

https://dspace.org/

Determination of the kinetics of contaminant degradation processes as a precursor to improved constructed wetland design

Aylward, Lara

2022
https://hdl.handle.net/10539/34382

Downloaded from a DSpace repository. https://dspace.org/



Determination of the Kinetics of Contaminant Degradation Processes as a Precursor to Improved Constructed Wetland Design

A dissertation for the fulfilment of the requirements of Master of Engineering

Prepared by

Lara Aylward

300324

Submitted to

School of Chemical and Metallurgical Engineering, Faculty of Engineering and the Built Environment, University of the Witwatersrand, Johannesburg, South Africa

Supervisor(s):

Dr Craig Sheridan Pr Eng. (Wits University)

Dr Uwe Kappelmeyer (UFZ, Leipzig, Germany)

May, 2019

Declaration

I declare that this dissertation is my own unaided work. It is being submitted for the degree of Master of Engineering to the Faculty of Engineering and the Built Environment, University of the Witwatersrand, Johannesburg.
It has not been submitted previously for any degree or examination to any other University.

_____

Lara Anne Aylward

23rd day of May 2019

Acknowledgements

I would like to thank the following people and organizations for their generous funding and invaluable advice and support:

- Prof. Craig Sheridan and Dr Uwe Kappelmeyer for their exceptional supervision and endless patience;
- The staff of the School of Chemical and Metallurgical Engineering at the University of the Witwatersrand;
- The staff of the Department of Environmental Biotechnology, as well as Dr Marie Kurz, Dr Christian Schmidt and Dr Tanja Brandt, at the Helmholtz Center of Environmental Research (UFZ), Leipzig, Germany;
- Ricky Bonner for his inspirational work ethic, his dedication to our shared experimental work and his contributions to each of my published papers;
- Philipp Hecht (TU Dresden), Michael van Zyl (Wits University) and Alyona Lepilova (University Thübingen) for their assistance in gathering and analysing data for this research as part of their diploma (Philipp) and masters (Michael, Alyona) research stays at the UFZ and their great company over many hours outside at the wetlands, in all weather conditions.
- My mom and dad for their unwavering support and encouragement and always providing a listening ear.

For financial assistance:

- Golder Associates South Africa
- The South African Water Research Commission
- The South African Department of Science and Technology
- The University of the Witwatersrand *Friedel Sellschop Award 2015*
- The Helmholtz Center of Environmental Research
- The National Research Foundation (NRF)
- The German Academic Exchange Service (DAAD)
- *Water4Crops* (an EU initiative)

Table of Contents

Table of Figures 8

List of Tables 13

List of Nomenclature 15

List of Acronyms 18

Chapter 1 Introduction 20

1.1. Background 20

1.1.1. The water conundrum in South Africa 20

1.1.2. Contamination of South Africa's water resources 20

1.1.3. South African water legislation 21

1.1.4. Sustainable water infrastructure and the green economy 21

1.1.5. The role of constructed wetlands and biomimicry 22

1.2. The relevance of this research 23

1.3. Research objectives 24

1.4. Structure of the thesis 24

1.5. List of Publications from this study 25

Chapter 2 Literature Review 26

2.1. Introduction to constructed wetlands 26

2.1.1. Natural wetland ecosystems 26

2.1.2. Historical development of constructed wetlands 27

2.1.3. Types of constructed wetlands 28

2.1.4. Wetland vegetation 29

2.1.5. Advantages of constructed wetlands 34

2.2. Wastewater quality 34

2.3. Remediation of wastewater using constructed wetlands 34

2.3.1. Contaminant removal mechanisms in constructed wetlands 34

2.3.2. Removal of organic carbon 35

2.3.3. Removal of nitrogen 36
2.3.4. Removal of phosphorus 38
2.3.5. Removal of additional contaminants 39
2.4. Constructed wetland hydraulics 39
2.4.1 Chemical engineering reactor theory 39
2.4.2. Types of fluid flow 41
2.4.3. Hydraulic tracer tests 43
2.4.4. The residence time distribution for steady-flow systems 44
2.4.5. Normalization of flow data 45
2.4.6. The residence time distribution for variable flow systems 45
2.4.7. Moments of the RTD 46
2.4.8. Flow behaviour in constructed wetland systems 47
2.4.9. Hydraulic efficiency 49
2.4.10. Hydraulic indexes 51
2.5. Chemical kinetics 54
2.6. Biomimicry and constructed wetland design 54
2.6.1. Ecological and Life's Principles 54
2.6.2. Biomimetic approach to wastewater treatment 56
Chapter 3 Materials and Methods 59
3.1. Experiments at the University of the Witwatersrand 59
3.1.1. Constructed wetland description 59
3.1.2. Wits Experimental timeline 60
3.1.3. Wetland preparation 61
3.1.4. Hydraulic studies 61
3.2. Experiments at the Helmholtz UFZ 62
3.2.1. Constructed wetland description 62
3.2.2. UFZ Experimental timeline 64

3.2.3. Hydraulic studies 64
3.2.4. Chemical and kinetic studies 66
Chapter 4 A comparison of three different residence time distribution modelling methodologies for horizontal subsurface flow constructed wetlands 69
4.1. Summary 69
4.2. Statement of individual contribution 69
4.3. Ecol. Eng. (2017). Vol. 99 pp. 99-113 70
4.3.1. Abstract 70
4.3.2. Introduction 71
4.3.3. Background 71
4.3.4. Research objectives 75
4.3.5. Materials and methods 76
4.3.6. Results and discussion 86
4.3.7. Conclusion 96
Chapter 5 Investigation into the kinetics of constructed wetland degradation processes as a precursor to biomimetic design 99
5.1. Summary 99
5.2. Statement of individual contribution 99
5.3. Water SA (2017) Vol. 43 No. 4 pp. 655-665 99
5.3.1. Abstract 99
5.3.2. Introduction 100
5.3.3. Materials and methods 103
5.3.4. Results and discussion 106
5.3.5. Conclusion 115
Chapter 6 Hydraulic study of a non-steady horizontal sub-surface flow constructed wetland during start-up 117
6.1. Summary 117
6.2. Statement of individual contribution 117

6.3. Sci. Tot. Environ. (2019) Vol. 646 pp. 880-892 117
6.3.1. Highlights 117
6.3.2. Graphical abstract 117
6.3.3. Abstract 118
6.3.4. Introduction 118
6.3.5. Theoretical background 119
6.3.6. Research objectives 125
6.3.7. Materials and methods 125
6.3.8. Results and discussion 129
6.3.9. Conclusion 139
Chapter 7 Contaminant degradation in a pilot-scale constructed wetland in the early start-up phase 140
7.1. Summary 140
7.2. Statement of Individual Contribution 140
7.3. Experimental Results 140
7.3.1. Baseline physico-chemical characteristics 140
7.3.2 Contaminant degradation and transformation 145
Chapter 8 Discussion and concluding remarks 157
8.1. Discussion 157
8.2. Conclusion 167
Chapter 9 References 169
Appendix A: Experimental Data, UFZ Leipzig 180
Appendix B: Matlab Code for Flow Test Data Analysis 209
Appendix C: Tracer Flow Test Data, UFZ Leipzig 241
Appendix D: Climatic Data (2016) 266
Appendix E: Supplementary information for *Sci. Tot. Environ. (2019) Vol. 646 pp. 880-892* 280
Appendix F: *Phragmites australis* fluoride tolerance experiments 286

Table of Figures

Figure 2-1: The definition of natural wetlands, their distinguishing characteristics and their classification according to the dominant plant species (Kivaisi, 2001). 26
Figure 2-2: The functional roles of a natural wetland (the dashed arrows represent contaminant removal by the wetland system) (Kivaisi, 2001). 27
Figure 2-3: Classification of constructed wetlands (Brix, 1994b). 28
Figure 2-4: The impulse and step change output concentration curves for ideal (dotted lines) and non-ideal (dashed lines) reactors in response to an impulse or step increase in input concentration (bold lines with arrow heads). (a) and (b) depict plug flow and (c) and (d) represent complete mixing (Headley and Kadlec, 2007). 43
Figure 2-5: (a) Hypothetical concentration breakthrough curve for an idealized impulse-response tracer test and (b) the corresponding residence time distribution function. 44
Figure 2-6: (a) Three hypothetical RTD's showing the effect of the degree of dispersion on peak shape, breadth and position and (b) Four hypothetical RTDs showing the influence of the amount of dead volume on the position of the RTD (Thackston et al., 1987). 48
Figure 2-7: The typical exponentially decaying concentration time profile of a perfectly mixed reactor and hypothetical concentration time breakthrough curves for two systems displaying various distributions of advective and stagnant zones (Thackston et al., 1987). 49
Figure 3-1: The experimental constructed wetlands at the IMWaRU site, Wits University showing the five zones of vegetation (left), the planted and unplanted wetlands side-by-side and the Jojo tank set-up (right). The outlet configurations (inlet configurations are not shown but are of the same design), the syphon break and the sample ports are also visible (right). 59
Figure 3-2: IMWaRU (Wits University) constructed wetland configuration showing a removable cage and sample tubing to three depths. The outlet distribution network is also visible and the inlet distribution network is of the same arrangement. The red dashed lines illustrate the division of the wetland system into a grid of sample points. 60
Figure 3-3: Experimental timeline for the experiments conducted in the constructed wetlands at the University of the Witwatersrand, 2015. 60
Figure 3-4: (a) Aerial view of the constructed wetland showing seven internal sample ports, three inlet valves and one outlet valve and (b) cross-sectional view showing the gravel bed and valve heights. 63
Figure 3-5: (a) Photograph of the pilot, gravel horizontal subsurface flow constructed wetland at the Helmholtz UFZ, Leipzig (July 2015) and (b) the middle basket when removed from the wetland showing a well-developed root system (Sept 2015). 63

Figure 3-6: Timeline of experiments conducted in the constructed wetlands at the Helmholtz UFZ during 2015. 64
Figure 3-7: Timeline of experiments conducted in the constructed wetlands at the Helmholtz UFZ during 2016. 64
Figure 3-8: Stainless steel sampling devices (samplers), peristaltic pump, flow cell and fluorometer configuration for the impulse-response flow tests. 65
Figure 4-1: Overview of the three different RTD modelling methodologies used in this study. The initial phase consists of data generation in the form of the hydraulic tracer study being performed on the wetland system and subsequent development of the concentration-time curve. The second phase consists of data processing and various numerical methods to obtain the hydraulic characteristics of the system. 76
Figure 4-2: Generic concentration-time data generated from the impulse and step change tracer experiments (Fogler, 1999). The response curves of both the impulse and step change tracer experiments typically differ considerably from their corresponding injection curves which indicates non-ideal flow patterns such as dispersion and short-circuiting effects. 77
Figure 4-3: The relationship between the concentration-time curve and the RTD function used in the impulse response modelling methodology (Levenspiel, 1999a). The mathematical transformation includes computing the area underneath the concentration-time curve and hence the use of numerical integration techniques such as Simpson's integration formulae. 78
Figure 4-4: Determining the mean residence time of the fluid by computing the area above the F(t) curve (Levenspiel, 1999a). 79
Figure 4-5: The relationship between the RTD function, E(t), and the cumulative distribution function, F(t) (Levenspiel, 1999a). The conversion of F(t) to E(t) requires the use of numerical integration techniques such as the central difference approximation. 80
Figure 4-6: TIS model demonstrated for the real reactor (left) using a combination of idealised tanks in series (right). Adapted from (Fogler, 1999). 81
Figure 4-7: Normalized E(t) (left) and F(t) (right) curves for different values of n (Fogler, 1999). As the number of stirred tanks in series increases the system approaches plug flow behaviour whereas the number of tanks in series approach unity the degree of back mixing increases and the system resembles a completely stirred tank reactor. 81
Figure 4-8: Spatial arrangement of inlet, outlet and internal sampling ports as well as the system grid resolution. All dimensions are expressed in mm. Samples were taken from three different depths within each of the thirteen sampling wells as well as at the system outlet. 83

Figure 4-9: Zonal distribution of wetland vegetation in planted system. Five different species were used and were strategically planted according to their tolerance of wastewater with the more resistant species planted towards the inlet of the wetland where higher contaminant concentrations would be expected. 84
Figure 4-10: E(t) and F(t) curves from the impulse and step change experiments, respectively. In Fig. 10(a) and (c) hydraulic data from the impulse response experiment on unplanted and planted systems are presented respectively and likewise in Fig. 10(b) and (d) using the step change response experiment. 87
Figure 4-11: RTD curves from the impulse experiments on the planted and unplanted systems. In Figures (a) and (b) hydraulic data from the surface layer are presented. In Figures (c) and (d) data from the intermediate layer are presented and in Figures (e) and (f) data from along the bottom of the wetland bed are presented. Each curve within the figures represents hydraulic data collected from a sampling point a specified distance from the system inlet thus allowing for the evolution of the RTD curve to be depicted as a function of system length. 92
Figure 4-12: Cumulative distribution curves from the impulse experiments on the planted and unplanted systems. In Figures (a) and (b) hydraulic data from the surface layer are presented. In Figures (c) and (d) data from the intermediate layer are presented and in Figures (e) and (f) data from along the bottom of the wetland bed are presented. Each curve within the figures represents hydraulic data collected from a sampling point at a specified distance from the system inlet. 93
Figure 4-13: Comparison of $tm\tau$ for when 3-point subintervals and when one subinterval is used for numerical integration using Simpson's 1/3 rule. The comparison performed on the hydraulic data obtained from the unplanted system is presented in Fig. 13(a) and for the planted system in Fig. 13(b) and is performed in each case for the impulse response as well as the step change derivative and step change integral modelling approaches..... 95
Figure 4-14: Normalized E(t) for planted and unplanted systems with regions of noise highlighted on the E(t) curves from the step change derivative approach. 96
Figure 5-1: (a) Aerial view of the CW showing the sample port, three inlet valve and single outlet valve locations and (b) cross-sectional view of the CW showing one stainless steel sampling tube. 103
Figure 5-2: (a) A photograph of the pilot-scale, horizontal subsurface flow CWs at the Helmholtz UFZ (July 2015) and (b) the stainless steel basket removed from the centre of the wetland showing an already well-developed root system (September 2015). 104
Figure 5-3: A schematic diagram of the sampling device, pump, flow cell and fluorometer configuration for the tracer flow tests..... 105

Figure 5-4: Baseline characterization showing (a) the dissolved oxygen concentration and (b) the oxidation-reduction potential prior to the introduction of artificial wastewater. Data was obtained from 24 cm below the gravel bed surface and at increasing distance along the flow path during August, September and October 2015. 108
Figure 5-5: The normalized RTD function for the pilot CW determined from an impulse-response tracer test, with τ = 2.16 d (θ = 0.78), t_m = 2.89 d (θ = 1.0) and a peak time at maximum concentration of 2.31 d (θ = 0.80). 110
Figure 5-6: (a) Total organic carbon concentration (avg. inlet [TOC] = 573 ± 62 mg/ℓ; baseline TOC = ± 3.0 mg/ℓ) and (b) total nitrogen concentration (avg. inlet [TN] = 230 ± 21 mg/ℓ; baseline TN = ± 1.7 mg/ℓ) as a function of time at the wetland outlet up to 7 weeks after the introduction of artificial wastewater into the system. 112
Figure 5-7: An illustration of the general trend in (a) TOC concentration (avg. inlet [TOC] = 573 ± 62 mg/ℓ) and (b) the dissolved oxygen concentration at increasing distance from the wetland inlet over the 7 week experimental period (avg. inlet [DO] = 11.158 ± 1.208 mg/ℓ; avg. inlet temp = 10.9 ± 2.6°C).....113
Figure 5-8: The change in oxidation-reduction potential as a function of time at the wetland outlet up to 7 weeks after the introduction of artificial wastewater into the system (avg. inlet potential = 336.1 ± 30.1 mV). 114
Figure 5-9: The variability in the rate of decomposition of total organic carbon, k_{TOC}, and the rate of transformation of total nitrogen, k_{TN} 115
Figure 6-1: Summary and comparison of the mathematics underlying hydraulic theory for steady versus variable flow systems 122
Figure 6-2: (a) An aerial view of the constructed wetland showing seven internal sample ports, three inlet valves and one outlet valve and (b) cross-sectional view showing the gravel bed and valve heights. ...126
Figure 6-3: (a) 2015 and (b) 2016 idealized concentration breakthrough curves at various distances from the wetland inlet and mid-depth (24cm) below the gravel surface, assuming a tracer mass of 30 mg and hydraulic residence time of 7 days.....131
Figure 6-4: Normalized RTDs, assuming steady flow, at various distances along the flow path at (a) mid-depth (2015) and (b) 12 cm, (c) 24 cm and (d) 36 cm depth (2016). 133
Figure 6-5: Comparison of the 2015 and 2016 normalized RTDs at various distances along the flow path and at mid-depth (24cm) below the gravel surface. 134
Figure 6-6: 2016 normalized RTDs at the wetland outlet for experiments in duplicate, calculated using standard (dashed line) and variable flow (solid line) methodologies.....135

Figure 6-7: Evapotranspiration, rainfall, relative humidity and global radiation measured in Leipzig during April, August and October 2016.....138
Figure 7-1: (a) Redox potential and (b) dissolved oxygen concentration along the constructed wetland at a depth of 12cm over the 5 week baseline sampling period.....142
Figure 7-2: (a) Redox potential and (b) dissolved oxygen concentration along the constructed wetland at a depth of 24cm over the 5 week baseline sampling period.....143
Figure 7-3: (a) Redox potential and (b) dissolved oxygen concentration along the constructed wetland at a depth of 36cm over the 5 week baseline sampling period.....144
Figure 7-4: Total organic carbon hydraulic loading (avg. inlet TOC loading = 10.1 ± 1.7 $g/m^3.d$; baseline TOC loading = 0.81 ± 0.22 $g/m^3.d$) as a function of time at the wetland outlet up to 10 weeks after the introduction of artificial wastewater into the system against the variation in volumetric flowrate (avg. inlet flowrate = 6.2 ± 0.3 L/d; avg. outlet flowrate = 5.3 ± 0.4 L/d for week 1-5).....146
Figure 7-5: Total nitrogen hydraulic loading (avg. inlet TN loading = 4.5 ± 0.8 $g/m^3.d$; baseline TN loading = 0.34 ± 0.16 $g/m^3.d$) as a function of time at the wetland outlet up to 10 weeks after the introduction of artificial wastewater into the system against the variation in volumetric flowrate (avg. inlet flowrate = 6.2 ± 0.3 L/d; avg. outlet flowrate = 5.3 ± 0.4 L/d for week 1-5).....147
Figure 7-6: The change in dissolved oxygen concentration as a function of time at the wetland outlet up to 10 weeks after the introduction of artificial wastewater into the system (inlet dissolved oxygen concentration and saturated oxygen concentration also shown).....148
Figure 7-7: The change in oxidation-reduction potential as a function of time at the wetland outlet up to 10 weeks after the introduction of artificial wastewater into the system (avg. inlet potential = 109.2 ± 42.4).....148
Figure 7-8: (a) Total organic carbon concentration profile (avg. inlet [TOC] = 78.6 ± 11.0 mg/L) and (b) total nitrogen concentration profile (avg. inlet [TN] = 35.1 ± 5.0 mg/L) at 24cm below the bed surface over 5 weeks in July 2016.....149
Figure 7-9: (a) Dissolved oxygen concentration profile (avg. inlet [DO] = 8.80 ± 0.37 mg/L) and (b) redox potential profile 24cm below the bed surface over 5 weeks in July 2016.....150
Figure 7-10: The TOC hydraulic loading density profile for the week 15^{th} – 21^{st} July 2016 (key in top right-hand side indicates range of hydraulic loading rates in $g/m^3.d$).....154
Figure 7-11: The TN hydraulic loading density profile for the week 15^{th} – 21^{st} July 2016 (key in top right-hand side indicates range of hydraulic loading rates in $g/m^3.d$).....154

List of Tables

Table 2-1: Common species of macrophyte (Brisson and Chazarenc, 2008).....29
Table 2-2: Investigation of the removal efficiencies of various pollutants between Phragmites australis and a sub-species of Typha in a horizontal subsurface flow mesocosms (Brisson and Chazarenc, 2008) 32
Table 2-3: The primary contaminants and their mechanisms of removal from CW systems (Vymazal, 2005, Brisson and Chazarenc, 2008).....35
Table 2-4: Classes of chemical reactors (Froment et al., 2011) 40
Table 2-5: The Biomimetic Ecological Principles 55
Table 2-6: Summary of successful biomimetic wetland designs (Dama-Fakir et al., 2015).....57
Table 3-1: Legal limits on environmental discharges for a treatment plant of Class 2 in Germany (based on an inflow of 300–600 $kg \cdot d^{-1}$ BOD_5) 67
Table 3-2: Feed water and artificial wastewater inflow loading rates during 2015 68
Table 3-3: Feed water and artificial wastewater inflow loading rates during 2016 68
Table 4-1: Average flow rates used for hydraulic tracer studies as well as the nominal retention time for each experiment. 84
Table 4-2: Dynamic sampling regime employed for the impulse tracer studies where X indicates a sample being taken 85
Table 4-3: Dynamic sampling regime employed for the step change tracer studies where X indicates a sample being taken.....86
Table 4-4: Calculated hydraulic parameters for the planted and unplanted systems using the impulse and step change modelling methodologies.....88
Table 4-5: Comparison of hydraulic parameters for the unplanted system, scaled to a flow rate of 4.5 l/min ..89
Table 4-6: Comparison of hydraulic parameters for the planted system, scaled to a flow rate of 4.5 l/min 89
Table 5-1: Primary contaminants and mechanisms of removal from CW systems.....101
Table 5-2: Average bed temperature, pH, TOC and TN concentration with the saturated oxygen concentration (fresh water, 760 mm Hg) at the time of the baseline measurements.....106
Table 5-3: Various hydraulic parameters describing the behaviour of the pilot CW as determined from the impulse-response tracer test and system RTD.....111
Table 6-1: A comparison of steady and non-steady systems with regards to flow conditions, retention time and standard residence time distribution theory.....120
Table 6-2: Time to maximum peak concentration at various distances along the flow path (2015 versus 2016) 131

Table 6-3: Peak time and hydraulic moments at the wetland outlet using standard and variable flow methodologies (sample distance = 6.0 m; system volume = 1009 L).....136
Table 7-1: Average baseline pH, TOC concentration and TN concentration with the average temperature and saturated oxygen concentration (fresh water, 760 mm Hg) in the pilot CW 141
Table 7-2: Inlet temperature and dissolved oxygen concentration with the saturated oxygen concentration (fresh water, 760 mm Hg) at the baseline 141
Table 7-3: Average weekly total organic carbon and total nitrogen hydraulic loading rates and percentage removal (day of sampling is the second date mentioned).....146
Table 7-4: Estimated internal TOC and TN hydraulic loading **12cm** below the wetland surface.....153
Table 7-5: Estimated internal TOC and TN hydraulic loading **24cm** below the wetland surface.....153
Table 7-6: Estimated internal TOC and TN hydraulic loading **36cm** below the wetland surface.....153

List of Nomenclature

α	exposed wetland surface area
A	wetland cross sectional area
B	width of the wetland
C_{A0}	concentration of species A in the feed
C_A	concentration of species A at the system outlet
C_{max}	concentration of dye as $t \rightarrow \infty$
C(t)	time variant tracer concentration (for a steady flow system)
$C(\theta)$	dimensionless concentration (for a steady-flow system)
$C(\Phi)$	dimensionless concentration (non-steady flow system)
d	dispersion index
D	dispersion number
D_p	equivalent spherical diameter of the packing material
e	effective volume utilisation ratio
E(t)	residence time distribution function (for a steady flow system)
$E(\theta)$	normalized residence time distribution (for a steady-flow system)
$E(\Phi)$	dimensionless residence time distribution (non-steady flow system)
ET	water lost by evapotranspiration
F(t)	cumulative distribution function
$F(\theta)$	Normalized cumulative distribution function
h	wetland water level
k_{TOC}	reaction rate constant for the decomposition of TOC
k_{TN}	reaction rate constant for the transformation of TN
L	length of the wetland
M, m_i	total mass of tracer injected (at the start of the flow test)
M_0	zeroth moment of the residence time distribution
M_1	first moment of the residence time distribution (equivalent to $\bar{t}_m$)
M_2	second moment of the residence time distribution
n	number of tanks in series (T-I-S model)
N	fractional recovery of tracer material
Pe	Peclet number
Q	steady-state volumetric flow rate
$\overline{Q}_{in}$	average inlet volumetric flow rate (assuming a steady-flow system)
$Q_{internal}$, Q_i	estimated local flow rate at a specified distance from the wetland inlet

$\overline{Q}_{out}$	average outlet volumetric flow rate (assuming a steady-flow system)
$Q_{in}(t)$	time-variant inlet volumetric flow rate (non-steady flow system)
$Q_{out}(t)$	time-variant outlet volumetric flow rate (non-steady flow state)
$\overline{Q}_{sys}$	average volumetric flow rate (assuming a steady-flow system)
q_{in}	inlet hydraulic loading rate
q_{in}	outlet hydraulic loading rate
R	percentage recovery of tracer
Re_p	Reynold's number for packed beds
r_i	rate of formation ($r_i > 0$) or consumption ($r_i < 0$) of species i
t	time after injection, or age
t_0	time signalling the start of a tracer experiment, or time of injection
t_f	time marking the end of the flow test
t_{10}	time taken 10% of the injected tracer mass to reach the system outlet
t_{90}	time taken for 90% of the injected tracer mass to reach the system outlet
t_{99}	time taken for 99% of the injected tracer mass to reach the system outlet
t_m, $\bar{t}_m$	mean residence time (1st moment of the RTD)
t_p, t_{peak}	time corresponding to the maximum peak concentration recorded at the wetland outlet
U_s, u_s	superficial fluid velocity
V, V_{sys}	total system fluid volume (taking into account material voidage)
V_{eff}	effective volume utilisation (volume of fluid inside reactor, excluding the dead volume)
V(t)	time-variant system volume
$V_{out}(t)$	cumulative discharge volume
v_0, $\dot{v}$	system volumetric flowrate
x_i	position along the length of the wetland, where i = 1 - 6 and designates a sampling point
X	conversion or extent of reaction

Greek and Special Characters

ε	voidage of the gravel
δ	increase in depth of water due to rainfall
λ	hydraulic efficiency
Φ	dimensionless flow weighted time
ρ	fluid density
ρ_{veg}	vegetation density
σ^2	variance (2nd moment of the RTD)

τ nominal residence time, or hydraulic retention time, for a steady flow system

θ normalized time for a steady flow system

θ_i dimensionless short-circuiting index

θ_{peak} normalized peak time

μ fluid viscosity

Chemical Species Formulae

C	carbon
CH_2O	formaldehyde
CO_2	carbon dioxide
CO_3^{2-}	carbonate
H^+	hydronium ion
HCO_3^-	bicarbonate
H_2O	water
N_2	nitrogen gas
N_2O	nitrous oxide
NH_3	ammonia
NH_4^+	ammonium
NO_2^-	nitrite
NO_3^-	nitrate
O_2	oxygen gas
OH^-	hydroxide
PO_4^{3-}	phosphate

List of Acronyms

AMD	acid mine drainage
ANAMMOX	anaerobic ammonia oxidation
AWW	artificial wastewater
BOD	biological oxygen demand
BTC	(concentration) breakthrough curve
COD	chemical oxygen demand
CSTR	continuous stirred tank reactor
CW	constructed wetland
DEA	Department of Environmental Affairs
DNRA	dissimilatory nitrate reduction, or nitrate ammonification
DO	dissolved oxygen
DST	Department of Science and Technology
DWS	Department of Water and Sanitation
FC	faecal coliforms
HRT	hydraulic residence time
HSSF	horizontal sub-surface flow
IMWaRU	Industrial and Mining Wastewater Research Unit
IC	inorganic carbon
MDI	Morril Dispersion Index
MI	Moment Index
M_{pre}	pre-nominal moment about the nominal divide
NDP	National Development Plan
NPOC	non-purgeable organic carbon
NRM	National Resource Management programme
NWRS	National Water Resource Strategy
PFR	plug flow reactor
RTD	residence time distribution
SANBI	South African National Biodiversity Institute
SIP	Strategic Integrated Project
SPACE	Systems for People to Access a Clean Environment
TC	total carbon
T-I-S	Tanks-In-Series model
TKN	total Khejdahl nitrogen

TN	total nitrogen
TOC	total organic carbon
TP	total phosphorus
TSS	total suspended solids
VF	vertical flow
WRC	Water Research Commission
WSA	water source area

Chapter 1 Introduction

1.1. Background

1.1.1. The water conundrum in South Africa

South Africa is a water scarce country – ranked 30th driest globally (GreenCape, 2016) – with an annual rainfall of just 50% of the world average (WWF-SA, 2016). Moreover, precipitation is seasonal and fluctuates (WWF-SA, 2016) and rainfall patterns could be further impacted by climate change (GreenCape, 2016). As a consequence, South Africa's fresh water supply in its catchments, rivers, wetlands and aquifers is not guaranteed to be replenished at the time and to the extent required.

South Africa's water source areas (WSAs) – the land areas that produce run-off into the river systems – are located in a belt along the coastal region of the country, inland toward the mountainous Drakensberg area and then in the north along the Mozambican border (WWF-SA, 2016). The WSAs are of key importance because the country relies predominantly on surface water from the river systems into which they drain. At present, only 16% of the WSAs are protected in national parks, nature reserves and nature conservancies. This percentage is too low, given that these areas are some of South Africa's most valuable natural assets. It is concerning that some of the WSAs in the Drakensberg, Mfolozi and Mpumalanga regions are overlapped by coalfields (WWF-SA, 2016). Coal mining and coal fired power contribute significantly to the South African economy (DOE, 2018, Koko, 2018). This is just one example of the challenge that faces multiple industries and government departments alike: ensuring that productivity is maximized within the constraints of sufficient protection of the natural environment.

1.1.2. Contamination of South Africa's water resources

Poor water quality has a major negative impact on the livelihood of all South African citizens, as well as the surrounding ecosystem. Water quality in South Africa's natural resources has declined over the previous two decades; in some cases to such an extent that the water has become a serious health threat. The primary contributors to the pollution of the country's water resources are:

- Release of raw sewage
- Acid mine drainage
- Release of untreated industrial effluent
- Excess nutrients from agricultural runoff (WWF-SA, 2016)

Exacerbating the problem is the number of municipal water service authorities plagued by poor service delivery and any of a range of factors, including increased urbanization, aging of the engineered infrastructure, lack of maintenance and shortage of skills could be blamed. To compound this, many inhabited areas of the country are

either in remote locations or are unplanned, rapidly expanding informal settlements; neither of which are serviced by the existing, although deteriorating, water treatment facilities (WWF-SA, 2016, Swartz, 2009). Without urgent attention, South Africa could be faced with a serious water quality and availability crisis.

1.1.3. South African water legislation

South Africa's constitution declares that access to clean, safe water is a basic right for every citizen. The manner in which this constitutional right is upheld is also important because the unique constitution also grants the environment the basic right to water. Hence, provision of water in South Africa becomes a careful balance between adequate supply and protection of the country's natural water resources (WWF-SA, 2016).

South Africa's water resources are governed by the Water Services Act of 1997 and the National Water Act of 1998 (WWF-SA, 2016, Govt.SA., 2017). The South African Department of Water and Sanitation (DWS) is mandated to protect, manage, develop and control the use of the country's water resources. Closely related to this is the provision of sanitation services; also falling under the DWS umbrella. In line with the requirements of the two water acts and government's National Development Plan (NDP), the DWS issued the revised National Water Resource Strategy (NWRS2). The NWRS2 outlines how the department and other key role players will achieve effective management of the national water resources. The strategy includes security of water supply, managing environmental degradation and curbing pollution of water resources.

The National Resource Management Programme (NRM) was initiated in 1995 by the South African Department of Environmental Affairs (DEA) with the 'working for water' initiative. This programme aimed to conserve water by eliminating invasive alien plant species. Subsequently, the NRM has expanded to include the 'working for fire', 'working for forests', 'working for wetlands' and 'working for ecosystems' programmes. The country has, since 2002, achieved a 5% improvement in the provision of fresh water to households. However, there are still approximately 2.5 million people without access to this essential resource (Govt.SA., 2017) and new and innovative programmes will be required to reduce this figure further.

1.1.4. Sustainable water infrastructure and the green economy

The increasing demand for water, coupled with the low average annual rainfall input, means that planning and development are essential to increase capacity and maintain an adequate supply of fresh water, but all too often this is done without sufficient consideration of the ecological infrastructure. The DEA and the South African National Biodiversity Institute (SANBI) define ecological infrastructure as "the nature-based equivalent of built infrastructure". In other words, the ecosystems, as a result of their natural functionality, provide essential services to society and support socio-economic development in terms of, for example, the provision of water and soil and climate control. The DEA and SANBI have, thus, announced the 19th Strategic Integrated Project

(SIP 19) in order to rehabilitate, develop and protect "Ecological Infrastructure for Water Security" (WWF-SA, 2016). This project is still in its early phases, but pilot projects are underway (SANBI, 2014).

As South Africa works towards developing its ecological infrastructure, opportunity arises to move from centralized to decentralized wastewater treatment facilities; examples of which include point-of-use household technologies (SEAL, 2018, CWC, 2015, Nimbus, 2017), rainwater harvesting installations, grey-water green roofs and water recycling and reclamation systems (GreenCape, 2016). The popularity of decentralized systems is growing as a result of the need to:

- reduce or eliminate transport and pumping costs
- improve access to water and sanitation services; particularly in remote areas and establishments that are not connected to the sewage infrastructure
- prevent pollution of water bodies and
- find solutions that are easy to install, quick to implement, span a broader range of treatment capacities, have minimal power requirements and have low maintenance costs (GreenCape, 2016).

1.1.5. The role of constructed wetlands and biomimicry

Constructed wetlands (CWs) are engineered systems, designed to utilize the soil, vegetative and microbial processes of natural wetlands to assist in the treatment of wastewater of different origins (Vymazal, 2005). CWs have been identified as a viable, green technology solution to water management in the following areas:

- regulation of water supply
- drought alleviation
- regulation of water quality (and particularly for biological and temperature control)
- purification of water (GreenCape, 2016)

Biomimicry is defined as "the practice of learning from and then emulating nature's genius to solve human problems and create more sustainable solutions" (Biomimicry.SA., 2015). As the types of wastewater become more diverse, so the need for more economical, efficient and robust systems to cope with the treatment demands emerges. The biomimetic principles (incorporating both the ecological and life's principles) (Todd and Josephson, 1996, Benyus, 2017) provide valuable tools to inform the design of improved CW systems. Biomimetic wetlands are self-contained, ecologically engineered systems where waste streams are recycled wherever practicable. In addition, they can be a source of nutrient-rich fertilizers and renewable energy and can act as carbon sinks, air quality regulators, temperature regulators and habitats for biodiversity (Dama-Fakir et al., 2015).

The Department of Science and Technology (DST) is at the helm of creating awareness around and moving forward with the ecological infrastructure work initiated by the DWS and SANBI. In addition, stakeholders in

environmental consultancy, research institutions, the Water Research Commission (WRC) and Biomimicry SA are coordinating research projects to develop biomimetic design solutions for the country's water-related challenges. There is real scope for CWs to provide a valuable addition to South Africa's ecological infrastructure. They offer all of the advantages of decentralized systems and, when designed using biomimetic principles, can offer benefits beyond just water remediation. A case in point is the successful prototype in the Langrug informal settlement close to Franschoek (Biomimicry.SA., 2018). This is one of the first Systems for People to Access a Clean Environment (SPACE) projects, initiated five years ago by the Western Cape government and carried out in full co-operation with the local community. Langrug has been converted into an Eco-machine (JTED, 2014, U.S.EPA, 2002), which uses biomimicry to address water purification, stormwater and solid waste management, as well as provide potential for revenue generation (WWF-SA, 2016). Overall, CWs have an important role to play in expanding the ecological infrastructure and biomimicry offers a more holistic and sustainable approach to the design and implementation of these systems.

1.2. The relevance of this research

Much of the literature views CWs as "black boxes" and an in-depth knowledge of the complexities and interdependencies of the chemical, hydraulic, kinetic and microbiological processes is still lacking; even though more recent studies have begun to report data from various internal of locations along the length of the wetland bed (Sheridan et al., 2014a, Bonner et al., 2017b, Bonner et al., 2017a). This research focuses on an in-depth hydraulic characterization and baseline physico-chemical description of a newly established pilot-scale CW; followed by a five month period of feeding artificial domestic wastewater into the wetland and continually monitoring the chemical and physical changes. In addition, external climatic conditions and vegetation development will be monitored. The analytical procedure involves dividing the CW into a grid of sample ports: seven ports down the length of the bed, each of which is divided into three depths. The multitude of sampling locations and samples will provide insight into the internal spatial development and operation of the wetland system. More specifically, the hydraulic characterization will describe fluid flow behaviour throughout the wetland and provide insight into the validity of making steady-state mathematical assumptions in a real, dynamic system. The chemical characterisation will provide insight into the kinetics of carbon and nitrogen transformation. It is envisaged that this research may enhance the existing body of knowledge on design methodology and visual representation of CW systems by including more information on the internal fluxes and, thus, act as a framework for future research and development.

1.3. Research objectives

1. To use impulse-response tracer tests to determine the hydraulic characteristics of the Industrial and Mining Water Research Unit's (IMWaRU) pilot-scale CWs (namely the residence time distribution, velocity profiles, reactor behaviour, location of dead zones and areas of short-circuiting/bypass) and then to compare, and possibly validate, the findings using step-change tracer studies in the same systems (in conjunction with Ricky Bonner).
2. To investigate the hydraulic and chemical kinetic performance of a pilot-scale CW in the start-up phase at the Helmholtz Centre for Environmental Research (Helmholtz UFZ) in Leipzig, Germany. The investigative method was to be chosen based on the conclusions drawn from objective 1.
3. To collate and analyse the data collected and develop a framework for improved CW design from the perspective of:
    a. optimizing fluid flow pathways
    b. maximizing fluid residence time in the areas of the bed where the rates of contaminant removal are greatest
4. To compare the impulse-response performance of a fluoride probe with that of a fluorescent chemical tracer to investigate the suitability of a salt-based tracer.
5. To determine whether micro-organisms may be used as reliable tracers.

1.4. Structure of the thesis

This thesis comprises 8 chapters plus the appendices of experimental data. Chapters 4, 5 and 6 are made up of published papers in *Ecological Engineering*, *Water SA* and *Science of the Total Environment*, respectively. The authors plan to submit the experimental findings in Chapter 7 for publication. Certain sections of the theory presented in the literature review (Chapter 2) and the materials and methods (Chapter 3) may be repeated in similar sections of the papers. The author requests the reviewers' patience in this regard.

The appendices contain the experimental data, Matlab code and other supplementary information to support this thesis. More data and information is given on the CDs and anything additional can be made available on request. The experimental data supporting the paper in Chapter 4 is presented in the thesis written by Ricky Bonner and submitted to the Faculty of Engineering and the Built Environment of the University of the Witwatersrand.

1.5. List of Publications from this study

i. Bonner, R., **Aylward, L.A.**, Kappelmeyer, U. and Sheridan, C.M. 2017. A comparison of three different residence time distribution modelling methodologies for horizontal subsurface flow constructed wetlands. *Ecological Engineering*, 99, 99 – 113.

ii. Bonner, R., **Aylward, L.A.**, Kappelmeyer, U. and Sheridan, C.M. 2017. Heat as a hydraulic tracer for horizontal subsurface flow constructed wetlands. *Journal of Water Process Engineering*, 16, 183 – 192.

iii. **Aylward, L.A.**, Kappelmeyer, U., Bonner, R., Hecht, P. and Sheridan, C.M. 2017. Investigation into the kinetics of constructed wetland degradation processes as a precursor to biomimetic design. *Water SA*, 43(4), 655 – 665.

iv. Luciana Schultze-Nobre, L., Wiessner, A., Bartsch, C., Paschke, H., Stefanakis, A.I., **Aylward, L.A.** and Kuschk, P. 2017. Removal of dimethylphenols and ammonium in laboratory-scale horizontal subsurface flow constructed wetlands. *Engineering in Life Science*, 17 (12), 1224 – 1233.

v. Kappelmeyer, U. and **Aylward, L.A.** 2018. Chapter 2 Rhizospheric processes for water treatment: background principles, existing technology and future use. In: Artificial or constructed wetlands – a suitable technology for sustainable water management. Durán-Domínguez-de-Bazúa, M.C., Navarro-Frómeta, A.E. and Bayona, J.M. (Eds.). CRC Press Taylor & Francis Group, Mexico.

vi. **Aylward, L.A.**, Bonner, R., Kappelmeyer, U. and Sheridan, C.M. 2019. Hydraulic study of a non-steady horizontal sub-surface flow constructed wetland during start-up. *Science of the Total Environment*, 646, 880 – 892.

vii. Bonner, R., **Aylward, L.A.**, Kappelmeyer, U. and Sheridan, C.M. 2018. Combining tracer studies and biomimetic design principles to investigate clogging in constructed wetlands. *Water SA*, 44(4), 764 – 770.

Chapter 2 Literature Review

2.1. Introduction to constructed wetlands

2.1.1. Natural wetland ecosystems

Natural wetlands are areas intermediate between water and land; examples of which include swamps, marshes and bogs. Figure 2-1 gives the definition and classification of natural wetland systems (Kivaisi, 2001).

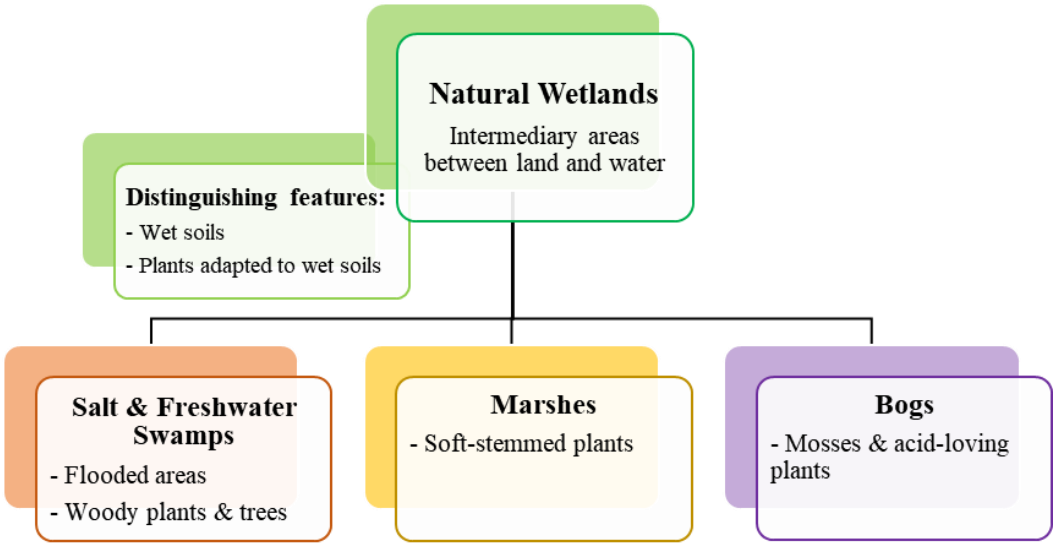


Figure 2-1: The definition of natural wetlands, their distinguishing characteristics and their classification according to the dominant plant species (Kivaisi, 2001).

Natural wetlands have a number of important ecological functional roles; namely water purification, water capture and storage, flow regulation, flood attenuation and shoreline stabilization and protection. These roles are represented diagrammatically in Figure 2-2. Without their diversity of vegetation, microbial and aquatic species and wildlife, wetland ecosystems would not support these functions (Kivaisi, 2001). It is, thus, not surprising that natural wetlands should be the inspiration for a solution to water treatment challenges; namely the constructed wetland.

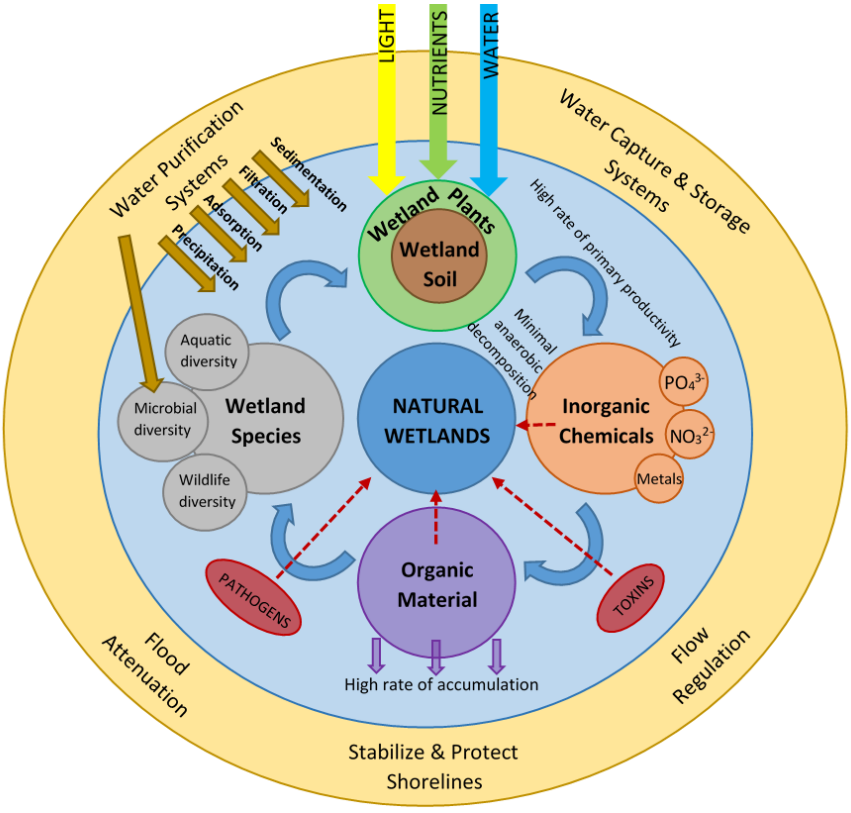


Figure 2-2: The functional roles of a natural wetland (the dashed arrows represent contaminant removal by the wetland system) (Kivaisi, 2001).

2.1.2. Historical development of constructed wetlands

Historically, wetlands were considered wastelands of little use and poor aesthetic appeal and often converted into landforms of supposed better value. However, as knowledge grew of how vital a part of the natural environment these ecosystems were, focus turned towards their preservation and protection and the development of CWs for wastewater remediation (Reed, 1993). Quoting Jan Vymazal of the *Duke University Wetland Centre*, "CWs are engineered systems that have been designed and constructed to utilize the natural processes involving wetland vegetation, soils and the associated microbial assemblages to assist in treating wastewaters" (Vymazal, 2005); often acting as polishing systems following the primary and secondary water treatment stages (Brix, 1994b). CWs have three characterising features:

1. A soil, gravel or sand filled bed (Brix, 1994b, Haberl et al., 2003).
2. One of more types of specialised macrophyte, which are adapted to the hydric and oxygen depleted conditions, known to aid in the removal of various types of wastewater contaminants and withstand harsh chemical environments (Brix, 1994b, Haberl et al., 2003).

3. Specific hydrologic conditions in that the soil matrix be saturated with water up to a depth of 2m, either continually or intermittently, during the vegetation's growth season (Haberl et al., 2003).

Organic matter and nutrients are removed from the water flowing through the wetland owing to its ability to transform or store these species (Brix, 1994b). Originally, CWs treated domestic and municipal sewage, but their use was later extended to industrial and agricultural wastewater, landfill leachate, acid mine drainage (AMD) and stormwater and mining run-off remediation (Vymazal, 2005, Reed, 1993). High levels of removal of sulphate, manganese, iron and certain heavy metals from acid mine water have also been observed (Smith, 1997).

2.1.3. Types of constructed wetlands

CWs are broadly categorized according to the class of dominant macrophyte and then the major type of fluid flow through the system. This classification is illustrated by means of the diagram in Figure 2-3. Free-floating macrophyte systems were developed largely as a means of enhancing the performance of stabilization ponds; whereas submerged macrophyte systems were intended to act as polishing systems post the primary and secondary water treatment stages. These two classes of CWs are not widely used and it is the emergent macrophyte systems that dominate; hence their further classification based on the primary fluid flow path (Brix, 1994b).

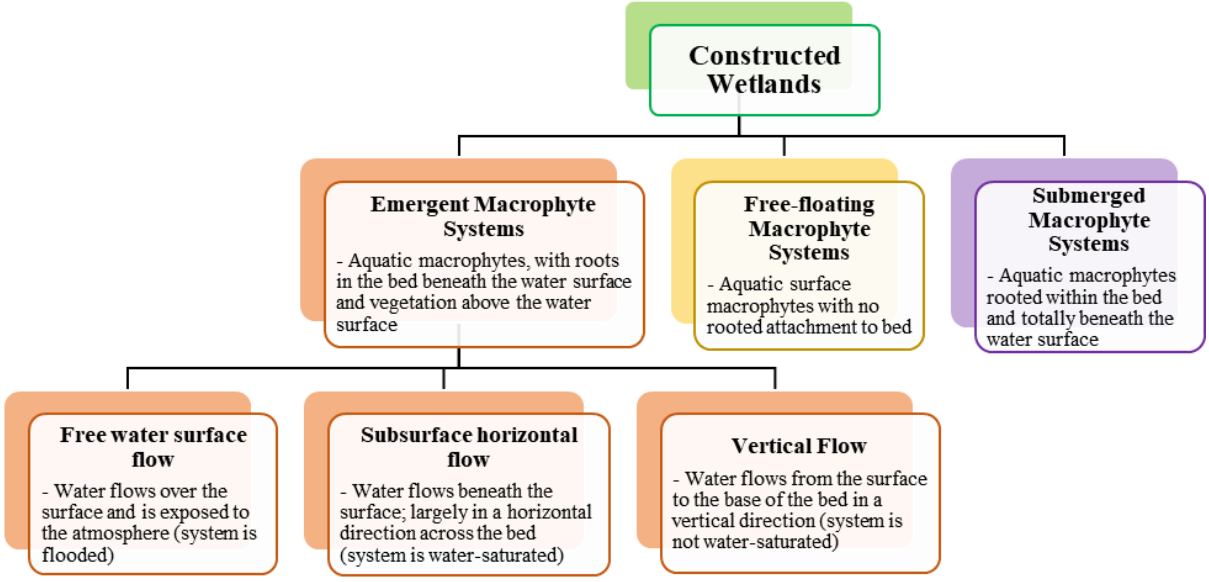


Figure 2-3: Classification of constructed wetlands (Brix, 1994b).

The horizontal subsurface flow (HSSF) CW emerged as the preferred system for wastewater remediation and wetlands of this type find were most commonly installed. However, as the number of classes of wastewaters requiring treatment continued to increase, it became evident that single-stage HSSF CW systems were not always adequate, depending on the level of treatment required. This lead to the development of hybrid CWs. Hybrid CWs consist of two or more classes of wetlands connected together, in various configurations of series or parallel units, to better utilize the treatment capabilities of the individual systems. For example, nitrogen removal efficiency is poor in single-stage HSSF systems, but HSSF and vertical flow (VF) hybrid CWs improve the overall efficiency of nitrogen removal (Vymazal, 2005).

2.1.4. Wetland vegetation

There have been a number of debates over the importance of CW's being planted versus unplanted, but the majority of studies have concluded that wetland vegetation play a vital part in wastewater remediation in these systems (Brix, 1994a, Brisson and Chazarenc, 2008, Brix, 1997, Stottmeister et al., 2003, Tanner, 2001).

Types of wetland vegetation

CWs may be planted with one or more types of macrophyte. The term macrophyte broadly describes macroscopic, aquatic species which may be emergent, submerged or free-floating. The distinguishing feature of the macrophytes is their ability to survive in water-saturated soils or in aquatic environments. In addition, they also show fast growth, quick establishment, high rates of biomass generation and have well-developed root and support systems (Brix, 1994a, Brisson and Chazarenc, 2008). Table 2-1 summarizes the macrophytes most commonly used or studied in treatment wetland systems. Brisson and Chazarenc (2008) reviewed 35 different experiments involving a variety of wetland species. *Phragmites australis* and *Typha latifolia* appear in the most studies; followed by *Typha angustifolia* and *Schoenoplectus validus*.

Table 2-1: Common species of macrophyte (Brisson and Chazarenc, 2008)

Species	**Sub-species**
Baumea	*articulata*
Bolboschoenus	*fluviatilis*
Canna	*indica*
Carex	*lacustris, rostrata*
Commelina	*communis*
Cyperus	*corymbosus, dubius, grandis, immensus, involucratus, papyrus*
Digitaria	*bicornis*
Echinochloa	*pyramidalis, cordifolius*
Eriocaulon	*sexangulare*
Glyceria	*maxima*
Iris	*pseudacorus*
Juncus	*effusus*
Kyllinga	*erectus*

Leptochloa	*fusca*
Ludwigia	*octovalvis*
Pennisetum	*purpureum*
Phalaris	*arundinacea*
Phragmites	*sp., australis, mauritianus, vallatoria*
Sagittaria	*latifolia*
Schoenoplectus	*sp., acutus (Syn. Scirpus acutus), mucronatus (Syn. Scirpus mucronatus), pungens (Syn. Scirpus pungens), validus (Syn. Scirpus validus)*
Scirpus	*sp., atrovirens, cyperinus, globulosus, grossus*
Spartina	*patens*
Stenotaphrum	*secundatum*
Typha	*sp., angustifolia, capensis, domingensis, latifolia, orientalis, subulata*
Urochloa	*mutica*
Vetiveria	*zizanoides*
Zizania	*latifolia*
Zizaniopsis	*bonariensis*

Role of vegetation in contaminant removal

Wetland plants have important physical and metabolic functions in CWs (Brix, 1994a), which will be discussed in this section. The physical functions are the following:

- Wetland surface stabilization, particle filtration and light attenuation

  Primarily, wetland vegetation prevents erosion of the surface layers of soil (Brix, 1994a); although this function is somewhat less important in gravel-based HSSF CWs which are bounded by impermeable walls. The dense root region created by macrophyte species aids in trapping suspended solids travelling through the wetland. The aerial vegetation reduces the intensity of ultra-violet light reaching the surface of the wetland; thereby preventing excessive algal growth (Brix, 1994a).
- Preventing clogging in vertical flow systems
- Insulating the wetland

  Decaying plant matter forms a litter layer on the wetland surface which shelters the soil from frost during winter and keeps it cool and moist during summer (Brix, 1994a).
- Provision of oxygen in the root zone (rhizosphere)

  The water saturated state of a CW lends itself towards being anaerobic and supporting anaerobic mechanisms of pollutant removal. However, macrophytes have efficient mechanisms of internal oxygen transport from their aerial organs to their submerged roots; thereby providing an oxygen-rich zone which is essential for aerobic degradation processes and nitrification in the rhizosphere (Brix, 1994a). Most of the oxygen is released from the apical region (region of new growth) behind the root apex, or tip (Armstrong, 1979). Some oxygen may leak into the rhizosphere from young fine laterals protruding from the root base, but no oxygen is released from established roots or rhizomes (Armstrong and

Armstrong, 1988). The vegetation provides in excess of 90% of the oxygen available in the root zone via their various internal transport mechanisms (Reddy et al., 1989).

- A habitat for wildlife
- Aesthetic appeal

  Flowering wetland plants, such as the *Iris pseudacorus* (Yellow Flag), *Canna indica* (Canna lily or Indian shot) (Brix, 1994a) or *Zantedeschia aethiopica* (Arum lily) (Bonner et al., 2017b) can be chosen to increase the visual appeal of a CW.

The metabolic functions include:

- Providing a large surface area (specifically in the root zone) for microbial (biofilm) attachment and growth
- Plant uptake of nutrients from the wastewater

Due to their characteristic high productivity, wetland plants absorb and store larger amounts of nutrients in their biomass. However, this amount is typically small in comparison to the influent contaminant loading from the wastewater (Brix, 1994a, Haberl et al., 2003).

Macrophyte species selection

A number of factors must be considered and off-set against one another when choosing the most suitable vegetation for a planted CW, such as root depth, wastewater loading tolerance and plant health and productivity. Wetland design, the type of wastewater and contaminants, climate and the time available for wetland establishment also play a role (Brisson and Chazarenc, 2008). For example, *Phragmites australis* take up to three years to reach full maturity (Vymazal and Krőpfelová, 2005). Moreover, if aerobic degradation processes and, thus, oxygenation of the rhizosphere are important for the type of wastewater being treated, then plants supporting high convective through-flow of gases should be chosen (Brix, 1994a). *Phragmites australis* are a good example of macrophyte which transport gases via convective through-flow (Armstrong and Armstrong, 1991).

Brisson and Chazarenc (2008) reviewed 35 studies regarding the influence of macrophyte species on pollutant removal efficiency in various types of CW. The focus was largely on microcosm studies comparing at least two species of macrophyte cultivated under identical experimental conditions and measuring the influent and effluent concentrations as an indication of pollutant removal efficiency. Microcosm experiments are not truly representative of real systems and replication was minimal (and often carried out in the same unit rather than across identical units), so the results should be treated with caution (Fraser and Keddy, 1997). Nevertheless, they do give an indication of the relative performance between common wetland species within the constraints

of reasonable cost and time. Validation of the microcosm findings in a pilot-scale or full-scale wetland system is still required (Brisson and Chazarenc, 2008).

The pollutants under consideration in the studies reviewed by Brisson and Chazarenc (2008) were total suspended solids (TSS), organic matter in terms of chemical or biological oxygen demand (COD or BOD), total Khejdahl nitrogen (TKN), total nitrogen (TN), nitrate (NO_3^-), total phosphorus (TP), phosphate (PO_4^{3-}) and ammonium (NH_4^+). Overall, they found that removal efficiency for a number of contaminants was different from species to species, but no generalizations (based on definite correlations across the board) could be formulated.

Differences in nitrogen (and particularly NO_3^-) removal efficiencies between species were most commonly observed; most likely because nitrogen is known to be assimilated in the biomass or transformed by aerobic microbial activity in the root zone. This is evidence of the advantage of combining more than one species of macrophyte in CWs to utilize the differences in removal efficiencies under different conditions. No trends were apparent for suspended solids, organic matter and phosphorus removal (Brisson and Chazarenc, 2008). The studies involving HSSF mesocosms planted with *Phragmites australis* are summarized in Table 2-2. In general, no difference in removal efficiency was seen between *Phragmites australis* and *Typha latifolia* or *Typha angustifolia*, with the exception of experiment 2 where *Typha latifolia* showed a higher removal efficiency for nitrogen and phosphorus.

Table 2-2: Investigation of the removal efficiencies of various pollutants between Phragmites australis and a sub-species of Typha in a horizontal subsurface flow mesocosms (Brisson and Chazarenc, 2008)

Experiment number	**Macrophyte species**	**Removal efficiency observations**
2	*Phragmites australis* *Typha latifolia*	• BOD, COD: no difference • Typha lat. Showed higher removal of TKN, TP, NH_4^+, PO_4^{3-}
26	*Phragmites australis* *Typha angustifolia*	• COD, TSS, TKN, TP: no difference
27	*Phragmites australis* *Typha angustifolia*	• BOD, COD, TSS, TKN, TP, PO_4^{3-}: no difference
28	*Phragmites australis* *Typha angustifolia*	• COD, TSS, TSS: no difference

The majority of studies reviewed by Brisson and Chazarenc (2008) showed that there were differences in removal efficiencies between many species; even though these were experimental condition specific and the results should be treated with caution. Nonetheless, the review is evidence that macrophyte selection is an important consideration in CW design. It is not yet possible to make a set of general guidelines for macrophyte species selection as more research is required into the different mechanisms of contaminant removal between

the common types of wetland plants and better factors correlating measureable plant features to treatment efficiency must be found.

Importance of root exudates

As part of their metabolic activities (Marschner, 1995), plant roots secrete a mixture of compounds (Flores et al., 1999), collectively referred to as root exudates. These exudates are thought to play a vital role in the maintenance of rhizospheric microbial communities, which are, in turn, essential for some of the remediative processes occurring in CWs.

Specialized transporter protein molecules are responsible for the active transport of exudate material across the root plasma membrane (Baetz and Martinoia, 2014). Plants can alter the chemical composition of the exudate material in response to various internal and external stimuli and it is the make-up of the exudates that largely defines the surrounding soil environment and microbial community structure (Baetz and Martinoia, 2014). There are few studies devoted to a detailed characterization of the exudate composition according to plant species, but they can be grouped broadly into two categories. The first is the low molecular weight class, examples of which include amino acids, organic acids, simple sugars and phenolic compounds. The second category is the high molecular weight species, such as long chain polysaccharides and proteins (Walker et al., 2003). The expressed proteins often act as transporter molecules for other root exudate constituents (Baetz and Martinoia, 2014).

Plant root exudates have a number of important functions; namely regulation of the microbial community in the surrounding soil, alteration of the soil's physical and chemical characteristics, plant defence, support of symbiotic relationships in the rhizosphere and prevention of invasion by competing plant species (Nardi et al., 2000). Root exudates are also the medium of transport of photosynthetically fixed carbon from the plant to the rhizosphere (Marschner, 1995) and it is believed that they serve as chemical messengers between plant roots, the rhizosphere and soil micro-organisms (Walker et al., 2003). As an example, parasitic plants secrete root exudates to stimulate the growth of invasive organs which can suffocate or drain nutrients from other plant species (Keyes et al., 2000).

The role of root exudates in plant defence is a vital but complex one (Baetz and Martinoia, 2014). Root secretions may contain antimicrobial compounds for the protection of the plant against herbivorous species, fungi and pathogens (Nardi et al., 2000). Many of the compounds initially associated with defence were low molecular weight species and enzymes, but it has been subsequently discovered that high molecular weight proteins and extracellular DNA also play a role by binding, trapping and aggregating pathogenic bacteria (Wen et al., 2007a, Wen et al., 2007b, Wen et al., 2009). Exudates can also contain a mix of regulatory compounds.

Regulators are required, in one instance, for tightly controlling the release of photosynthetically synthesized carbon from the plant which, if excessive, is a large carbon drain for the plant (Baetz and Martinoia, 2014).

2.1.5. Advantages of constructed wetlands

Provided that an adequate area of land is available at an affordable price, CWs are reliable, cost-effective, energy-efficient and low-maintenance systems that pose minimal risk of public exposure to contaminants within the system (Reed, 1993). They can also provide various additional benefits; namely carbon sequestration, air quality regulation, evapotranspiration, temperature regulation, a habitat for biodiversity and nutrient cycling (Dama-Fakir et al., 2015).

2.2. Wastewater quality

There are various physicochemical parameters which provide information about water quality. For example:

- A positive redox potential indicates an oxidizing solution. Many pollutants require strong oxidants to facilitate their decomposition (Bellingham, 2012) yet some of the oxidative processes (processes requiring oxygen) generate sulphur dioxide, nitrate and nitrite. These reduced species produce a drop in redox potential which could impede further oxidative decomposition.
- NH_4^+ is a by-product of the decomposition of urea. High levels of NH_4^+ can produce an environment which is toxic to aquatic organisms.
- Organic carbon is also an important water quality indicator, for which maximum allowable limits are commonly published in environmental legislation; particularly for the chemical oxygen demand (COD) and biological oxygen demand (BOD).

2.3. Remediation of wastewater using constructed wetlands

2.3.1. Contaminant removal mechanisms in constructed wetlands

Contaminants are removed from CWs via physical, chemical and biological routes (Brix, 1994b). Physical removal relies upon sedimentation and entrapment of solids within the wetland bed. Chemical removal involves reactions which convert harmful contaminants into less dangerous compounds. Some of these reactions rely upon reducing conditions associated with the saturated wetland soils (Haberl et al., 2003) but many are driven by biological processes in the root region of the wetland vegetation (Headley and Kadlec, 2007). Table 2-3 summarizes the primary contaminants and their mechanisms of removal from CW systems.

Table 2-3: The primary contaminants and their mechanisms of removal from CW systems (Vymazal, 2005, Brisson and Chazarenc, 2008)

Contaminant	Mechanism of Removal
Organic Matter	Aerobic and anaerobic degradation by bacteria attached to plant roots, rhizomes and media surfaces
Suspended solids	Filtration and sedimentation
Nitrogen (ammonia/nitrate)	Nitrification / denitrification and adsorption (if soil grain is sufficiently fine)
Phosphorus (phosphate)	Ligand exchange reactions in the presence of iron, aluminium or calcium hydrous oxides

2.3.2. Removal of organic carbon

The potential for degradation of organic compounds is measured by COD and BOD. COD is a measure of the oxygen required to oxidise organic matter by any means. BOD measures the amount of dissolved oxygen required by micro-organisms to metabolize organic compounds. Therefore, COD is representative of all organic matter present, while BOD is an indicator of the organic matter which can only be biologically decomposed. BOD and COD are widely utilised sum parameters for the removal of organic matter, but studies into the removal of specific types of organic compounds have also been conducted. Examples include hydrocarbons (petrochemical compounds), oil and grease, mineral oil, chlorinated volatile organic compounds, aromatic compounds, cyanide, glycols, atrazine (a herbicide), trinitrotoluene (TNT), RDX or cyclonite (an explosive) and general organics found in dairy farm, pig farm, slaughterhouse and olive mill wastewater plus landfill leachate. In these studies, emphasis has been placed on the selection of the particular plant species best suited to the removal of the specific organic compound (Haberl et al., 2003). CWs produce BOD_5 due to the degradation of dead plant matter. As a result, there may be a residual BOD_5 within the system and complete removal will seldom be achieved (Reed, 1993).

Although the primary mechanisms of organic matter removal are biological, for example fermentation, aerobic respiration, anaerobic respiration and bio-augmentation (Table 2-3), other degradative processes such as volatilization, oxidation (photochemical), sorption by plants and sedimentation can also be effective. Research into the mechanistic details of the removal pathways for organic compounds is still ongoing. The removal efficiency for organic compounds in CWs is high, but will vary depending on the type of organic compound and the plant species selected. As such, the genetic modification of plants in such a way as to enhance the uptake of a specific organic compound could be one way to improve CW removal efficiency. With these factors in mind, and careful consideration of the environmental conditions, CWs can be designed for maximum removal efficiency of organic matter (Haberl et al., 2003).

2.3.3. Removal of nitrogen

The primary mechanisms of nitrogen removal are microbial processes (Adler et al., 1996). Higher nitrogen removal efficiencies are achieved in planted, gravel-based systems (Yang et al., 2001, Brix, 1994a) with adequate oxygen, minimal algal growth and sufficient hydraulic residence time (Reed, 1993). Nitrogen is involved in many processes and reactions within a constructed wetland, yet often it is only transformed from one nitrogenous species to another. The processes that ultimately remove nitrogen from wetland waste water are volatilization, denitrification, anaerobic ammonia oxidation (ANAMMOX), adsorption, plant uptake coupled with biomass harvesting and burial (Vymazal, 2007).

Ammonia volatilization

Volatilization is the loss of ammonia (NH_3) gas from the wetland surface to the atmosphere. This is an equilibrium reaction represented by Eq. 2-1:

$$NH_3(g) + H_2O(aq) \rightleftharpoons NH_4^+(aq) + OH^-(aq) \quad [2_1]$$

A pH above 7.0 shifts the equilibrium towards the left, while a pH below 7.0 shifts the equilibrium towards the right. Hence, losses of NH_3 by volatilization are greater at higher pH; particularly above 9.3 (Reddy and Patrick, 1984).

Nitrification

Nitrification is the aerobic transformation of NH_4^+ into NO_3^- by nitrifying bacteria and is influenced by temperature, pH, inorganic carbon (IC) availability, the microbial population, the concentration of NH_4^+ ions, the dissolved oxygen (DO) concentration and the bicarbonate (HCO_3^-) concentration. Nitrification is a two-step process, represented by the overall Eq. 2-4:

$$NH_4^+ + 1.5O_2 \rightarrow NO_2^- + 2H^+ + H_2O \quad [2_2]$$

$$NO_2^- + 0.5O_2 \rightarrow NO_3^- \quad [2_3]$$

$$NH_4^+ + 2O_2 \rightarrow NO_3^- + 2H^+ + H_2O \quad [2_4]$$

In Eq. 2-2, a nitrite (NO_2^-) intermediate is formed by the action of ammonia oxidising bacteria. These bacteria draw their energy from inorganic carbon, carbon dioxide (CO_2) or carbonate (CO_3^{2-}) (Hauck, 1984, Paul and Clark, 1996). NO_2^- is then transformed into NO_3^- by nitrite oxidizing bacteria (Eq. 2-3), which may also derive energy from organic compounds in addition to NO_2^- (Paul and Clark, 1996, Schmidt et al., 2001, Schmidt et al., 2003). In low oxygen environments, only partial nitrification takes place. Eq. 2-2 proceeds in the same way, but a lack of oxygen means that NO_2^- is transformed into nitrous oxide (N_2O) or nitrogen gas (N_2) rather than into NO_3^- (Bernet et al., 2001).

Denitrification

Denitrification is the anaerobic transformation of NO_3^- to N_2. Under anaerobic or anoxic conditions, nitrogen acts as an electron acceptor (Reddy and Patrick, 1984), but the rate of denitrification is fastest under anoxic conditions. The process, shown in Eq. 2-5, is induced by denitrifying bacteria which use organic carbon, such as formaldehyde (CH_2O), as a source of energy (Hauck, 1984, Jetten et al., 1997, Paul and Clark, 1996). Denitrification is influenced by the DO concentration, redox potential, temperature, pH, soil characteristics, presence of organic matter, the concentration of NO_3^- and the presence of free water on the wetland surface (Vymazal, 2005, Focht and Verstraete, 1977).

$$6(CH_2O) + 4NO_3^- \rightarrow 6CO_2 + 2N_2 + 6H_2O \quad [2_5]$$

Denitrification may also proceed in the presence of oxygen; in which case organic carbon is oxidized (oxygen acts as an electron acceptor) and CO_2 and water (H_2O) are produced as by-products (Reddy and Patrick, 1984).

Anaerobic ammonium oxidation (ANAMMOX)

ANAMMOX is the anaerobic transformation of NH_4^+ and either NO_3^- or NO_2^- to nitrogen. The ANAMMOX process can be described by Eq. 2-6 and 2-7 (Mulder et al., 1995, van de Graaf et al., 1995). Although both NO_3^- and NO_2^- can act as electron acceptors in the ANAMMOX reaction, NO_2^- is the key electron acceptor (Strous et al., 1997).

$$5NH_4^+ + 3NO_3^- \rightarrow 4N_2 + 9H_2O + 2H^+ \quad [2_6]$$

$$NH_4^+ + NO_2^- \rightarrow N_2 + 2H_2O \quad [2_7]$$

Dissimilatory nitrate reduction (DNRA)

DNRA, also known as nitrate ammonification, is the reduction of NO_3^- to NH_4^+ by nitrate-reducing or nitrate-ammonifying bacteria. The process is influenced by the C:NO_3^- ratio, the DO concentration and temperature (Vymazal, 2007). DNRA is described by three reactions, which are given below, with Eq. 2-8 being a form of bacterial cellular respiration (Megonigal et al., 2004).

$$NO_3^- + H_2 \rightarrow NO_2^- + H_2O + ATP \quad [2_8]$$

$$NO_2^- + 3H_2 + 2H^+ \rightarrow NH_4^+ + 2H_2O \quad [2_9]$$

$$NO_3^- + 4H_2 + 2H^+ \rightarrow NH_4^+ + 3H_2O \quad [2_10]$$

The NH_4^+ produced may be taken up by the wetland plants (high levels of uptake, however, can lead to eutrophication), assimilated by micro-organisms or adsorb to various negatively charged surfaces (Vymazal, 2007).

Assimilatory nitrate reduction

Macrophytes, algae and heterotrophic bacteria take up inorganic nitrogen and convert it into organic nitrogen containing compounds, such as amino acids. By this process, they assimilate nitrogen. Soluble forms of nitrogen, such as NO_3^- to NH_4^+, are the preferred nitrogen containing species for this process (Vymazal, 2007).

Ammonification

Ammonification describes the transformation of organic nitrogen into NH_3. Ammonification is biologically driven and influenced by temperature, pH, the C:N ratio, nutrient availability, the type of soil matrix and the presence of oxygen (Vymazal, 2007); with the rate of ammonification being fastest under aerobic conditions (Reddy and Patrick, 1984). Ammonification occurs via a number of intermediate steps, known as deamination steps, and may be either an oxidation or reduction process. Oxidative deamination is described by Eq. 2-11 (Savant and DeDatta, 1982) and reductive deamination by Eq. 2-12 (Rose, 1976).

$$\text{amino acids} \rightarrow \text{imino acids} \rightarrow \text{keto acids} \rightarrow NH_3(g) \quad [2_11]$$

$$\text{amino acids} \rightarrow \text{saturated acids} \rightarrow NH_3(g) \quad [2_12]$$

Nitrogen fixation

Fixation is an enzyme (nitrogenase) catalyzed reaction by which N_2 gas is converted to NH_3 (Stewart, 1973) under anaerobic, or reduced, conditions (Buresh et al., 1980). Macrophytes, heterotrophic bacteria and cyanobacteria are all capable of N_2 fixation (Johnston, 1991).

Adsorption

NH_4^+ ions can adsorb to negatively charged sites on detritus, sediments and soils. This is an equilibrium reaction which establishes a balance with NH_3 in the wetland water (see Eq. 2-1). The equilibrium can be shifted by a change in the concentration of NH_4^+ and O_2 in the water. For example, nitrification decreases the concentration of NH_4^+ ions in solution and would drive desorption of ammonia from the sediment (Kadlec and Knight, 1996).

Organic nitrogen burial

Detritus is composed partly of organic nitrogen. Nitrogen locked up in peat and decaying organic matter, such as leaves, becomes permanently unavailable in the nitrogen cycle, but is only removed from the bed if the wetland is cleared of this debris. Organic nitrogen removal has only been reported to contribute to nitrogen removal in natural wetlands rather than CWs (Vymazal, 2007).

2.3.4. Removal of phosphorus

Phosphorus is largely removed by chemical adsorption; particularly onto iron, aluminium and calcium hydrous oxides (Adler et al., 1996). The removal of phosphorus may be ineffective, largely due to limited contact time

between the flowing water and the soil (Reed, 1993), but higher removal efficiencies have been reported for mineral soil containing wetlands as compared to gravel based systems (Yang et al., 2001).

2.3.5. Removal of additional contaminants

The removal of faecal coliforms (FC) is normally insufficient (Reed, 1993). Although high FC removal efficiencies, in the region of 90%, may be achieved (Neralla et al., 2000), this is largely dependent on favourable climatic conditions and levels of FC reduction that can be achieved in wetland systems often do not comply with regional discharge standards (Smith et al., 2005), (Kassim, 2007). In addition, removal of pathogenic microorganisms and viruses are seldom killed. Therefore, additional disinfection of the effluent may be required, such as chlorination (Neralla et al., 2000).

2.4. Constructed wetland hydraulics

CW hydraulics broadly describes flow behaviour within CW systems. The geometry, as well as various physical properties, can influence how water moves through a CW and both should be carefully selected during the design process in relation to site-specific loading and treatment requirements. Ultimately, CW performance and sustainability will be governed by how successfully designers can optimize and operators can control the hydrological regime and flow behaviour (Reed et al., 1995, Persson et al., 1999).

2.4.1 Chemical engineering reactor theory

Chemical engineering is the branch of engineering characterised by the commercialization of chemical reactions to turn raw materials into a desired product. Hence, the discipline of chemical engineering involves, predominantly, the design and operation of chemical reactors as well as the supporting processes to take the process from start (material feed) to end (separation and purification of desired product and adequate treatment of waste generated) (Levenspiel, 1999b).

The wide variety of industrial chemical reactions are carried out in various types of chemical reactor. The choice of reactor depends on:

i. the number and sequence of reactions (a single reaction, reactions in series, reactions in parallel, complex reactions)
ii. whether the reactions are to be carried out in a continuous or non-continuous process
iii. whether the reactions are exothermic or endothermic
iv. the effect of temperature on the selectivity and reaction kinetics (which governs the distribution of products)
v. whether a catalyst is required (Levenspiel, 1999b)

Table 2-4 summarizes the main classes of chemical reactors, their operational features and examples of where each may be used (Froment et al., 2011). Industrial reactors could also be designed as combinations of these types.

Table 2-4: Classes of chemical reactors (Froment et al., 2011)

Type of Reactor	**Operational Features**	**Areas of Application (select examples)**
Batch reactor	• Single vessel (may contain an agitator) • All reactants are fed into the reactor at once, after which the reaction is left to run to completion • Uniform composition and temperature throughout the reactor at any point in time • Composition changes with time as the reaction proceeds • Isothermal or non-isothermal	• Specialty chemicals • Polymers • Pharmaceuticals
Semi-batch reactor	All characteristics of a batch reactor but • Reactants are fed into or removed from the reactor intermittently	• Specialty chemicals • Polymers • Pharmaceuticals
Plug flow reactor (PFR)	• Tubular reactor • Fluid is assumed to move as a "plug" and with uniform velocity along the reactor • Fluid conditions (velocity, temperature, composition) are uniform at any cross section along the reactor at a point in time • Isothermal or non-isothermal • Adiabatic or non-adiabatic • Pressure drop can be large • May contain a solid packing material depending • Perfect plug flow (no intermixing between successive fluid elements) is an idealized case	• Gasoline production • Oil cracking (olefin production) • Ammonia synthesis
Mixed flow reactor or continuous stirred tank reactor (CSTR)	• Reactor is a well agitated vessel • Continuous flow process • Assume concentration and temperature are uniform throughout the reactor (therefore the effluent has the physical and chemical properties as the contents of the reactor) • Opposite extreme to plug flow (perfect mixing is an idealized case)	• Biazzi process (temperature control is critical) • Polymerization of butadiene & styrene (reaction requires constant composition) • Two-phase reactions • Ziegler catalytic reactions & Hercules Distillers process (catalyst must be kept in suspension)
Fixed bed catalytic reactor	• Tubular reactors packed with solid catalyst particles, over which the reactant-containing fluid stream flows	• Steam reforming • Water-gas shift reaction • Carbon monoxide methanation

	• Catalyst bed is fixed (catalyst particles are bound to a surface) • Isothermal or non-isothermal • Adiabatic or non-adiabatic • Pressure drop can be large • Reactor must be shut-down to regenerate catalyst	• Ammonia, methanol & sulfuric acid synthesis • Petroleum refining
Fluidized bed reactor	• A portion of solid catalyst particles move against the flow of reactant-containing fluid • Suitable for highly exothermic reactions (require close temperature control) • Opportunity to recycle and regenerate catalyst in a continuous process	• Catalytic cracking of gas oil (gasoline production) • Oxidation of naphthalene • Oxychlorination of ethylene • Union Carbide process
Transport or riser reactor	• Fluidized bed reactor in which all catalyst particles are entrained in the reaction fluid stream	• Fischer-Tropsch process
Biological reactor	• Reactor in which reactions are brought about by the action (metabolism) of micro-organisms	• Brewing

A HSSF CW closely resembles a horizontal flow packed bed reactor. The CW is packed with a solid medium and bounded by an impermeable barrier. The packing material creates the many channels through which wastewater can flow, acts as support for the root systems of the wetland vegetation and provides the surface on which various micro-organisms can attach (as a biofilm). These micro-organisms play an important role in the degradation of organic contaminants (Alcocer et al., 2012).

2.4.2. Types of fluid flow

Fluid flow through any enclosed space can be described as one of two types; namely laminar or turbulent. Laminar flow occurs when fluid velocities are low. In this flow regime, flow patterns are smooth and Newton's law of viscosity applies. Flow can be visualized as parallel layers sliding alongside one another, without any mixing between the layers. In contrast, turbulent flow is the result of high fluid viscosities which result in the formation of eddies, or swirls, and unstable flow patterns. Turbulent flow can be visualized as streams of fluid moving in multiple directions and at many angles to the primary direction of movement. There is a distinct velocity, known as the critical velocity, at which flow transitions from laminar to turbulent (Geankoplis, 1993).

The flow regime within a system is dependent on a number of factors; namely fluid velocity, fluid density, fluid viscosity and channel diameter. The existence of laminar or turbulent flow conditions can be determined using the dimensionless Reynolds Number, Re (Geankoplis, 1993). The Reynold's Number for a packed bed reactor is given by Eq. 2-13 (Subramanian, 2004). The Reynold's Number should be less than 10 for laminar flow (Miller and Clesceri, 2002).

$$Re = \frac{D_p U_s \rho}{(1-\varepsilon)\mu} \quad [2_13]$$

where D_p is the equivalent spherical diameter of the packing material (m), U_s is the superficial fluid velocity ($m \cdot s^{-1}$), ρ is the density of the fluid ($kg \cdot m^{-3}$), ε is the fractional voidage of the packing material and μ is the fluid viscosity ($Pa \cdot s$).

The equivalent spherical diameter is estimated using Eq. 2-15 and the superficial velocity is calculated according to Eq. 2-16 (Mayo, 2014).

$$D_p = 6 \, x \frac{\text{volume of particle}}{\text{surface area of particle}} \quad [2_14]$$

$$U_s = \frac{Q}{hB} \quad [2_15]$$

where Q is the volumetric flow rate ($m^3 \cdot s^{-1}$), h is the water depth (m) and B is the breadth, or width, of the reactor (m).

Nominal Residence Time

The extent of pollutant degradation is closely related to the amount of time that these contaminants spend travelling through the CW. This is referred to as the residence time. It is desired that the flow regime be as close to ideal plug-flow as possible, as this condition would maximize the residence time of the fluid travelling through the system and result in maximum contaminant decomposition (Rengers et al., 2016). Under ideal plug-flow conditions, all material should experience the same time of detention within the system (Wahl et al., 2010). The time required for a single exchange of the entire wetland volume, referred to as the nominal residence time, τ, is defined by Eq. 2-16 (Fogler, 2006).

$$\tau = \frac{V}{Q} \quad [2_16]$$

where V is the total volume of fluid within the system and Q is the steady-state volumetric flow rate.

For gravel bed CW systems, the volume of fluid would be expressed by Eq. 2-17 (Alcocer et al., 2012).

$$V = hBL\varepsilon \quad [2_17]$$

where h is the water depth, B is the width of the wetland (perpendicular to the direction of flow), L is the length of the wetland from inlet to outlet and ε is the fractional voidage of the gravel medium.

2.4.3. Hydraulic tracer tests

Flow through a wetland system can be visualized as being composed of the sum of the movement of many consecutive elements of fluid. Due to the physical characteristics of the wetland system, some elements of water will travel through the wetland faster, or less impeded, than others; giving rise to a distribution of travel times from inlet to outlet (Headley and Kadlec, 2007).

In order to generate a picture of the distribution of residence times and describe the flow of water through a CW, a tracer test is performed. It is assumed that the tracer follows the same pathway as the portion of water with which it travels and, thus, provides a reasonable indication of the residence time distribution (RTD). In any type of tracer test, an inert tracer is injected into the inlet stream and tracked to the outlet. Samples are taken from the outlet stream at pre-defined time intervals, which are based on the average residence time of water in the wetland. The sampling frequency should be the greatest when the tracer concentrations are changing most rapidly (this is usually between 50 and 90 percent of the estimated residence time). The outlet volumetric flow rate should also be recorded with each sample. The concentration of the tracer is in each sample is determined by means of a suitable analytical technique. The time varying concentration data is the used to plot the residence time distribution function (Headley and Kadlec, 2007).

There are three types of tracer test; namely frequency tests, an impulse-response and the step-change tracer study. Frequency tests are not used and are thus excluded from this study. In an impulse-response type experiment, a single pulse of tracer of know mass is injected into the inlet stream at time t_0 to initiate the test. For the step-change test, the inflow is changed from feed water to a solution of known concentration of tracer at t_0. The input and output signals from the two types of tracer test are illustrated in Figure 2-4.

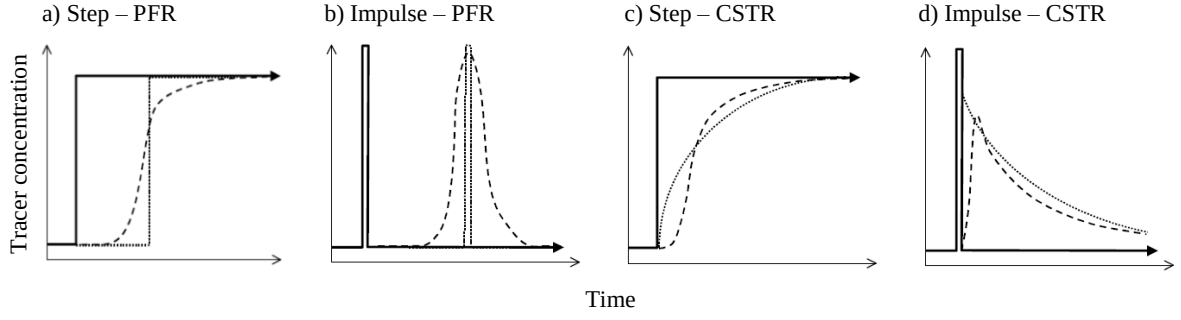


Figure 2-4: The impulse and step change output concentration curves for ideal (dotted lines) and non-ideal (dashed lines) reactors in response to an impulse or step increase in input concentration (bold lines with arrow heads). (a) and (b) depict plug flow and (c) and (d) represent complete mixing (Headley and Kadlec, 2007).

2.4.4. The residence time distribution for steady-flow systems

The RTD function, E(t), is the primary descriptor of wetland hydraulic behaviour. It is a plot of the spread of residence times for all elements of fluid flowing through the system (Persson et al., 1999) and is generated by means of either an impulse-response or a step change tracer experiment. The impulse-response tracer test is the more widely used and the mathematical equations relating to this type of flow test only are described in the sections to follow.

Consider a hypothetical impulse-response tracer test in which a known mass of inert tracer, m_i, is injected at the wetland inlet at time t_0 and the tracer concentration, C(t), is measured as a function of time, t, at the system outlet. The concentration breakthrough curve (BTC) can be obtained by plotting tracer concentration against time, as illustrated in Figure 2-5.

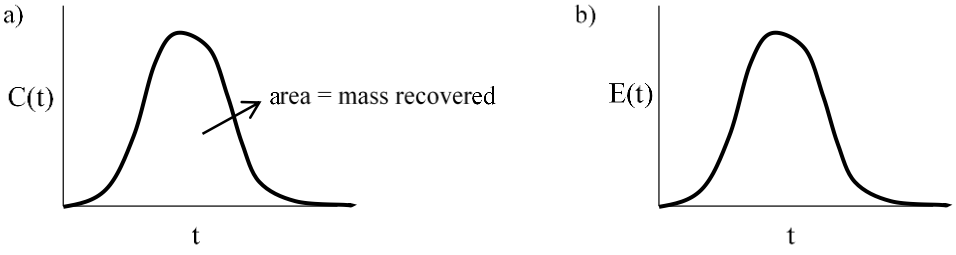


Figure 2-5: (a) Hypothetical concentration breakthrough curve for an idealized impulse-response tracer test and (b) the corresponding residence time distribution function.

The RTD function is defined by Eq. 2-18 (Fogler, 2006).

$$E(t) = \frac{C(t)}{\int_0^\infty C(t)\,dt} \qquad [2_18]$$

Furthermore, the fractional recovery of tracer material is calculated according to Eq. 2-19 (Fogler, 2006).

$$N = \frac{Q\int_0^\infty C(t)\,dt}{m_i} \qquad [2_19]$$

where N is the fractional recovery of tracer, Q is the steady flow rate over the duration of the tracer test (or the best approximation thereof), $\int_0^\infty C(t)\,dt$ represents the total mass of tracer recovered at the wetland outlet and m_i is the total mass of tracer injected at the start of the flow test.

One important assumption of RTD theory is that steady-state flow is maintained in the systems under investigation. When flow is variable, the fluid entering the wetland will not have the same residence time as that exiting and, as such, the same pulse of tracer will produce different concentration profiles depending on

whether the flowrate increases or decreases over time. This presents a number of challenges for the hydraulic calculations and subsequent analysis (Naumann, 1969).

2.4.5. Normalization of flow data

Normalization refers to the mathematical technique of converting physical data, such as time and concentration, into dimensionless quantities. When experimental conditions, such as flow rate, system volume and mass of tracer injected, are dissimilar, direct comparisons between different RTDs cannot be made unless the data has been normalized. The same applies to comparisons of RTDs from diverse CW systems (Bonner et al., 2017b, Wahl et al., 2010, Lange et al., 2011). However, flow must be in the laminar region (and, therefore, reversible) to make normalization of the RTD function possible. The normalized RTD function is given by Eq. 2-20 and Eq. 2-21 (Rengers et al., 2016):

$$\theta = \frac{t}{\tau} \qquad [2_20]$$

$$E(\theta) = \tau \frac{Q\, C(\theta)}{m_i} \qquad [2_21]$$

where θ is dimensionless time and τ is the nominal residence time.

2.4.6. The residence time distribution for variable flow systems

To account for non-steady flow conditions, Werner and Kadlec (1996) defined a dimensionless flow weighted time, Φ, and corresponding outflow concentration, C'(Φ), as given in Eq. 2-22 and Eq. 2-23, respectively. Φ is an expression of time in terms of total volume exchanges. $\phi = 1$ is the nominal residence time and is comparable to τ (Eq. 2-16). The area beneath the C'(Φ) vs Φ curve should be unity (representing 100% of the tracer mass).

$$\phi = \int_{t_0}^{t} \frac{Q(t')}{V(t')} dt' \qquad [2_22]$$

$$C'(\phi) = \frac{C(\phi)V(\phi)}{m_i} \qquad [2_23]$$

where Q(t') is the variable flowrate, V(t') is the variable system fluid volume, t' is a "dummy" variable of integration, t_0 is the time of tracer injection, V(Φ) is the system volume at a given flow weighted time and M is the mass of tracer injected.

2.4.7. Moments of the RTD

The moments of the RTD are used to evaluate hydraulic performance. In order to calculate the moments, a selection of mathematical equations are applied, all of which reduce the RTD function to a single value. This makes comparisons between different RTDs more convenient (Rengers et al., 2016). Eq. 2-24 to 2-27 outline the four important moments that have been defined (Fogler, 2006):

$$\text{0th moment: } M_0 = \frac{Q \int_0^\infty C(t)\, dt}{m_i} = N \qquad [2_24]$$

$$\text{1st moment: } M_1 = \int_0^\infty t\, E(t)\, dt = \bar{t}_m \qquad [2_25]$$

$$\text{2nd moment: } M_2 = \int_0^\infty (t - \bar{t}_m)^2\, E(t)\, dt = \sigma^2 \qquad [2_26]$$

$$\text{3rd moment: } M_3 = \frac{1}{\theta^{3/2}} \int_0^\infty (t - \bar{t}_m)^3\, E(t)\, dt = s^3 \qquad [2_27]$$

The moments of the dimensionless RTD are given in Eq. 28-31 (Rengers et al., 2016):

$$\text{0th moment: } \widehat{M}_0 = \int_0^\infty E'(\theta)\, d\theta \qquad [2_28]$$

$$\text{1st moment: } \widehat{M}_1 = \int_0^\infty \theta\, E'(\theta)\, d\theta \qquad [2_29]$$

$$\text{2nd moment: } \widehat{M}_2 = \int_0^\infty (\theta - M_1)^2\, E'(\theta)\, d\theta \qquad [2_30]$$

$$\text{3rd moment: } \widehat{M}_3 = \frac{1}{\theta^{3/2}} \int_0^\infty (\theta - M_1)^3\, E'(\theta)\, d\theta \qquad [2_31]$$

The zeroth moment (M_0) gives the fractional recovery of tracer material. The first moment (M_1) is the mean residence time, $\bar{t}_m$ (Fogler, 2006). When 100% of the tracer material is recovered ($M_0 = 1$), the first moment represents the centroid of the RTD. The variance, or spread of data about the mean, is given by the second moment (M_2) (Rengers et al., 2016). A large variance indicates significant departure from ideal plug-flow (Persson et al., 1999). The third moment (M_3), termed the 'skewness', represents the degree by which the distribution is skewed to either side of the mean (Fogler, 2006).

The dimensionless moments of the C'(Φ) vs Φ curve are given by the same Eq. 28-31 with the appropriate substitutions of the concentration and time normalized variables (Wahl et al., 2010). $M'_0 = M'_1 = 1$ and $M'_2 = 0$ under ideal conditions. Any deviations from ideality are used to quantify the hydraulic efficiency.

2.4.8. Flow behaviour in constructed wetland systems

Flow non-ideality (departure from plug-flow) is the symptom of physical, flow, geometric and physiological parameters; examples of which could include fluid density, water flow rate, wetland length and evapotranspiration, respectively. The presence of a packing medium also has a significant impact on flow behaviour. In addition, CW hydrodynamics may display varying levels of complexity depending on the extent of occurrence of short-circuiting, zones of stagnation (dead zones), zones of re-circulation, dispersion and mixing effects; the presence of which are seen in the shape and spread of the RTD (Rengers et al., 2016, Thackston et al., 1987).

Short-circuiting

In CW systems, water flows preferentially along the paths of least resistance. When a pocket of fluid moves through the system at a velocity markedly greater than the average of the bulk flow and reaches the outlet in a time much shorter than τ, this pocket is said to have 'short-circuited' through the wetland. Short-circuiting is characterized by a significant amount of material reaching the outlet in a normalized travel time of less than 0.4 (Thackston et al., 1987).

Dispersion

Dispersion has been widely used to quantifying the degree of departure from ideal flow in detention systems (Persson et al., 1999). Dispersion is the result of both vertical and lateral variation in the average velocity at a particular location within the wetland. As depicted in Figure 2-6a, dispersion can be identified by a noticeable broadening of the base of the RTD curve and high degrees of dispersion are accompanied by a change in peak shape (Thackston et al., 1987). One way of quantifying dispersion is by determining the dispersion index, d, according to Eq. 2-32:

$$d = \frac{\sigma^2}{\bar{t}_m{}^2} \qquad [2_32]$$

Plug-flow conditions will produce a sharp peak and small standard deviation in the close vicinity of the nominal residence time (Persson et al., 1999), a representation of which can be seen in curve 1 of Figure 2-6a. A large value of *d* is synonymous with a wide distribution of residence times and an increased broadening of the RTD peak (Figure 2-6a). This means that a significant quantity of material exits the wetland well ahead of or well behind the mean residence time (Thackston et al., 1987). It should be noted that the mean residence time is not dependent on the degree of dispersion or vice versa. All of the curves in Figure 2-6a have the same $\bar{t}_m$ and λ

but each a different value of *d*. Further, the four RTDs in Figure 2-6b have identical values of *d* but different values of $\bar{t}_m$ and λ (Thackston et al., 1987).

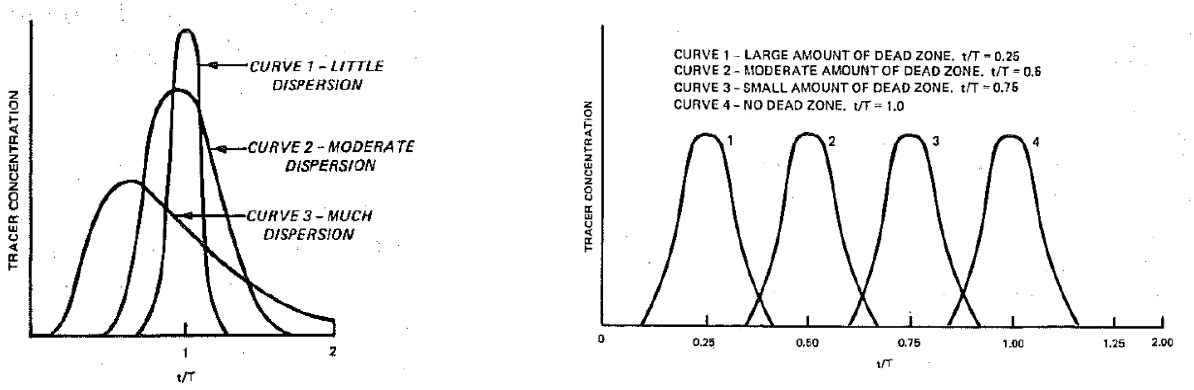


Figure 2-6: (a) Three hypothetical RTD's showing the effect of the degree of dispersion on peak shape, breadth and position and (b) Four hypothetical RTDs showing the influence of the amount of dead volume on the position of the RTD (Thackston et al., 1987).

As an alternative, Levenspiel (1972) used the dispersion number, D, given in Eq. 2-33. In this expression, D approaches zero under plug-flow conditions but approaches infinity as the extent of mixing nears completeness (Persson et al., 1999).

$$\left(\frac{\sigma}{\bar{t}_m}\right)^2 = 2D - 2D^2\left(1 - e^{1/D}\right) \qquad [2_33]$$

Dead (stagnant) zones

Dead zones often occur in shallow areas, corners and behind baffles or obstructions. The rate of exchange of water in and out of a stagnant zone is greatly reduced; velocities are significantly lower than in the main advective flow paths; eddy re-circulation is typical; mixing between stagnant water and the bulk flow is poor and fluid entering a dead zone will have a significantly longer residence time than the mean. As a consequence, the cumulative volume of the dead zones is considered essentially unavailable and the effective treatment volume, V_{eff}, becomes smaller than the actual wetland volume, V. The presence of dead zones tends to reduce the mean residence time of the body of water as a whole; resulting in a shift of the RTD towards lower normalized times, as is illustrated in Figure 2-6b (Thackston et al., 1987).

Mixing effects

The concentration-time profile of a completely mixed system is an exponentially decaying function, as shown by the dashed curve in Figure 2-7. In such reactors, the combined effect of a high degree of mixing and steady flow results in a continually diminishing tracer concentration detected at the system outlet (Persson et al., 1999).

In general, a system whose flow behaviour is predominantly advective produces a RTD with a sharp, narrow peak. Advective zones provide channels for unimpeded flow through the wetland, with minimal lateral dispersion. Therefore, the mean residence time can be significantly shorter than the nominal residence time. On the other hand, water which enters a dead zone during its passage through the system will be held-up within this area for an extended period and only emerge gradually. For this reason, the resultant RTD will have a straight, elongated tail. These two cases are illustrated by the solid and dotted hypothetical BTCs in Figure 2-7, both of which indicate sharp peaks for advective flow dominated systems. The larger the amount of dead space, the longer the tailing (Thackston et al., 1987).

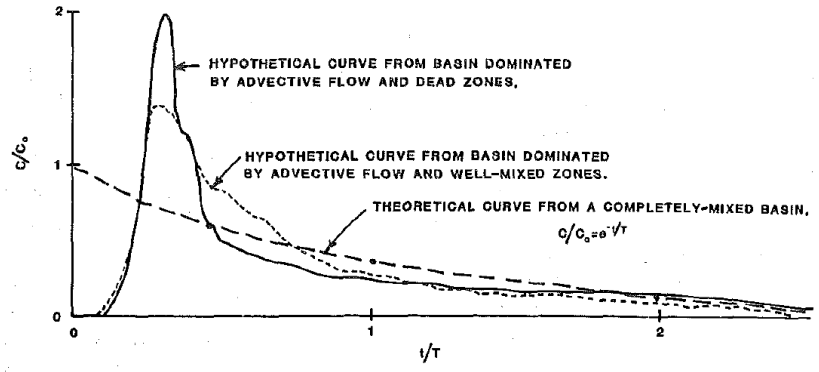


Figure 2-7: The typical exponentially decaying concentration time profile of a perfectly mixed reactor and hypothetical concentration time breakthrough curves for two systems displaying various distributions of advective and stagnant zones (Thackston et al., 1987).

Further, systems displaying less advective flow dominance but still a high degree of mixing will also produce long-tailed RTDs. The extent of tailing will be directly related to the degree of mixing; in other words the tail extends further as the system approaches a fully mixed state. In comparison to the hypothetical RTDs given in Figure 2-6, the peak will be flatter (display a lower maximum value) and broader and possibly multi-modal (Persson et al., 1999).

2.4.9. Hydraulic efficiency

Wetland systems utilizing a maximal amount of the available treatment volume and maintaining near plug-flow conditions are hydraulically efficient (Persson et al., 1999) and, in general, will yield a high degree of contaminant degradation or transformation. Thus, efficiency is a balance between the degree of pollutant removal, the wetland area or volume required to achieve this extent of removal and the corresponding treatment time. For this reason, the RTD is an important pre-requisite for the determination of treatment efficiency, and a variety of design factors including the mean residence time, the inlet and outlet valve position, the vegetation and the type, size and shape of the wetland will bear influence (Persson et al., 1999, Thackston et al., 1987). If

meaningful comparisons between wetland systems or across a selection of experimental conditions are to be made, then the calculation of hydraulic efficiency should be based on the normalized RTD function (Wahl et al., 2010).

In reality, the attainment of ideal plug-flow is not possible. Thus, the observed mean residence time, $\bar{t}_m$, will not be equal to the nominal residence time, τ. Thackston et al. (1987) maintained that $\bar{t}_m$ was the primary determinant of hydraulic efficiency and quantified it in terms of an effective volume utilization ratio, e, given in Eq. 2-34.

$$e = \frac{\bar{t}_m}{\tau} = \frac{V_{eff}}{V} \qquad [2_34]$$

Persson et al. (1999) explained the combined importance of both uniformity of flow and maximal use of effective volume for assessing hydraulic efficiency. Plug-flow conditions alone may not guarantee good wetland design because plug-flow could be the result of a high degree of short-circuiting. Similarly, approximately equal mean and nominal residence times do not always imply high efficiency as these times could be very similar even in the undesirable case that the peak of the RTD is broad and flat. Hence, in the development of their expression for hydraulic efficiency, λ, given in Eq. 2-35 below, the ratio assigned to effective volume utilization, e, by Thackston et al. (1987) and a term involving the equivalent number of tanks in series, n, (Fogler, 2006, Kadlec and Knight, 1996) were combined. Both terms are equally weighted (between 0 and 1) in the equation.

$$\lambda = e\left(1 - \frac{1}{n}\right) = \frac{t_p}{\tau} \qquad [2_35]$$

where t_p is the maximum concentration peak time recorded at the wetland outlet.

The number of tanks in series, n, is the parameter in the Tanks-In-Series (T-I-S) model, which was developed to account for non-ideal flow behaviour in reactor systems. This model has been widely applied to the modelling of HSSF CWs containing a gravel bed, as these systems are considered a category of packed bed reactor. Fogler (2006) defined the number of tanks by Eq. 2-36:

$$n = \frac{\tau^2}{\sigma^2} \qquad [2_36]$$

However, Eq. 2-36 relies upon the determination of the mean, variance and standard deviation of the RTD. If these descriptors are determined experimentally, the shape of the curve, the extent of the tailing and the often arbitrary selection of the end-point of the tracer test can have a large influence on the statistical results (Persson et al., 1999). For this reason, alternative expressions for the mean and standard deviation have been suggested and rely upon determination of the time at which specified mass recoveries are achieved or concentration

maxima are detected. Hence, the number of tanks in series may be also be calculated by Eq. 2-37 (Kadlec and Knight, 1996):

$$n = \frac{\tau}{\tau - t_p} \qquad [2_37]$$

2.4.10. Hydraulic indexes

In order to quantify the extent of flow non-ideality, simplify RTD analysis and allow for meaningful comparison between different systems, various hydraulic indexes have been defined (Teixeira and Siqueira, 2008). As has been discussed in the previous section, departure from plug-flow has an adverse impact upon wetland treatment efficiency and it is the shape of the RTD that alludes to the occurrence of non-ideal flow within the system. Yet, the RTD function itself is only a qualitative indication of flow behaviour.

The hydraulic indexes reduce the RTD to a single value by means of various mathematical operations. In this way, they provide a quantitative assessment of hydraulic performance by comparing the flow behaviour in a real wetland system to that which would be expected in the same system operating under ideal flow conditions (Teixeira and Siqueira, 2008). However, although these indexes give good insight into fluid flow behaviour, they have been found to be poorly correlated to effluent pollutant composition (Rengers et al., 2016).

There are two main categories of hydraulic indexes; namely short-circuit and mixing indexes. Various other indexes have been defined, but these do not fit into one particular class. Teixeira and Siqueira (2008) summarized seventeen hydraulic indexes already existing in the literature and assessed each according to its

1) Definition and adequate representation of identified physical phenomenon
2) Sensitivity to changes in that phenomenon
3) Statistical variability

Their motivation for such a study was the apparent lack of standards for the assessment of wetland hydraulic performance and that different indexes measuring the same phenomenon can yield different results. Their investigation considered RTDs for five flow regimes (from disperse plug-flow to completely mixed) and identified the hydraulic index most suited to evaluating the short-circuiting and mixing phenomena. Their findings are presented below.

Short-circuiting index

Short-circuiting is the result of the development of preferential flow paths and typically results in a mean residence time shorter than the nominal residence time (Teixeira and Siqueira, 2008). Visually, the RTD will be shifted below τ (Wahl et al., 2010). Teixeira and Siqueira (2008) assessed eight short-circuit indexes based on the assumption that they describe the advective movement of the tracer front. It was concluded that the t_{10} index is the best measure of short-circuiting because it is closely related to advective flow, it displays low

statistical variability and it is a good indicator of channelling through the system. The t_{10} index is defined as the amount of time taken for the first 10% of the injected mass of tracer mass to reach the system outlet. In addition, t_i (the time taken for the first concentration above baseline to be recorded at the outlet) is a valuable index because it indicates the degree of short-circuiting within the system without requiring measurement of the full RTD. Expressed in terms of dimensionless variables, the short-circuiting indexes can be expressed as Eq. 2-38 and Eq. 2-39 (Rengers et al., 2016).

$$\theta_i = \frac{t_i}{\tau} \qquad [2_38]$$

$$\theta_{10} = \frac{t_{10}}{\tau} \qquad [2_39]$$

Mixing index

Mixing is a manifestation of the random spreading of material owing to diffusion, recirculation and the presence of zones of stagnation. The result is an extended period of detention (or the mean residence time exceeding the nominal residence time) (Teixeira and Siqueira, 2008). Visually, mixing will result in a broadening of the RTD function (Wahl et al., 2010). The inlet and outlet configurations can bear large influence over the extent mixing; particularly for closed systems. Teixeira and Siqueira (2008) evaluated six mixing indexes with the assumption that this index best describes the arbitrary dispersal of the fluid. It was concluded that σ^2 (see Eq. 2-26), or the dimensionless second moment $\widehat{M}_2$(see Eq. 2-30), is the most suitable index for quantifying mixing effects, due to its close relation to the physical phenomenon and the fact that it is widely used in many kinetic models. However, σ^2 does have the disadvantage of high statistical variability when mixing effects are minimal. The $t_{90} - t_{10}$ index shows better statistical reproducibility for all degrees of mixing, but Teixeira and Siqueira still suggested that σ^2 be the index of choice due to its other advantages. In instances of a low degree of mixing, the Morril Index, MDI, in Eq. 2-40 is preferred (Teixeira and Siqueira, 2008, Rengers et al., 2016).

$$\mathrm{MDI} = \frac{t_{90}}{t_{10}} \qquad [2_40]$$

where t_{90} is the time taken for 90% of the injected mass of tracer to exit the system.

Moment index

Wahl et al. (2010) proposed a new index for hydraulic efficiency; termed the Moment Index. They identified the major limitation of the existing hydraulic indexes to be their susceptibility to being skewed by the tail effect. Tailing refers to the often encountered long extension of the end section of the RTD function which asymptotically approaches zero. In general, it is assumed that a flow test is complete and the tail of the RTD has returned close enough to the initial baseline (zero) concentration after a minimum of three mean detention

times (Levenspiel, 1999b). In this context, residence, or detention, time is defined as the flow rate and volume-dependent total travel time from system inlet to outlet. However, in many practical situations it may be impractical to continue experiments for this length of time. The Moment Index, thus, aims to resolve the uncertainty regarding measurement of the residence time as this can have a significant impact upon the RTD and, therefore, the computed hydraulic efficiency (Wahl et al., 2010).

The Moment Index is determined using the RTD and the hold back parameter (HBT). The HBT was defined by Stamou and Noutsopoulos (1994) as the pre-nominal area, which is the area under the RTD function for all φ up until the nominal divide (corresponding to a flow weighted time φ = 1). This new index is defined based on a single exchange of the reactor volume only, so the arbitrary truncation of flow data defining the end point of the flow test does not impact upon the result. In other words, the Moment Index is not subject to tail effects. In addition, it has no connection to either the short circuit or mixing indexes; it shows greater sensitivity than many other indexes; it can be correlated to the effluent pollutant composition for first order reactions and it accounts for vegetation density, wetland shape and wetland bathymetry (Wahl et al., 2010).

The Moment Index, MI, given in Eq. 2-41, is based on the following two assumptions:

i. If the residence time is equal to or longer than τ, the system is operating at 100% efficiency.
ii. The fraction of material reaching the outlet prior to the nominal divide (Φ = 1) counts against hydraulic efficiency. Hence, the most weight is given to the shortest residence times.

$$\mathrm{MI} = 1 - \mathrm{M_{pre}} \qquad [2_41]$$

where M_{pre} is the pre-nominal moment taken about the nominal divide.

The pre-nominal moment is defined by Eq. 2-42. A decrease in hydraulic efficiency produces a proportional increase in the magnitude of the pre-nominal moment and, thus, a decrease in the value of the Moment Index (Wahl et al., 2010).

$$\mathrm{M_{pre}} = \int_0^1 (1 - \phi)\, C'(\phi)\, d\phi \qquad [2_42]$$

To illustrate the value of the Moment Index, Wahl et al. (2010) considered 42 hypothetical RTDs. For select cases, the normalized concentration against flow weighted time curves were plotted and used to evaluate hydraulic efficiency. Firstly, the functions were qualitatively ranked from most to least efficient based on function shape and position relative to φ = 1 (being representative of the nominal detention time). Then, MI, (t_p/τ), e $(\bar{t}_m/\tau)$ and λ $(e(1 - 1/n))$ were calculated and used to again rank the hypothetical reactors from most

to least efficient. The results were compared and it was found that MI ranking was the closest to the qualitative predictions in each case. In order to further quantitatively substantiate their findings, plots of MI, (t_p/τ), e and λ versus effluent pollutant fraction were produced for the 42 RTDs and a linear regression analysis performed. It was again found that MI displayed the best fit with R^2 being closest to 1.

2.5. Chemical kinetics

The term 'kinetics' broadly describes the rate at which a chemical species is transformed from one form into another. The kinetics of the contaminant degradation processes are an important indication of the treatment efficiency of a CW (Sheridan et al., 2014a).

In order to investigate the kinetics of contaminant degradation in CW's, it is essential to have a thorough understanding of the flow hydraulics. Although research into the hydraulic performance of HSSF CW's has been limited, there have been a number of studies reporting on how the various micro-organisms and plant species interact in order to break-down pollutants in the wastewater. Although each CW system is unique and should be dealt with on a case-by-case basis, it is generally accepted that wetlands operating as close to ideal plug-flow as possible will yield greater kinetic efficiencies. Higher aspect (length-to-width) ratios, higher loading rates and packing of smaller diameter is helpful in inducing nearer to ideal plug flow behaviour in packed bed systems (Alcocer et al., 2012).

2.6. Biomimicry and constructed wetland design

Biomimicry is a design methodology whereby natural or biological processes are simulated in man-made systems (Biomimicry.SA., 2015). It is the principles of self-organization, self-regulation and self-invention that enable biological systems to successfully adapt to changing, and threatening, environmental conditions. This ability to adapt and survive is possible only because of species diversity (Kauffman, 1993). Given their origins, CW's are inherently biomimetic systems. However, the design of CW's can be improved by the application of the more recently developed biomimetic principles.

2.6.1. Ecological and Life's Principles

In order to stimulate biomimetic design, two sets of guidelines known as the ecological and life's principles have been developed. These guidelines are based upon extensive observation of natural ecosystems, a thorough understanding of the fundamental principles underlying natural processes and abstraction of those traits which ensure that living species survive and thrive in their particular environment (Benyus, 2017).

Ecological Principles

The ecological principles are a set of general criteria to be used in the design of technologies based on natural ecosystems (Todd and Josephson, 1996). The eleven principles, with brief explanations, are provided in Table 2-5 (Benyus, 2017).

Table 2-5: The Biomimetic Ecological Principles

Ecological Principle	**Description**
Geological diversity and nutrient complexity	Soils rich in a variety of minerals are better able to support biological diversity. The wider the nutrient variety, the greater the species diversity and the better the capability of the system as a whole to adapt and optimize.
Nutrient and micro-nutrient reservoirs	The assortment of nutrients in the soil must be in a bio-available form to support life.
Steep gradients	A living system in which there are distinct or large differences in or between measurable physical and chemical properties supports a greater diversity of chemical reactions/transformations and creates many alternative pathways through the system. The recycling of material is one way of creating gradients within a system.
High exchange rates	The surface area for chemical reactions in biological-type reactors must be accessible to the greatest volume of material as is possible. It must neither be disturbed by the flow regime nor itself obstruct flow. Increasing the diversity of the reactive surfaces increases the diversity of chemical reactions/transformations supported.
Periodic and random pulsed exchanges	Exposing a living system to simulated, regular changes as well as arbitrary disturbances helps it to adapt to and recognize alterations in the environment. In this way, the system becomes more robust and the impact of change becomes less during steady operation.
Cellular design and structure of mesocosms	The cell is the basic building block of living organisms. Individual cells are able to function independently or together with other cells via a communication network. Cells are also able to specialize to carry out specific functions. Cellular design of living systems means that resources are used more efficiently, systems can increase or decrease in size as the need arises and non-functioning cells can be removed without jeopardizing the system as a whole.
Law of the Minimum	No ecosystem functions in isolation of the environment or adjacent ecosystems. At least three separate sub-systems (linked only by flows) should be incorporated into design. This is the generally accepted norm in creating a self-sustaining system over the long term.
Diverse microbial communities	Many reactions taking place in living systems are catalyzed by bacteria. In addition, nucleated algae, water

	and slime mold, slime nets, fungi and protozoa are also capable of supporting many important reactions. The greater the diversity of bacteria and micro-organisms incorporated into the design of a living system, the greater the number of reactions supported by the system.
Photosynthetic communities	Plants in living systems provide the site for biological reactions (the root zone). In addition, their own photosynthetic metabolism can play an important role in contaminant and pathogen removal. Living systems with greater plant diversity are more successful in managing their energy, oxygen and chemical balances.
Phylogenetic diversity	Different animal species, of different levels of genetic complexity, play an important role in regulating, controlling and maintaining living systems.
Microcosm as a tiny mirror image of a macrocosm	A living system must be designed in harmony with its surrounds and be capable of harnessing external resources to sustain itself, while not disturbing surrounding ecosystems, and also offer benefit to its surrounds.

Life's principles

The life's principles are a set of criteria which should be applied in the innovation, design and evaluation stages of a biomimetic system – with emphasis placed on evaluation of how a system functions as a sum of its parts. Life's principles are based on the over-arching patterns found amongst living species surviving and thriving in their particular environment (Benyus, 2017).

2.6.2. Biomimetic approach to wastewater treatment

The biomimetic approach says that the most sustainable solutions to water treatment, and mankind's problems in general, are found in nature. In short, nature should act as a model, measure and mentor (Benyus, 2017). As the types of wastewater to be treated increase and become more diverse, so the need for more economical, efficient and robust systems to cope with the treatment demands emerges.

Successfully designed biomimetic water treatment systems should be developed as ecosystem technologies and function according to the ecological and life's principles. As in any natural ecosystem, all components must sync harmoniously with one another and it must be realised that the system as a whole cannot operate efficiently without contribution from all of its individual parts (Benyus, 2017). Biomimetic wetlands are, thus, self-contained, ecologically engineered systems, which effectively and efficiently mimic the natural actions of and

interactions between bacterial communities, microbial communities, algae, plants, trees and aquatic organisms (Dama-Fakir et al., 2015).

The biomimetic approach would, ideally, lead to the design of zero-waste systems and systems that display multiple functionality. CWs can act as carbon sinks, air quality and temperature regulators and habitats for biodiversity. Furthermore, multiple functionality could be achieved through, for example, the recycling of waste streams, the production of nutrient-rich fertilizers and the generation of renewable energy. Therefore, there is potential for additional income generation from these systems. For example, wetland vegetation may be harvested and sold as a means of income generation (Dama-Fakir et al., 2015). Table 2-6 outlines some examples of successful projects from companies at the forefront of biomimetic water treatment technologies.

Table 2-6: Summary of successful biomimetic wetland designs (Dama-Fakir et al., 2015)

Company Name	- *Floating Island International* - *Bright Water Company*	- *John Todd Ecological* - *Worrel Water Technologies*	- *Natural Systems Utilities* - *Naturally Wallace Consulting* - *Whole Water Systems*
Natural system being mimicked	Wetland and aquatic ecosystems	Natural wetland systems	Natural wetland systems
Biomimetic product/process	- *Biohaven Wild Floating Islands* - *Bright Water Company Floating Islands*	- *Living Machines* - *EcoMachines*	- *Natural Systems* - *Treatment Wetlands* - *CW Bioreactor*
Principles of natural system operation	The role of floating plants in the removal of excess nutrients from natural wetland waters	Aerobic and anoxic water treatment as observed in facultative ponds	Multi-functionality of natural wetlands in organic, inorganic and biological contaminant removal
Biomimetic system description	- Bouyant islands constructed out of layers of polymer batting and containing pockets of wetland plants/vegetation - Plant roots extend into the water and the associated microbes remove excess nutrients from the water	1) **Pre-treatment:** anaerobic zone 2) **Flow equalization:** zone to ensure uniformity of flow 3) **Primary treatment:** independent tanks in series containing different combinations of gravel/rocks, plants/vegetation and aquatic species for decomposition of organic/inorganic matter and consumption of by-products (Living Machines may contain screens, biofilters, plumbing systems and other mechanical	- Integration of natural systems with on-site wastewater treatment and re-use - Decentralization of wastewater treatment to expand water purification capabilities across a range of wastewaters and contaminants and create (self) sustainable water treatment/

		devices to accelerate the natural purification process) 4) **Polishing:** Ecological Fluidized Bed or small CW	recycling/re-use solutions
Type of water/wastewater treated	Water bodies, such as livestock ponds, golf course ponds, wildlife habitat areas etc.	- High strength industrial wastewater - Sewage	- Municipal - Commercial - Industrial
Availability of technology	Currently available e.g. Du Noon township, Western Cape	Currently available in USA, UK, Australia, China & Ghana e.g. construction phase of Langrug project, Western Cape, soon to be initiated	Currently available in USA e.g. **"eMonti Green Hub"** (an anaerobic digester using industrial wastewater and sewage sludge, with other wastes) in the development phase by PPA, Eastern Cape, South Africa (Middleton, 2012)

In summary, the biomimetic approach relies upon careful observation and multi-disciplinary partnerships to develop a deeper understanding of the hydraulic, biological, chemical, physical and kinetic processes occurring within wetland systems and then transferring this knowledge to improved design guidelines for CWs (Benyus, 2017).

Chapter 3 Materials and Methods

A description of the materials and methods is given in this chapter. The detail underlying the hydraulic and kinetic calculations is left to be described in the individual chapters dealing with each topic. This is done to avoid repetition and also to aid the flow and understanding of the results presented in the subsequent chapters. The author requests the reviewers' patience as the information presented below may also be included in the published papers.

3.1. Experiments at the University of the Witwatersrand

3.1.1. Constructed wetland description

The CWs were stationed at the IMWaRU outdoor research facility on the east campus at Wits University. Two pilot-scale CWs, each a custom-made plastic trough (4.2m x 0.8m x 0.8m) filled with quarry gravel, were used. One wetland contained only gravel, while the second contained gravel and was planted with a variety of indigenous macrophytes (*Arum lily*, *Cyperus papyrus nana, Typha capensis, Juncus effuses*, *Chondropetalum tectorum*). The wetland was divided into five zones defined by the vegetation within each section, as shown in Figure 3-1. In both cases, the height of the gravel bed was approximately 0.7m.



Figure 3-1: The experimental constructed wetlands at the IMWaRU site, Wits University showing the five zones of vegetation (left), the planted and unplanted wetlands side-by-side and the Jojo tank set-up (right). The outlet configurations (inlet configurations are not shown but are of the same design), the syphon break and the sample ports are also visible (right).

The wetlands were fed by two JoJo water tanks (Figure 3-1). One tank contained an impellor and the other a submersible pump so that water could be circulated between the two; thereby ensuring homogeneity of the feed solution. Each wetland was fitted with identical inlet and outlet water distribution networks (built using PVC elbows and T-pieces, high quality garden hose-pipe and metal worm clamps). The JoJo tanks were connected

to the wetland inlets via a length of hosepipe, into which a municipal flow meter and dye injection port (consisting of a PVC T-piece and rubber bung) was fitted. A syphon break was fitted to each outlet to control the level within the wetland.

Thirteen sample ports were inserted into the wetlands. These ports were constructed of plastic-coated wire mesh so as not to disturb the flow path of water through the CW (Figure 3-1). All sample ports were fitted with three different lengths of PVC tubing; thereby dividing the bed into a grid-like network and allowing for sampling at three depths. The experimental set-up is illustrated in Figure 3-2. The five sample ports positioned down the centre of the bed contained removable cages packed with the same gravel as found in the larger system. The gravel was divided into three different height sections, with open spaces between them. The remaining eight sample ports were located at fixed points along the edges of the wetlands.

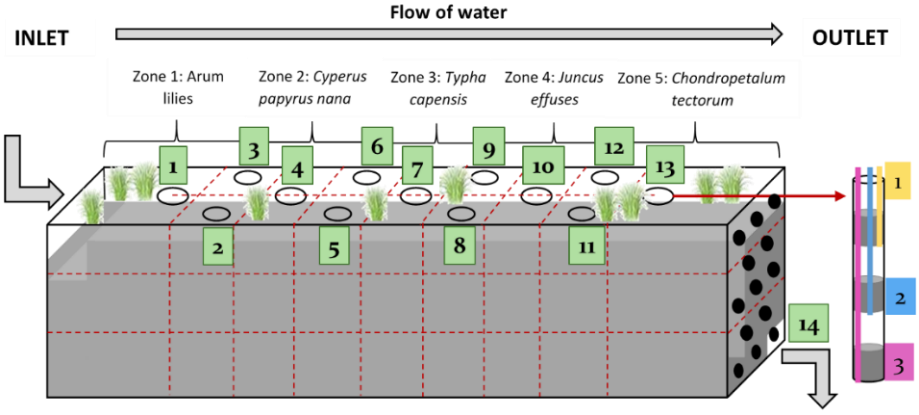


Figure 3-2: IMWaRU (Wits University) constructed wetland configuration showing a removable cage and sample tubing to three depths. The outlet distribution network is also visible and the inlet distribution network is of the same arrangement. The red dashed lines illustrate the division of the wetland system into a grid of sample points.

3.1.2. Wits Experimental timeline

The timeline of the experimental regime in 2015 is presented in Figure 3-3. The experimental procedure is elaborated on in the sections to follow.

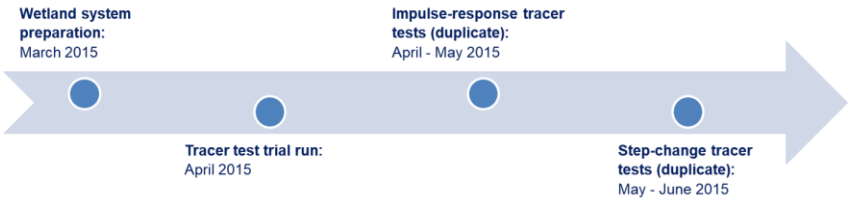


Figure 3-3: Experimental timeline for the experiments conducted in the constructed wetlands at the University of the Witwatersrand, 2015.

3.1.3. Wetland preparation

Before commencing with the experiments, the wetlands were drained of all residual water and flushed twice with tap water available on-site to ensure any residual chemicals were removed. The tap water from the site was analysed to determine the baseline for the spectrophotometric measurements.

3.1.4. Hydraulic studies

Tracer test trial run

A tracer test trial run was conducted to investigate the operational characteristics of the system (and, specifically to set the valve positions on the inlet configuration to give an evenly distributed inflow), to perfect the tracer dye injection and sample removal techniques and to briefly observe the movement of tracer dye through the wetlands and determine the sampling regime.

Once the inlet valve positions has been set, the influent and effluent water flow rates were monitored to determine the range of inflow and outflow rates achievable. Based on this, an inflow rate of 20 L/min was chosen for the trial run; yielding an experimental time of 10 hours. The trial run was an impulse-response tracer test, using FWT Red fluorescent dye. Based on the experience gained and results obtained from the trial run, an inflow rate of 5 L/min (for an experiment of 24 hours in duration) was chosen for the subsequent impulse-response and step-change tracer tests.

Impulse-response tracer tests

The inlet valves were opened to the positions determined during the trial run and the outlet valves were opened fully. The outlet valve from the JoJo tank was opened and adjusted to achieve the pre-determined inflow rate of 5 L/min. The syphon break at the outlet was also adjusted to ensure that the water level in the wetland coincided with the gravel surface. Once the water level was being maintained and the flow had reached pseudo steady-state, the pulse of FWT Red liquid dye (30ml) was injected into the feed line.

Samples were removed from each of the three depths at each sample port at 30 minute intervals until the peak of the concentration had been surpassed. Thereafter, samples were taken at 2 min, 15 min and 30 min after injection; then on a half-hourly basis and then a two hourly basis up to 12 hours after injection. Thereafter, samples at 24 and 29 hours after injection were collected to complete the RTD tail. Based on the flow rate (distance moved in a specified time interval) and visual observation of the intensity of the pink colour of the samples removed, sampling was conducting in a cascade fashion. More samples were removed from the front section of the wetland soon after injection but none at the back end of the wetland until the dye front had moved closer to the latter sample ports. As such, the time of the greatest sampling frequency was determined on a port-by-port basis.

The FWT Red concentration in each sample was analysed using a Merck Spectroquant (and absorbance-concentration calibration curve) after filtration. The time-variant FWT Red concentration data was used to plot the experimental RTD, from which various hydraulic parameters were calculated (see Chapter 4).

Step-change tracer tests

The valves were opened and adjusted as described for the impulse-response tracer tests. Once the water level had stabilized and the flow had reached pseudo steady-state, the feed was changed over to a solution of known concentration of FWT Red. The same sampling regime was followed and sample analysis performed as for the impulse response tracer tests and the same hydraulic parameters calculated; although by a different mathematical technique (see Chapter 4).

3.2. Experiments at the Helmholtz UFZ

3.2.1. Constructed wetland description

The pilot CW is located at the Helmholtz Zentrum für Umweltforschung (UFZ) in Leipzig, Germany. Construction was completed in October 2013 and the first experiments commenced in August 2015. Figure 3-4 is a schematic diagram of the wetland system, which is a horizontal sub-surface flow (HSSF) CW. The stainless steel container is 6 m in length and 0.70 m in height and one longitudinal boundary is constructed at 16° from the vertical, such that the widths at the top and base of the container are 1.2 m and 1.0 m, respectively (Figure 3-4b). The CW is an unusual shape as it was built using a pre-constructed SS container. The wetland has been dug into the ground, such that the upper rim and 20 cm of the boundary wall protrude above the ground. The system is filled with glacial gravel (bed height 0.50 m; particle size 4 - 8 mm; 36% voidage) and planted with *Phragmites australis*. Three fully removable, stainless-steel baskets (height 0.7 m; diameter 0.30 m) have been inserted into the central flow path (Figure 3-5a). Each basket contains the same gravel and vegetation as in the surrounding wetland system. The basket cages have evenly distributed pores of the same diameter as the average gravel particle size to minimize flow disruption. The purpose of the baskets is to analyse, in more detail, a predominantly undisturbed section of the CW under laboratory conditions. This part of the methodology has been developed from previous studies on laboratory-scale planted fixed bed reactor (PFBR) systems (Kappelmeyer et al., 2002, Lünsmann et al., 2016). Photographs of the wetland are given in Figure 3-5.

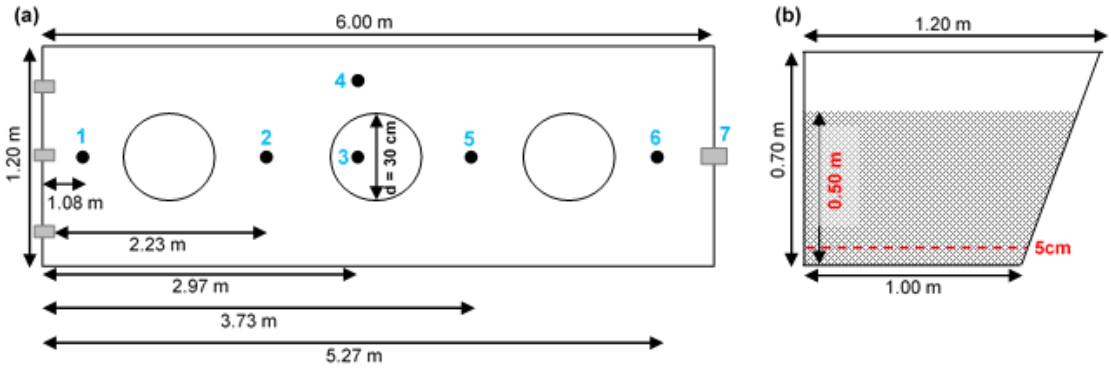


Figure 3-4: (a) Aerial view of the constructed wetland showing seven internal sample ports, three inlet valves and one outlet valve and (b) cross-sectional view showing the gravel bed and valve heights.

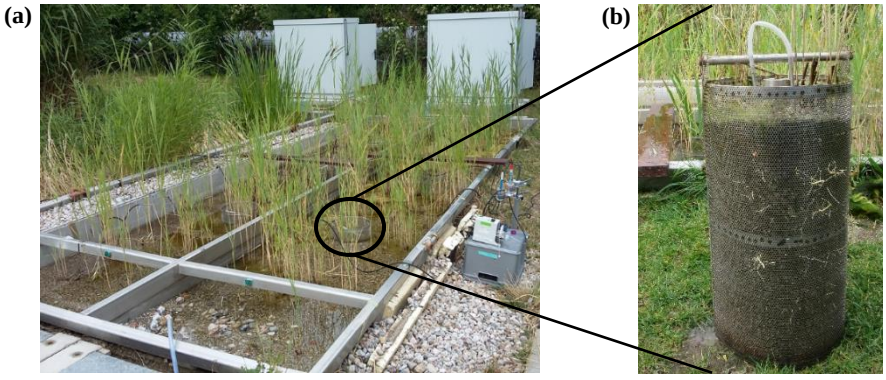


Figure 3-5: (a) Photograph of the pilot, gravel horizontal subsurface flow constructed wetland at the Helmholtz UFZ, Leipzig (July 2015) and (b) the middle basket when removed from the wetland showing a well-developed root system (Sept 2015).

The system is fed by three evenly spaced valves (Figure 3-4a), positioned 5 cm above the wetland base. The discharge is removed via a single outlet valve (Figure 3-4a), centred and also 5 cm above the wetland base. The inlet and outlet water flow rate is regulated via a gear pump (VGS120, Verder Pump, Germany), a motor (SEV6324, SEVA Tec, Germany) and a frequency controller (DF51-322-025, MOELLER, Germany). Data is logged to allow for continual flow rate monitoring. The water level within the wetland is controlled by means of a syphon at the wetland outlet.

The system was allowed to establish naturally, without any external nutrient source, from October 2013 to July 2015. During this time, municipal tap water was fed into the system in the spring, summer and autumn. The feed was shut off during the coldest winter months (December – February).

3.2.2. UFZ Experimental timeline

Timelines of the experimental regimes in 2015 and 2016 are presented in Figure 3-6 and 3-7. The experimental procedures are elaborated upon in the sections to follow.

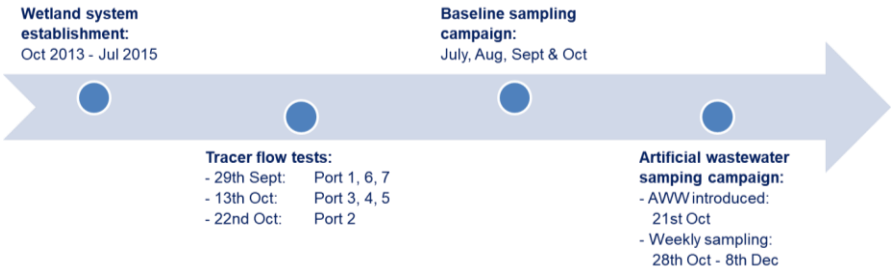


Figure 3-6: Timeline of experiments conducted in the constructed wetlands at the Helmholtz UFZ during 2015.

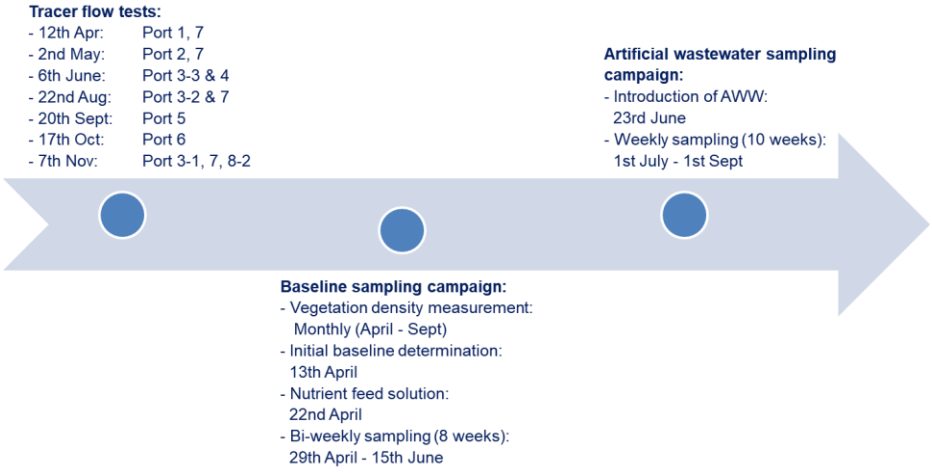


Figure 3-7: Timeline of experiments conducted in the constructed wetlands at the Helmholtz UFZ during 2016.

3.2.3. Hydraulic studies

Investigation into the suitability of fluoride as a tracer

Phragmites australis were harvested from the outdoor wetland and equal masses were placed in five brown bottles in the laboratory. One bottle was left as the control and the other four were filled with solutions of different fluoride concentrations (500 mg/L, 1g/L, 2 g/L and 5 g/L). The experiments, specifically the health of the plants in each bottle, were monitored over a period of two weeks (24th August – 7th September 2016) by measuring the amount of evapotranspiration and the diffusion conductance of the leaf surfaces (AP4 Porometer, AT Delta-T Devices) (see Appendix F).

Impulse-response tracer tests

Stainless-steel sampling devices (hereafter referred to as samplers) were inserted into the gravel bed at six locations (Figure 3-4). The samplers were L-shaped, hollow tubes containing several holes at the base of their long ends. These openings were too small to allow for gravel to enter, but large enough to allow for easy movement of water. The long end was inserted into the gravel bed and the short end, containing a single opening, extended above the surface.

The samplers were connected in pairs; one being the outlet tube (from which water was removed from the wetland) and the second the return tube. The return tube was fixed to the outlet tube such that the base of its long end was positioned 6 cm above the base of the outlet tube. This arrangement ensured that water was removed from and returned to the wetland in a roughly spherical zone, so as to minimize flow disturbances. The short ends were connected to a peristaltic pump (BVP_Z, ISMATEC SA, Switzerland), a custom-made stainless-steel flow cell (Schnegg, 2002) and a fluorometer (GGUN-FL, Albillia, Switzerland) using black norprene tubing. A schematic diagram of this set-up can be found in Figure 3-8. The fluorometer was calibrated before each experiment using a two-point calibration.

30mg of Uranine fluorescent tracer powder was dissolved into 1L of distilled water and injected as a single pulse. For the duration of each flow test, water was pumped from the wetland, into the flow cell and returned to the bed at the same location (Figure 3-8) to ensure that the total system volume was maintained. The peristaltic pump rate was kept low to minimize impact on flow behaviour. The fluorometer was programmed to record a potential (mV) at 10 second intervals, which was converted to Uranine concentration.

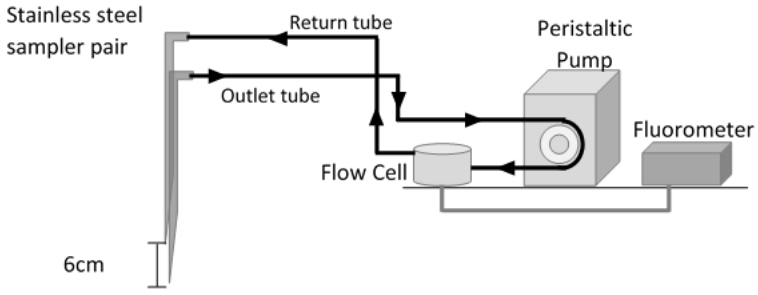


Figure 3-8: Stainless steel sampling devices (samplers), peristaltic pump, flow cell and fluorometer configuration for the impulse-response flow tests.

Flow tests in 2015

Flow tests were conducted at each of the internal sample ports and at the system outlet during September and October 2015. These were the very first hydraulic tests in the pilot wetland. Samplers were inserted to mid-depth (24cm below the gravel surface). The inlet flow rate was set to provide a retention time of approximately

five days and the syphon was adjusted to maintain a water level of 0.5 m (coinciding with the gravel surface). The inlet and outlet flowrates were monitored three times daily: 6 am, 12 noon and 6 pm. During the start-up phase, the system was fed with only tap water.

Flow tests in 2016

The hydraulic investigation was extended during 2016, with flow tests being run from April through November at the six internal sample ports and at the system outlet (in duplicate). Three pairs of samplers were inserted at each port (12 cm, 24 cm and 36 cm below the gravel surface), with 6 cm separating each pair. The inlet flow rate was set to provide a retention time of approximately seven days and the syphon at the outlet was adjusted to maintain a water level of 0.44m (6cm below the gravel bed surface). In addition, vegetation density was determined monthly, inlet and outlet flow rates were monitored throughout each day and weather data (air temperature, global radiation, humidity and wind speed) was compiled hourly at the on-site weather station. During the April flow test, the system was fed with only tap water. In May and June, the wetland received a nutrient solution (urea). For the remaining tests, the feed was artificial wastewater (AWW). An AWW concentrate was prepared, based on a published standard, and contained 30 g/L casein peptone, 20.62 g/L meat extract, 5.62 g/L urea, 5.25 g/L dipotassium hydrogen phosphate. The concentrate was diluted as 1:400 with municipal tap water before entering the wetland (FMJC., 2001).

3.2.4. Chemical and kinetic studies

Water sampling protocol

Samplers were inserted into the gravel bed at three depths (12cm, 24cm and 36cm) at each of six internal locations (Figure 3-4) and in the same arrangement as described for the tracer tests above. In addition, black norprene tubing was connected directly to the discharge valve at the system outlet. The short ends of the sampler pairs were connected, in turn, to a small peristaltic pump (REGLO MS 2/6, ISMATEC SA, Switzerland) via identical lengths (1.2m) of black norprene tubing. Water was pumped continually through three consecutive plastic flow cells for the measurement of dissolved oxygen (DO) (Fibox 3, Presens, Germany), oxidation-reduction (redox) potential (Multi-i340, WTW, Germany) and pH (Multi-i340, WTW, Germany). The temperature within the bed and of the water passing through the flow cells was also recorded. 20ml samples were collected and filtered through 0.45μm syringe filters. 3ml aliquots were prepared and submitted to the analytical laboratory for carbon and nitrogen analysis (Multi N/C 21005, Analytikjena, Germany), while the remaining volume was used for ammonium (NH_4^+ - N) and nitrate (NO_3^- - N) analyses (Nova 60 Spectroquant, Merck, Germany).

Introduction of artificial wastewater

An artificial wastewater (AWW) concentrate containing casein peptone, meat extract, urea and dipotassium hydrogen phosphate was prepared, autoclaved and injected into the CW system via a metering pump (Gamma L GALA1000, ProMinent, Germany). The concentrate was formulated from a published standard based on the average composition of the water released from a treatment plant of Class 2 in Germany; representing between 1 000 and 5 000 inhabitant equivalents (FMJC., 2001). A typical analysis of German Class 2 effluent is given in Table 3-1.

Table 3-1: Legal limits on environmental discharges for a treatment plant of Class 2 in Germany (based on an inflow of 300–600 kg·d^{-1} BOD_5)

Component	**Concentration (mg·L^{-1})**
[a] COD	110.0
[a] BOD_5	20.0
[b] TOC	22.80
[b] TN	9.14

[a] legal standard

[b] measured in laboratory (Helmholtz UFZ, Leipzig) from AWW concentrate

Before the AWW was introduced into the wetland, a full set of baseline samples were taken (samples were taken from the inlet, outlet and at three depths at each internal sample port. This was done once a month for three months leading up to the AWW sampling campaign in 2015 and every week for five weeks prior to AWW introduction in 2016.

The separate feed water and AWW feed lines were combined into a single pipe and the two fluid streams mixed before entry into the wetland. The AWW flow rate was monitored regularly via the 'bucket and stopwatch' method. Weekly sampling commenced 1 week after the introduction of the wastewater and continued for 7 to 10 weeks. Samples were taken from 24 cm below the gravel surface at each sample port, as described previously.

Detailed description of feed water composition 2015

Prior to the introduction of the AWW (21 October 2015), the system was fed with municipal tap water only. The AWW concentrate used for this set of experiments contained 37.50 g·L^{-1} casein peptone, 25.78 g·L^{-1} meat extract, 7.03 g·L^{-1} urea and 6.56 g·L^{-1} dipotassium hydrogen phosphate. The individual feed water and AWW loading rates are presented in Table 3-2.

Table 3-2: Feed water and artificial wastewater inflow loading rates during 2015

Week	Date (2015)	HLR ($L \cdot m^{-2} \cdot d^{-1}$)		HLR ($L \cdot m^{-3} \cdot d^{-1}$)		Flow ratio (inflow:AWW)
		Inflow	AWW	Inflow	AWW	
1	21 Oct – 28 Oct	76.14	0.0982	452.4	0.583	776
2	28 Oct – 4 Nov	76.95	0.0899	457.2	0.534	856
3 – 7	4 Nov – 8 Dec	20.54	0.0806	122.0	0.479	255

Detailed description of feed water composition 2016

Prior to the introduction of the AWW (23 June 2016), the system was fed first with municipal tap water and then with a nutrient solution containing 7.03 $g \cdot L^{-1}$ casein peptone (0.48 $g \cdot m^{-2} \cdot d^{-1}$ / 3.80 $g \cdot m^{-3} \cdot d^{-1}$). The AWW concentrate used for this set of experiments contained 30 $g \cdot L^{-1}$ casein peptone, 20.624 $g \cdot L^{-1}$ meat extract, 5.624 $g \cdot L^{-1}$ urea and 5.250 $g \cdot L^{-1}$ dipotassium hydrogen phosphate. The individual feed water and AWW loading rates are presented in Table 3-3.

Table 3-3: Feed water and artificial wastewater inflow loading rates during 2016

Week	Date (2016)	HLR ($L \cdot m^{-2} \cdot d^{-1}$)		HLR ($L \cdot m^{-3} \cdot d^{-1}$)		Flow ratio (inflow:AWW)
		Inflow	AWW	Inflow	AWW	
1	23 June – 1 Jul	22.20	0.0588	131.9	0.3491	378
2	1 Jul – 7 Jul	20.91	0.0588	124.2	0.3491	356
3	7 Jul – 15 Jul	21.19	0.0588	125.9	0.3491	361
4	15 Jul – 21 Jul	23.18	0.0588	137.7	0.3491	394
5	21 Jul – 29 Jul	20.08	0.0588	119.3	0.3491	342
6	29 Jul – 4 Aug	12.91	0.0608	76.7	0.3610	213
7	4 Aug – 11 Aug	16.71	0.0608	96.1	0.3610	266
8	11 Aug – 18 Aug	11.80	0.0608	70.1	0.3610	194
9	18 Aug – 25 Aug	40.84	0.0608	242.7	0.3610	672
10	25 Aug – 1 Sept	22.93	0.0608	136.3	0.3610	377

Chapter 4 A comparison of three different residence time distribution modelling methodologies for horizontal subsurface flow constructed wetlands

4.1. Summary

The following chapter comprises the paper entitled: "A comparison of three different residence time distribution modelling methodologies for horizontal subsurface flow constructed wetlands", which was published in Ecological Engineering in 2016. In the context of this research, the purpose of the experiments was two-fold. Firstly, to become familiar with the theory behind and techniques involved in tracer testing and, secondly, to gain a deeper understanding of the mathematics underlying the hydraulic output of impulse-response versus step-change tracer tests and under which circumstances either type of test should be employed. Key to this latter objective is understanding and appreciating the limitations of each mathematical technique and how to interpret the results, seeing as different conclusions may be drawn from the same system depending on the method of tracer test chosen. This first set of experiments was a fundamental step in developing the tools required for the later work conducted at the Helmholtz UFZ in Leipzig, Germany.

4.2. Statement of individual contribution

This research was carried out in collaboration with Ricky Bonner, who is first author on the paper. The following is a list of tasks to which I made a significant contribution:

- Preparation of the IMWaRU site on which the pilot-scale CWs are located
    - Securing site access and overseeing maintenance of the grass
    - Coordinating with the workshop with regards to the construction and fitting of the impellar and circulation pump in the Jojo water tanks on site
- Preparation of the experimental CWs
    - Construction of the inlet and outlet distribution networks
    - Fitting of the tubing to the sample ports for sample removal
    - Planting of the wetlands
- Developing the experimental procedure
- Conducting the tracer test trial run
- Conducting the impulse-response and step-change tracer tests, in duplicate
- Analyzing all samples for tracer dye concentration in the laboratory using the Merck Spectroquant
- Developing the spreadsheet to capture the results and conduct the numerical integration (impulse-response tracer test) or differentiation (step-change tracer test)
- Proof-reading of the paper prior to and during the review process

4.3. Ecol. Eng. (2017). Vol. 99 pp. 99-113

4.3.1. Abstract

In this paper three different residence time distribution modelling methodologies for horizontal subsurface flow constructed wetlands were compared and these were the impulse response, step change derivative and step change integral modelling methodologies. Impulse response and step change tracer studies were conducted on pilot scale horizontal subsurface flow constructed wetlands to generate the concentration-time data to be fed into the impulse response and step change modelling approaches, respectively. For the unplanted reactor, the two step change modelling methodologies suggested the same fluid flow behaviour reflected by almost identical values for the mean residence time ($\bar{t}_m$) and the same value for the number of stirred tanks in series (n) and Peclet number (Pe). The impulse response modelling approach suggested a 7% higher $\bar{t}_m$ and a lower degree of dispersion. For the planted system each modelling methodology suggested different fluid flow behaviour. Practical limitations were attempted to be identified for the two types of tracer experiments. The limitations of the experiments could be considered limitations of the modelling methodologies as they depended on the tracer experiments for data generation. We were unable to collect sufficient data on the peak of the impulse response curve for the unplanted reactor and may have affected the impulse response modelling methodology results. Sampling down the length of the reactor revealed that tracer dispersion had an effect of broadening the impulse response curves to the extent that it was almost impossible to identify non-ideal flow behaviour such as short-circuiting. The mathematical techniques employed by each modelling methodology were also critically assessed. We found that varying the size and hence number of subintervals used in Simpson's 1/3 rule for numerical integration resulted in different values for $\bar{t}m/T$ for each modelling approach. The lower the sensitivity of the modelling methodology the better as choosing a parameter as arbitrary as subinterval size should not have a noticeable effect on reported hydraulic behaviour. For both reactor systems the step change derivative approach was least sensitive to subinterval selection, reporting a 1% and 4% variation in $\bar{t}_m/T$ for the planted and unplanted system, respectively whereas $\bar{t}_m/T$ determined by the step change integral and impulse response modelling methodologies varied by 10% or more in some cases. We highlighted the differentiation of F(t) to obtain E(t) to be a potential weakness of the step change derivative methodology as it had the capability to amplify background noise which may have affected the calculation of the hydraulic parameters. It was concluded that each modelling methodology had the potential to output a different reactor model for the same reactor and that each approach has its own inherent strengths and weaknesses. The choice of modelling methodology is ultimately dictated by availability of experimental equipment and the designer's confidence in using each of the respective approaches.

Keywords: Residence time distribution modelling, wastewater treatment, packed bed reactor, horizontal sub-surface flow constructed wetland, reactor model

4.3.2. Introduction

An horizontal subsurface flow constructed wetland (HSSF CW) is an example of a packed bed reactor (Vymazal and Krőpfelová, 2009, Sheridan et al., 2014a, Sheridan et al., 2014b), which utilizes a series of interrelated physical, chemical and biological processes to treat various types of wastewater (Dordio and Carvalho, 2013, Ligi et al., 2014, Scholz and Hedmark, 2010). These systems are typically packed with a solid matrix such as soil, gravel, clay aggregates or metallurgical slags (Dotro et al., 2011, Drizo et al., 1999, Sheridan et al., 2013). They may also be planted with different types of macrophytes to enhance the treatment processes (Leto et al., 2013). Some of the benefits of using macrophytes in the system include their ability to transfer oxygen from the atmosphere to the root zone to facilitate aerobic pollutant degradation processes as well as accumulation of toxic heavy metals in the plant tissue (Stottmeister et al., 2003).

As is the case with other types of packed bed reactors, the hydrodynamic behaviour of CWs has historically been over-simplified as being ideal plug flow (Werner and Kadlec, 2000). The presence of complex plant root structures; the growth of bacterial biofilms within the wetland matrix; the entrapment of suspended solids and the precipitation of heavy metals originating from the feed wastewater results in both spatially and temporally-dependent flow resistance (Knowles et al., 2011, Sheoran and Sheoran, 2006, Suliman et al., 2006a, Suliman et al., 2006b). The flow resistance causes non-uniform flow velocity profiles and, hence, different pockets of water reside within the system for different lengths of time, giving rise to a residence time distribution (RTD) and a mean residence time which is smaller than or equal to the ideal theoretical residence time (Levenspiel, 1999a). Pollutant degradation models built on the ideal plug flow assumption have, thus, proved to be in the large part inaccurate (Galvão et al., 2010, Marsili-Libelli and Checchi, 2005, Sheridan et al., 2014a, Sheridan et al., 2014b), since there is no way of incorporating the varying lengths of time spent by different pockets of wastewater in contact with elements of the system which can facilitate their degradation. This may lead to the installation of an under-sized constructed wetland and an unsatisfactory production performance. Consequently, a pilot scale reactor is built beforehand and an RTD study is conducted to develop a reactor model accounting for the non-ideal flow behaviour which when coupled with kinetic data can facilitate more accurate sizing of the reactor equipment (Lima and Zaiat, 2012, Rüdisüli et al., 2012).

4.3.3. Background

HSSF CWs use a variety of treatment processes to improve the quality of ground and surface water (Galletti et al., 2010, Marchand et al., 2010), some of which will be discussed below.

4.3.3.1. Physical treatment processes

Adsorption of phosphates

Soluble inorganic phosphates are transferred from the soil-pore water to the surface of the soil matrix via adsorption (Huett et al., 2005, Vohla et al., 2011). Adsorption rates are dependent on the granular medium's texture, grain size distribution, iron, calcium, magnesium and aluminium content (Garcia et al., 2010) as well as environmental factors such as redox potential and pH (Vymazal et al., 1998). The higher the iron, calcium, magnesium and aluminium content the higher the adsorption capacity becomes as a result of more iron, aluminium, magnesium and calcium hydroxide groups on the granular surface (Drizo et al., 1999, Shenker et al., 2005). Adsorbed phosphate can be released back into the water under reduced conditions due to the reductive dissolution of ferric and manganese phosphate minerals (Palmer-Felgate et al., 2010). According to Lüderitz and Gerlach (2002) phosphates can also be adsorbed onto humic substances produced as a result of vegetation breakdown.

Sedimentation and filtration of metals

Sedimentation of metals in HSSF systems is facilitated by the vegetation and substrate present as they decrease water flow velocity and increase hydraulic retention time (Lee and Scholz, 2007). Johnston (1993) noted that the efficiency of settling and sedimentation of metals is proportional to the particle settling velocity and wetland length. Sedimentation of metals is enhanced by flocculant formation as flocs tend to adsorb metals onto their surface (Marchand et al., 2010). Flocculation formation rates are high under alkaline conditions, a strong presence of suspended solids, high ionic strength and high algal density (Matagi et al., 1998).

4.3.3.2. Biochemical treatment processes

Nitrification

Nitrification is the biological oxidation of ammonium to nitrate, with nitrite as an intermediate (Burgin and Hamilton, 2007, Vymazal, 2007). The process can be described using the following reaction steps:

$$NH_4^+ + 1.5O_2 \rightarrow NO_2^- + 2H^+ + H_2O$$

$$NO_2^- + 0.5O_2 \rightarrow NO_3^-$$

The first reaction step is performed by aerobic bacteria which derive energy from the oxidation of ammonium to nitrite and use carbon dioxide as a carbon source (Tanner et al., 2012). The second step involves the activity of nitrite-oxidising bacteria to convert nitrite to nitrate (Kim et al., 2010). Oxygen is supplied to the nitrifying bacteria via two methods, namely diffusion from the atmosphere to the subsurface layers of the system and translocation from the atmosphere to the rhizome via plant structure (Van de Moortel et al., 2010, Yalcuk et al., 2010). Since the diffusion of oxygen is approximately $3x10^5$ times smaller than in air (Verberk et al., 2011), translocation of oxygen via vegetation is the primary method for oxygen supply to the nitrifying bacteria.

Albuquerque et al. (2009) notes, however, that oxygen supply via the rhizomes is consumed rapidly and there is competition for oxygen with other aerobic bacteria. Consequently, nitrification rates are low in HSSF systems with values between 0.01 and 2.15 $gNm^{-2}d^{-1}$ being reported in literature (Reddy and D'Angelo, 1997, Tanner et al., 2002). The optimum temperature for the process to occur is between 30 and 40°C and between a pH of 6.6 and 8.0 (Bradley et al., 2002).

Denitrification

Denitrification is the process in which nitrate is converted to dinitrogen gas via a series of intermediates such as nitric oxide and nitrous oxide (Warneke et al., 2011), as shown in the reaction step provided by Vymazal (2007):

$$2NO_3^- \rightarrow 2NO_2^- \rightarrow 2NO \rightarrow N_2O \rightarrow N_2$$

The overall reaction depicting the process is provided by (Hauck, 1984):

$$6(CH_2O) + 4NO_3^- \rightarrow 6CO_2 + 2N_2 + 6H_2O$$

The process occurs under anaerobic conditions with organic compounds being utilised by bacteria as a carbon source (Wen et al., 2010) and nitrogen being used as an electron acceptor instead of oxygen (Fleming-Singer and Horne, 2002, Noorvee et al., 2007). Jakubaszek and Wojciech (2014) report that for 1 g of nitrate being converted to nitrogen gas, 0.7 g of carbon are required for the bacteria to perform the process. Optimal pH for the process is between 7 and 7.5 whereas optimal temperatures lie between 20 and 25°C (Reddy et al., 2014).

Organic transformation and removal

Dissolved organic matter from the influent wastewater and that produced from the disintegration of particulate organic matter can then be decomposed via aerobically or anaerobically-facilitated processes (Garcia et al., 2010). Aerobic degradation is performed by aerobic heterotrophic bacteria which use oxygen as a final electron acceptor (Vymazal and Krőpfelová, 2009):

$$C_6H_{12}O_6 + 6O_2 \rightarrow 6CO_2 + 6H_2O + 12e^- + \text{energy}$$

Oxygen transfer rates in HSSF systems are typically low, as noted by Rousseau and Santa (2007) who estimated it to be approximately 0.7 g O_2 $m^{-2}day^{-1}$. Consequently, aerobic degradation pathways are not prominent in such systems. Anaerobic degradation is thus the dominant transformation pathway for dissolved organic matter and is a multi-phase process. The first step of the process entails the microbial conversion of complex soluble polymers into simpler monomers such as amino acids (Megonigal et al., 2004). These amino acids then undergo fermentation to produce primarily fatty acids, alcohols as well as hydrogen and carbon dioxide. Sulphate-reducing bacteria then convert the fatty acids into carbon dioxide, water and hydrogen sulphide:

$$CH_3COOH + H_2SO_4 \rightarrow 2CO_2 + 2H_2O + H_2S$$

Methanogenic bacteria also convert fatty acids as well as carbon dioxide and hydrogen into methane as shown in the following two reaction steps:

$$CH_3COOH + 4H_2 \rightarrow 2CH_4 + 2H_2O$$

$$4H_2 + CO_2 \rightarrow 2CH_4 + 2H_2O$$

4.3.3.3. Modelling treatment processes in HSSF CWs

One of the most popular models used to predict HSSF CW treatment performance is the k-C* model, which was presented by Kadlec and Knight (1996) and discussed by Rousseau et al. (2004):

$$\frac{C_{out} - C^*}{C_{in} - C^*} = e^{-kt} \qquad [4_1]$$

This model, like many others found in literature assume ideal plug flow conditions (Sheridan et al., 2014a, Sheridan et al., 2014b). Spatial and temporal variation of flow resistance inside the packed media cause the hydraulics to deviate considerably from ideal plug flow, as has been reported in studies on HSSF CWs (Ranieri et al., 2013). Only recently have researchers attempted to include the non-ideal fluid flow behaviour in treatment models (Sheridan et al., 2014a, Sheridan et al., 2014b).

4.3.3.4. Types of hydraulic modelling approaches for HSSF CWs

Apart from the method of performing a tracer study to obtain residence time distribution data, which will be the focus of this paper, other types of approaches have been developed by researchers to describe the non-ideal flow behaviour inside wetland systems. A prominent example is the finite element approach developed and discussed by Knowles and Davies (2010). The model attempts to describe, via a three-dimensional output, the dependence of hydraulic performance on clogging due to particle transport using COMSOL Multiphysics 3.5 FEA software (COMSOL A.B., Sweden) and a coupling of hydraulic and clogging sub-models using a reactive transport model. In the hydraulic model the system is resolved into an upper sub-domain with flow described using Richard's Law for variably saturated flow and the water table flow described using Darcy's Law. The clogging model is based on the work performed by Cui et al. (2008) which uses a filter coefficient used to describe the extent of clogging within a wetland bed. The filter coefficient exponentially increases with time and is dependent on the clean system filter coefficient, media porosity and a factor accounting for feed and operating conditions of the system under study. The model was tested by conducting a hydraulic tracer study on an existing HSSF CW in the United Kingdom (UK). Clogging was found to be underestimated by the model due to the exclusion of processes besides particle accumulation which affect clogging such as biomass growth and the development of dense plant root structures.

The focus of this study is the development of a comparison between three different types of RTD modelling methodologies which could be used for horizontal subsurface flow constructed wetlands; one of which required

the generation of concentration-time data from an impulse response tracer experiment and the other two from a step change tracer experiment. The impulse response experiment and its associated modelling procedures is the most popular (Headley and Kadlec, 2007). To the authors' knowledge, the step change experiment has been used less frequently with only a few studies coming to mind such as that performed by Suliman et al. (2006a,b). The tracer studies and subsequent hydraulic modelling was performed on two HSSF CWs; both of which were packed with dolomitic gravel with the one being planted and the other unplanted.

4.3.4. Research objectives

In this study, the primary aim was to build a comparison between three available RTD modelling methodologies for horizontal subsurface flow constructed wetlands. To accomplish this, the following 2 research objectives first needed to be met:

1. To conduct impulse and step change tracer studies on packed bed reactors to generate the concentration-time data which could be fed into the three modelling methodologies outlined in Figure 4-1; and
2. To determine hydraulic parameters such as the mean residence time, the number of equally sized CSTRs in series, the Peclet number and the hydraulic efficiency using the three different modelling approaches.

The comparison between the methodologies could then be built by attempting to meet the next 3 objectives:

3. To compare the hydraulic parameters obtained using each of the three approaches against ideal theoretical conditions;
4. To identify practical limitations encountered when conducting the impulse and step change tracer experiments. The limitations of the tracer studies can be considered limitations of the respective methodologies as they depend on the tracer studies for data generation; and
5. To critically assess the mathematical techniques which the modelling methodologies employ.

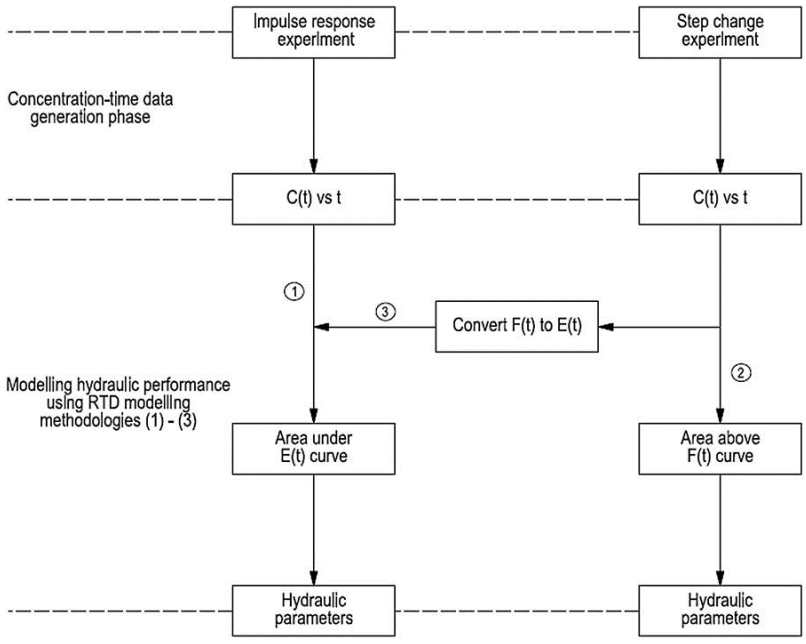


Figure 4-1: Overview of the three different RTD modelling methodologies used in this study. The initial phase consists of data generation in the form of the hydraulic tracer study being performed on the wetland system and subsequent development of the concentration-time curve. The second phase consists of data processing and various numerical methods to obtain the hydraulic characteristics of the system.

4.3.5. Materials and methods

4.3.5.1. Overview of theoretical framework for modelling methodologies

In Figure 4-1 an overview is provided of the necessary steps involved in each of the three RTD modelling methodologies. Modelling methodology (1) is referred to as the impulse response modelling methodology and requires concentration-time data generated from an impulse response experiment. Methodologies (2) and (3) are called the step change integral modelling methodology and the step change derivative modelling methodology, respectively. These two approaches require concentration-time data generated from a step change tracer experiment. The sections which follow describe each step in more detail.

4.3.5.2. Generating concentration-time data using tracer experiments

A flow tracer study is a stimulus-response experiment (Chazarenc et al., 2003), in which an inert soluble tracer is injected either as an impulse or as a step change in concentration into the system inlet pipe and the tracer concentration is measured continuously at the system outlet. The data are then fed into the modelling methodologies to ascertain the flow characteristics of the system. In Figure 4-2 generic concentration-time curves generated from the impulse and step change tracer experiments are shown.

The nominal residence time of fluid inside the system is calculated according to Eq. 4-2 (Fogler, 1999):

$$\tau = \frac{V}{\dot{v}} \qquad [4_2]$$

The reactor volume must account for the bed porosity, which is determined using Eq. 4-3 (Alcocer et al., 2012):

$$V = hBL\varepsilon \qquad [4_3]$$

A successful tracer study requires the flow to be in the laminar range (Sheridan et al., 2014a, Sheridan et al., 2014b), which is the case when the Reynolds number is less than 10 (Miller and Clesceri, 2002). The Reynolds number for packed beds is given by Eq. 4-4 (Subramanian, 2004):

$$Re_p = \frac{D_p u_s \rho}{(1-\varepsilon)\mu} \qquad [4_4]$$

The superficial velocity is determined using Eq. 4-5 (Mayo, 2014):

$$u_s = \frac{\dot{v}}{hB} \qquad [4_5]$$

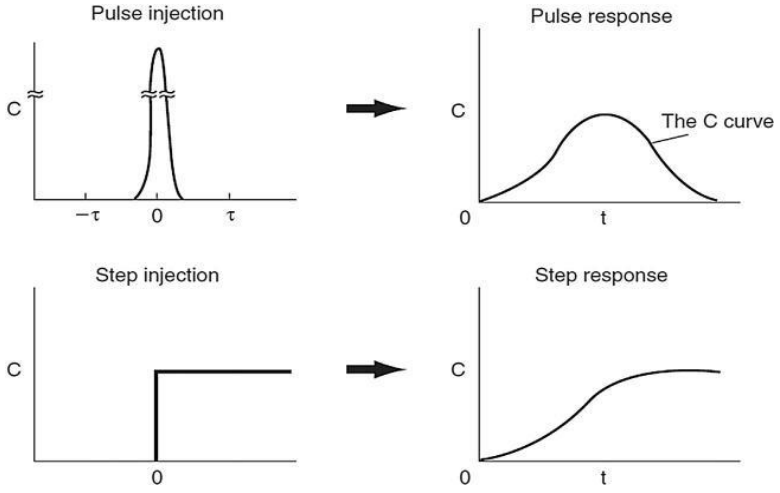


Figure 4-2: Generic concentration-time data generated from the impulse and step change tracer experiments (Fogler, 1999). The response curves of both the impulse and step change tracer experiments typically differ considerably from their corresponding injection curves which indicates non-ideal flow patterns such as dispersion and short-circuiting effects.

4.3.5.3. Modelling hydraulic performance using RTD modelling methodologies

The RTD modelling methodologies outlined in Figure 4-1 use the concentration-time data generated from the flow tracer study experiments to calculate the mean residence time of the fluid inside the reactor system as well

as the variance, which provides an indication of the flow inhomogeneity's around the mean hydraulic residence time. The sections which follow describe the mathematical techniques which each approach uses in the modelling process.

Methodology 1: impulse response modelling methodology

The residence time distribution function, E(t), is determined from the concentration-time curve at the system outlet according to Eq. 4-6. A visual description of the mathematical relationship between the two curves is presented in

Figure 4-3.

$$E(t) = \frac{C(t)}{\int_0^\infty C(t)dt} \qquad [4_6]$$

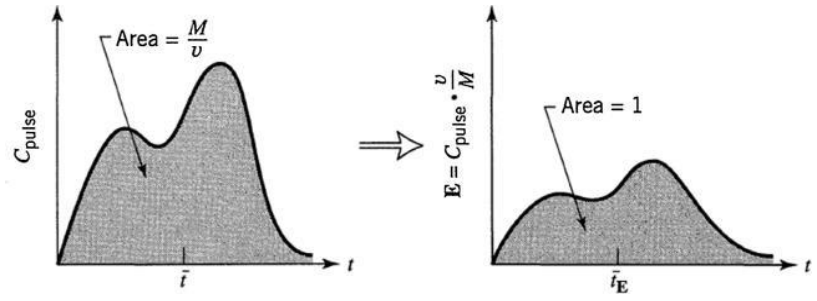


Figure 4-3: The relationship between the concentration-time curve and the RTD function used in the impulse response modelling methodology (Levenspiel, 1999a). The mathematical transformation includes computing the area underneath the concentration-time curve and hence the use of numerical integration techniques such as Simpson's integration formulae.

The mean residence time of the fluid is then calculated using E(t) as shown in Eq. 4-7:

$$\bar{t}_m = \int_0^\infty tE(t)dt \qquad [4_7]$$

The variance is calculated using Eq. 4-8:

$$\sigma^2 = \int_0^\infty t^2E(t)dt - \bar{t}_m{}^2 \qquad [4_8]$$

The recovery of tracer is determined using Eq. 4-9:

$$\% \text{ recovery} = \frac{\dot{v}\int_0^\infty C(t)dt}{M} \times 100 \qquad [4_9]$$

Methodology 2: step-change integral modelling methodology

The cumulative distribution curve, F(t), is constructed based on the concentration-time curve using the relation provided in Eq. 4-10:

$$F(t) = \frac{C(t)}{C_{max}} \qquad [4_10]$$

The mean residence time is determined from the F(t) curve, as shown in Eq. 4-11 and in Figure 4-4.

$$\bar{t}_m = \int_0^\infty [1 - F(t)]dt \qquad [4_11]$$

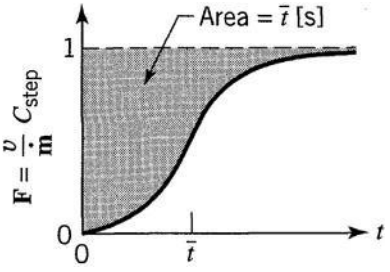


Figure 4-4: Determining the mean residence time of the fluid by computing the area above the F(t) curve (Levenspiel, 1999a).

The variance is then determined using Eq. 4-12:

$$\sigma^2 = \int_0^\infty t[1 - F(t)]dt - \bar{t}_m{}^2 \qquad [4_12]$$

Methodology 3: step-change derivative modelling methodology

The step-change derivative methodology requires differentiating the F(t) curve to obtain the E(t) curve as shown in Eq. 4-13 and Figure 4-5.

$$E(t) = \frac{dF(t)}{dt} \qquad [4_13]$$

Once the E(t) curve is obtained, Eq. 4-7 and Eq. 4-8 are then used to determine the mean residence time and the variance, respectively.

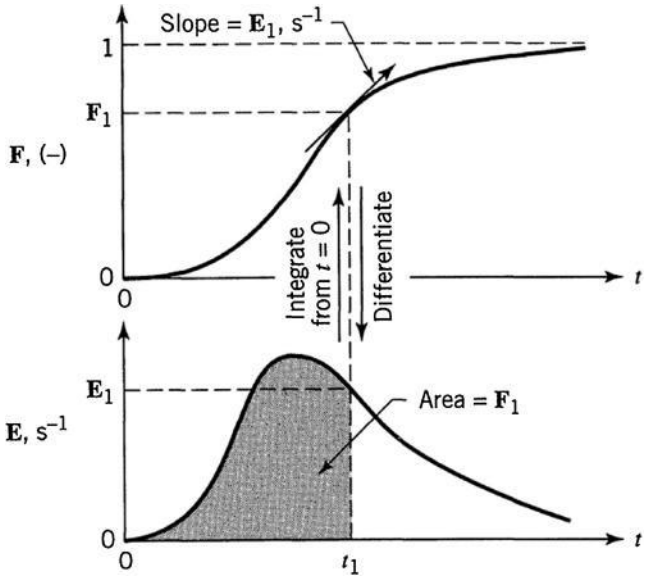


Figure 4-5: The relationship between the RTD function, E(t), and the cumulative distribution function, F(t) (Levenspiel, 1999a). The conversion of F(t) to E(t) requires the use of numerical integration techniques such as the central difference approximation.

4.3.5.4. Using $\bar{t}_m$ and σ^2 to generate additional hydraulic performance parameters

Normalizing the E(t) and F(t) curves

The reversible property of flow in the laminar flow region makes it possible to normalize the E(t) and F(t) curves with respect to time. This is useful for comparing hydraulic data generated at different experimental flow rates and comparing hydraulic performance of systems with different volumetric capacities (Lange et al., 2011, Wahl et al., 2010). The data set is normalized by converting it into dimensionless variables as is shown in Eq. 4-14 through Eq. 4-16 (Fogler, 1999).

$$\theta = \frac{t}{\bar{t}_m} \qquad [4_14]$$

$$E(\theta) = \bar{t}_m E(t) \qquad [4_15]$$

$$F(\theta) = F(t) \qquad [4_16]$$

where θ effectively represents the number of reactor volumes of fluid which have flowed through the system at a particular point in time.

Developing the tanks in series (T-I-S) model

The hydraulic data generated from each of the modelling methodologies can be used to determine the number of ideal, equally sized continuously stirred tank reactors (CSTRs) in series that will give the same residence

time distribution as that of the system under study (Levenspiel, 1999a). A demonstration of this rationale is provided in Figure 4-6.

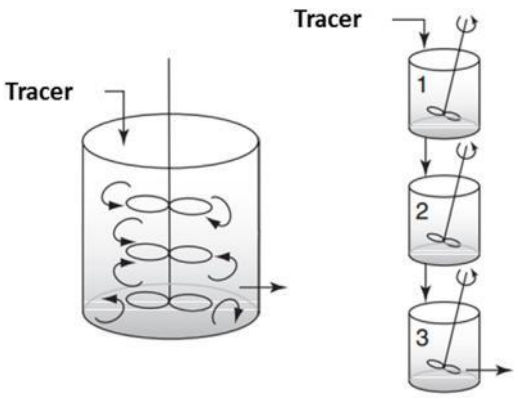


Figure 4-6: TIS model demonstrated for the real reactor (left) using a combination of idealised tanks in series (right). Adapted from (Fogler, 1999).

The number of tanks in series, n, is determined using Eq. 4-17:

$$n = \frac{\bar{t}_m{}^2}{\sigma^2} \qquad [4_17]$$

A graphical interpretation of the model is provided in Figure 4-7. As n → 1, the hydrodynamics approach completely mixed flow. As n → ∞, the hydrodynamics approach ideal plug flow behaviour.

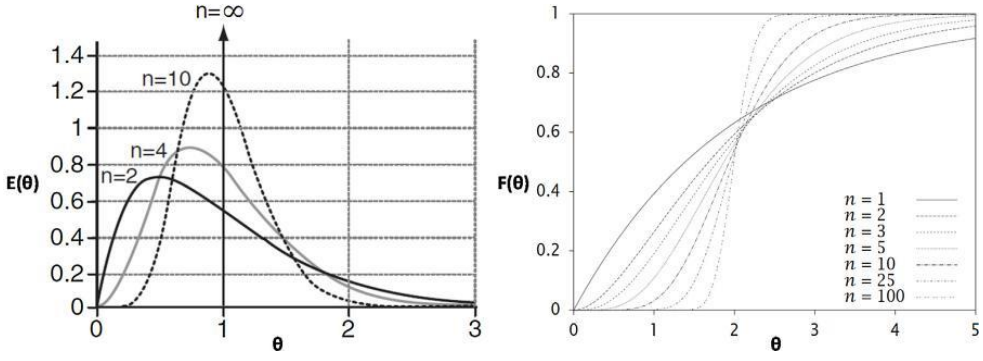


Figure 4-7: Normalized E(t) (left) and F(t) (right) curves for different values of n (Fogler, 1999). As the number of stirred tanks in series increases the system approaches plug flow behaviour whereas the number of tanks in series approach unity the degree of back mixing increases and the system resembles a completely stirred tank reactor.

Developing the dispersed plug flow model

The dispersed plug flow model allows for packed bed reactors to be modelled as plug flow reactors with a certain degree of back mixing by adjusting the mass balance to include a dimensionless dispersion number (Levenspiel, 1999a). The dispersion number is defined using Eq. 4-18 (Fogler, 1999).

$$D = \frac{\text{rate of transport by diffusion}}{\text{rate of transport by convection}} = \frac{1}{Pe} \quad [4_18]$$

Pe can be determined using the correlation provided in Eq. 4-19:

$$\frac{\sigma^2}{\bar{t}_m{}^2} = \frac{2}{Pe} - \frac{2}{Pe^2}(1 - e^{-Pe}) \quad [4_19]$$

As Pe decreases, the amount of axial dispersion inside the system increases and the hydrodynamics approach completely mixed flow. As Pe increases, the axial dispersion decreases and the system approaches plug flow behaviour.

Effective volume utilization

The effective volume ratio indicates how much of the reactor volume is being utilised to provide the necessary contact between the fluid and bed matrix. The portion of the reactor which is not being used for this purpose is considered dead volume (Albertini et al., 2012). It is calculated using Eq. 4-20 (Thackston et al., 1987):

$$e = \frac{\bar{t}_m}{\tau} = \frac{V_{eff}}{V} \quad [4_20]$$

Hydraulic efficiency

Hydraulic efficiency is used to evaluate the hydraulic performance of non-ideal reactors, with ideal plug flow systems being 100% efficient (Wahl et al., 2010). The hydraulic efficiency can be described as the capacity of a reactor to utilize its entire volume by uniformly distributing flow to maximize residence time (Holland et al., 2004). One of the most commonly used correlations is that provided by Persson et al. (1999) and is shown in Eq. 4-21.

$$\lambda = e\left(1 - \frac{1}{n}\right) \quad [4_21]$$

4.3.5.5. Experimental apparatus description

The packed bed reactors used in this study were HSSF CWs located at the Industrial and Mining Water Research Unit (IMWaRU) facility at the University of the Witwatersrand, Johannesburg. Both systems were built using

HDPE external support troughs and then filled with dolomite gravel (mean particle size 20 mm). The reactors had a length of 4.2 m, width of 0.9 m and depth of 0.7 m.

Thirteen sample ports, constructed from PVC mesh (mesh opening = 20 mm), were installed into both systems in order to accommodate sampling within different regions of the CWs. Three lengths of silicon tubing were cut and attached to each of the sampling wells using cable ties so that samples could be drawn from three different depths, ultimately resolving each system into a three-dimensional grid. The projected surface (normal to the feed) was divided into regions A, B and C. Each system was also divided into Zones 1 to 5 down its length. The spatial distribution of the sampling points, inlet and outlet ports, as well as the designated zones is provided in Figure 4-8.

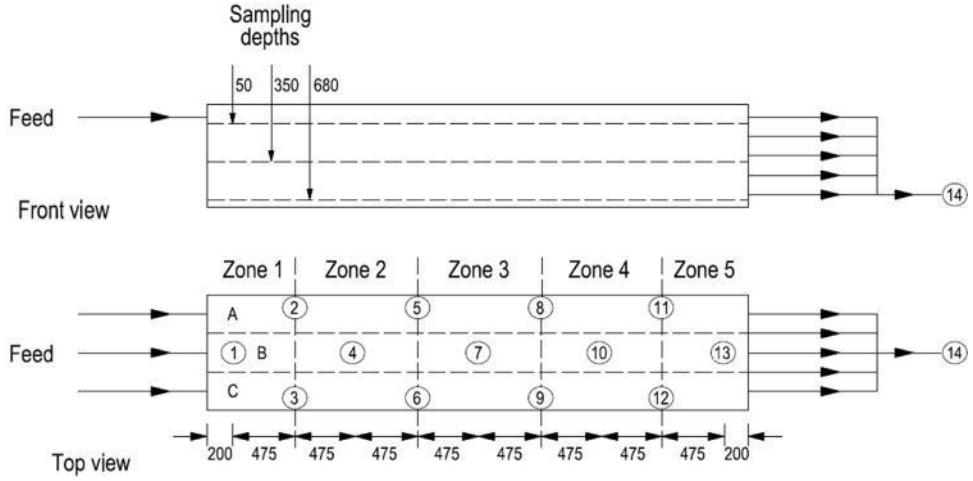


Figure 4-8: Spatial arrangement of inlet, outlet and internal sampling ports as well as the system grid resolution. All dimensions are expressed in mm. Samples were taken from three different depths within each of the thirteen sampling wells as well as at the system outlet.

Planted wetland vegetation

Each of the five zones within the planted CW contained a different species of vegetation. Polyculture was selected over monoculture due to better treatment performance reported in literature (Karathanasis et al., 2003). Images of the different plant species within the system are provided in Figure 4-9. All of the five species are indigenous to South Africa (Coetzee et al., 1999, Kritzinger et al., 1997, Reinten et al., 2011, Rubin et al., 2001, Schiegl et al., 2004). Zone 1 was planted with *Zantedeschia aethiopica* due to their tolerance of various types of high-strength wastewaters (Zurita et al., 2006). Each subsequent zone was planted with a species which had a successively lower tolerance for impacted water (Tanner, 1996).



Zone 1 *Zantedeschia aethiopica* | Zone 2 *Cyperus papyrus nana* | Zone 3 *Typha capensis* | Zone 4 *Juncus effusus* | Zone 5 *Chondropetalum tectorum*

Figure 4-9: Zonal distribution of wetland vegetation in planted system. Five different species were used and were strategically planted according to their tolerance of wastewater with the more resistant species planted towards the inlet of the wetland where higher contaminant concentrations would be expected.

4.3.5.6. Determining system porosity

The presence of plant root structures decreases the pore volume of subsurface flow systems and has been discussed extensively (Knowles et al., 2011). Thus, despite both systems used in this study having the same external physical dimensions their internal effective volumes had the potential to differ. A porosity test was performed on both systems prior to the hydraulic tracer studies. First, both systems were drained completely and the inlet and outlet valves were closed. A hosepipe, fitted with a flow meter (Gardena, Germany), was inserted into sampling port l and each system was filled until the water level coincided with the gravel bed surface. The total volume measured by the flow meter represented the effective volume of each system. The porosity was determined by dividing this effective volume by the total volume of the system.

4.3.5.7. Experimental flow rate

The inflow and outflow rates were measured once every 30 min, with the average flow rates for each of the experiments shown in Table 4-1.

Table 4-1: Average flow rates used for hydraulic tracer studies as well as the nominal retention time for each experiment.

Experiment	System	Average flow rate (l/min)	τ (min)
Impulse	Unplanted	4.59	268
	Planted	4.30	264
Step change	Unplanted	4.39	281
	Planted	4.13	275

4.3.5.8. Tracer studies

Both the impulse and the step-change tracer experiments were conducted concurrently throughout the month of June 2015. FWT Red fluorescent dye (Cole-Parmer, USA) was used as the tracer for both sets of tracer studies.

Impulse response tracer studies

Prior to the commencement of each experiment, a 5 m^3 vertical cylindrical feed tank was completely filled with tap water and the tank outlet connected to the CW inlet. The CW inlet and outlet valves were opened to allow the inflow and outflow rates to equalise. A tap continuously supplied water to the feed tank in order to maintain a constant hydrostatic pressure and, hence, constant feed flow rate to the systems. Once the flow rates had equalized, 30 ml of FWT Red was injected into the feed line to the CW. Samples were collected through ports 1 to 14 for the duration of the experiment. A dynamic sampling regime was designed to maximize the resolution of the concentration-time curves (Headley and Kadlec, 2007). A summary of the sampling regime employed is presented in Table 4-2.

Table 4-2: Dynamic sampling regime employed for the impulse tracer studies where X indicates a sample being taken

Time (min)	Ports 1-4	Ports 5-7	Ports 8-13	Port 14
0	X	X	X	X
10	X	X		
20	X	X		X
30	X	X	X	X
60	X	X	X	X
90	X	X	X	X
120	X	X	X	X
150	X	X	X	X
180	X	X	X	X
210	X	X	X	X
240	X	X	X	X
270		X	X	X
300	X	X	X	X
330			X	X
360	X	X	X	X
420			X	X
480	X	X	X	X
600			X	X
720	X	X	X	X

Step change tracer studies

Two 5 m^3 vertical cylindrical tanks were filled with tap water and 300 ml of FWT Red was then added to each tank. In order to ensure solution homogeneity, one of the feed tanks was fitted with a two-blade agitator extending to the bottom of the tank. A pump (ViaAqua VA-300A, USA) was placed inside the second feed tank such that the contents of both tanks were allowed to circulate for 24 h before commencing the experiments to ensure the tracer was completely mixed. The inlet and outlet flow rates were allowed to equalise, at which time the feed to the CW was switched over from tap water to the tracer solution. A sampling regime was also designed to maximize the resolution of the cumulative concentration-time curves and is presented in Table 4-3.

Table 4-3: Dynamic sampling regime employed for the step change tracer studies where X indicates a sample being taken

Time (min)	Ports 1-4	Ports 5-6	Port 7	Ports 8-9	Ports 10-13	Port 14
0	X	X	X	X	X	X
15	X	X	X			
30	X	X	X			X
60	X	X	X	X		X
90	X	X	X	X	X	X
120	X	X	X	X	X	X
150	X	X	X	X	X	X
180	X	X	X	X	X	X
210		X	X	X	X	X
240		X	X	X	X	X
270	X	X	X	X	X	X
300	X	X	X	X	X	X
330			X	X	X	X
360	X	X	X	X	X	X
390				X	X	X
420	X	X	X	X	X	X
480	X	X	X	X	X	X
540				X	X	X
600	X	X	X	X	X	X
720	X	X	X	X	X	X

4.3.5.9. Sample analysis

Samples were not pre-treated and were analysed within 48 h of collection. A spectrophotometer (Merck Spectroquant Pharo 300) was used to measure the absorbance of each sample at 550 nm. Plastic cuvettes with a path length of 10 mm were filled with sample solution and inserted into the spectrophotometer to obtain the absorbance data. Absorbance readings were converted into concentration values by constructing a calibration curve, which had an R^2 of 0.99.

4.3.6. Results and discussion

4.3.6.1. Determining hydraulic performance parameters using each modelling methodology

The RTD functions obtained from the impulse experiments, as well as the cumulative distribution functions obtained from the step-change experiments, are shown in Figure 4-10. These functions were plotted using data obtained from the system outlets.

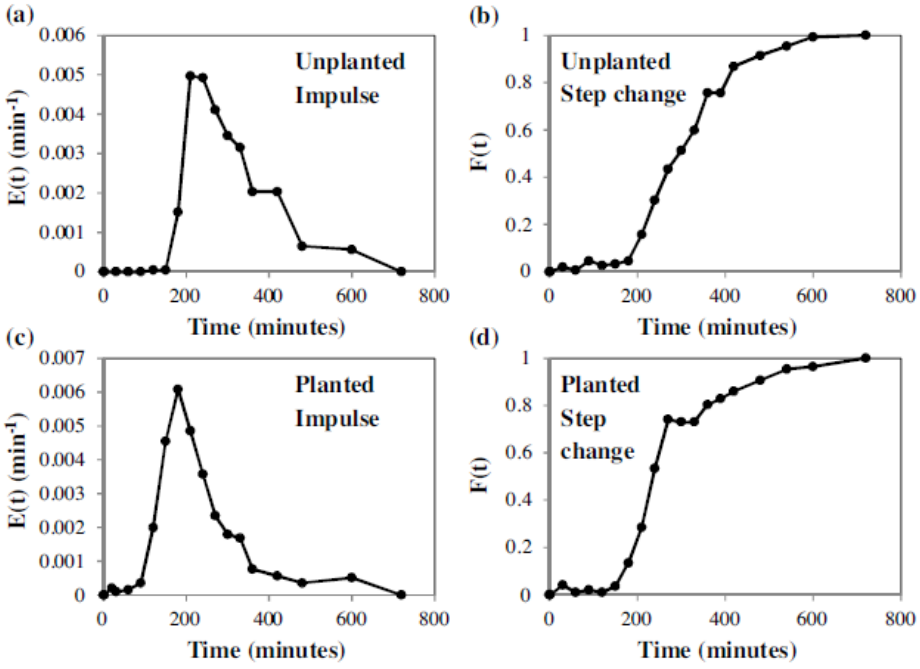


Figure 4-10: E(t) and F(t) curves from the impulse and step change experiments, respectively. In Fig. 10(a) and (c) hydraulic data from the impulse response experiment on unplanted and planted systems are presented respectively and likewise in Fig. 10(b) and (d) using the step change response experiment.

Each of the curves in Figure 4-10 displayed a time delay between injection and breakthrough of the tracer at the system outlet. For the impulse response experiments, this was approximately 180 min for the unplanted system and 120 min the planted system. The time delay was closer to 210 min for the unplanted step-change experiment and 180 min for the planted step-change experiment. The well-defined peak and long tail found for both the planted and unplanted impulse response curves is indicative of deviation from plug flow behaviour. Researchers have found this to be the case in other wetland systems with similar system properties using hydraulic tracer studies (García et al., 2004, Sheridan et al., 2014a, Sheridan et al., 2014b). The finite element model used by Knowles and Davies (2010) to describe hydraulic flow patterns in an HSSF CW with similar system dimensions and packed material also suggested similar results and was attributed to the spatial variation of hydraulic conductivity as a result of clogging processes. The model described a stagnant region of water near the inlet and a rapidly advancing front along the surface of the bed which subsequently percolates through the bed and then exits the system much faster than the pockets of fluid which were trapped near the inlet.

The E(t) and F(t) curves were used to calculate the hydraulic parameters of the two systems; the results of which are shown in Table 4-4.

Table 4-4: Calculated hydraulic parameters for the planted and unplanted systems using the impulse and step change modelling methodologies

Parameter	Unplanted			Planted		
	Impulse	Step change		Impulse	Step change	
		Derivative	Integral		Derivative	Integral
ε (%)	47	47	47	43	43	43
V_{eff} (l)	1 231	1 231	1 231	1 136	1 136	1 136
$\dot{v}$ (l/min)	4.59	4.39	4.39	4.30	4.13	4.13
τ (min)	268	281	281	264	275	275
Tracer recovery (%)	100			100		
$\bar{t}_m$ (min)	319	311	309	259	265	277
σ^2 (min)	11 071	11 927	11 726	17 333	13 257	14 845
N	9	8	8	4	5	5
Pe	17.12	15.38	15.38	6.67	9.52	9.52
e	1.19	1.11	1.10	0.97	0.96	1.01
λ	1.06	0.97	0.97	0.73	0.78	0.81

The planted system had a 4% lower porosity and this can explain why it was calculated to have a smaller V_{eff} when compared to the unplanted system. The lower porosity could be attributed to the presence of the plant roots in the bed voids and is consistent with results obtained by other researchers (IWA, 2000). The tracer studies were conducted approximately six weeks after planting. Consequently, root zone growth was still in the initial development phase (Tanner, 1996). It is expected that the root zone will develop over the next six months as a result of the correct supply of nitrogen and phosphorus as key nutrients for the wetland plants (Ong et al., 2010) as well as the start of the Southern Hemisphere Spring in the month of September. The growth process should increase the plant root density in the bed voids and hence contribute to further reductions in porosity (Knowles et al., 2011).

A tracer mass recovery of approximately 100% was obtained for both impulse response experiments, indicating that sufficient time was allocated for the tracer studies. This is a consequence of automated sampling. There is further evidence of this in Figure 4-10, in which the E(t) curves reached a value of zero and the F(t) curves reached a value of 1 within 720 min.

All three modelling methodologies suggested smaller values for N and Pe for the planted system when compared to the unplanted system; implying that the planted system had a higher degree of back mixing. Similar values for N and Pe have been reported for other horizontal subsurface flow systems having similar bed porosities and compositions (Ríos et al., 2009).

For each of the experiments, the mean residence time ($\bar{t}_m$) was comparable with the nominal retention time (τ), resulting in an effective volume utilization (e) close to and, in some cases, greater than 1. The effective volume utilization figures are higher than those reported in literature for other horizontal subsurface flow systems (El

Hamouri et al., 2007, Sheridan et al., 2014a, Sheridan et al., 2014b, Suliman et al., 2006a, Suliman et al., 2006b). For instance, the system studied by Sheridan et al. (2014a,b) had outlet ports level with the inlet port and at a single depth; thereby inducing a hull-shaped flow profile and, thus, a larger dead zone volume. In this study, the configuration of the outlet ports allowed the fluid to exit the system at a multitude of depths and, in effect, created an open boundary.

The hydraulic efficiency parameter (λ) depends on the magnitudes of N and e. The lower degree of back mixing and higher effective volume utilization resulted in a higher hydraulic efficiency for the unplanted system, for all three modelling approaches.

4.3.6.2. Building the modelling methodology comparison: evaluating the results obtained from the three modelling approaches against ideal theoretical conditions

Since the flow rates were slightly different for each experiment, they have been normalized with each other. This was possible because in the laminar flow region the physical properties could be reversed. Both experiments were scaled to a flow rate of 4.5 l/min, with the results shown in Table 4-5 and Table 4-6 for the unplanted and planted systems, respectively. The other hydraulic parameters have not been scaled and remained the same as those presented in Table 4-4.

Table 4-5: Comparison of hydraulic parameters for the unplanted system, scaled to a flow rate of 4.5 l/min

Parameter	**Impulse**	**Step change**	
		Derivative	**Integral**
$\dot{v}$ (l/min)	4.5	4.5	4.5
τ (min)	274	274	274
$\bar{t}_m$ (min)	325	304	302
N	9	8	8
Pe	17.12	15.38	15.38
e	1.19	1.11	1.10
λ	1.06	0.97	0.97

Table 4-6: Comparison of hydraulic parameters for the planted system, scaled to a flow rate of 4.5 l/min

Parameter	**Impulse**	**Step change**	
		Derivative	**Integral**
$\dot{v}$ (l/min)	4.5	4.5	4.5
τ (min)	252	252	252
$\bar{t}_m$ (min)	247	243	254
N	4	5	5
Pe	6.67	9.52	9.52
e	0.98	0.96	1.01
λ	0.73	0.78	0.81

Unplanted system

$\bar{t}_m$ was greater than τ for each of the modelling methodologies, resulting in an effective volume utilization greater than 100% in each case. All three methodologies, thus, indicated an absence of dead zones and short circuiting effects within the system, which are phenomena that should be avoided in the design of subsurface flow CWs and heterogeneous reactors in general (Chazarenc et al., 2003, Mendoza et al., 2013). Evaporative processes can also reduce subsurface fluid velocities, resulting in experimental retention times being longer than their theoretical equivalents (Headley et al., 2012) and might be a cause of an effective volume utilization greater than 100%. The step-change modelling techniques indicated an almost identical $\bar{t}_m$, which is 11% higher than τ. The impulse response technique indicated a $\bar{t}_m$ which was 19% greater than the τ. Both step-change techniques estimated the same values for N and Pe, whereas the impulse modelling technique suggested a lower degree of dispersion, with an 11.3% higher Pe and an extra CSTR in series.

Planted system

Each methodology produced a different $\bar{t}_m$ for the planted system. The step change integral technique indicated a $\bar{t}_m$ higher than the τ, resulting in an effective volume utilization slightly higher than 100%. The step-change derivative and impulse techniques both indicated a $\bar{t}_m$ smaller than the theoretical retention time, resulting in a dead volume of 4% and 2% for the two techniques, respectively. Nevertheless, both step change techniques estimated the same degree of back mixing within the system, indicated by the same values for N and Pe. The impulse technique suggested a higher degree of back mixing, reflected by a 30% lower Pe and one less CSTR placed in series. All three techniques reported hydraulic efficiencies lower than 100% and these are attributed to the high degree of dispersion within the system.

4.3.6.3. Building the modelling methodology comparison: practical limitations of the tracer studies

Capturing sufficient concentration-time data for adequate definition of system response

There were a lack of data points in the region surrounding the peak of the E(t) curve for the unplanted system, as seen in Figure 4-10. This may have affected the shape of the response, as well as the hydraulic parameters calculated for the system. Researchers remark that this can be a likely occurrence, even with a well-designed sampling regime put in place (Teefy, 1996). The step-change experiment has no such drawback. This is shown by the consistent distribution of data points on the F(t) curves, for both planted and unplanted system, in Figure 4-10.

Effect of tracer dispersion on concentration-time curves derived from tracer experiments

In Figure 4-11and Figure 4-12 the RTD curves and the cumulative distribution curves from sampling ports 1, 4, 7, 10 and 13 from the impulse and step change experiments are presented, respectively. In each of Figure

4-11 (a)–(f) the peak of the response was largest in magnitude at 0.2 m where after it broadened as the tracer travelled through the reactor. In Figure 4-12 (a)–(f) the gradient of the response curve was steepest at 0.2 m and then flattened out with each successive sampling port. These trends observed in Figure 4-11 and Figure 4-12 are indicative of dispersion of tracer as it moved through the system and has been confirmed by other researchers conducting hydraulic studies on HSSF CWs (Sheridan et al., 2014a, Sheridan et al., 2014b).

The cumulative distribution curve obtained from the sampling port at a length of 4 m in Figure 4-12 (f) experienced an unexpected increase in gradient between 210 and 240 min, where after it returned to the trend observed before 210 min. This suggests short-circuiting behaviour (Sheridan et al., 2011). The corresponding impulse response curve had broadened to the extent that it was difficult to identify multi-modal distributions. This was also the case at a length of 4 m in Figure 4-11 (a) and Figure 4-12 (a). Tracer dispersion can thus affect the qualitative description of the reactor hydraulics when using the impulse response experiment and may also have a knock-on effect when quantifying the hydraulic parameters using the impulse response modelling methodology.

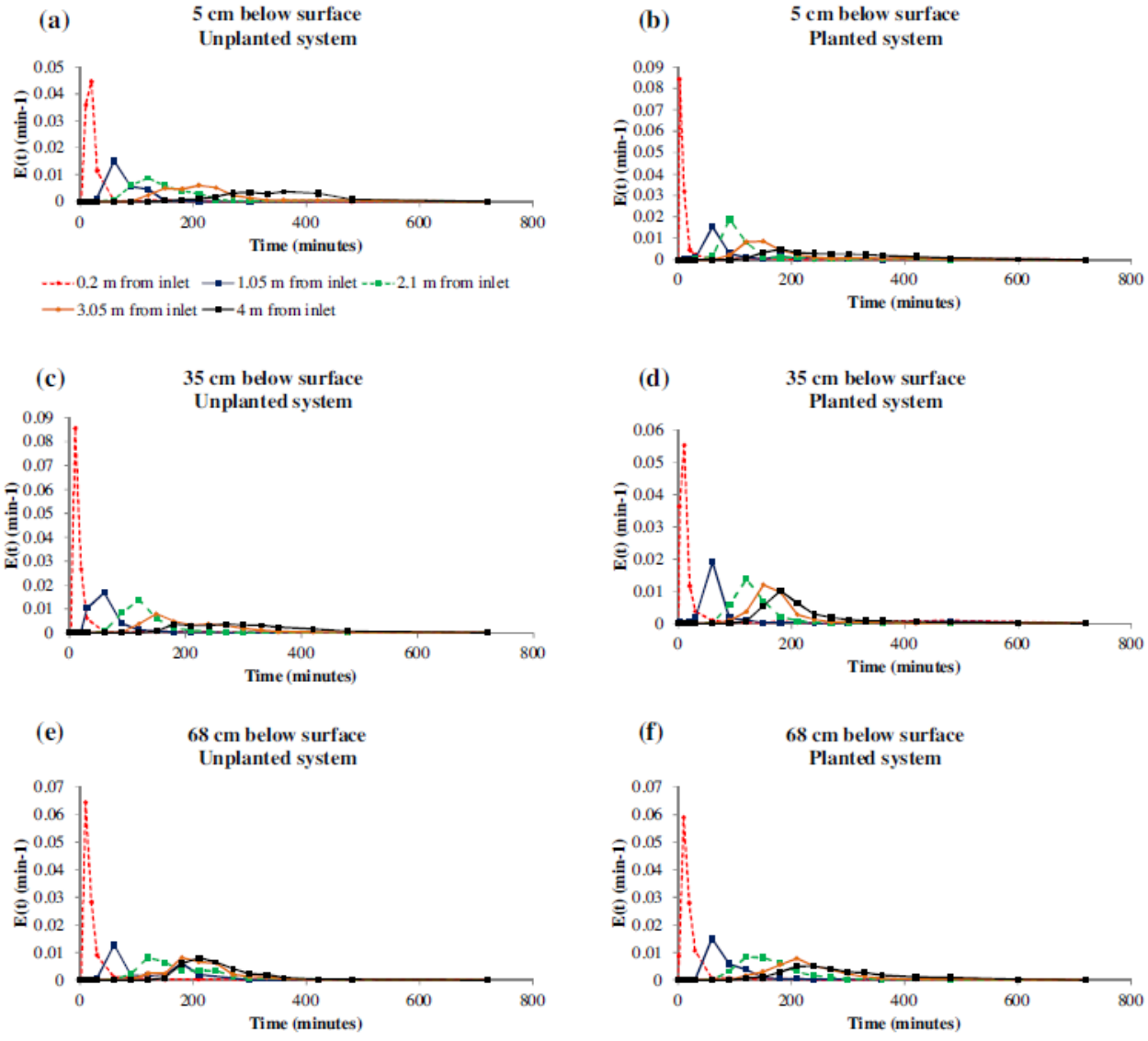


Figure 4-11: RTD curves from the impulse experiments on the planted and unplanted systems. In Figures (a) and (b) hydraulic data from the surface layer are presented. In Figures (c) and (d) data from the intermediate layer are presented and in Figures (e) and (f) data from along the bottom of the wetland bed are presented. Each curve within the figures represents hydraulic data collected from a sampling point a specified distance from the system inlet thus allowing for the evolution of the RTD curve to be depicted as a function of system length.

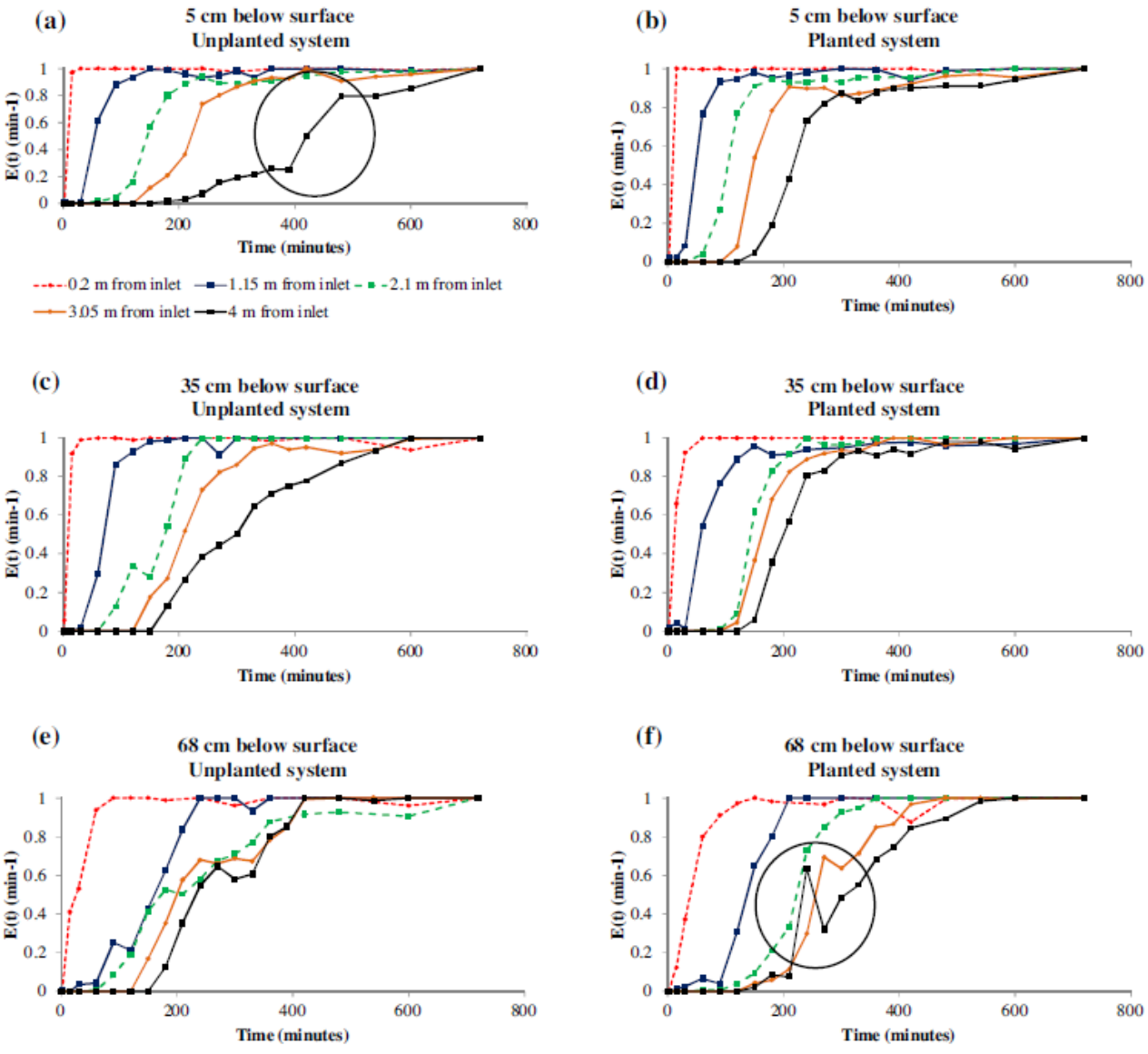


Figure 4-12: Cumulative distribution curves from the impulse experiments on the planted and unplanted systems. In Figures (a) and (b) hydraulic data from the surface layer are presented. In Figures (c) and (d) data from the intermediate layer are presented and in Figures (e) and (f) data from along the bottom of the wetland bed are presented. Each curve within the figures represents hydraulic data collected from a sampling point at a specified distance from the system inlet.

4.3.6.4. Building the modelling methodology comparison: critical assessment of the mathematical techniques used by modelling methodologies

Modelling approach sensitivity to selection of numerical integration procedure

Each modelling approach required numerical integration for the computation of the hydraulic parameters and for this study, Simpson's 1/3 rule was selected. The method works by approximating the curve as a parabola in

multiple equally sized subintervals. The areas under the parabolas are then evaluated and summed together to arrive at the approximation provided in Eq. 4-22 (Pozrikidis, 1998).

$$I = \frac{h}{3}[f(x_0) + 4f(x_1) + 2f(x_2) + \cdots + 4f(x_{n-1}) + f(x_n)] \quad [4_22]$$

where:

$$h = \frac{b - a}{2} \quad [4_23]$$

with n being the number of equally sized subintervals.

The number of subintervals used is left to the discretion of the user and can range from using one interval in which $h = a - b = x_n - x_0$, to the maximum number of subintervals possible in which a minimum of three data points are required viz. $h = \frac{a-b}{2}$. It would thus be desirable for the modelling approach to display the least sensitivity as possible to the number of subintervals employed as it would allow the user to have more confidence in the final answer.

The hydraulic parameter $\bar{t}_m/\tau$ was calculated for different sizes of subintervals to determine how sensitive each modelling approach was to the subinterval selection with the results presented in Figure *4-13*. Each modelling approach displayed a degree of sensitivity to the subinterval selection. For both systems the step change derivative approach was the least sensitive, with a 1% and 4% variation in $\bar{t}_m/\tau$ for the planted and unplanted system, respectively. The other two approaches displayed higher degrees of sensitivity. For example, the impulse response modelling methodology suggested a value of 0.86 for $\bar{t}_m/\tau$ and hence a 14% dead volume for the planted system when one subinterval is used and this changes to a $\bar{t}_m/\tau$ of 0.98 and hence a 2% dead volume when 3-point subintervals are used. A similar variation in $\bar{t}_m/\tau$ was seen for the unplanted system when using the step change integral route.

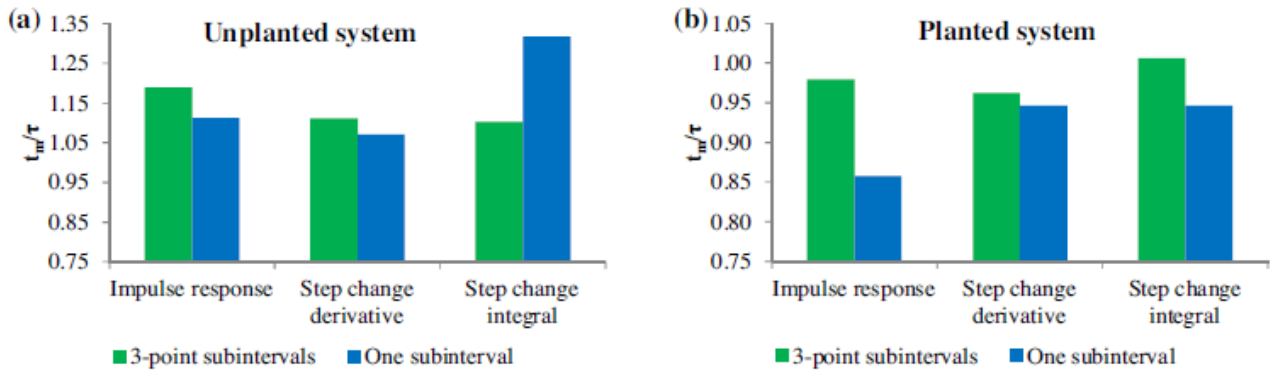


Figure 4-13: Comparison of $\bar{t}_m/\tau$ for when 3-point subintervals and when one subinterval is used for numerical integration using Simpson's 1/3 rule. The comparison performed on the hydraulic data obtained from the unplanted system is presented in Fig. 13(a) and for the planted system in Fig. 13(b) and is performed in each case for the impulse response as well as the step change derivative and step change integral modelling approaches.

Modelling approach sensitivity to noisy data generated during data collection phase

Both impulse and step change experiments are capable of generating noisy data, particularly during the sample analysis procedure. At very low concentrations of tracer the relative contribution of background noise to the absorbance measurement is large. Background noise in the system may be caused by slight scratches on the cuvettes or from the presence of fine suspended solids in the sample which deflect the light beam and alter the Spectroquant reading. It would thus be expected that the F(t) curves used for the step change derivative modelling approaches and the C(t) curve used for the impulse response approach would have contained some degree of noise.

In Figure 4-14 (a) and (b), E(t) from the step change derivative and impulse response approaches were compared. In the region 0 < 0 < 0.5, E(t) from the step change derivative approach was noisier than E(t) from the impulse experiment and this was the case for both reactor systems. This may be attributed to the differentiation of F(t) to obtain E(t) as differentiating noisy data amplifies the noise (Bequette, 2003) and transfers it to the next stage of the modelling process. The step change derivative approach was thus more sensitive to noisy data compared to the other two approaches, and could potentially contribute to inaccuracies in computing the hydraulic performance parameters.

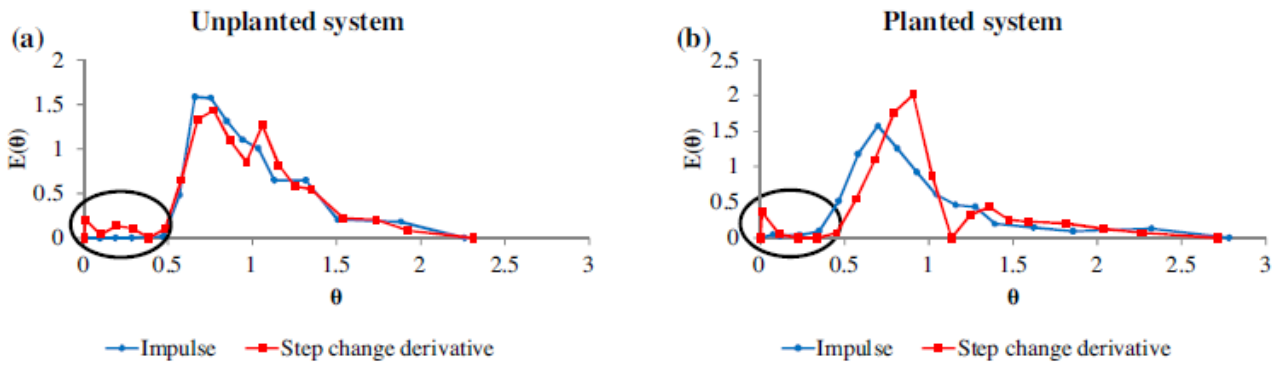


Figure 4-14: Normalized E(t) for planted and unplanted systems with regions of noise highlighted on the E(t) curves from the step change derivative approach.

4.3.7. Conclusion

Sizing of constructed wetlands for wastewater treatment requires the integration of treatment kinetics into a reactor model which attempts to reflect the non-ideal flow behaviour through the packed media. One way to build the reactor model is to conduct RTD studies on a pilot scale system. In this paper three different RTD modelling methodologies were compared using two pilot scale HSSF CWs. These were the impulse response, step change integral and step change derivative modelling methodologies. Impulse response and step change tracer experiments were conducted to generate the concentration-time data for the impulse response and step change modelling methodologies, respectively. Hydraulic parameters were then calculated for the two systems using each of the modelling approaches. The comparison between the modelling approaches was then built by attempting to meet the following research objectives:

- To compare the hydraulic parameters obtained using each of the three approaches against each other and ideal theoretical conditions. For the unplanted system, we found that $\bar{t}_m$ was greater than 'r for each of the modelling methodologies. The two step change modelling methodologies suggested the same fluid flow behaviour reflected by almost identical values for $\bar{t}_m$ and the same values for N and Pe. The impulse modelling methodology indicated a 7% higher $\bar{t}_m$ compared to the step change modelling approaches and a lower degree of dispersion. Each modelling methodology suggested different hydraulic behaviour for the planted system. Both step change methodologies quantified the same degree of dispersion for the system; however the step change integral approach determined a $\bar{t}_m$ slightly greater than τ and thus no dead volume in the system whereas the step change derivative approach determined a 4% dead volume caused by $\bar{t}_m$ being slightly less than τ. The impulse response modelling methodology suggested a higher degree of dispersion than both step change modelling approaches and a 2% dead volume for the system.

- To identify practical limitations encountered when conducting the impulse and step change tracer experiments. The limitations of the tracer studies can be considered limitations of the respective methodologies as they depend on the tracer studies for data generation. Despite a well-designed sampling regime put in place for the impulse response tracer experiment, we were unable to capture sufficient data on the peak of the concentration-time curve for the unplanted system. This affected the shape of the response curve and may have also impacted the modelling results. No such difficulties were encountered with the step change experiments. Sampling down the length of the reactor made it possible to identify another limitation of the impulse response experiment: tracer dispersion had the effect of broadening the impulse response curves to the extent that it was almost impossible to identify non-ideal flow behaviour such as short-circuiting towards the end of the reactor systems. Although tracer dispersion also had an effect on the step change response curves, it was still possible to identify non-ideal flow behaviour which was prevalent in both systems.
- To critically assess the mathematical techniques which the modelling methodologies employ. A sensitivity analysis was performed to determine the effect of changing the size and hence number of subintervals used in Simpson's 1/3 rule for numerical integration on $\bar{t}_m/\tau$ for each modelling methodology. The lower the sensitivity of the modelling methodology the better as choosing a parameter as arbitrary as subinterval size should not have a noticeable effect on reported hydraulic behaviour. The step change derivative modelling methodology was least sensitive for both reactor systems; displaying a 1% and 4% variation in $\bar{t}_m/\tau$ for the planted and unplanted system, respectively. This was in contrast to the $\bar{t}_m/\tau$ determined by the step change integral and impulse response modelling methodologies which varied by 10% or more in some cases. The differentiation of F(t) to obtain E(t) using the step change derivative methodology was identified as a potential weakness as it had the capability of amplifying background noise which may have affected the calculation of the hydraulic parameters. This is due to the sensitivity of the method to the gradient of the line which introduces this.

The ramifications of this comparison are that each modelling methodology has the potential to output a different reactor model for the same system under study which, when combined with kinetic data may produce a different reactor size for the treatment process. Each modelling methodology also has its own strengths and weaknesses. The absence of an analytical answer to the problem means the choice of modelling methodology is ultimately dictated by other criteria such as experimental equipment availability and the reactor designer's confidence in the respective approaches.

Acknowledgements

We wish to thank the School of Chemical and Metallurgical Engineering Workshop at the University of the Witwatersrand for their assistance with the experimental set up. This research was supported by the NRF-DAAD joint research initiative under the project reference SFH14062972489 as well as by the WRC through project K5/2096/3, entitled *Exploring knowledge on natural processes for novel approaches to constructed wetlands design and performance for wastewater*.

Chapter 5 Investigation into the kinetics of constructed wetland degradation processes as a precursor to biomimetic design

5.1. Summary

The following chapter comprises the paper entitled: "Investigation into the kinetics of constructed wetland degradation processes as a precursor to biomimetic design", which was published in Water SA in 2017. This research paper was initially accepted for an oral presentation at the WISA biennial conference held at the Durban ICC in May 2016.

The paper details the very first sets of experiments conducted in the newly established pilot-scale, horizontal subsurface flow CWs, which were important in terms of developing an understanding of the baseline chemical characteristics, fluid flow patterns and the carbon and nitrogen degradation and transformation kinetics. The results of this investigation were used as the basis for improving upon the methodology for the follow-up experiments in 2016.

5.2. Statement of individual contribution

The experimental design, preparation, work and analysis was carried out by myself with Dr Uwe Kappelmeyer advising and overseeing the work at the Helmholtz UFZ in Leipzig Germany. Some of the analytical results (TOC, IC, TC/NPOC and TN) were provided by Frau Puschendorf, who operated the Multi N/C 2100 S analyser (Analytik Jena AC). For a period, Philip Hecht (a student completing his honours in engineering at the University of Dresden and conducting his practical at the Helmholtz UFZ) assisted with the collection of samples in the field. I had the support of Prof. Craig Sheridan and Ricky Bonner in various stages of the method selection, design and write-up phases of this paper.

5.3. Water SA (2017) Vol. 43 No. 4 pp. 655-665

5.3.1. Abstract

As the types of wastewater become more diverse, so the need for more economical, efficient and robust treatment systems emerges. Biomimetic constructed wetlands (CWs) are a green technology solution and could provide a valuable addition to South Africa's ecological infrastructure.

This study involved the characterisation of a start-up, pilot-scale, horizontal subsurface flow CW. The objectives were to break into the CW 'black box', understand the natural baseline state and initial internal development and incorporate biomimetic principles into the design and methodology.

The wetland was left to establish with no external nutrient source. Sample ports were inserted at multiple locations and depths throughout the bed. The background characteristics were determined first, followed by the hydraulic tracer studies and then the introduction of artificial domestic wastewater and a weekly sampling regime. All samples were analysed for dissolved oxygen (DO), pH, redox potential, total organic carbon (TOC) and total nitrogen (TN).

After 18 months, the *Phragmite* root system was well developed; having penetrated to the bottom of the wetland. The residence time distribution at the system outlet showed two distinct peaks before the mean retention time (t_m), indicating channelling. There were multiple small peaks after t_m and a long tail to suggest tracer hold-up and diffusional mixing effects. It was also found that the flow behaviour was commensurate to 6 CSTRs in series. At the baseline, the system displayed average residual TOC and TN concentrations of ±3.0 mg/ℓ and ±1.7 mg/ℓ, respectively, and lower DO and redox potentials were observed in summer than autumn. After the introduction of artificial wastewater, the majority of TOC and TN removal occured in the first half the wetland; accompanied by DO consumption and a drop in potential. The rate of removal was higher in autumn than winter and a temperature-related decrease in the rate constant was observed.

Keywords: constructed wetlands, background analysis, hydraulics, kinetics, biomimicry

5.3.2. Introduction

South Africa is a water scarce country – ranked 30th driest globally (GreenCape, 2016) – with an annual rainfall of just 50% of the world average. The country relies predominantly on water from catchments, rivers, wetlands and aquifers (WWF-SA, 2016). Poor water quality has a major negative impact on the livelihood of all South African citizens, as well as the surrounding ecosystem. Water quality in South Africa's natural resources has declined over the previous two decades; in some cases to such an extent that the water has become a serious health threat. The primary contributors to the pollution of the country's water resources are:

- Release of raw sewage
- Acid Mine Drainage (AMD)
- Release of untreated industrial effluent
- Excess nutrients from agricultural runoff
- Poor service delivery from municipal Water Service Authorities

Without urgent attention, South Africa could be faced with a serious water quality crisis (WWF-SA, 2016).

South Africa's water resources are governed by the Water Services Act of 1997 (RSA, 1997) and the National Water Act of 1998 (RSA, 1998). In line with the requirements of the two water acts and Government's National Development Plan (NDP), the South African Department of Water and Sanitation (DWS) issued the National Water Resource Strategy (NWRS2). The NWRS2 is a water quality management strategy which covers security of water supply, managing environmental degradation and curbing pollution of water resources. The DWS, in conjunction with the South African National Biodiversity Institute (SANBI), has proposed a 19th Strategic Integrated Project (SIP) which will use the 'Investment in Ecological Infrastructure (IEI)' model to find joint ecological and

engineering solutions to South Africa's water treatment challenges (SANBI, 2014). As South Africa works towards developing its ecological infrastructure, opportunity arises to move from centralized to decentralized wastewater treatment facilities, examples of which include point-of-use household technologies, rainwater harvesting installations, grey-water green roofs and water recycling and reclamation systems (GreenCape, 2016).

Constructed wetlands (CWs) are engineered systems, designed to utilize the soil, vegetative and microbial processes of natural wetlands in the treatment of wastewater of different origins, including domestic and municipal sewage, industrial and agricultural wastewater, landfill leachate, AMD, storm-water run-off and mining wastewater (Reed, 1993, Vymazal, 2005). CWs typically consist of a soil, gravel or sand-filled bed planted with various types of macrophyte (most commonly *Phragmites australis*) (Brix, 1994b). Table 5-1 summarizes the primary contaminants and their mechanisms of removal from CW systems (Vymazal, 2005).

Table 5-1: Primary contaminants and mechanisms of removal from CW systems

Contaminant	**Mechanism of Removal**
Organic Matter	Aerobic and anaerobic degradation by bacteria attached to plant roots, rhizomes and media surfaces
Suspended solids	Filtration and sedimentation
Nitrogen (ammonia or nitrate)	Nitrification / denitrification process and adsorption (if soil grain is sufficiently fine)
Phosphorus (phosphate)	Ligand exchange reaction in the presence of iron, aluminium or calcium hydrous oxides

In the past, CWs have most often been used as polishing systems following the primary and secondary water treatment stages (Brix, 1994b) but have more recently been identified as a viable, green technology solution to water management in the following areas:

- regulation of water supply
- drought alleviation
- regulation of water quality (particularly for biological and temperature control) (GreenCape, 2016)

Biomimicry is defined as "the practice of learning from and then emulating nature's genius to solve human problems and create more sustainable solutions" (Biomimicry.SA., 2015). Throughout the process of evolution, living organisms have survived and adapted to changing conditions in such a way as to ensure continual access to water. For this reason, natural ecosystems and their inhabitants provide many examples of successful water purification processes (Dama-Fakir et al., 2015). For example:

- The ability of the Namibian Fog Beetle to capture water from the air (Kenny et al., 2012);
- The ability of 'curly-whirlies' (desert plants of the Namaqualand) to capture fog from the air with modified leaves and stems (Vogel and Müller-Doblies, 2001);

- The action of worms, beetles and micro-organisms in decomposing forest litter into humus, thereby creating a mat for water filtration on the forest floor (the chemical-free *Biolytix*™ water filtration system mimics this process) (Kenny et al., 2012); and
- The ability of natural wetland ecosystems to filter sediments and nutrients from surface water (Kenny et al., 2012).

Natural wetlands have a number of important functions; namely water purification, water capture and storage, flow regulation, flood attenuation, shoreline stabilization and protection, carbon sequestration, air quality regulation, temperature regulation and habitats to support biodiversity (Dama-Fakir et al., 2015). Without their variety of vegetation, micro-organisms, aquatic species and wildlife, wetland ecosystems would not support these functions (Kivaisi, 2001).

As the types of wastewater to be treated become more diverse, so the need for more economical, efficient and robust systems to cope with the treatment demands emerges. Biomimetic principles (Benyus, 2017, Todd and Josephson, 1996) could provide valuable tools to inform the design of improved CW systems. Biomimetic CWs are self-contained, ecologically engineered systems in which waste streams are recycled wherever practicable. In addition, they can be a source of nutrient-rich fertilizers and renewable energy and can act as carbon sinks, air quality regulators, temperature regulators and habitats for biodiversity (Dama-Fakir et al., 2015).

There is real scope for CWs to provide a valuable addition to South Africa's ecological infrastructure. They offer all of the advantages of decentralized systems (GreenCape, 2016) and, when designed using biomimetic principles, can offer benefits beyond just water remediation. A case in point is the successful prototype in the Langrug informal settlement close to Franschoek (WWF-SA, 2016). Langrug has been converted into an Eco-machine (U.S.EPA, 2002, JTED, 2014), which uses biomimicry to address water purification, stormwater and solid waste management, as well as provide potential for revenue generation (WWF-SA, 2016).

Although the use of CWs for wastewater treatment was documented as early as 1904 (Brix, 1994b), much of the pioneering literature views CWs as "black boxes" and understanding of how these systems operate internally is limited (Albertson, 1998, Haberl et al., 2003, Garcia et al., 2010, Rengers et al., 2016). This research focuses on an overall hydraulic characterization of a newly established pilot-scale CW and an in-depth physico-chemical baseline description to act as points of reference. This is followed by two months of feeding artificial domestic wastewater into the wetland and continually monitoring the chemical and physical changes. The chemical characterisation will provide insight into the kinetics of total carbon and total nitrogen transformation. The analytical procedure involves dividing the CW into a grid of sample ports: seven ports down the length of the bed, each of which is divided into three depths. The multitude of sampling locations and samples will provide insight into the internal development and operation of the wetland system. This preliminary data is to form the basis of a long-

term study into the internal behaviour of CWs, from start-up into steady operation, and will provide the start of a framework to inform improved biomimetic design.

5.3.3. Materials and methods

5.3.3.1. Pilot-scale CWs at the Helmholtz Zentrum für Umweltforschung (UFZ)

The pilot-scale wetlands at the Helmholtz UFZ are planted, horizontal subsurface flow (HSSF) CWs. The system is filled with glacial gravel (particle size 4 – 8 mm; voidage 36%; bed height 0.50 m) and planted with *Phragmites australis*. A schematic diagram of the wetland is given in Figure 5-1. The boundary structure is an approximately rectangular, stainless steel container (6 m length x 0.70 m height). One side down the length of the wetland is constructed at 16° from the vertical, such that the width at the top and base of the container is 1.2 m and 1.0 m, respectively. Three fully removable, stainless-steel baskets (height 0.7 m; diameter 0.30 m) have been inserted into the central flow path. Each basket contains glacial gravel and has been planted with *Phragmites autralis* just as in the surrounding wetland system. The basket cages have evenly distributed pores of the same diameter as the average gravel particle size to minimize disruptions to the flow of water. The purpose of the baskets is to be able to transport a predominantly undisturbed section of the CW to the laboratory for more detailed analysis.

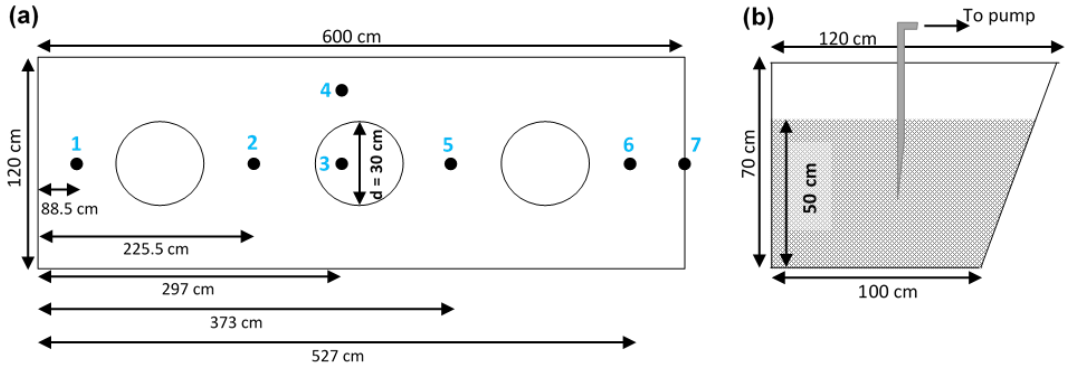


Figure 5-1: (a) Aerial view of the CW showing the sample port, three inlet valve and single outlet valve locations and (b) cross-sectional view of the CW showing one stainless steel sampling tube.

The wetland is fed by three evenly spaced inlet valves, which are positioned 5 cm above the base of the container. The discharge is removed via a single, centred outlet valve, also 5 cm above the wetland base. The flow rate of water into and out of the wetland is regulated via a gear pump (VGS120, Verder Pump, Germany), motor (SEV6324, SEVA Tec, Germany) and frequency controller (DF51-322-025, MOELLER, Germany) and data is logged to allow for continual monitoring of the flow rates. The water level within the wetland is maintained at 0.5 m by means of a syphon at the wetland outlet. Construction

was completed in October 2013. Figure 5-2(a) shows a photograph of the wetlands at the UFZ taken in July 2015. The wetland has been dug into the ground, such that the upper rim and 20cm of the boundary walls are visible. Figure 5-2(b) shows a photograph of the middle basket when it was removed from the wetland in September 2015.

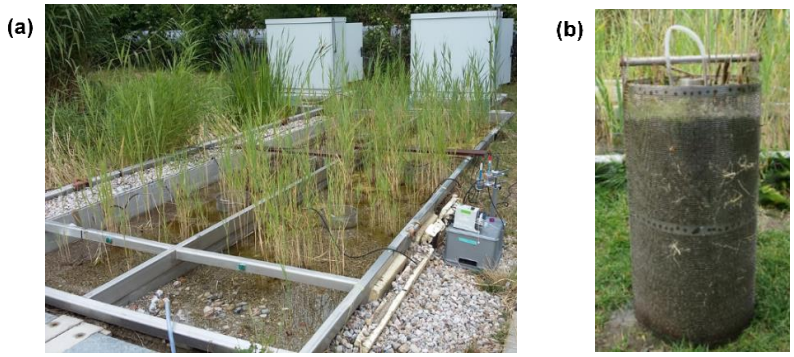


Figure 5-2: (a) A photograph of the pilot-scale, horizontal subsurface flow CWs at the Helmholtz UFZ (July 2015) and (b) the stainless steel basket removed from the centre of the wetland showing an already well-developed root system (September 2015).

5.3.3.2. Collection of Baseline Samples

From October 2013 to July 2015, the wetland was allowed to establish naturally, without any external nutrient source. Municipal tap water was fed into the system during spring, summer and autumn and shut off during the coldest winter months. In order to determine the baseline characteristics of the newly constructed CW, a set of samples, hereafter referred to as baseline samples, were taken before the commencement of any other experiments. The samples were taken from 24 cm below the gravel surface. Sampling devices, hereafter referred to as samplers, were inserted into the bed at the locations indicated in Fig. 1(a), but not at the system outlet (port 7) where black norprene tubing was connected directly to the discharge valve. The samplers were L-shaped, stainless steel tubes (Figure 5-1(b)), open at both ends, to allow for the easy movement of water. The long end was inserted into the gravel bed and contained several pore-like holes at the base. These holes were too small to allow for gravel to enter the hollow interior. The short end sat above the surface of the gravel bed and contained a single opening.

The short end of each sampler was connected, one at a time, to a small peristaltic pump (REGLO MS 2/6, ISMATEC SA, Switzerland) via 1.2 m of black, norprene tubing. Water was pumped continually through flow-through cells for the measurement of dissolved oxygen (DO) (Fibox 3, Presens, Germany), oxidation-reduction (redox) potential (Multi-i340, WTW, Germany), pH (Multi-i340, WTW, Germany) and temperature, after which 20ml aliquots were collected, through 0.45 μm syringe filters and submitted to the analytical laboratory for total organic carbon (TOC) and total nitrogen (TN) analysis (Multi N/C 21005, Analytikjena, Germany).

5.3.3.3. Impulse-Response Tracer Tests

For the hydraulic investigation, samplers were inserted into the bed at each internal port (Figure 5-1(a)); 24 cm below the gravel surface. The samplers were connected in pairs. One sampler was the outlet tube, from which water was removed from the wetland, and the second was the return tube. The return tube was fixed to the outlet tube such that the holes at the base of its long end were positioned 6 cm above those of the outlet tube. Both short ends of the samplers making up each pair were connected to a peristaltic pump (BVP_Z, ISMATEC SA, Switzerland), a stainless steel flow cell (Schnegg, 2002) and a fluorometer (GGUN-FL, Albillia, Switzerland) using black norprene tubing. This configuration is shown in Figure 5-3.

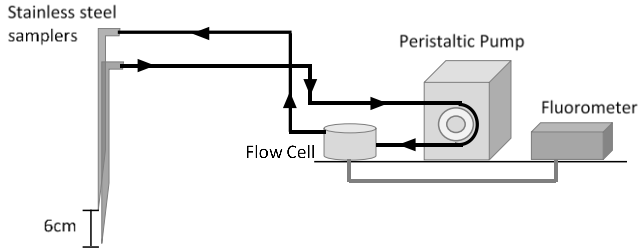


Figure 5-3: A schematic diagram of the sampling device, pump, flow cell and fluorometer configuration for the tracer flow tests.

A known mass of Uranine fluorescent tracer dye was dissolved in 1 ℓ of distilled water and injected into the wetland inlet as a single pulse. For the duration of each flow test, water was pumped out of the wetland and through the flow cell, which was connected to the fluorometer, before being returned to the bed at the same location (Figure 5-3). The return flow ensured that the total system volume was maintained. The fluorometer was programmed to record data at 10 s intervals and provided a potential (mV) reading, which was converted to Uranine concentration after calibration with feed water from the site (baseline) and a standard Uranine solution (70 ppb).

5.3.3.4. Introduction of Artificial Wastewater

An artificial wastewater (AWW) concentrate containing 37.50 g/ℓ casein peptone, 25.78 g/ℓ meat extract, 7.03 g/ℓ urea and 6.56 g/ℓ dipotassium hydrogen phosphate was prepared, autoclaved and introduced into the CW system via a metering pump (Gamma L GALA1000, ProMinent, Germany). The concentrate was formulated from a published standard based on the average composition of the water released from a treatment plant of class 2 in Germany; representing between 1000 and 5000 inhabitant equivalents (DIN38412). The separate water and AWW feed lines were combined into a single feed pipe and the two fluid streams mixed before entry into the wetland. To achieve the desired inflow nutrient load (in terms of carbon, nitrogen and phosphorous), the flow rate maintained by the AWW metering pump was set to 1/500 of the inlet water flow rate. Weekly sampling commenced one

week after the introduction of the wastewater and continued for 7 weeks. Samples were taken from 24 cm below the gravel surface at each sample port as described previously.

5.3.4. Results and discussion

It was desired that the pilot-scale CWs at the Helmholtz UFZ resemble a natural wetland ecosystem as closely as possible. For this reason, the CWs were allowed to establish naturally, without any external nutrient source, from October 2013 until summer 2015, when these first experiments were scheduled to commence. The results to follow represent the baseline and the very first set of measured data. Due to the complexity and continual internal development of these systems, such experiments will be repeated seasonally and annually into long-term operation of these wetlands. Knowledge and resources from several disciplines in the sciences will be drawn upon to develop a databank of information, to gain a deeper understanding of the operation and continual fluxes within wetland systems and, ultimately, to recommend a methodology and a set of design parameters for engineering scale-up.

5.3.4.1. Wetland Baseline Characterization

Samples for the baseline characterization were taken in August, September and October of 2015, at which time the wetland was a working system with unknown flux, no additional carbon source and low organic load. The bed temperature, pH, TOC and TN concentration were measured down the length of the wetland and are presented in Table 5-2.

Table 5-2: Average bed temperature, pH, TOC and TN concentration with the saturated oxygen concentration (fresh water, 760 mm Hg) at the time of the baseline measurements

Period	Average bed temp (°C)	Saturated oxygen (mg/ℓ)	pH	TOC (mg/ℓ)	TN (mg/ℓ)
Aug 2015	24.1 ± 2.1	8.5	6.85 ± 0.14	3.11 ± 0.24	0.54 ± 0.05
Sept 2015	20.5 ± 0.3	9.0	7.50 ± 0.21	3.60 ± 0.30	0.44 ± 0.02
Oct 2015	16.8 ± 1.1	9.7	7.44 ± 0.19	2.39 ± 0.11	0.72 ± 0.06

The pH of the wetland was found to remain relatively constant (Table 5-2) and within the physiological range of natural fens and freshwater wetland ecosystems (Kadlec and Wallace, 2009). The TOC and TN concentrations reported in Table 5-2 give the average natural background levels, below which the measured outlet concentrations are not expected to fall (Kadlec and Knight, 1996). This residual carbon and nitrogen can be accounted for by inherent production of organic substances and carbonaceous material (root exudates) which contribute to the biological oxygen demand (BOD) and decaying plant matter (Bavor et al., 1988, IWA, 2000, Reed, 1993).

The variation in DO and potential within the wetland are plotted in Figure 5-4(a) & (b), respectively. For clarity, the DO and redox potential at sample port 3, located inside the middle basket (Figure 5-2(a)),

has been plotted as individual points. In general, the wetland microcosm within the basket does not show behaviour markedly different to that in the surrounding system, except during October when the DO and potential aligned with the data obtained in August (Figure 5-4, 'x').

There was a clear consumption of oxygen during August (Figure 5-4(a), round markers), accompanied by a lower potential (Figure 5-4(b), round markers), and a general increase in both wetland DO and potential from August to October. August was the warmest month during the summer of 2015 with the high levels of solar radiation. The average daily air temperature and global radiation maxima were measured to be 28.4°C and 716 Wm^{-2}, respectively, at the weather station on-site. These were measured between 11 am and 2 pm. The plants were green and their growth rate and level of activity would have been at a maximum under these climatic conditions (Kadlec and Wallace, 2009); hence the greater consumption of oxygen during August.

In the autumn months of September and October, when the average ambient and bed temperatures had begun to decrease (Table 5-2), there was a reduction in oxygen consumption (Figure 5-4(a), diamond & square markers) and a more positive potential (Figure 5-4(b), diamond & square markers). Overall, this would be expected because plant activity should have decreased in the autumn period. Also evident is that the oxygen concentrations were closer to the saturation values. In both September and October, approximately 9 mg/ℓ of O_2 was measured in the feed water. The water remained oxygen-saturated within the first 100 cm of the wetland, which would suggest no oxidative processes or exudate transformation up to 100 cm. (Figure 5-4(a), diamond and square markers). In September, oxygen was consumed faster within the second 100 cm of the wetland before reaching a minimum and then increasing until the water was oxygen saturated again close to the outlet (Figure 5-4(a), diamond markers). The plant roots are a source of oxygen to the rhizosphere (Kadlec and Wallace, 2009), but it cannot be confirmed that this is the reason for this re-introduction of oxygen into the wetland. The September trend in DO close to the wetland outlet is dissimilar to that in both August and October and, due to the lack of confirmatory experimental data, should be treated with caution. In contrast, the oxygen level decreased progressively down the bed in October (Figure 5-4(a), square markers). This indicated that plant activity decreased down the bed (it was observed that the vegetation density also decreased down the bed) but that the plants were still active although not at the same high level as at the height of the summer.

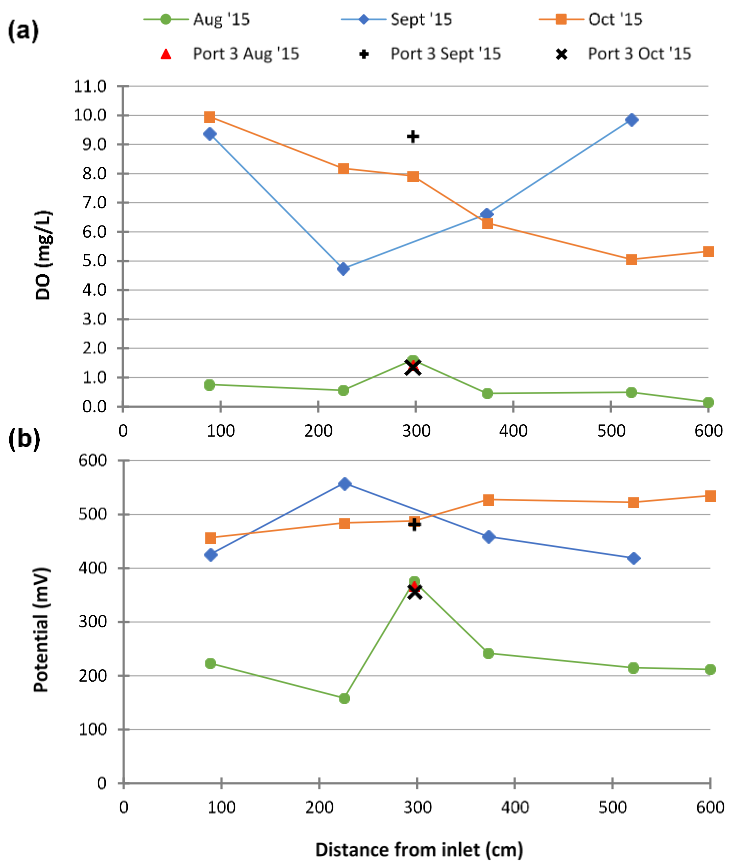


Figure 5-4: Baseline characterization showing (a) the dissolved oxygen concentration and (b) the oxidation-reduction potential prior to the introduction of artificial wastewater. Data was obtained from 24 cm below the gravel bed surface and at increasing distance along the flow path during August, September and October 2015.

In summary, Figure 5-4(a) & (b) suggest a seasonal influence on the DO concentration and redox potential, but it cannot be said with certainty whether this is due to changes in the plants or changes in microbial activity in the root zone. However, model experiments have indicated that oxygen input from the plants is dependent on the light intensity and the redox state of the root zone (Kadlec and Wallace, 2009).

5.3.4.2. Hydraulic Characterisation

A gravel HSSF CW can be considered to be a type of packed-bed reactor (Sheridan et al., 2014a, Sheridan et al., 2014b, Vymazal and Krőpfelová, 2005). An understanding of wetland hydraulics is a pre-requisite for an investigation into the kinetics of contaminant degradation (Headley and Kadlec, 2007, Fogler, 2006). The hydraulic investigation of the pilot CW at the Helmholtz UFZ was performed by means of an impulse-response tracer test according to the methodology described by Headley and Kadlec (2007).

Tracer studies should be conducted under laminar, or reversible flow, conditions (Sheridan et al., 2014a, Sheridan et al., 2014b). Before commencing the flow test, the Reynolds number was calculated for the

wetland system (Subramanian, 2004) and verified to be less than 10, which confirmed that flow was well within the laminar region (Miller and Clesceri, 2002).

Subsequent to the completion of the tracer test, the recovery of tracer material was calculated, according to [5-1], as the first check on the reliability of the experimental data. Data obtained from a tracer test with a low percentage recovery of material at the system outlet should be treated with caution (Headley and Kadlec, 2007).

$$R = \frac{v_0 \int_0^\infty C(t)dt}{M} \times 100 \qquad [5_1]$$

The method outlined in Fogler (2006), and summarized below, was used to calculate the residence time distribution (RTD) function for the reactor, defined by:

$$E(t) = \frac{C(t)}{\int_0^\infty C(t)dt} \qquad [5_2]$$

C(t) is the time-variant concentration data collected during the flow test and the denominator represents the area under the C(t) curve. The RTD is important because it visually describes dynamic wetland behaviour and fluid flow patterns and is the basis for the calculation of many important hydraulic parameters, one of which is the mean residence time, t_m, or first moment:

$$\bar{t}_m = \int_0^\infty tE(t)dt \qquad [5_3]$$

The mean residence time, t_m, was compared to the nominal residence time, τ, which is the hypothetical time taken for a pulse of tracer to move from inlet to outlet assuming ideal plug flow:

$$\tau = \frac{V}{v_0} \qquad [5_4]$$

V is the reactor volume and accounts for the porosity of the packing material, and v_0 is the system the volumetric flowrate. $t_m = \tau$ for a closed, steady-state system with no dead volume.

The variance, σ^2, or second moment of the RTD, is an indication of the spread of the data about the mean and was calculated according to:

$$\sigma^2 = \int_0^\infty (t - \bar{t}_m)^2 E(t)dt \qquad [5_5]$$

Owing to the fact that flow was laminar and, thus, completely reversible, the RTD function could be normalized against the mean residence time according to:

$$\theta = \frac{t}{\bar{t}_m} \qquad [5_6]$$

$$E(\theta) = E(t)\bar{t}_m \qquad [5_7]$$

[5-2], [5-6] and [5-7] were employed to produce the normalized RTD function for the reactor outlet in Figure 5-5. The shape of the RTD in suggests that that this system displays behaviour intermediate between plug flow and complete mixing (Headley and Kadlec, 2007). There are two main features in Figure 5-5. Firstly, the distribution is multi-modal. There are two distinct peaks prior to $t = t_m$ ($\theta = 1.0$). This is typical of a reactor in which there is channelling or by-pass and dead zones (Headley and Kadlec, 2007). The small peaks after $t = t_m$ ($\theta = 1.0$) could indicate hold-up in densely vegetated areas or possibly adsorption and desorption of the tracer material onto the gravel (Headley and Kadlec, 2007, Smart and Laidlaw, 1977). Secondly, there is long tailing evident. This can be the result of mixing between the pore spaces, diffusion between regions of faster and slower flow and, again, dead zones (Fogler, 2006).

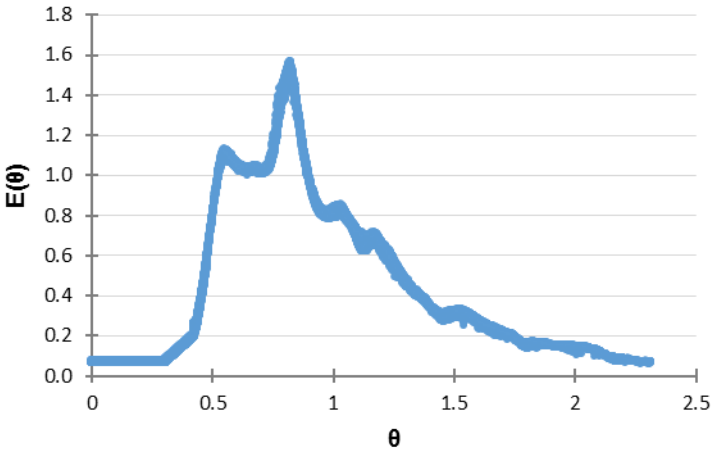


Figure 5-5: The normalized RTD function for the pilot CW determined from an impulse-response tracer test, with τ = 2.16 d (θ = 0.78), t_m = 2.89 d (θ = 1.0) and a peak time at maximum concentration of 2.31 d (θ = 0.80).

Various hydraulic parameters, calculated from [5-1], [5-3], [5-4], [5-5] and the RTD, are summarized in Table 5-3. The mean residence time, or time taken for the bulk of the injected pulse of Uranine to reach the outlet, was 2.89 days. Ninety-nine percent (99%) of the injected mass of tracer had exited the wetland after 6.54 days. In general, it takes at least three retention times for material to be flushed from the system. Making this assumption, it would take an additional 2 days (2.89 d x 3 = 8.67 d) for the tail of the RTD curve to reach baseline concentration again.

Table 5-3: Various hydraulic parameters describing the behaviour of the pilot CW as determined from the impulse-response tracer test and system RTD

Hydraulic Parameter	**Value**
Mean volumetric flowrate (ℓ/hr)	22.28
Reynold's no. (Re)	0.11
Reactor volume (ℓ)	1156.2
Mean Residence Time, t_m (d)	2.89
Nominal Residence Time, τ (d)	2.16
Variance (σ^2)	1.116E+10
Peak time at max. concentration (days after injection)	2.31
t_{99} (d)	6.54
Recovery (%)	100

5.3.4.3. Contaminant Transformation Indicators

Various physicochemical parameters provide information about water quality. DO is essential for aerobic degradation processes. The ammonium (NH_4^+) ion is a by-product of the decomposition of urea and high levels of NH_4^+ can produce an environment which is toxic to aquatic organisms. A positive redox potential indicates an oxidizing solution and many pollutants require strong oxidants to facilitate their decomposition (Bellingham, 2012). Organic carbon and the chemical oxygen demand (COD) are important water quality indicators (Kadlec and Wallace, 2009), for which maximum allowable limits are commonly published in environmental legislation.

For the purpose of this very first investigation into the behaviour of this CW system, the TOC and TN concentrations were measured. TOC was chosen because it is a more accurate measure of the degradation of carbon in the system, as opposed to COD which is a cumulative measure of all oxidisable components. Similarly, TN, which is the sum parameter of the nitrogen contributions from ammonium (NH_4^+), nitrate (NO_3^-), nitrite (NO_2^-) and organic nitrogen, was considered for this preliminary set of results. The next set of experiments will involve more detailed analysis of the species making up these sum parameters.

The TOC and TN concentrations at the system outlet over the 7 week experimental period are shown in Figure 5-6(a) & (b). The inlet and outlet concentration data for week 1 and 2 is plotted as individual points because the system was yet to achieve a state of steady operation. Figure 5-6(a) indicates TOC degradation and Figure 5-6(b) shows TN transformation. There is a general decrease in TOC and TN removal from late October to early December, indicated by the increasing outlet TOC and TN concentrations over this period. The change of season and the resultant colder ambient temperatures would have lowered microbial activity and any decomposition of dead bio-matter could have introduced additional nitrogen into the system (Kadlec and Wallace, 2009).

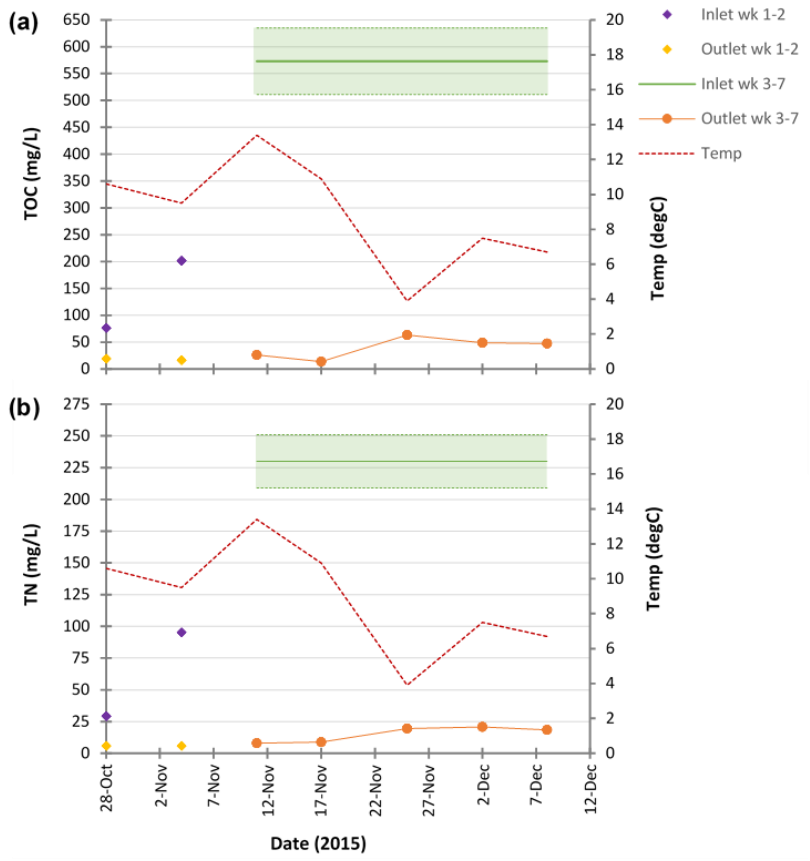


Figure 5-6: (a) Total organic carbon concentration (avg. inlet [TOC] = 573 ± 62 mg/ℓ; baseline TOC = ± 3.0 mg/ℓ) and (b) total nitrogen concentration (avg. inlet [TN] = 230 ± 21 mg/ℓ; baseline TN = ± 1.7 mg/ℓ) as a function of time at the wetland outlet up to 7 weeks after the introduction of artificial wastewater into the system.

Figure 5-7 shows the DO concentration of the outlet stream. Each week, the DO was found to be below 0.75 mg/ℓ, which indicates high oxygen consumption when compared to the 11.158 ± 1.208 mg/ℓ DO at the wetland inlet. This is thought to be due to the action of micro-organisms in degrading organic carbon (Kadlec and Wallace, 2009). To support this hypothesis, the general trend in TOC concentration as a function of distance along the flow path is also plotted in Figure 5-7(a) and shows that organic carbon is definitely degraded in the first half of the bed. In general, oxygen consumption appears to be higher in the first 300 cm of the bed, where the largest reduction in TOC is also observed. It is also noted that the standard deviation at each sample port increases with distance down the wetland bed. This spread of data points is most pronounced at the wetland outlet (600 cm). In general, the DO concentration is greater at the start of the experiment (28th October) and lower towards the end of the sampling campaign (8th December). In the autumn (October/November 2015), the plants could still have been contributing oxygen to the system (Kadlec and Wallace, 2009); hence the higher DO data on 28th October, 11th and 17th November in the sample ports after 300 cm, where TOC degradation had largely ceased. As the experiment proceeded into the beginning of winter (December 2015), oxygen input by the plants should have been much less, but the plants were still observed to be active up until the 8th

December. The continued activity, even if slower at this time, coupled with reduced oxygen input from the roots could explain the lower DO data on 2nd and 8th December in the sample ports after 300 cm and the larger spread of data points these latter sample ports.

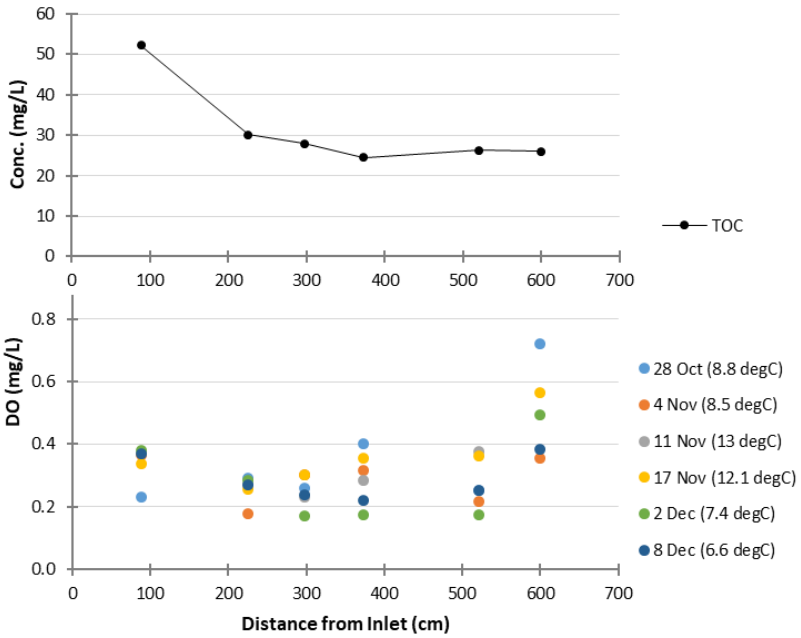


Figure 5-7: An illustration of the general trend in (a) TOC concentration (avg. inlet [TOC] = 573 ± 62 mg/ℓ) and (b) the dissolved oxygen concentration at increasing distance from the wetland inlet over the 7 week experimental period (avg. inlet [DO] = 11.158 ± 1.208 mg/ℓ; avg. inlet temp = 10.9 ± 2.6°C).

The redox potential as a function of time at the wetland outlet is plotted in Figure 5-8 and a progressive decrease in potential can be seen over the 7 week experiment. This decrease in potential indicates that the system became more anoxic, as would be expected if oxidative degradation processes were taking place. Oxidative degradation may have produced a number of reduced species, such as sulphur dioxide (SO_2), nitrate (NO_3^-) and (NO_2^-). The presence of these reduced species would have contributed to the observed decline in redox potential (Kadlec and Wallace, 2009).

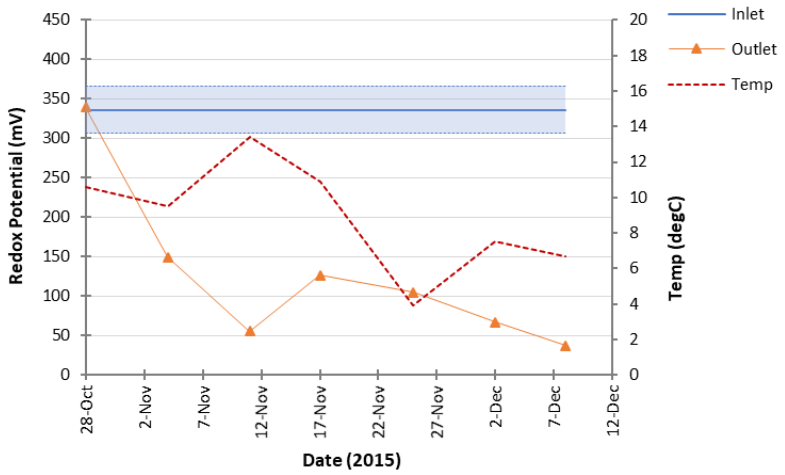


Figure 5-8: The change in oxidation-reduction potential as a function of time at the wetland outlet up to 7 weeks after the introduction of artificial wastewater into the system (avg. inlet potential = 336.1 ± 30.1 mV).

5.3.4.4. Kinetics of Contaminant Degradation

For the purposes of this paper, the rates of transformation of TOC and TN (from urea) were considered. The RTD was used to guide the choice of a reactor model to describe the system so that the rate constants for these transformations could be calculated. The Tanks-in-Series (T-I-S) model, along with a first order rate law, was chosen for this preliminary investigation. According to the T-I-S model, a packed bed reactor can be described by a number of continuously stirred tank reactors (CSTRs) of equal volume in series. The number of tanks in series, *n*, was calculated by:

$$n = \frac{\tau^2}{\sigma^2} \qquad [5_8]$$

This method requires a constant inflow concentration and volumetric flow rate. The conversion, *X*, of the reacting species was related to the mean residence time and reaction rate constant by:

$$X = 1 - \frac{1}{(1 + \tau_i k)^n} \qquad [5_9]$$

$$\text{where } \tau_i = \frac{V}{v_0 n} \qquad [5_10]$$

Where conversion is defined by the quotient of the number of moles of the species reacted to the number of moles of the same species fed into the system. Hence, in terms of concentration:

$$C_A = C_{A0}(1 - X) \text{ or } \frac{C_A}{C_{A0}} = (1 - X) \qquad [5_11]$$

Substituting [5-11] into [5-9] yields:

$$C_A = \frac{C_{A0}}{(1 + \tau_i k)^n} \qquad [5_12]$$

[5-12] was used to solve for the reaction rate constants (Fogler, 2006). Figure 5-9 shows the rate constants for the degradation of TOC and the transformation of TN from week 3 of the experiment when the system was operating more stably. A similar trend of variation in rate constants can be seen. A certain degree of variation in the rate constants may be expected because TOC and TN are sum parameters and dependent on multiple chemical processes. In addition, the temperature dependence of the rate constant should also be considered. The reaction rate constant of most chemical reactions is directly related to the reaction temperature and increases with an increase in temperature, or vice versa (Atkins and De Paula, 2006). The temperature in the wetland decreased as the weeks progressed from autumn into the beginning of winter (Figure 5-9) and this could account for the reduction in the reaction rate constant, particularly beyond the third week of the experiment. As the micro-organisms acclimatize to the different types and quantities of nutrients available and plant activity increases significantly with the onset of spring in 2016, it is expected that the rate constants will change. Thus, the values calculated here should be treated as a point of reference.

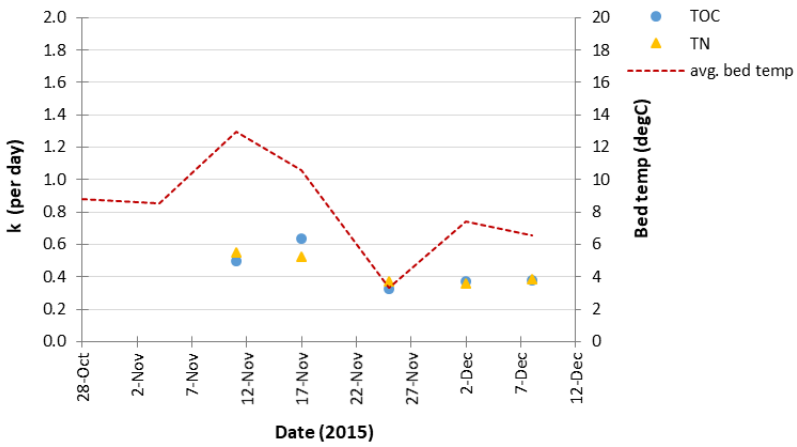


Figure 5-9: The variability in the rate of decomposition of total organic carbon, k_{TOC}, and the rate of transformation of total nitrogen, k_{TN}

5.3.5. Conclusion

Biomimicry involves the mimicking of natural processes to solve human problems and relies upon careful observation and an in-depth understanding of the fundamentals governing these processes. It is known that CWs successfully remediate wastewater, as evidenced by the number of operational CWs worldwide. However, it would be useful to merge the fields of engineering, microbiology and chemistry, while incorporating the biomimetic principles to break into the 'black box' that is many of these systems and better understand how they operate.

As such, this paper suggests a methodology for handling new or proposed CW systems; starting with a detailed investigation of natural wetlands. This is to be followed by wetland construction and establishment and then a start-up background characterization, hydraulic characterization and kinetic

investigation. The baseline, hydraulic and kinetic studies should then be repeated into long-term operation. The experiments were conducted at the Helmholtz UFZ (Leipzig, Germany) where the equipment and resources available allowed for much more detailed investigation and analysis and the methodology and findings can still act as a useful point of reference for similar research in South Africa; at least qualitatively if not quantitatively.

These results are just the first set in a series. The planned repetition of flow tests and kinetic studies will generate a databank and create a picture of the internal development and performance of CW systems over time, which will in turn form the basis of a framework to inform improved biomimetic design.

Acknowledgements

The authors would like to acknowledge the following people for their significant contribution towards the results presented in this paper:

1. The Helmholtz Zentrum für Umweltforschung (UFZ), Dept. of Environmental Biotechnology for access to their outdoor wetlands and laboratory facilities.
2. Frau Puschendorf (Helmholtz UFZ, Dept. of Environmental Biotechnology) for her assistance with sample analysis.
3. Marie Kurz and Christian Schmidt (Helmholtz UFZ, Dept. of Hydrogeology) for their assistance with the fluorometers.
4. Golder Associates South Africa
5. The South African Water Research Commission
6. University of the Witwatersrand *Friedel Sellschop Award 2015*
7. The National Research Foundation (NRF)
8. The German Academic Exchange Service (DAAD)
9. *Water4Crops* (an EU initiative)

Chapter 6 Hydraulic study of a non-steady horizontal sub-surface flow constructed wetland during start-up

6.1. Summary

This chapter comprises my second published paper describing the hydraulic studies carried out in 2016. It was been written as a follow up to (Aylward et al., 2017) and extended the tracer studies to a multi-depth investigation, as well as compared the mathematical output from the standard hydraulic equations (which rely on steady-state flow) with equations modified for a non-steady flow system. The influence of environmental conditions is also taken into account. The Matlab code is provided in Appendix B and a summary of the flow test data in Appendix C. More detailed information is provided on the CDs (due to data volume). The supplementary information for this paper is provided in Appendix E.

6.2. Statement of individual contribution

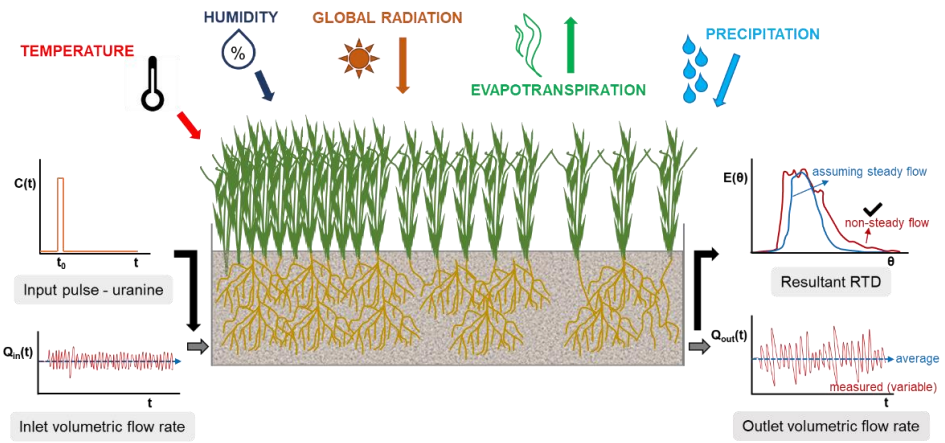
The experimental design, preparation, work and analysis was carried out by myself with Dr Uwe Kappelmeyer advising and overseeing the work at the Helmholtz UFZ in Leipzig Germany. For a large part of the field work, I had the assistance of Alyona Lepilova (also conducting the experimental work for her masters in engineering at the Helmholtz UFZ). I had the support of Prof. Craig Sheridan and Ricky Bonner in various stages of the method selection, design and write-up phases of this paper.

6.3. Sci. Tot. Environ. (2019) Vol. 646 pp. 880-892

6.3.1. Highlights

- Impulse-response tracer tests in a start-up, non-steady flow, pilot-scale HSSF CW
- Fluctuations in outflow linked to vegetation and climatic conditions
- Comparison of results of classic RTD theory with Werner & Kadlec's modified method
- Significant difference between outlet RTDs calculated using standard RTD theory
- Variable flow method should be used preferentially as outlet RTDs are comparable

6.3.2. Graphical abstract



6.3.3. Abstract

This paper describes the hydraulic performance of a start-up, pilot-scale, horizontal sub-surface flow constructed wetland (CW), located outdoors at the Helmholtz UFZ, Leipzig. This paper aims to investigate the impact of the method of hydraulic calculation in a pilot-scale system. Impulse-response tracer tests were conducted at multiple depths and locations throughout the system and the uranine concentration was measured using a fluorometer. In addition, the volumetric flow rate was closely monitored and climatic data was gathered to support the hydraulic results. Werner and Kadlec's modified residence time distribution (RTD) theory (originally developed for systems with large flow rate and volume fluctuations) was applied and the results compared to those obtained using classic RTD theory.

Progressive uranine dispersion, broadening of the RTD base, a change in peak shape and extended tailing were observed with increasing distance. All of these factors indicated deviation from plug flow and mixing effects with low-to-moderate dead volume. As this was a non-steady flow system, application of modified RTD theory ensured that the first moments of the normalized breakthrough curves and RTD functions were always unity. The Student's t-test (95% confidence) showed that the outlet RTDs calculated assuming steady-flow were significantly different, but those determined using the modified theory were closely comparable.

In general, a decrease in flow rate from inlet to outlet was observed and fluctuations in the outflow were linked to climatic conditions. August was characterized by the highest temperatures, high global radiation and high rates of evapotranspiration. Low or no outflow was recorded in conjunction with high evapotranspiration. The lowest temperatures, low global radiation, low evapotranspiration and high humidity were recorded in October, as well as the second highest rainfall (82 mm) after June (115 mm). Surges in outflow were observed with rain events.

Keywords: tracer studies, uranine, non-steady flow, climatic factors, evapotranspiration

6.3.4. Introduction

Natural wetland ecosystems form a key component of the ecological infrastructure and provide essential environmental services including water capture, purification and storage; flow regulation; protection and stabilization of shorelines and flood attenuation (Kivaisi, 2001). From the perspective of sustainability, protection of natural wetlands is essential and constructed wetlands (CWs) have the potential to play a key role in wetland conservation. CWs are engineered, biological reactors which rely on a combination of physical, chemical and microbial processes to treat various types of wastewater (Brix, 1994b, Reed, 1993, Vymazal, 2005). If designed optimally, CWs can treat high loads of diverse pollutants at relatively low cost and still be aesthetically appealing.

CW performance is quantified by both hydraulic and kinetic efficiency. Since the water acts as the transport medium, the level of treatment will be impacted by its specific flow path and average retention time within the system. In other words, the calculation and prediction of CW treatment performance is not possible without an understanding of the hydraulics of the system.

Hydraulic performance is normally determined from impulse-response or step-change tracer studies and residence time distribution (RTD) theory. Although a widely utilized technique, many of the mathematical relationships hold only if the system is operating under steady flow conditions. In real CW systems, the condition of steady flow is, at best, an assumption. Factors such as evapotranspiration (relative humidity), bed medium, vegetation density, rainfall and temperature; amongst others can contribute to flow non-ideality by either directly or indirectly affecting the discharge flow rate.

Most of the CW literature still views these systems as "black boxes" (Albertson, 1998, Garcia et al., 2010, Haberl et al., 2003, Rengers et al., 2016) and only a few studies have dealt with conducting hydraulic flow tests internally (Bonner et al., 2017a, Bonner et al., 2017b, Sheridan et al., 2014a, Sheridan et al., 2014b). For this reason, the methodology of Levenspiel (1972), Fogler (2006) and Headley and Kadlec (2007) has been expanded in this study and tracer tests have been conducted at multiple depths and locations throughout the bed to better describe the internal flow paths and fluxes. Werner and Kadlec's modified RTD theory for non-steady flow systems (1996), initially developed to account for the large flow rate and system volume fluctuations in storm water treatment systems, has been applied to this hydraulic investigation of a horizontal sub-surface flow (HSSF) CW and compared to the standard RTD theory output.

6.3.5. Theoretical background

6.3.5.1. Non-ideal and non-steady flow behaviour

A distinction should be made between non-ideal and non-steady flow. Non-ideal flow is a result of physical, geometric and physiological characteristics; examples of which include fluid density, flow rate, wetland length and evapotranspiration. Evapotranspiration is the amount of water lost due to evaporation and transpiration and is subject to diurnal and seasonal variation. Evaporation accounts for water loss from water bodies and soils, while transpiration is water loss through the leaves of vegetation (W.M.O., 2008). In a HSSF CW, evaporation should be minimal because the water surface lies beneath the gravel surface. Hence, water loss from a wetland system water mass balance should be primarily the result of transpiration. The packing medium, short-circuiting, stagnant zones, re-circulation, dispersion and mixing also impact flow behaviour and their presence can be inferred from the shape and spread of the RTD (Rengers et al., 2016, Thackston et al., 1987). These non-ideal flow phenomena occur in the majority of CWs, even when a steady-flow rate is maintained.

Non-steady flow refers to a variable flow rate. The application of standard RTD theory to non-steady flow systems is limiting because the fluctuating flow rate can have a large impact on the shape and position of the RTD; thus making it difficult to differentiate non-ideal flow behaviour from variable flow effects (Werner and Kadlec, 1996).

6.3.5.2. Hydraulic behaviour in steady versus non-steady flow systems

The application of residence time distribution (RTD) theory to non-steady flow systems was explored by Cha and Fan (1963) and later addressed by Naumann (1969) and McCord (1972). Subsequently, various publications have extended the methods developed by these researchers, but not in a broadly applicable manner. In response, Werner and Kadlec (1996) combined the available analytical tools (Kadlec, 1994, Levenspiel, 1972) with the theoretical ideas proposed in the literature to develop a modified RTD theory. It was developed specifically for storm water treatment systems but can be applied to a wide range of variable flow systems.

RTD theory describes the mathematical relationships required to infer hydraulic behaviour from the concentration profiles generated in tracer studies (Fogler, 2006, Levenspiel, 1972, Werner and Kadlec, 1996). The application of traditional RTD theory requires steady-flow conditions to be maintained. However, there are many instances in which steady flow is not, or cannot, be sustained (for example, storm water treatment systems) and different tracer concentration profiles will be obtained depending on when, relative to a surge or disruption in flow, the tracer pulse is injected. Table 6-1 summarizes the most important hydraulic performance indicators for steady flow systems and highlights where standard RTD theory is not adequate to describe flow behaviour in non-steady flow systems.

Table 6-1: A comparison of steady and non-steady systems with regards to flow conditions, retention time and standard residence time distribution theory

	Steady Flow System	**Variable (Non-steady) Flow System**
System volume	$V_{sys} = k$	$V_{sys} \neq k$
Volumetric Flow Rate	$Q_{sys} = Q_{in}(t) = Q_{out}(t)$	$Q_{in}(t) \neq Q_{out}(t)$
Nominal Retention Time	τ	-
The RTD	Entrance and exit RTDs are equivalent $C(\theta) = E(\theta)$ for all θ	$E(t)$ and $E(\theta)$ are greatly influenced by variation in volumetric flow rate $C(\theta) \neq E(\theta)$
Zeroth moment	$C(t) = M / Q_{sys}$ $E(t) = 1$ $C(\theta) = 1$ $E(\theta) = 1$	$C(t) \neq M / Q_{sys}$ $E(t) = 1$ $C(\theta) \neq 1$ $E(\theta) = 1$
First moment	$E(t) = \bar{t}_m = \tau$ $C(\theta) = 1$ $E(\theta) = 1$	$\bar{t}_m \neq \tau$ - -

In practice, it is not possible to maintain steady flow in CW systems and the application of standard RTD theory requires determination of an average flow rate. There are various methods of mean flow rate estimation, but no generally accepted approach to establishing which resultant profile is the correct or best representation of system behaviour. Werner and Kadlec (1996) developed a method of RTD analysis in which the impact of a variable volumetric flow rate has been eliminated. The basis of Werner and Kadlec's modified RTD function is the use of the outlet cumulative discharge volume (Eq. 6-1), rather than the residence time.

$$V_{out}(t) = \int_{t_0}^{t_f} Q_{out}(t)\, dt \qquad [6_1]$$

where $V_{out}(t)$ is the cumulative discharge volume and $Q_{out}(t)$ is the flow rate at the wetland outlet measured as a function of time.

The cumulative discharge volume, $V_{out}(t)$, is normalized against the average total system volume, V(t), to yield the flow weighted time, Φ. V(t) and the total mass of tracer recovered are used to calculate the normalized concentration, C(Φ). A plot of C(Φ) against Φ can be compared directly to the C(θ) or E(θ) functions for a steady-state system. Failure to account for variation in the exit flow rate could result in qualitative (visual) similarities between different flow systems being overlooked. The non-steady RTD function, C(Φ), has the following properties:

- The 0^{th} moment is unity and provides a check on the mass balance.
- The 1^{st} moment is approximately unity, depending on the accuracy of measurement of V(t) and provides a check on the reliability of the data.
- The 2^{nd} moment and peak time (mode of the RTD) are not greatly influenced by non-steady flow conditions.
- If C(Φ) is calculated for a steady-flow system, it will be identical to C(θ) (Werner and Kadlec, 1996).

For comparison, Werner and Kadlec's variable flow method has been summarized and presented alongside Fogler (2006) and Levenspiel (1972) standard RTD (Figure 6-1). All equations are applicable to an impulse-response tracer experiment, but can be replaced by those relating to a step-change tracer test, as the analytical procedure outlined is applicable to both types of study.

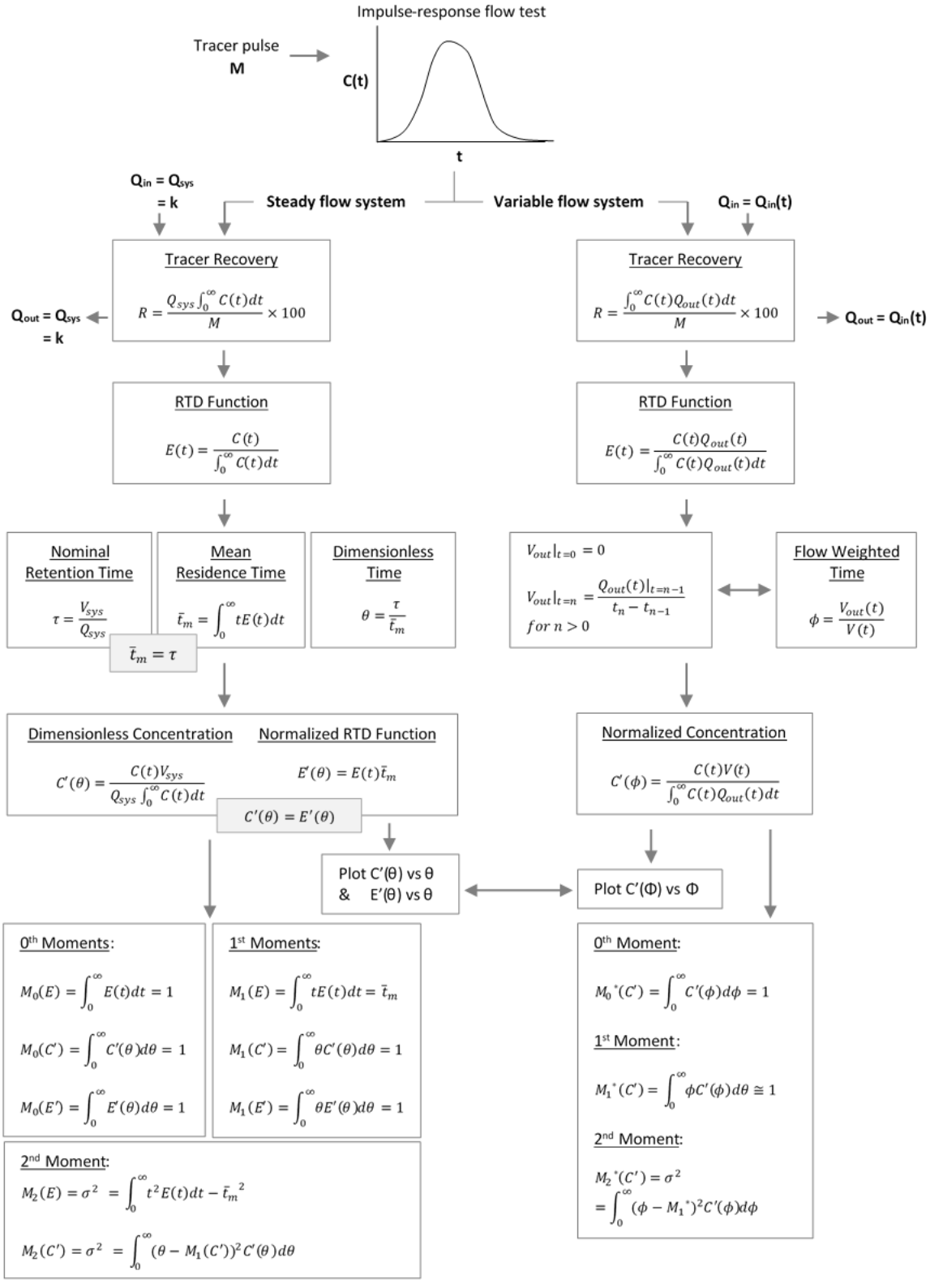


Figure 6-1: Summary and comparison of the mathematics underlying hydraulic theory for steady versus variable flow systems

6.3.5.3. Hydraulic efficiency

Wetland systems utilizing a maximal amount of the available treatment volume and maintaining near plug-flow conditions are hydraulically efficient (Persson et al., 1999) and, in general, will yield a higher degree of contaminant degradation or transformation. A variety of design factors including the mean residence time ($\bar{t}_m$), the inlet and outlet valve positions (Sheridan et al., 2014b), the vegetation and the type, size and shape of the wetland will bear influence (Persson et al., 1999, Thackston et al., 1987).

Thackston et al. (1987) proposed that $\bar{t}_m$ is the primary determinant of hydraulic efficiency and quantified efficiency in terms of the effective volume utilization ratio, e (Eq. 6-2).

$$e = \frac{\bar{t}_m}{\tau} = \frac{V_{eff}}{V_{sys}} \quad [6_2]$$

where $\bar{t}_m$ is the mean of the residence time distribution, τ is the nominal residence time, V_{eff} is the portion of the wetland volume used for effective treatment and V_{sys} is the total system fluid volume.

Persson et al. (1999) explained the combined importance of flow uniformity and maximum use of the available wetland volume for assessing hydraulic efficiency, λ, and proposed the following equation:

$$\lambda = e\left(1 - \frac{1}{n}\right) = \frac{t_p}{\tau} \quad [6_3]$$

where e is the effective volume utilization, t_p is the maximum concentration peak time recorded at the wetland outlet and n is the parameter from the Tanks-In-Series (T-I-S) model.

The Tanks-In-Series (T-I-S) model accounts for non-ideal flow behaviour in reactor systems. n represents the number of continuously stirred tank reactors (CSTR's) of equal volume in series. As $n \rightarrow \infty$, flow approaches ideal plug flow, while n = 1 indicates perfect mixing (Fogler, 2006, Kadlec and Knight, 1996). Fogler (2006) defined the number of tanks in series as:

$$n = \frac{\bar{t}_m{}^2}{\sigma^2} \quad [6_4]$$

where σ^2 is the variance, or the second moment, of the RTD.

6.3.5.4. Hydraulic efficiency indexes

The RTD function is a qualitative indication of flow behaviour as its shape alludes to non-ideal flow within the system. The hydraulic indexes reduce the RTD to a single value by comparing the flow behaviour in a real (or experimental) wetland system to that which would be expected in the same system if it were operating under ideal flow conditions (Teixeira and Siqueira, 2008).

Teixeira and Siqueira (2008) summarized and assessed seventeen hydraulic indexes published in the literature. The motivation for their study was the lack of standards for the assessment of wetland hydraulic performance and the fact that different indexes measuring the same phenomenon could yield different results. Their investigation considered RTDs for five flow regimes (from disperse plug-flow to complete mixing) and identified the hydraulic indexes most suited to quantifying the degree of short-circuiting and mixing, as discussed in the next sections.

Short-circuiting index

Teixeira and Siqueira (2008) concluded that the θ_{10} index (Eq. 6-5) is the best measure of short-circuiting because it is closely related to advective flow, displays low statistical variability and is a good indicator of channelling through the system.

$$\theta_{10} = \frac{t_{10}}{\tau} \qquad [6_5]$$

where t_{10} is the amount of time taken for the first 10% of the injected mass of tracer to reach the system outlet.

The smaller the value of the θ_{10} index, the greater the degree of short-circuiting, or channelling, through the system. This is undesirable because the residence time of pollutants in the root zone is decreased and the extent of removal will be reduced.

Mixing index

The variance, σ^2, or second moment, M_2, of the RTD (Figure 6-1) is the most suitable index for quantifying mixing effects, due to its close relation to the physical phenomenon and the fact that it is widely used in many kinetic models (Teixeira and Siqueira, 2008). The lower the value of σ^2, the smaller the spread of the data and the lower the degree of mixing. However, σ^2 has the disadvantage of high statistical variability when mixing effects are minimal.

In situations where the degree of mixing is low, the Morril Dispersion Index, MDI, (Eq. 6-6) is preferred (Rengers et al., 2016, Teixeira and Siqueira, 2008). The larger the value of MDI, the longer it takes for the bulk of the material to exit the system and the greater the degree of mixing.

$$\mathrm{MDI} = \frac{t_{90}}{t_{10}} \qquad [6_6]$$

where t_{90} is the amount of time taken for 90% of the injected mass of tracer to reach the system outlet.

Moment index

Wahl et al. (2010) proposed the Moment Index, MI, for hydraulic efficiency. They identified that a major limitation of the existing hydraulic indexes is their susceptibility to being skewed by the tail effect. MI is determined using the RTD and the hold back parameter (Stamou and Noutsopoulos, 1994), which is the area under the RTD function for all θ up until the nominal divide (where $\theta = 1$). Wahl

refers to this parameter as the pre-nominal moment, M_{pre} (Eq. 6-8). MI is defined based on a single exchange of the reactor volume only and is, hence, not subject to tailing effects. MI (Eq. 6-7) is based on the following assumptions:

i. If the residence time is equal to or longer than τ, the system is operating at 100% efficiency.
ii. The fraction of material reaching the outlet prior θ = 1 counts against hydraulic efficiency. Hence, the most weight is given to the shortest residence times.

$$MI = 1 - M_{pre} \quad [6_7]$$

$$M_{pre} = \int_0^1 (1 - \theta)\, C'(\theta)\, d\theta \quad [6_8]$$

A decrease in hydraulic efficiency produces a proportional increase in the magnitude of the pre-nominal moment and, thus, a decrease in the value of MI (Wahl et al., 2010). Hence, the smaller the value of MI, the lower the hydraulic efficiency.

6.3.6. Research objectives

The aim of the research presented in this paper was to investigate the following:

i. The appropriateness, or reliability, of applying the steady-state assumption to hydraulic calculations in a non-steady flow system.
ii. The impact of climatic conditions on the water balance and hydraulic behaviour.
iii. The value of a multiple depth and multiple location sampling campaign.
iv. An improved methodology for investigating CW systems.

6.3.7. Materials and methods

6.3.7.1. Pilot-scale constructed wetland

Construction of the pilot CW at the Helmholtz UFZ in Leipzig was completed in October 2013 and the first experiments on this system commenced in June 2015. The system was allowed to establish naturally, without any external nutrient source, from October 2013 to June 2015. During this time, municipal tap water was fed into the system in the spring, summer and autumn (March to November). The feed was shut off during the coldest winter months (December to February).

The wetland was buried, such that only the rim and upper 20 cm of the boundary walls protruded above the ground. The system was filled with glacial gravel (bed height 0.50 m; particle size 4 - 8 mm; voidage 36%) and planted with *Phragmites australis*. Each basket contained the same gravel and vegetation as in the surrounding wetland system. The basket cages had evenly punched holes of the same diameter

as the average gravel particle size to minimize flow disruption. The purpose of the baskets was to analyse, in more detail, a predominantly undisturbed section of the CW outside of the real system by its removal and transfer to the laboratory; for which the methods and procedures had been developed from previous studies on laboratory-scale planted fixed bed reactor (PFBR) systems (Kappelmeyer et al., 2002, Lünsmann et al., 2016). Photographs of the wetland system can be found in Figure E1 of Appendix E.

Figure 6-2 is a schematic diagram of the pilot HSSF CW. The stainless steel container is 6 m length x 0.70 m height. The system is fed by three evenly spaced valves (Figure 6-2a), positioned 5 cm above the wetland base. The discharge is removed via a single outlet valve (Figure 6-2a), centred and also 5 cm above the wetland base. Three fully removable, stainless-steel baskets (height 0.7 m; diameter 0.30 m) have been inserted into the central flow path (Figure 6-2a). One boundary down the length of the wetland is constructed at 16° from the vertical, such that the widths at the top and base of the container are 1.2 m and 1.0 m, respectively (Figure 6-2b).

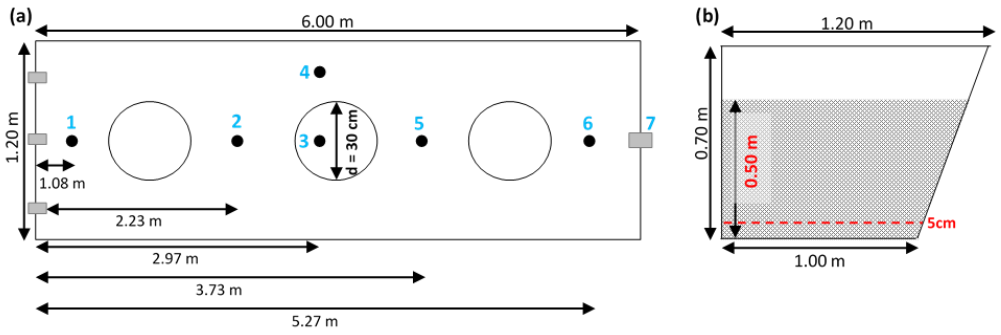


Figure 6-2: (a) An aerial view of the constructed wetland showing seven internal sample ports, three inlet valves and one outlet valve and (b) cross-sectional view showing the gravel bed and valve heights.

The inlet and outlet water flow rate was regulated via a gear pump (VGS120, Verder Pump, Germany), a motor (SEV6324, SEVA Tec, Germany) and a frequency controller (DF51-322-025, MOELLER, Germany). The Data was logged to allow for continual flow rate monitoring. The water level within the wetland was controlled by means of a syphon at the wetland outlet.

6.3.7.2. Impulse-response tracer tests

Stainless-steel sampling devices (hereafter referred to as samplers) were inserted into the gravel bed at six locations (Figure 6-2). The samplers were L-shaped, hollow tubes containing several holes at the base of their long ends. These openings were too small to allow for gravel to enter, but large enough to allow for easy movement of water. The long end was inserted into the gravel bed and the short end, containing a single opening, extended above the surface. The samplers were connected in pairs; one being the outlet tube (from which water was removed from the wetland) and the second the return tube. The return tube was fixed to the outlet tube such that the base of its long end was positioned 6 cm above

the base of the outlet tube. This arrangement ensured that water was removed from and returned to the wetland in a roughly spherical zone, so as to minimize flow disturbances. The short ends were connected to a peristaltic pump (BVP_Z, ISMATEC SA, Switzerland), a specialised stainless-steel flow cell (Schnegg, 2002) and a fluorometer (GGUN-FL, Albillia, Switzerland) using black norprene tubing. A schematic diagram of this set-up can be found in Figure E3 of Appendix E. The fluorometer was calibrated before each experiment using a two-point calibration.

30mg of uranine (fluorescent tracer powder) was dissolved into 1L of distilled water and injected as a single pulse. The tracer solution was prepared directly before injection and protected from light in a brown glass bottle. For the duration of each flow test, water was pumped from the wetland, into the flow cell and returned to the bed at the same location (Figure E3, Appendix E) to ensure that the total system volume was maintained. The peristaltic pump rate was kept low to minimize potential impact on flow behaviour. The fluorometer was programmed to record a potential (mV) at 10 second intervals, which was converted to a corresponding uranine concentration using the results of the calibration.

2015 tracer flow tests

Flow tests were conducted at each of the sample ports (Figure 6-2a) during September and October 2015. These were the very first hydraulic tests to be conducted in the pilot wetland. Samplers were inserted to mid-depth (24cm below the gravel surface). The inlet flow rate was set to provide a retention time of approximately five days and the syphon was adjusted to maintain a water level of 0.5 m (coinciding with the gravel surface). The inlet and outlet flow rates were monitored three times daily: 6 am, 12 noon and 6 pm. The system was fed with tap water only.

2016 tracer flow tests

The hydraulic investigation was extended during 2016, with flow tests being run from April through November at the designated sample ports (Figure 6-2a). The flow test at the system outlet was performed in duplicate. Three pairs of samplers were inserted at each port (12 cm, 24 cm and 36 cm below the gravel surface), with 6 cm separating each pair. The inlet flow rate was set to provide a retention time of approximately seven days and the syphon at the outlet was adjusted to maintain a water level of 0.44m (6cm below the gravel bed surface).

In addition, the vegetation density was measured monthly, the inlet and outlet flow rates were monitored throughout each day and the weather data (air temperature, global radiation, humidity and wind speed) was recorded hourly at the on-site weather station. During the April flow test, the system was fed with tap water only. In May and June, the wetland received a nutrient solution of urea (6.62 mg/L). For the remaining tests, the feed was artificial wastewater (AWW). The AWW concentrate was prepared based on published standards and contained 30 g/L casein peptone, 20.62 g/L meat extract, 5.62 g/L urea, 5.25 g/L dipotassium hydrogen phosphate. The concentrate was diluted as 1:400 with municipal tap water before entering the wetland (FMJC., 2001).

6.3.7.3. Hydraulic calculations

The equations underlying the hydraulic calculations are summarized in Figure 6-1. All data was normalized before proceeding with any further analyses. When tracer recovery was less than 100%, the data was normalized against the actual mass of tracer recovered, rather than the total mass injected, to ensure that the area under the E(t) and E(θ) curves was unity (Holland et al., 2004) but this hydraulic data was treated as a guideline only.

As a preliminary step, the system was visualized in real-time. Steady-flow was assumed and the normalized concentration break-through curves (C(θ) vs θ) were calculated. Scaling factors (HRT_{adj} and C_{adj}) were defined using a theoretical HRT, HRT_{ideal}, of 7 days and theoretical tracer mass, M_{ideal}, of 30 mg (Eq. 6-9 to 6-11). Dimensions were re-introduced by multiplying θ by HRT_{adj} and C(θ) by C_{adj}.

$$HRT_{adj} = \frac{HRT_{ideal} \times L_{port}}{L} \quad [6_9]$$

$$C_{adj} = \frac{M_{ideal}}{Q_{adj} \times HRT_{adj}} \quad [6_10]$$

$$Q_{adj} = \frac{V_{sys}}{\tau_{adj}} \quad [6_11]$$

where HRT_{adj} is the adjusted or scaled HRT, L_{port} and L are the respective distances from the inlet to the sample port and wetland outlet, C_{adj} is the adjusted concentration and Q_{adj} is the adjusted volumetric flow rate.

Further to this, the normalized RTDs (E(θ) versus θ) were plotted on the same set of axes to investigate self-similarity (Sheridan et al., 2014a).

The 2016 flow tests investigated the causes and impacts of variable flow in more detail. The hydraulic parameters (RTDs, moments, efficiency indexes etc.) were calculated using standard RTD theory (Fogler, 2006, Levenspiel, 1972) and, again, using the method developed by Werner and Kadlec (1996) for non-steady flow systems. Standard RTD theory requires calculation of an average volumetric flow rate, $\overline{Q}_{sys}$, over the duration of the flow tests. This was computed by:

$$\bar{Q}_{sys} = \frac{\bar{Q}_{in} + \bar{Q}_{out}}{2} \quad [6_12]$$

where $\overline{Q}_{in}$ is the average inlet volumetric flow rate and $\overline{Q}_{out}$ the average outlet volumetric flow rate over the duration of the flow test.

The hydraulic calculations were repeated using, firstly, $\overline{Q}_{out}$ and, secondly, an estimate of the local flow rate at an internal sample port, $Q_{internal}$, in place of $\overline{Q}_{sys}$. To determine $Q_{internal}$, it was assumed that the

flow rate decreased linearly from inlet to outlet and expressions relating stem density to volumetric flow rate were obtained (refer to Appendix E). Ports 2, 3 and 5 were selected for illustrative purposes.

Climatic data was also collected to calculate the wetland water budget, which is given by:

$$m_{in} + m_{precip} = m_{out} + m_{evap} \quad [6_13]$$

$$Q_{in}\Delta t\rho + \frac{(\sum \delta_i)a\rho}{10^6} = Q_{out}\Delta t\rho + \frac{ETa\rho}{10^6} \quad [6_14]$$

where m_{in}, m_{precip}, m_{out} and m_{evap} [kg] are the total masses of water from inflow, precipitation, outflow and ET, respectively.

Eq. 6-14 expresses the mass balance (Eq. 6-13) in terms of measured parameters. Δt [d] represents the total duration of the flow test. $\sum\delta_i$ [mm] is the increase in water depth due to rainfall and ET [mm] is the water loss due to evapotranspiration, summed over the duration of the flow test. a [mm^2] is the wetland surface area. Eq. 6-14 was used to estimate the amount of water lost my evapotranspiration.

6.3.8. Results and discussion

6.3.8.1. Overview of wetland hydraulic behaviour

Tracer selection

Uranine was the tracer chosen for the flow tests due to its low environmental impact, its economy of use (it is highly soluble and detectable at low concentrations in water), its non-biodegradability (Gutowski et al., 2015, Käss, 1998, Merck, 2011, Smart and Laidlaw, 1977) and convenience, as the fluorometers contained three optical lamps for simultaneous measurement of uranine, resazurin (Raz) and resorufin (Rru). Only uranine was injected due to the cost of the other tracers.

Prior to selection, however, various properties of uranine were considered. Uranine is photosensitive and degraded by direct sunlight (Eriksson et al., 1997). Being an organic species, uranine is also susceptible to both biotic and non-biotic degradation (hydrolysis, redox reactions etc.) (Gutowski et al., 2015) even though studies regarding biodegradation of fluorescein are not conclusive (Käss, 2004, Kranjc, 1997) and research regarding microbial degradation is minimal (Gutowski et al., 2015). It has been found that biodegradation is negligible in experiments of 5 to 48 hours (Alaoui et al., 2011, Anderson et al., 2009, Duwig et al., 2008). After 28 day laboratory experiments, Gutowski et al. (2015) concluded, in accordance with (Smart and Laidlaw, 1977), that uranine and its transformation products are not readily biodegradable, but agreed with Käss (2004) that biodegradation in the natural environment cannot be completely disqualified.

Uranine contains negatively charged functional groups and is prone to sorption on numerous media (Kasnavia et al., 1999), the extent of which is governed by pH, temperature, water composition, uranine concentration and gravel porosity (Eriksson et al., 1997, Smart and Laidlaw, 1977). The adsorption capacity is higher for media with higher organic content (Kasnavia et al., 1999, Mikulla et al., 1997). In experiments carried out by Kasnavia et al. (1999), fluorescein sorbed strongly to alumina based materials (net positive charge), but weakly to silica based materials (net negative charge).

Percentage recovery

100% recovery of Uranine was obtained at the wetland outlet in 2015, but only 31% and 36% in duplicate experiments in 2016. Non-biotic degradation would have impacted tracer recovery over the extended retention time of these experiments (compared to typical flow tests). The contribution of biodegradation cannot be quantified with any certainty, but the longer residence time and the outdoor system may have presented greater opportunity for Uranine biodegradation.

The pH of the water decreased with distance from the wetland inlet, with depth beneath the bed surface and with time. The average pH decreased from 6.4 (at the front section and surface) to 5.0 (at the back section and base). As the strength of Uranine fluorescence decreases with decreasing pH and the effect on photo-detection is noticed at a pH < 7.0 (Smart and Laidlaw, 1977), the more acidic conditions in the wetland could have suppressed the signal strength and given false low concentration readings.

Plant uptake and premature termination of the flow tests are likely to have had an impact on Uranine recovery in the 2016 experiments, although the role of plant uptake was not investigated directly. Experiments to measure the extent of plant uptake are suggested for further studies. Due to time constraints, a maximum of two retention times were allowed for the flow tests in this study, although at least three retention times are recommended for the Uranine concentration to return to baseline.

Photodegradation is not thought to have had an impact on recovery because the tracer solution was prepared immediately before injection, stored in brown glass to be protected from light and then injected into the wetland below the gravel surface. Water turbidity was measured by the fluorometers and corrected for in the calibration, so this is not thought to have impacted the material recovery. Although the porosity of the gravel itself was not determined, it was silica based and the water was not highly acidic. Hence, sorption onto the gravel is not thought to have played a large role in lowering tracer recovery. It is recommended, however, that experiments to characterise the gravel medium are conducted in future.

Uranine break-through curves in real-time

The idealised concentration break-through curves are presented in Figure 6-3 and Table 6-2 shows the corresponding maximum peak concentrations and peak times. All hydraulic calculations were performed in *Matlab R2016b* and the RTD's were generated using the in-built figure plotting toolbox.

A detailed description of the code can be found in the GitHhub repository at https://github.com/kappelmeyer/WetlandFlow.

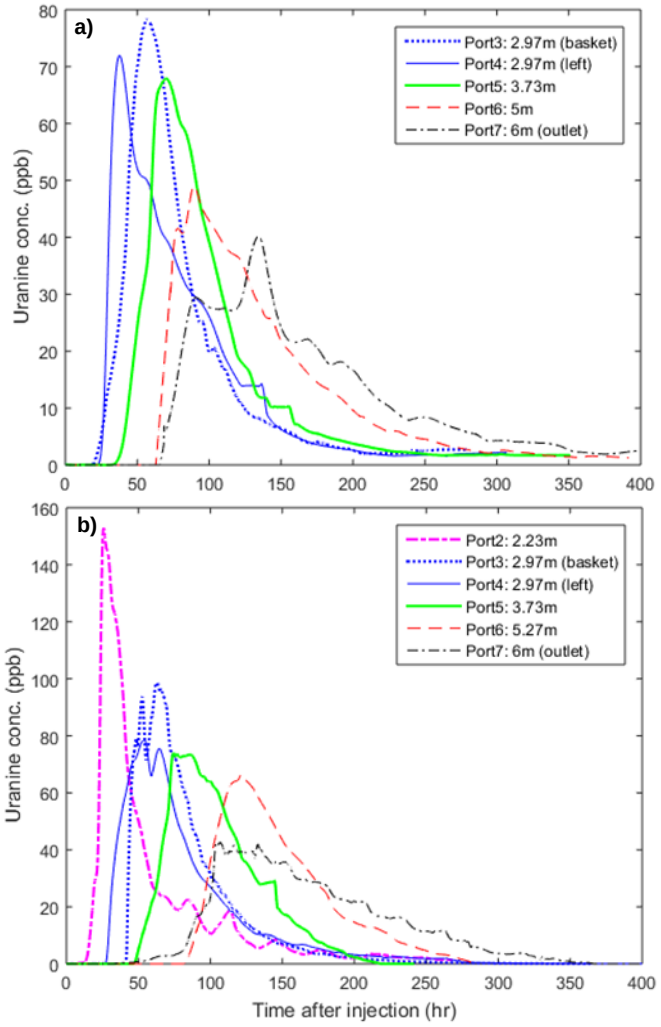


Figure 6-3: (a) 2015 and (b) 2016 idealized concentration breakthrough curves at various distances from the wetland inlet and mid-depth (24cm) below the gravel surface, assuming a tracer mass of 30 mg and hydraulic residence time of 7 days.

Table 6-2: Time to maximum peak concentration at various distances along the flow path (2015 versus 2016)

Port Number		**2**	**3**	**4**	**5**	**6**	**7**
Peak conc. (ppb)	**2015**	-	78.4	72.0	68.0	49.0	40.2
	2016	153.0	98.3	78.5	74.1	66.2	42.7
Peak time (h)	**2015**	-	56.7	37.7	70.1	89.6	134.1
	2016	25.8	63.3	54.4	74.1	121.3	106.7

Figure 6-3 a and b show a progressive broadening of the peak base and change in peak shape with increasing distance. The peaks are initially sharp and narrow and become rounded, flat and multi-modal and this is indicative of increasing dispersion as the tracer pulse travels from inlet to outlet. The peak

shapes indicate low dispersion in the first 2 m of the wetland, moderate dispersion in the middle section (2 m to 5 m) and high dispersion within the last 1 m of the bed.

The maximum peak concentration decreases with distance; also due to progressive dispersion of the Uranine. The peak maxima are observed later in time in 2016. This is likely due to development of the *Phragmites* root system and a thicker root mat providing increased resistance to flow. The peak at Port 4 appears earlier than at Port 3, with the time difference being more pronounced in 2015 (the peak at Port 3 appears 19 h after the peak at Port 4 in 2015; compared to just 9 h subsequent in 2016). This would suggest that flow through the basket was impeded and preferential flow paths had formed around the obstruction.

Contrary to what is observed at the internal ports, the maximum concentration peak at the outlet (Port 7) is detected later in 2015 than in 2016. However, the 2016 outlet RTD is broad and flat with multiple peaks (Figure 6-3) making it difficult to determine the exact location of the main peak. At least ten peaks of similar concentration can be identified, for which $\bar{t}_{peak}$ is 118.7 ± 9.3 h. The outlet peaks (broad, rounded and multi-modal) indicate dispersion of the tracer. The θ-position of the peaks, the extent of tailing and the many small peaks on an elongated RTD tail indicate dead space and hold-up.

Normalized RTDs

The normalized RTDs at three depths below the bed surface are given in Figure 6-4. In general, it was found that $\bar{t}_m$ exceeded τ, which alluded to a deviation from plug flow and mixing effects. Figure 6-4 shows the peaks shifted towards lower θ with straight, elongated tails; indicating dead zones within the system. θ_{peak} in the region 0.5 – 0.95 suggests a low to moderate amount of dead space (lower values indicate more dead volume). The multiple peaks on the RTD tails suggest hold-up within the system. In this context, hold-up means that some of the water becomes trapped or is impeded (its flow rate is reduced) and, consequently, does not reach the wetland outlet with the bulk water front travelling through the system. There could be a number of contributing factors for this, such as a dense root region, plant uptake and evapotranspiration, sedimentation, biofilm development, Uranine sorption and stagnant zones. There is no evidence of extensive short circuiting as the bulk of the tracer material does not reach any sampling location prior to θ = 0.4 (no peaks are detected prior to θ = 0.4).

Sheridan et al. (2014a) introduced the concept of the self-similarity of RTDs in systems displaying non-ideal flow behaviour. This principle is particularly useful in the interpretation of the results of multi-dimensional hydraulic experiments. The RTD measured at any internal location represents localized flow conditions, but if self-similarity between the RTDs can be demonstrated, it is reasonable to assume that hydraulic behaviour throughout the wetland (or at least a portion of it) is similar. This method allows for the comparison of RTDs from different locations and, if self-similarity is present, it can be concluded that different portions of the wetland behave in a similar manner (from a hydraulic point of view); despite increasing dispersion down the length of the wetland bed.

In 2015, self-similarity can be identified from 3 m to 5 m down the wetland (Figure 6-4a). Sheridan et al. (2014a) also showed self-similarity of the RTDs in the middle section of their experimental wetland. The only visual exceptions are Port 4 (where it is thought that flow channels around the central basket) and, to a lesser extent, Port 7 (where the distribution is multi-modal). Self-similarity is not evident again in 2016 (Figure 6-4b, c and d). The RTDs at Ports 2 and 6 are most distinctly different, which is consistent with the findings of Sheridan et al. (2014a). Mixing effects and a non-distinct flow profile could account for the clearly non-ideal behaviour in the front section of the bed (0 m to 2 m). Bypass and convergence of flow towards the outlet could be contributing factors in the final 1 m to 1.5 m. The RTDs are multi-modal at Ports 3, 4 and 5, with more peaks of lower concentration appearing at increasing depth. The outlet also shows a distinctly multi-modal profile (Figure 6-4c).

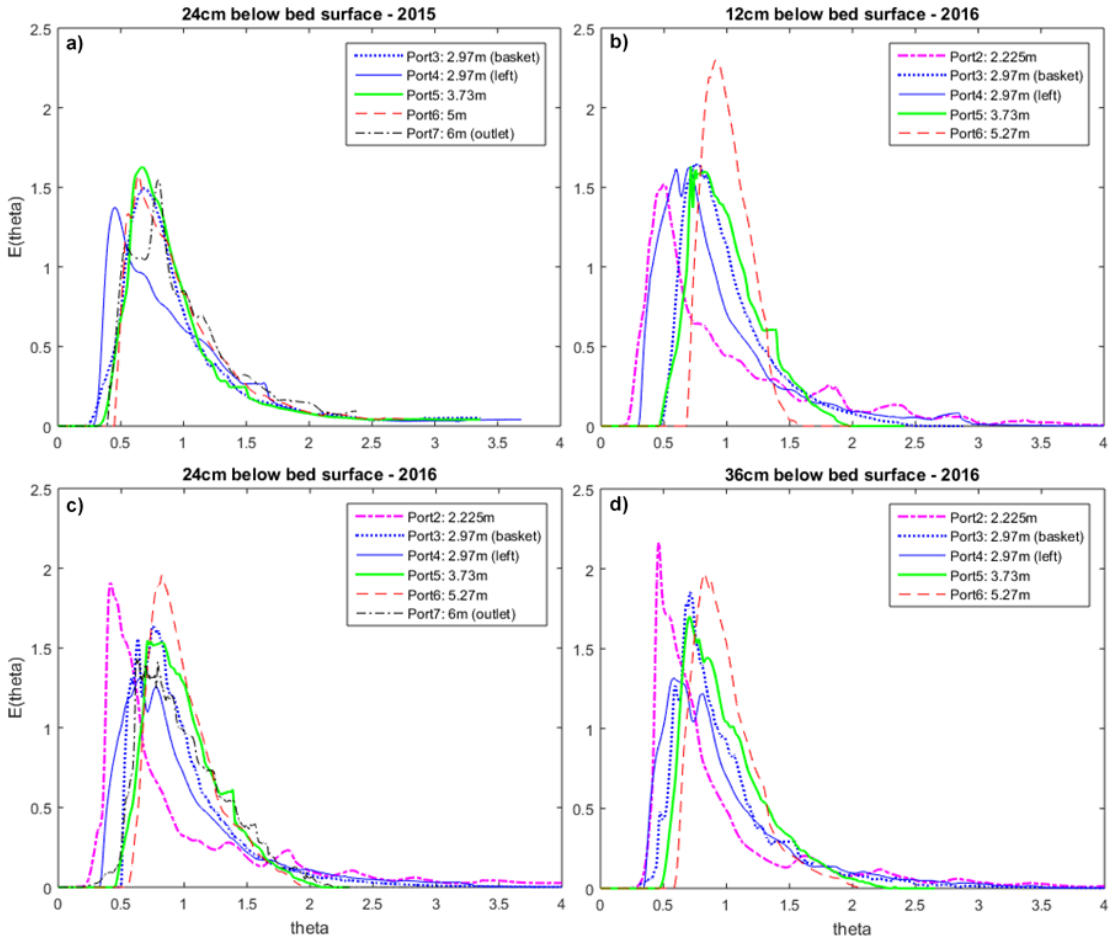


Figure 6-4: Normalized RTDs, assuming steady flow, at various distances along the flow path at (a) mid-depth (2015) and (b) 12 cm, (c) 24 cm and (d) 36 cm depth (2016).

Direct comparisons of fluid flow behaviour at each sample location are made by plotting the normalized RTDs obtained in 2015 and 2016 against one another (Figure 6-5). The outlet peaks are all multi-modal.

The outlet RTD obtained in 2015 shows two distinct peaks; the first ($\theta \cong 0.5$) indicates bypass and the second ($\theta \cong 0.9$) at maximum concentration is assumed to be the main peak. The 2016 outlet RTDs have multiple peaks. The main peak location cannot be identified, but the general peak shapes suggest similar flow behaviour for both 2016 flow tests.

There is a change in flow behaviour at Port 3 and 4, shown by the transition from a unimodal to a bimodal profile from 2015 to 2016. The curves are also shifted towards higher normalized time, θ, at the internal sample ports in 2016 (Figure 6-5) and this can be attributed to mixing effects. The measured wetland vegetation density was noticeably higher in 2016 than in 2015 (Figure E1 and E2, Appendix E) and the shapes of the internal RTDs could be evidence of the thicker *Phragmites* root mat obstructing flow. However, the flow tests were subject to variable flow conditions, which could have had a large impact on peak shape, and it cannot be said with certainty that the behaviour observed in 2016 is due only to internal system development and not fluctuations in flow rate.

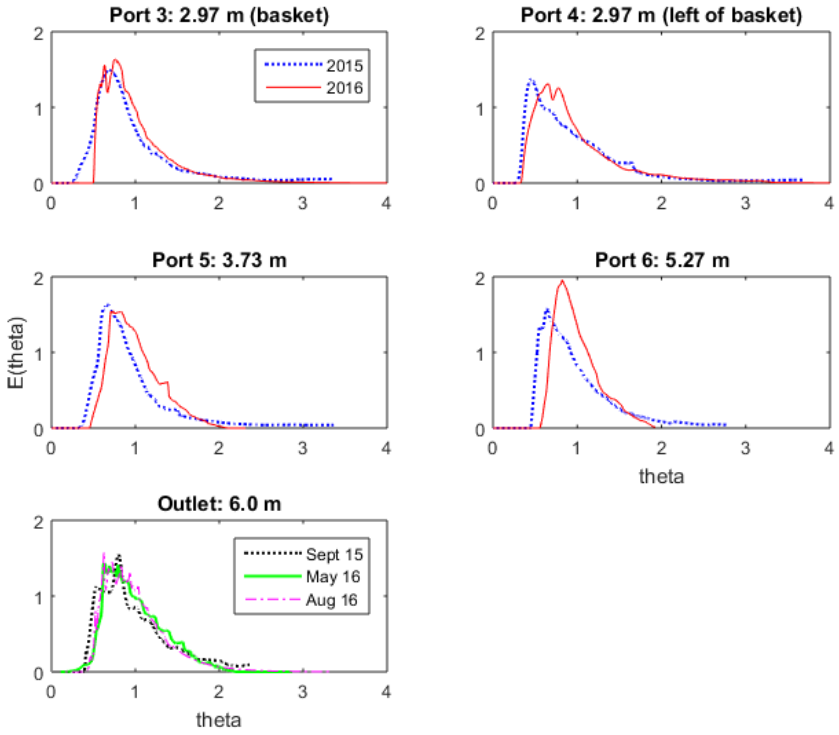


Figure 6-5: Comparison of the 2015 and 2016 normalized RTDs at various distances along the flow path and at mid-depth (24cm) below the gravel surface.

If self-similarity of the RTDs can be demonstrated from flow tests at multiple locations, it can be deduced that hydraulic behaviour in different portions of the wetland is very similar; even under non-ideal flow conditions. The RTDs at the front section of the wetland are affected by mixing and a non-distinct flow profile, while those at rear section are influenced by bypass and convergence of flow towards the outlet. Self-similarity was proven in the middle section of the wetland in 2015, but could

not be shown anywhere in 2016. Based on the outlet RTDs, the peak location with respect to normalized time, θ, indicates greater occurrence of bypass flow in 2015, but greater effect of mixing in 2016.

6.3.8.2. Impact of applying steady-state assumptions to a variable flow system

During the 2015 experiments, it was observed that $\bar{t}_m$ and τ were not equal and that the zeroth and first moments of C(θ) were not unity for any of the RTDs. This was a strong indication that the system was not operating under steady conditions; despite this being the assumption made for the hydraulic calculations. A single estimate of the system volume, measurement of the in- and outflow rates once daily and calculation of an average flow rate for the duration of each flow test was inadequate. Consequently, it was determined that closer monitoring of the inlet and outlet flow rates, better estimation of the total system volume, frequent vegetation (stem) density measurements and analysis of climatic data would improve the description of flow behaviour.

Comparison of Standard and Modified RTD Theory

The normalized RTDs at the wetland outlet, calculated first using standard RTD theory and again using the modified method for variable flow systems, are given in Figure 6-6. Selected hydraulic parameters and hydraulic indexes are also summarized in Table 6-3. The hydraulic indexes were calculated from the RTDs obtained assuming steady flow because the mathematical relations employed required use of a steady volumetric flow rate and expressions to handle a variable flow rate were not developed for this study.

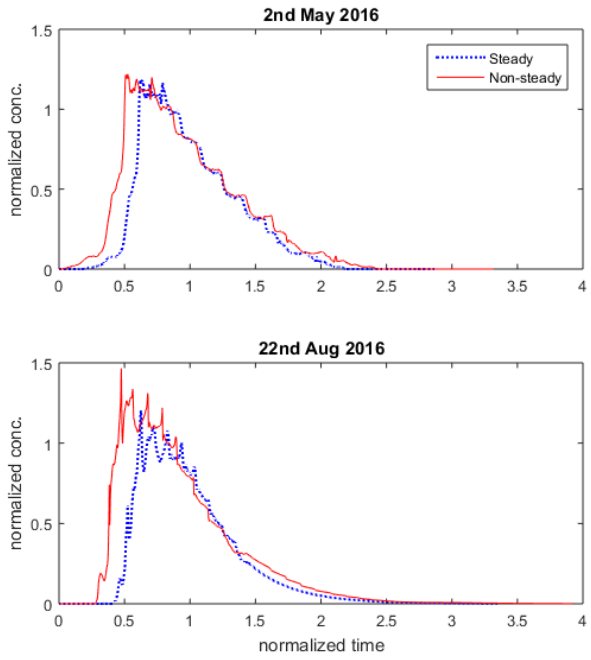


Figure 6-6: 2016 normalized RTDs at the wetland outlet for experiments in duplicate, calculated using standard (dashed line) and variable flow (solid line) methodologies.

Table 6-3: Peak time and hydraulic moments at the wetland outlet using standard and variable flow methodologies (sample distance = 6.0 m; system volume = 1009 L)

Date of flow test	**2 May 2016**		**22 August 2016**	
Method	**Steady flow**	**Variable flow**	**Steady flow**	**Variable flow**
θ_{peak} / Φ_{peak}	0.6352	0.5250	0.6247	0.4753
M_0 (E)	1.0000	1.0000	1.0000	1.0000
M_0 (C')	0.8240	1.0009	0.7577	1.0016
M_1 (E) = $\bar{t}_m$ (h)	149.4	150.0	231.3	241.1
M_1 (C')	0.8240	0.9591	0.7577	0.9309
θ_{10}	0.6208	-	0.6111	-
MDI	2.4183	-	2.4337	-
MI	0.8851	-	0.8926	-

When comparing the θ_{10}, MDI and MI indexes obtained from the duplicate experiments (May and August 2016), the results are similar. The degree of short circuiting is relatively low; indicated by a short-circuiting index (θ_{10}) closer to 1.0. The moment index, MI, is close to 0.90 in both cases and suggests good hydraulic efficiency. The higher values of the Morril Dispersion Index, MDI, would indicate some mixing, which is in agreement with the shape of the RTDs (Figure 6-6). These values should be treated with caution because of the questionable applicability of the steady state assumption made to perform the calculations, their inherent statistical variability and their reliability being subject to the system experiencing only a minor degree of mixing. It was assumed that the system would experience minimal mixing effects due to the low flow rate, which is well within the laminar region, but the extent of mixing was not otherwise quantified.

The Students t-test (at 95% confidence) was used to compare the outlet RTDs. For $\alpha = 0.05$, the null hypothesis H_0 ($\mu_d = 0$) indicated no significant difference between the RTDs. The value of the student's t-test for 25 evenly spaced time (and corresponding Uranine concentration) points (n = 24) was 2.064. The outlet RTDs obtained in 2016, by both the steady and the variable flow methods, were compared. The values of t were 2.046 and 2.368 for the May and August flow tests, respectively. The method of RTD calculation did not significantly impact the results extracted from the May test ($-2.064 < t < 2.064$), but the opposite is true for August ($t > 2.064$). When the plots of flow rate are considered (Figure E5 b and d, Appendix E), it is evident that the inlet and outlet flow rates are subject to greater variation in August as compared to May.

The May and August 2016 RTDs calculated by the steady flow method were also compared using the paired student's t-test, yielding a t-score of 4.763. This test was repeated for the RTDs obtained by the variable flow method and the t-score was 0.197. The RTDs calculated by the steady flow method are significantly different, while those calculated by the non-steady flow method are comparable. From

this, it can be concluded that a variable volumetric flow rate can have a significant impact on the RTDs and the inferred hydraulic behaviour.

The 2016 flow tests indicated that the wetland under study was characterised by a low degree of short-circuit flow (θ_{10} in the vicinity of 0.6), good hydraulic efficiency (MI close to 0.9) and mixing (shapes of the RTDs and high values of MDI). The degree of mixing was not otherwise quantified, but the low volumetric flow rate (within the laminar region) should have kept mixing effects to a minimum to enable use of these indexes. After a statistical analysis of the results of the duplicate tests at the wetland outlet, it was found that the RTDs calculated assuming steady flow and using standard RTD theory were significantly different. In contrast, the same RTDs calculated using the modified method for variable flow systems (Werner and Kadlec, 1996) were similar to one another. For more reliable results, the variable flow method should be used for hydraulic calculations on non-steady flow systems.

Impact of a variable volumetric flow rate

Plots of the inlet and outlet volumetric flow rates during the 2016 flow tests are given in Figure E5 of Appendix E. In general, the inlet flow rate exceeded the outlet flow rate, except during periods of heavy rainfall. This decrease in flow rate, which has also been observed by other researchers, motivated the estimation of an estimated local flow rate at each internal sample port. Table E1 of Appendix E contains detail of the calculations and the approximate internal flow rates. The local, internal volumetric flow rate was then used to re-calculate the RTDs (Figure E7, Appendix E). The RTDs calculated using the steady flow assumption and three different estimates of the average volumetric flow rate all lie closely on top of one another. It is only the RTD determined using the variable flow method that has a different shape and peak location. Hence, the method of estimation of the average volumetric flow rate does not have as large an impact on the shape and position of the RTD as does a fluctuating rate of outflow.

Impact of climatic factors

Climatic data from April, August and October is presented in Figure 6-7. August was the hottest month in Leipzig, with the highest daily global radiation maxima, highest levels of evapotranspiration and lowest humidity (Figure 6-7c, d). The outflow oscillated between 0 L/h and 7 L/h during the period 22 - 31 August (Figure E5 d, Appendix E) and no outflow was recorded during the day when the levels of evapotranspiration were at their highest.

October was the coldest month during the experimental period. The global radiation was noticeably lower than in August (Figure 6-7f) and there was no evapotranspiration, high humidity and numerous rain events (Figure 6-7e). The surges in the outflow rate from 18 - 25 October (Figure E5f, Appendix E) coincided with these rain events.

On some days during April and October, the water balance yielded slightly negative levels of evapotranspiration. In general, this was observed around the time of a rain event and could be due to a delay in the response of the system to correcting the water level.

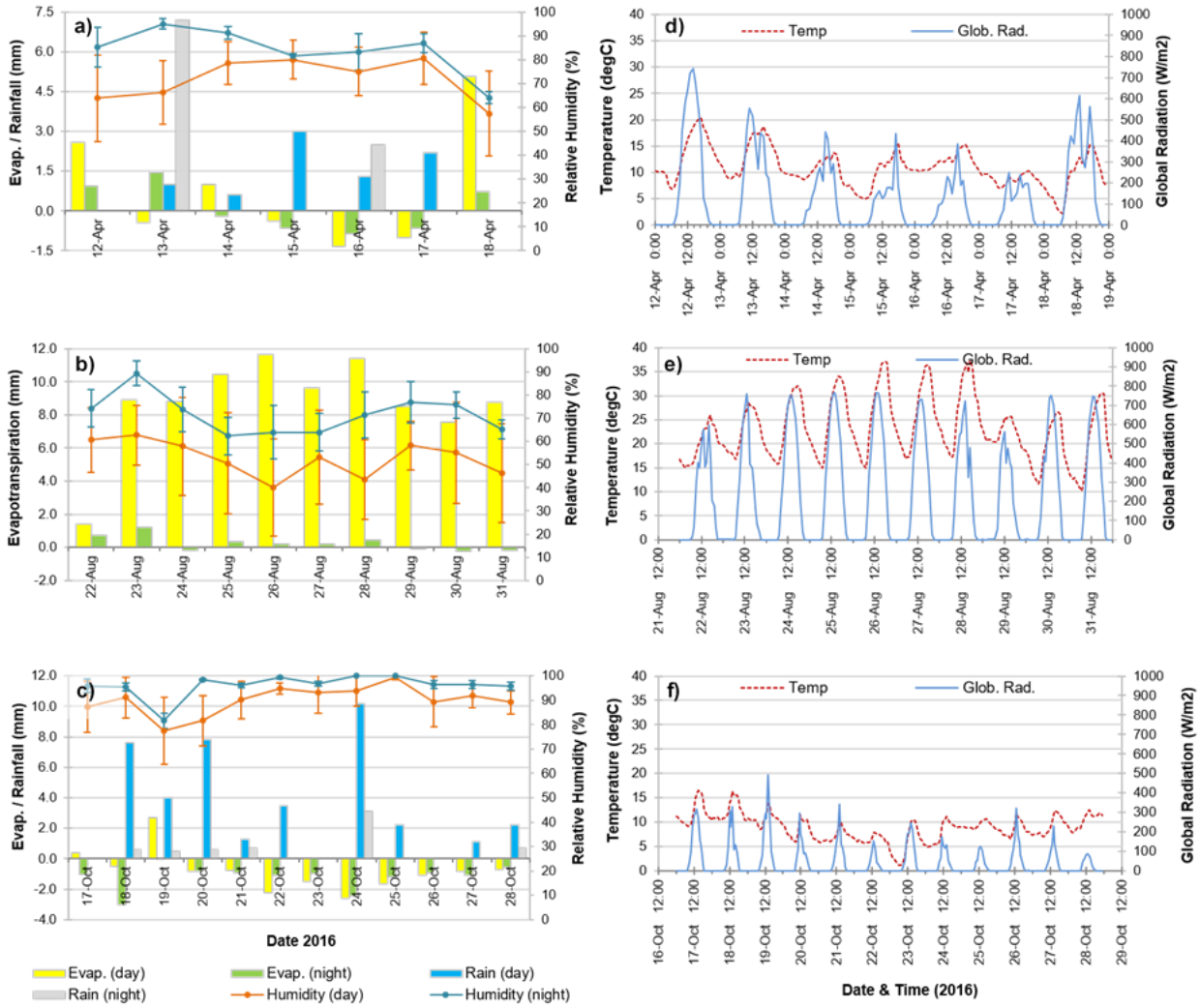


Figure 6-7: Evapotranspiration, rainfall, relative humidity and global radiation measured in Leipzig during April, August and October 2016.

The levels of global radiation and evapotranspiration are highest at the peak of summer and, since more water will be lost via the plants during this time, a drop in outlet flow rate can be observed. If accompanied by a period of low humidity and low rainfall, the outlet flow rate can drop to zero. When the opposite climatic conditions are experienced in the late autumn to early winter, there will be only a minor decrease in flow rate between the inlet and outlet. Periods of heavy rainfall will produce a surge in the outlet flow rate as a response of the wetland control system in maintaining the water level. In any outdoor wetland system, it is important to account for climatic factors in terms of calculating the water balance.

6.3.9. Conclusion

Impulse-response flow tests were conducted on a pilot scale CW at the Helmholtz UFZ during the spring, summer and autumn of 2015 and 2016, the results of which were used to hydraulically characterise the system.

At the time of the research, the CW was in its early start-up phase and, thus, impacted by internal plant root development and a noticeable increase in vegetation density was observed between the end of autumn 2015 and the end of spring 2016. The wetland was also exposed to various external climatic factors; both of which had varying levels of impact on the discharge volumetric flow rate over the experimental period. These variations in the outflow rate were observed to be closely related to weather events. When the highest temperatures, global radiation and evapotranspiration were logged in August, the outflow rate was low or zero. When ambient temperatures, global radiation and evapotranspiration were low in October, and high humidity was also recorded, the outflow rate remained higher. In addition, large surges in outflow were also recorded during rain events.

The RTDs obtained via two different methods were compared. The first method utilised standard RTD theory and the steady flow assumption; while the second was Werner and Kadlec (1996) modified RTD theory for variable flow systems. Although a visually reasonable approximation of hydraulic behaviour can be obtained using the standard RTD methodology, statistically significant differences were observed between the outlet RTDs when compared to the variable flow methodology.

The assumption that a real system operates under approximately steady flow conditions should not be made where variation in flow is either the norm or an intermittent occurrence; irrespective of size. Hence, Werner and Kadlec (1996) modified RTD theory should be used preferentially to calculate experimental RTDs. If the steady-flow methodology is preferred, preliminary investigations applying both methods are encouraged to validate the choice of the steady-state method. This, too, highlights the importance of regular and accurate inlet and outlet flow-rate monitoring.

In future, hydraulic experiments can be enhanced by determining the porosity of the gravel medium, quantifying the extent of plant uptake and developing mathematical relationships to calculate the hydraulic indexes for the variable flow method.

Acknowledgements

Michael van Zyl and Alyona Lepilova

Dr Marie Kurz and Dr Christian Schmidt

For financial assistance:

The South African DST and WRC; The University of the Witwatersrand Friedel Sellschop Award; The South African NRF; The DAAD and the Helmholtz UFZ, Leipzig

Chapter 7 Contaminant degradation in a pilot-scale constructed wetland in the early start-up phase

7.1. Summary

This chapter presents the results of the chemical studies carried out in the outdoor pilot-scale wetlands at the Helmholtz UFZ in Leipzig during 2016. Again, the focus was on TOC and TN as a follow-up to the experiments conducted in the summer and fall of 2015 (see Chapter 5). As in the preceding 2016 hydraulic investigation (see Chapter 6), the sampling regime was expanded to multiple depth network to better understand the changes occurring within the wetland bed. The experimental data supporting this chapter is provided in Appendix A.

7.2. Statement of Individual Contribution

The experimental design, preparation, work and analysis was carried out by myself with Dr Uwe Kappelmeyer advising and overseeing the work at the Helmholtz UFZ in Leipzig Germany and in close collaboration with Prof Craig Sheridan. Some of the analytical results (TOC, IC, TC/NPOC and TN) were, again, provided by Frau Puschendorf and the Multi N/C 2100 S analyser (Analytik Jena AC). Alyona Lepilova assisted with the collection of samples in the field.

7.3. Experimental Results

7.3.1. Baseline physico-chemical characteristics

Prior to the investigation into the degradation, or transformation, of select components from an artificial domestic wastewater, samples were collected over a period of three months (April - June 2016) in order to quantify the baseline characteristics of the pilot-scale CW. Samples were collected at three depths (12cm, 24cm and 36cm) from six sample ports down the length of the CW; as well as at the inlet and outlet (refer to Figure 3-4, Chapter 3). Table 7-1 summarizes the average pH, TOC concentration and TN concentration.

As discussed in Aylward et al. (2017) (Chapter 5), wetland systems are in a continual state of flux, due to both their internal development and the impact of external factors (such as environmental conditions). It was, thus, recommended that hydraulic and chemical-kinetic studies be repeated seasonally and annually into long-term operation in order to somewhat understand the extent of the change. The hydraulic tracer tests (Chapter 6) and the experiments presented in this section were the first set of follow-up studies. The feed of municipal water into the system was re-established at the beginning of April 2016 (early spring) once ambient temperatures had risen sufficiently after the European winter and continued through to the end of June 2016. At the time of the baseline sampling, the system had no additional carbon source and a low organic load.

Table 7-1: Average baseline pH, TOC concentration and TN concentration with the average temperature and saturated oxygen concentration (fresh water, 760 mm Hg) in the pilot CW

Date (2016)	Depth (cm)	Average temp (°C)	Saturated O_2 (mg.L^{-1})	pH	TOC (mg.L^{-1})	TN (mg.L^{-1})
April	inlet	14.0 ± 2.0	10.34	7.61 ± 0.00	3.00 ± 0.34	1.26 ± 0.39
	12	12.1 ± 2.8	10.80	6.62 ± 0.34	4.44 ± 1.19	2.75 ± 1.37
	24	12.0 ± 2.8	10.82	6.73 ± 0.38	4.13 ± 0.77	3.70 ± 2.03
	36	12.0 ± 2.8	10.82	6.80 ± 0.42	4.14 ± 0.95	4.29 ± 2.36
	outlet	16.0 ± 0.6	9.90	6.57 ± 0.25	8.55 ± 0.00	3.47 ± 0.86
May	inlet	18.1 ± 0.0	9.48	8.08 ± 0.00	8.21 ± 0.00	3.64 ± 0.00
	12	16.3 ± 0.8	9.84	6.93 ± 0.21	5.55 ± 1.19	1.43 ± 0.46
	24	16.3 ± 0.8	9.84	6.98 ± 0.19	5.36 ±0.82	1.99 ± 0.35
	36	16.3 ± 0.8	9.84	6.95 ± 0.21	5.35 ± 1.25	3.06 ± 1.37
	outlet	20.6 ± 0.0	9.00	6.80 ± 0.00	6.20 ± 0.00	2.45 ± 0.00
June	inlet	16.9 ± 0.1	9.72	7.22 ± 0.14	5.70 ± 0.79	3.06 ± 1.92
	12	18.8 ± 1.2	9.34	6.26 ± 0.29	6.95 ± 0.96	0.923 ± 0.285
	24	18.6 ± 0.8	9.38	6.28 ± 0.33	6.08 ± 0.74	1.08 ± 0.62
	36	18.5 ± 0.7	9.40	6.33 ± 0.40	6.36 ± 1.03	1.43 ±0.72
	outlet	21.3 ± 2.2	8.89	6.39 ± 0.15	9.81 ± 0.59	1.58 ± 0.22

The pH of the system remained constant (6.3 – 7.0), which is within the range reported for natural fens and freshwater ecosystems (Kadlec and Wallace, 2009). As seen by the data in Table 7-1, the wetland inherently contains carbon and nitrogen species, which are thought to be produced by the plants in the form of root exudates (Bavor et al., 1988, IWA, 2000, Reed, 1993). The baseline TOC and TN concentrations are useful points of reference after the introduction of the AWW stream. The concentrations of TOC and TN in the outlet stream, although it is possible, would not be expected to drop below the baseline level (Kadlec and Knight, 1996).

The measured DO and redox potential profiles at 12cm, 24cm and 36cm below the gravel bed surface are shown in Figure 7-1, Figure 7-2 and Figure 7-3; respectively. The inlet redox potentials and DO concentrations are given separately in Table 7-2. The saturated oxygen concentration reported in Table 7-1 is used for comparison against the measured DO, as a gauge of the level of aeration.

Table 7-2: Inlet temperature and dissolved oxygen concentration with the saturated oxygen concentration (fresh water, 760 mm Hg) at the baseline

Date (2016)	Temp (°C)	Redox (mV)	Inlet DO (mg/L)	Saturated O_2 (mg.L^{-1})
13 April	-		-	-
29 April	7.8	437.4	12.45	11.96
11 May	15.9	374.3	10.57	9.92
01 June	18.5	416.2	9.89	9.40
15 June	18.3	466.3	9.62	9.44

Table 7-2 shows that the municipal water entering the wetland is saturated with oxygen (the measured DO concentrations are larger than the saturation values). As expected, the feed water also has a largely positive redox potential. The temperature dependence of the DO concentration is also evident in Table 7-1 and Table 7-2; in particular the DO concentration decreases with increasing temperature.

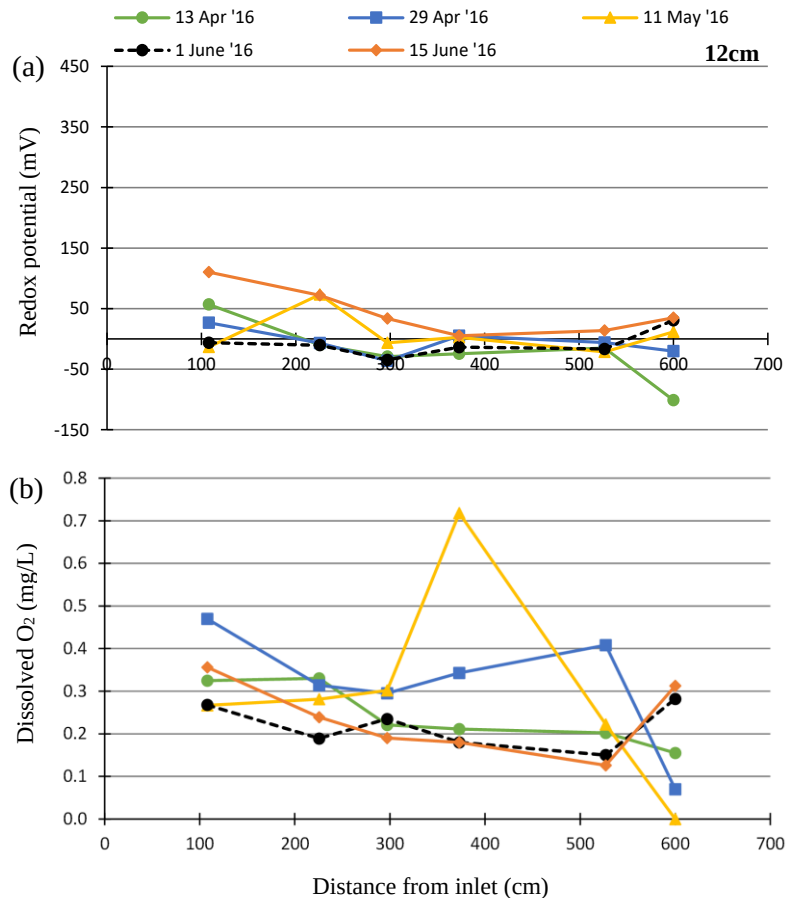


Figure 7-1: (a) Redox potential and (b) dissolved oxygen concentration along the constructed wetland at a depth of 12cm over the 5 week baseline sampling period.

There was a large decrease in the DO concentration and a noticeable reduction in potential within the first 100cm of the wetland (Figure 7-1b to Figure 7-3b). The DO concentration in the feed water was in the range of 9.6 – 12.45 mg/L, but had dropped below 1.0 mg/L throughout the wetland beyond 150cm from the inlet, which is well below the saturated oxygen concentration (see Table 7-1). This oxygen consumption is related to oxidative processes and/or root exudate transformation (Aylward et al., 2017). Figure 7-1, Figure 7-2 and Figure 7-3 show that the redox and DO profiles are very similar throughout the bed at all three sampling depths, with any differences being observed only in the first 150cm. In general, the redox potential lies in the range of -50mV to 50mV and remains relatively constant. Low levels of DO (0 mg/L – 0.5 gm/L) were observed and the DO concentration decreased with distance

along the bed; the only exception to this being a spike in DO on 11 May at port 4 (373cm). The plant roots can supply oxygen back into the root zone, depending on favourable light intensity and system potential (Kadlec and Wallace, 2009), but it cannot be said with certainty whether this spike is an erroneous data point or linked to plant physiology.

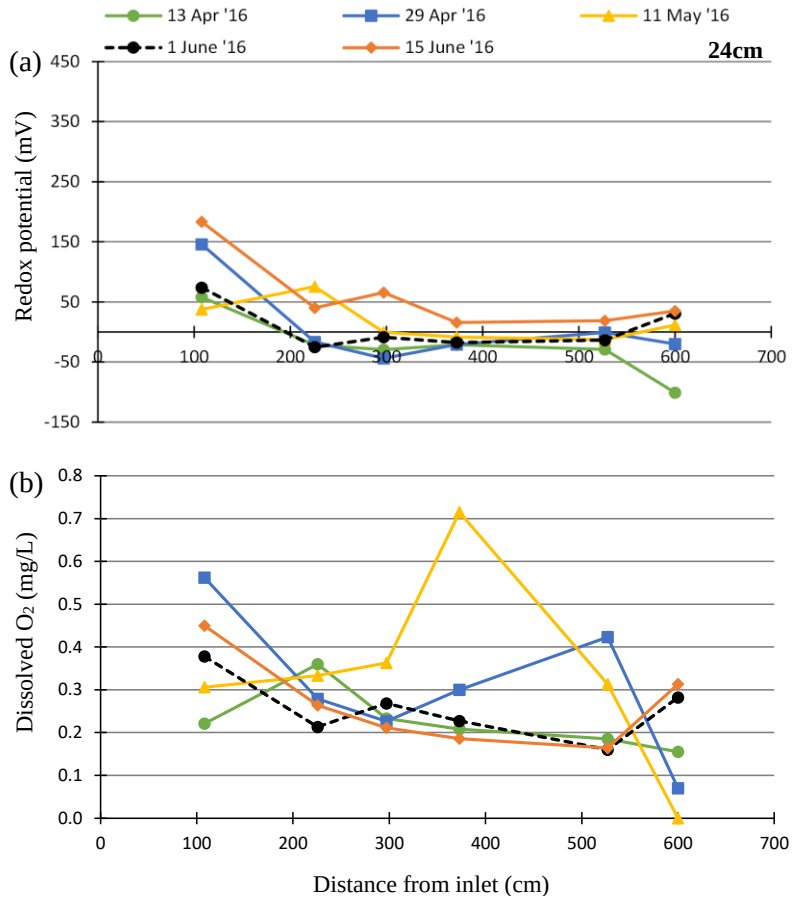


Figure 7-2: (a) Redox potential and (b) dissolved oxygen concentration along the constructed wetland at a depth of 24cm over the 5 week baseline sampling period.

Figure 7-3b shows a higher DO concentration at port 1 (108cm) for 29th April (3.88 mg/L), 1st June (1.14 mg/L) and 15th June (3.45 mg/L). This is accompanied by a higher redox potential on the 29th April (320 mV), 1st June (283 mV) and 15th June (385 mV), as would be expected. Figure 7-1, Figure 7-2 and Figure 7-3 also show rapid consumption of the oxygen entering the system within the first 100cm. The three inlet pipes carrying water into the wetland were located 5cm above the bottom of the wetland. It is likely that all of the oxygen carried into the wetland in the feed stream did not reach the sampling ports at, first, depth 2 and then depth 1; resulting in higher concentrations of oxygen being measured at depth 3. This could be the result of poor diffusive movement upwards within the first 100cm of the bed or because the oxygen entering the wetland was consumed so quickly in the bottom third of the system that it was not available to feed the top portions of the bed.

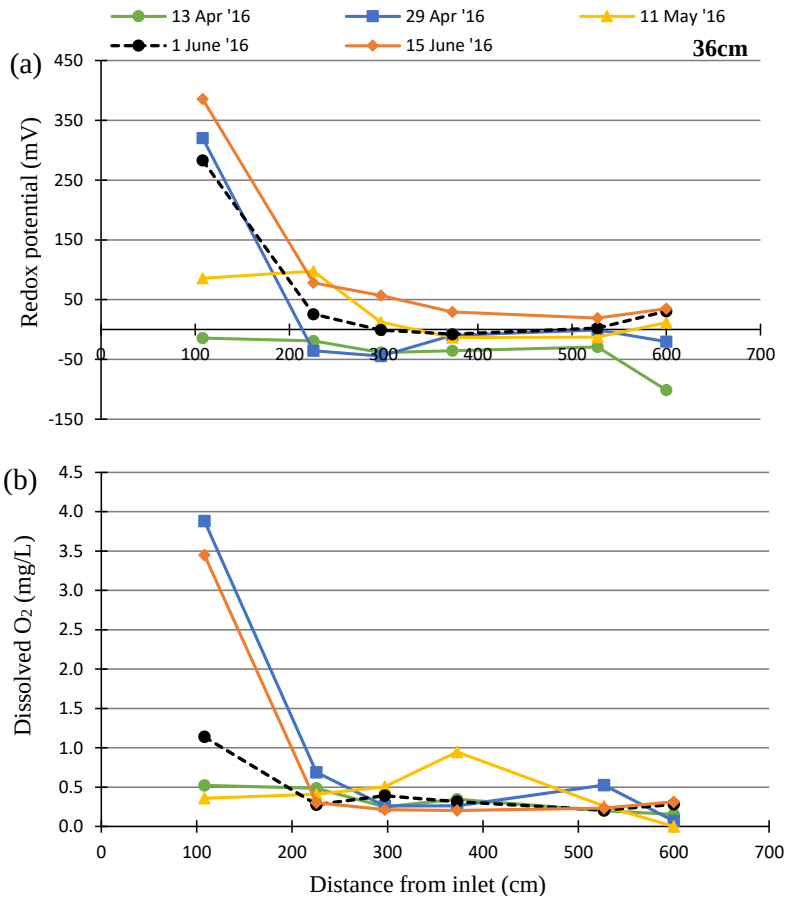


Figure 7-3: (a) Redox potential and (b) dissolved oxygen concentration along the constructed wetland at a depth of 36cm over the 5 week baseline sampling period.

The baseline sampling campaign began in the spring and ended in early summer; hence the rise in temperature both at the inlet (Table 7-2) and within the bed (Table 7-1). Although there is a clear consumption of oxygen and drop in redox potential from the inlet into the wetland in each case, there is no clear seasonal impact as was found during the previous sampling campaign in the European summer/autumn of 2015. In contrast, there was a general increase in DO and redox potential from August, through September and into October 2015. The low oxygen and potential in August was linked to the hot summer temperatures, high levels of solar radiation and the highest rates of plant growth and activity. Moving into the autumn, ambient temperatures began to decrease, as did the levels of plant activity; leading to lower oxygen consumption and an increase in redox potential (Aylward et al., 2017). Table 7-1 shows that, although the inlet and outlet concentrations of TOC fluctuate and do not show a particular trend, the baseline TOC concentration within the wetland increased gradually, but steadily, from April to June 2016. The measured concentrations were also similar at all three depths. It is also evident that the outlet TOC concentration is higher than what was measured inside the bed. In contrast, the TN concentration showed an overall decrease from April to June 2016 with a clear decline in TN in

the outlet stream. The inlet TN concentration was, as the TOC, subject to some fluctuation. There is also a depth profile evident. The TN concentration increases with depth below the bed surface.

7.3.2 Contaminant degradation and transformation

Artificial wastewater was introduced into the feed stream to the CW on 23rd June 2016. Thereafter, weekly samples were drawn, for a period of 10 weeks, until 1st September 2016. The samples were taken at the inlet, outlet and from three depths below the gravel bed surface (12cm, 24cm and 36cm) at the six sample ports along the length of the CW (refer to Figure 3-4, Chapter 3).

As was done for the 2015 experimental campaign, TOC and TN were measured as indicators of the degradation of organic carbonaceous species and nitrogenous species, respectively. The reasoning behind the choice is outlined in Aylward et al. (2017). In this study, it was also stated that a more detailed analysis should be conducted on the component species making up these sum parameters (Aylward et al., 2017). However, for consistency and completeness as well as due to time constraints, it was decided to collect one year's worth of data (the 2015 and 2016 experiments spanned different seasons) using the same methodology and measured parameters to improve the quality of the data set.

7.3.2.1 Overall degradation and transformation

Table 7-3 summarises the inlet and outlet contaminant loading and percentage removal of TOC and TN. TOC removal is the result of the degradation of organic carbon species, whilst TN removal is due to the transformation of nitrogen-containing contaminants into other forms via nitrification and denitrification. The speed of the pump regulating the flowrate of water into the wetland had been set to ensure a hydraulic residence time of approximately 7 days. The dosing pump administering the AWW concentrate into the feed stream was set accordingly to ensure the desired dilution ratio and, thus, concentration of each species entering the bed. The average inlet concentrations of TOC and TN during July 2016 were 78.6 ± 11.0 mg/L and 35.1 ± 5.0 mg/L, respectively. There were too many fluctuations in the flowrate during August for a reliable average to be reported (see Table A28 and Table A29, Appendix A). In Germany, CWs are most commonly used as tertiary treatment systems, or a polishing stage. The discharge limits for a German wastewater treatment plant of class 2 are 22.80 mg/L TOC and 9.14 mg/L TN. In these experiments, the pilot wetland received a high load of carbon and nitrogen relative to what a typical CW would receive from a primary water treatment facility in Germany.

The volumetric flowrate was monitored daily (see Table C3 and Table C4, Appendix C) and a weekly average then determined for the calculation of the hydraulic loading (see Table A28 and Table A29, Appendix A). The data collected for 7 days prior to each sampling day was used. This was done in response to the recommendation that a more detailed investigation into the in- and outflow variations be conducted (Aylward et al., 2017).

Table 7-3: Average weekly total organic carbon and total nitrogen hydraulic loading rates and percentage removal (day of sampling is the second date mentioned)

Week	[a]Date (2016)	Avg. bed temp (°C)	TOC			TN		
			HLR (g/m^3.d)		% removal	HLR (g/m^3.d)		% removal
			Inflow	Outflow		Inflow	Outflow	
1	23 Jun – 01 Jul	29.4	10.95	1.722	82.96	4.75	0.406	90.99
2	01 Jul - 07 Jul	26.1	10.27	1.564	84.52	4.43	0.386	91.43
3	07 Jul - 15 Jul	17.1	8.34	0.605	94.01	3.93	0.154	96.59
4	15 Jul - 21 Jul	24.5	12.73	1.910	81.08	5.88	0.376	91.64
5	21 Jul - 29 Jul	28.9	8.19	0.606	94.00	3.59	0.938	79.16
6	29 Jul - 04 Aug	27.8	27.00	2.096	92.24	11.97	0.292	97.56
7	04 Aug - 11 Aug	20.9	9.32	2.244	75.93	4.29	0.288	93.28
8	11 Aug - 18 Aug	32.1	4.87	1.481	69.59	1.98	0.213	89.24
9	18 Aug - 25 Aug	35.4	1.05	1.710	-63.47	0.37	0.487	-30.31
10	25 Aug - 01 Sept	26.3	12.72	0.849	93.32	5.24	0.095	98.19

Fluctuation in the inflow hydraulic load is evident in Table 7-3. This is not ideal for chemico-kinetic studies. Many of the existing equations and models for determining the rate constant for the chemical reactions taking place within the wetland are subject to the condition of steady-state operation (inflow rate and outflow rate are equal). The hydraulic loading rates of TOC and TN at the wetland inlet and outlet are shown in Figure 7-4 and Figure 7-5; respectively. Also included in Figure 7-4 and Figure 7-5 is the average volumetric flowrate. It is clear that the volumetric flowrate was not constant over the 10 week experiment and the system was not operating at steady state. It was difficult to maintain steady-state operation over a week, and then for 10 consecutive weeks, in an outdoor wetland which was fully exposed to the elements and unforeseen mechanical and technical breakdowns.

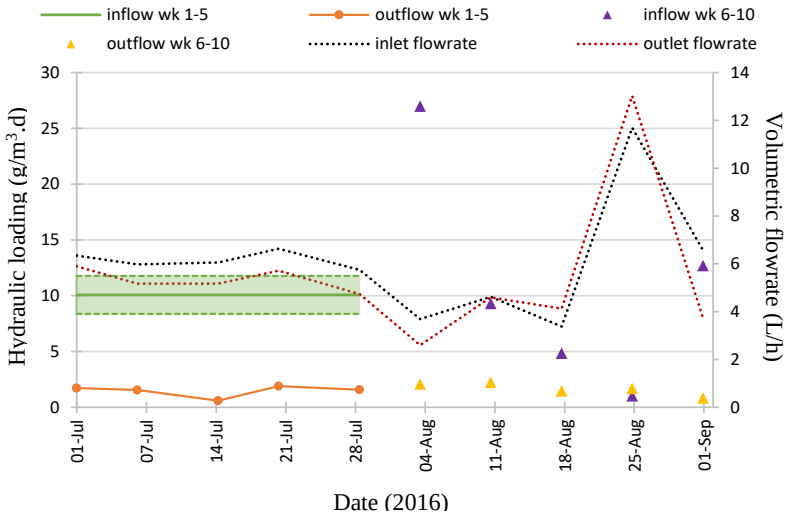


Figure 7-4: Total organic carbon hydraulic loading (avg. inlet TOC loading = 10.1 ± 1.7 g/m^3.d; baseline TOC loading = 0.81 ± 0.22 g/m^3.d) as a function of time at the wetland outlet up to 10 weeks after the introduction of artificial wastewater into the system against the variation in volumetric flowrate (avg. inlet flowrate = 6.2 ± 0.3 L/d; avg. outlet flowrate = 5.3 ± 0.4 L/d for week 1-5).

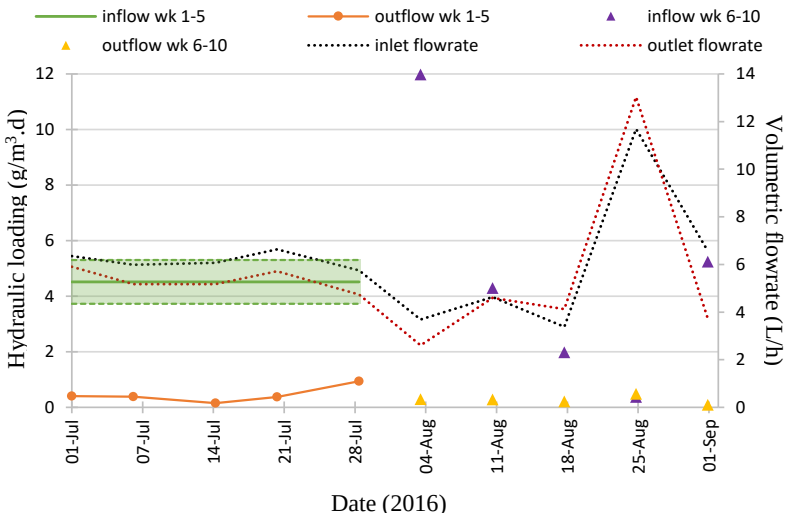


Figure 7-5: Total nitrogen hydraulic loading (avg. inlet TN loading = 4.5 ± 0.8 g/m^3.d; baseline TN loading = 0.34 ± 0.16 g/m^3.d) as a function of time at the wetland outlet up to 10 weeks after the introduction of artificial wastewater into the system against the variation in volumetric flowrate (avg. inlet flowrate = 6.2 ± 0.3 L/d; avg. outlet flowrate = 5.3 ± 0.4 L/d for week 1-5).

It was ensured that the system was in a mode of stable operation (relatively constant inlet and outlet volumetric flowrates) before in introduction of the AWW on 23rd June 2016. It is evident from Figure 7-4 and Figure 7-5 that, for the majority of the experimental period, the inlet flow rate exceeded the outlet flow rate. Stable operation was maintained for July, where an average inlet hydraulic load is plotted against the outlet load. Removal of both TOC and TN is evident. 83% - 94% TOC was degraded in July and over 90% TN was transformed during the same period.

In August, however, the inlet and outlet flowrates varied considerably. The decline in inlet flowrate at the beginning of the month was due to a power interruption to the site. The drop in flowrate at the inlet towards the middle of the month was linked to the build-up of biofilm in the feed tubes. The inflow pump speed had had to be increased to maximum (hence the spike) to flush out the tubes. The outlet flowrate responds in the same way to the changes in the inlet flowrate in order to maintain a constant water level. For this reason, the inlet and outlet hydraulic loads during August are plotted as individual points for each week in Figure 7-4 and Figure 7-5. The corresponding hydraulic loads and percentage TOC and TN removal are given in Table 7-3, but the accuracy of these results may be reduced because the erratic flow pattern meant that the hydraulic residence time was not 7 days. It is, thus, likely that the measured outlet loads did not corresponded to the recorded inlet loads during sampling the previous week.

The DO concentrations in the inflow and outflow are compared in Figure 7-6. It is evident that the feed water is saturated with oxygen and that this oxygen is almost completely depleted by the outlet. It also appears as if the oxygen concentration in the water leaving the wetland decreases with time. It is known

that aerobic micro-organisms play a large role in the degradation of organic carbon in wetland systems (Kadlec and Wallace, 2009) and it is thought that the oxygen was consumed by microbes inhabiting the root zone to support numerous oxidative degradation processes (Aylward et al., 2017). The system potential is also plotted as a function of time in Figure 7-7. In general, a progressive decline in potential can be seen, which is in line with the decrease in oxygen. Low to negative redox potentials are indicative of oxygen depleted to anoxic waters (Kadlec and Wallace, 2009).

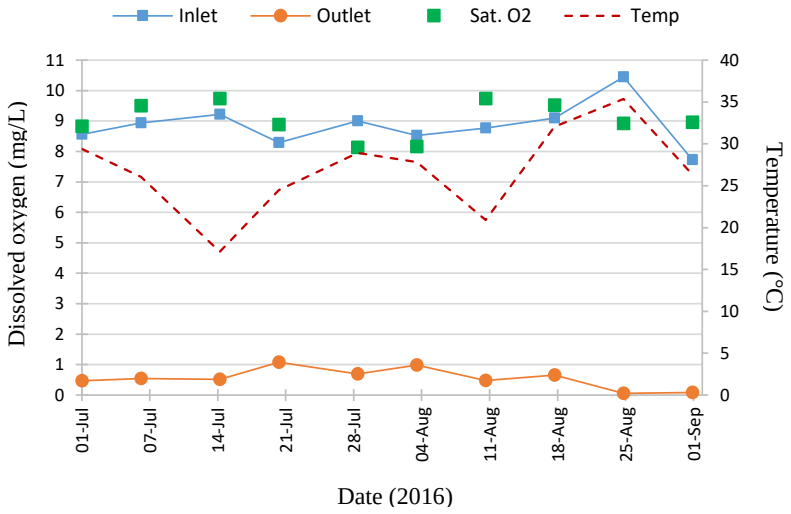


Figure 7-6: The change in dissolved oxygen concentration as a function of time at the wetland outlet up to 10 weeks after the introduction of artificial wastewater into the system (inlet dissolved oxygen concentration and saturated oxygen concentration also shown).

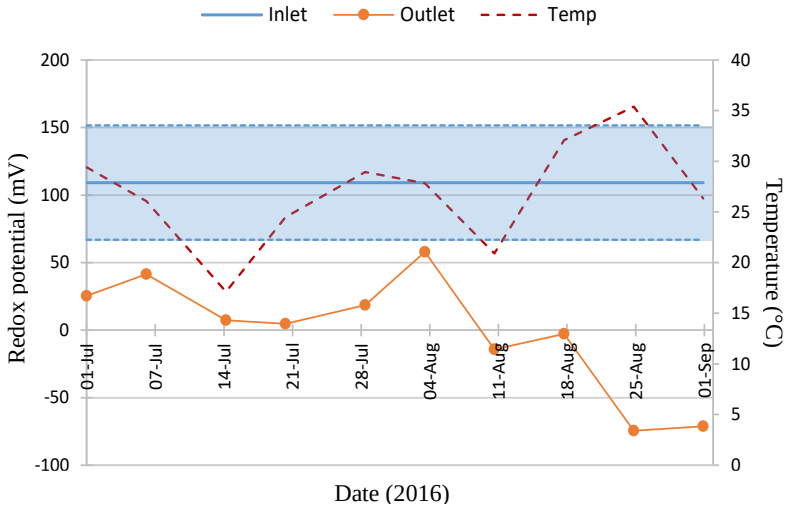


Figure 7-7: The change in oxidation-reduction potential as a function of time at the wetland outlet up to 10 weeks after the introduction of artificial wastewater into the system (avg. inlet potential = 109.2 ± 42.4).

7.3.2.2 Internal contaminant degradation and transformation

Section 7.2.1 investigated the overall bioremediation of the wetland over the duration of the experimental (sampling) period. This section examines the internal behaviour of the system and, in particular, the TOC and TN concentration profiles within the bed. Only data collected in July is considered due to the erratic nature of the August data and, consequently, uncertianty regarding its accuracy (refer to section 7.2.1). Figure 7-8 shows the TOC and TN profiles at depth 2, with the DO and redox profile provided in Figure 7-9. The data from depth 2 only has been presented as the trends were similar at all three depths. The figures showing the TOC, TN, DO and redox profiles relating to depths 1 and 3 are given in Figure A1 and Figure A2 of Appendix A.

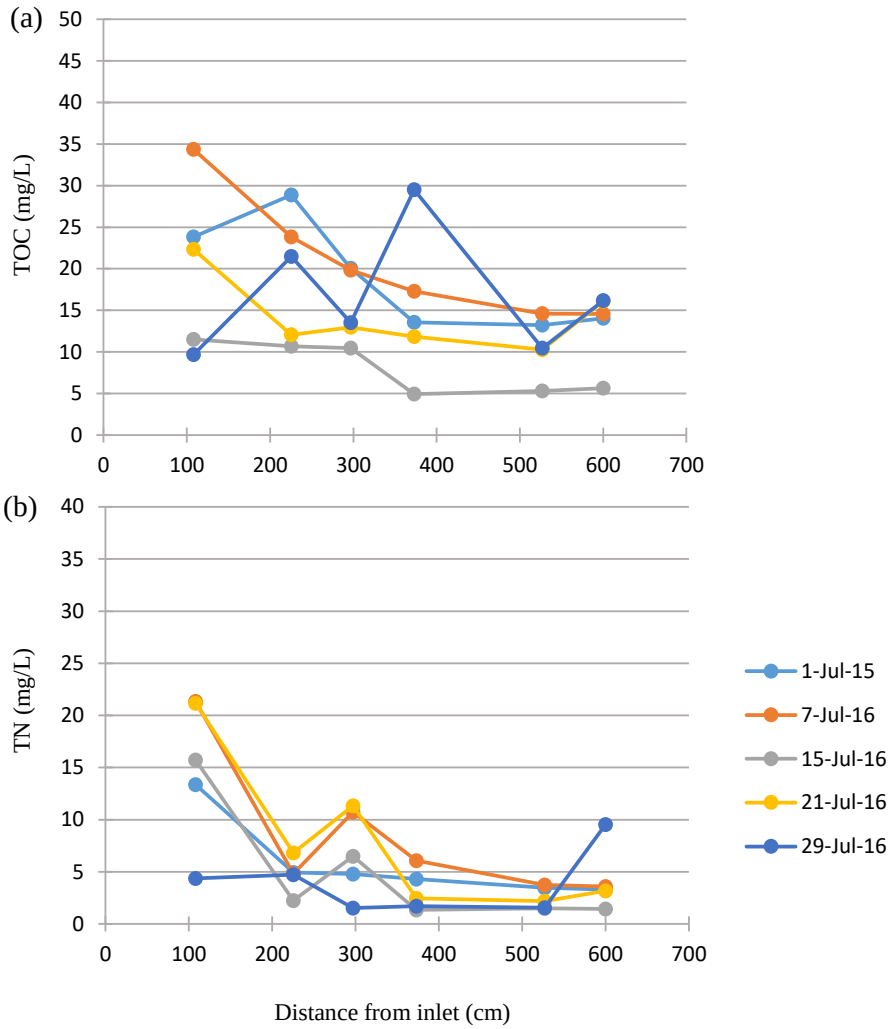


Figure 7-8: (a) Total organic carbon concentration profile (avg. inlet [TOC] = 78.6 ± 11.0 mg/L) and (b) total nitrogen concentration profile (avg. inlet [TN] = 35.1 ± 5.0 mg/L) at 24cm below the bed surface over 5 weeks in July 2016.

Figure 7-8 shows that the majority of the organic carbon degradation and nitrogen transformation occurs within the first half of the bed (up to 300cm). The TOC and TN profiles on 29th July seem to be an

exception. It is not certain whether the anomaly is due to operator error or a physical function of the system on the day. For this reason, this data is excluded from any of the general results drawn. The consumption of oxygen is also highest in the first 300cm of the wetland (Figure 7-9a), which supports the theory of oxidative TOC degradation. TOC degradation had largely ceased after 400cm (Figure 7-8a) and the oxygen concentration remained low but relatively constant to the outlet. There was, however, a slight increase in oxygen concentration towards the wetland outlet (Figure 7-9a). This is likely in response to the decrease in the rate of TOC degradation and lower oxygen consumption by the effecting microbes but could also be due to contributions from the plants (Kadlec and Wallace, 2009). The redox potential increased steadily down the length of the wetland; in line with the decline in contaminant degradation and oxygen consumption. The negative potentials up to 500cm indicate a largely anaerobic environment throughout most of the wetland.

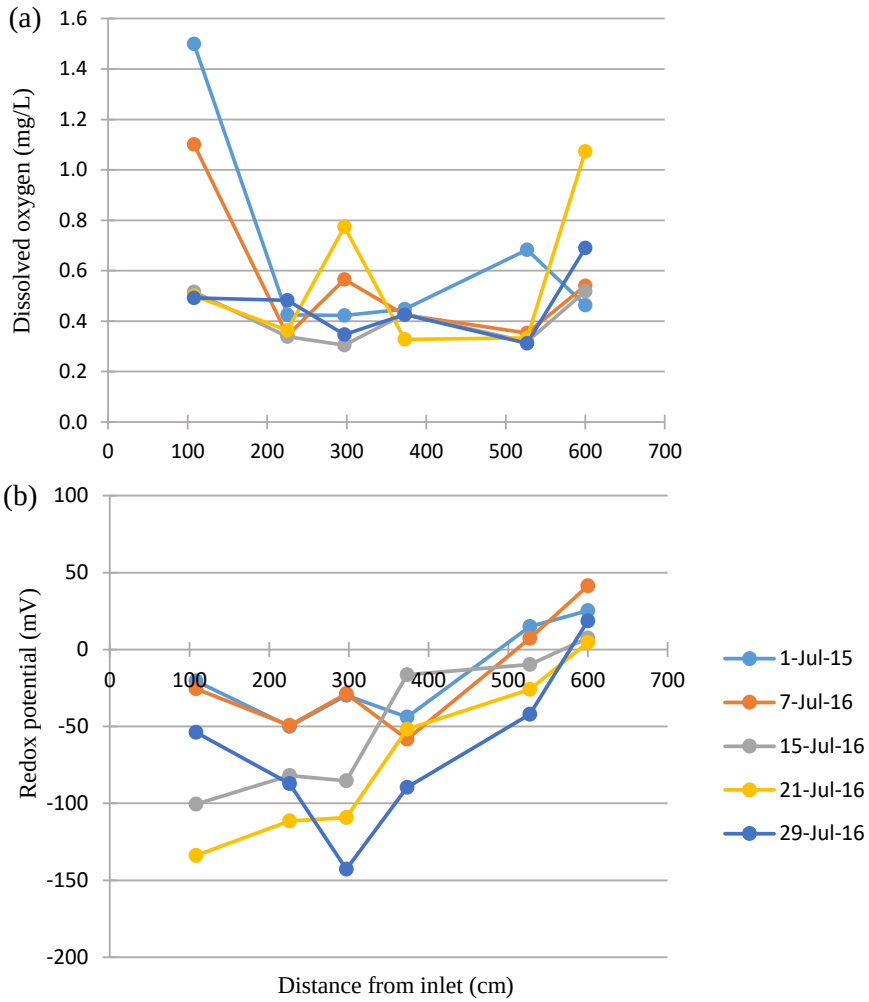


Figure 7-9: (a) Dissolved oxygen concentration profile (avg. inlet [DO] = 8.80 ± 0.37 mg/L) and (b) redox potential profile 24cm below the bed surface over 5 weeks in July 2016.

7.3.2.3 Internal contaminant loading profile

This section provides an overview of the performance of the CW with regards to the removal of TOC and TN from a stream of artificial wastewater. The aim is to present all of the chemical data gathered in a condensed, pictorial manner. This was inspired by the heat profile map generated in the study of heat as an alternative tracer in (Bonner et al., 2018). The method developed by Aylward et al. (2017) to relate the volumetric flow rate at an internal location in the wetland to the vegetation density in its vicinity was used to create a contaminant loading density map at multiple depths and locations in the wetland. This was done by estimating the local (internal) volumetric flowrate at each sample port and using this, together with the measured concentration, to calculate the local contaminant loading at that point. It was assumed that the volumetric flowrate across the depths was approximately the same.

The inflow pumps were set to achieve a hydraulic residence time of approximately 7 days. The inlet and outlet volumetric flow rates were closely monitored to determine the average daily flow rate. In general, it was observed that the volumetric flow rate decreased from inlet to outlet ($Q_{in} > Q_{out}$) although there were a few exceptions. An average weekly volumetric flowrate was then calculated using the data collected on each of the 7 days prior to sampling day. The average weekly flow rates for the duration of the experimental period are given in Table A28 and Table A29 of Appendix A.

For the purposes of the calculations in this section, and an illustration of the method, the data from the week of the 15th – 21st July 2016 was used. For this period, $\mathrm{Q_{in}} = 5.8790$ L/h and $\mathrm{Q_{out}} = 5.1311$ L/h. It was assumed that the flowrate decreased linearly down the length of the wetland. The two data points of inlet and outlet volumetric flow rate against distance from the wetland inlet were plotted and a linear trend line was fitted (see Figure A3, Appendix A). The expression relating volumetric flowrate to distance along the wetland was found to be:

$$\mathrm{Q_i} = -0.125\mathrm{x_i} + 5.879 \qquad [7_1]$$

where Q_i represents the local volumetric flow rate (L/h) and x_i the position along the length of the wetland (m) corresponding to one of the *i = 1-6* internal sampling points

As detailed in Chapters 3 and 6, the vegetation density in the CW was measured in stems per square metre from April to November 2016. For this, the wetland was divided into zones with the inlet, 6 internal sampling points and the outlet designating the zone boundaries. Zone 1 was marked from inlet (0cm) – 1.08m; zone 2 from 1.08m – 2.225m; zone 3 from 2.225m – 2.97m and so forth. The changes in vegetation density over this period are illustrated in Figure E6 of Appendix E (Aylward et al., 2017). The data upon which Figure E6 (Appendix E) is based is given in Table A30 of Appendix A. The vegetation density in the wetland as a whole increased on a month-to-month basis from April to November, with the most substantial increase from May to June as the summer growth period began.

Figure E6 (Appendix E) also shows that the vegetation density decreased with distance from the inlet (from zone 1 to zone 6).

The vegetation density was then plotted against distance from the wetland inlet and the best fit trend line was determined by trial and error (Figure A4, Appendix A). It was assumed that the vegetation density measured in each zone was the value at the mid-point of the zone. For example, in zone 1 (0m – 1.08m), the vegetation density was 325 stems/m^2 and in zone 2 (1.08m – 2.03m), the vegetation density was 322 stems/m^2. To estimate the vegetation density at each of the sample ports (which would have been on the zone boundaries), the average between the vegetation densities in each zone was taken. Hence, at 1.08m, the vegetation density was calculated to be $(325 + 322)/2$ stems/m^2. It was found that a polynomial of degree 2 resulted in the value of the r^2 parameter being closest to 1 ($r^2 = 0.9854$). The expression relating vegetation density to distance along the wetland was, thus, found to be:

$$\rho_{veg} = -6.5453 x_i^{\,2} - 0.6879 x_i + 333.6 \qquad [7_2]$$

where ρ_{veg} is the vegetation density (stems/m^2) and x_i the position along the length of the wetland (m) corresponding to one of the *i = 1-6* internal sampling points

After solving for x in Eq. 7-1 and substituting the result into Eq. 7-2, the expression relating the local volumetric flow rate to the vegetation density, ρ_{veg}, is:

$$0 = -6.5453 \left(\frac{5.879 - Q_i}{0.125}\right)^2 - 0.6879 \left(\frac{5.879 - Q_i}{0.125}\right) + 333.6 - \rho_{veg} \qquad [7_3]$$

The Microsoft Excel Solver tool was used to determine the value of Q_i which satisfied Eq. 7-3 using the values of ρ_{veg} corresponding to each sampling location. The local volumetric flowrate was then used to determine the TOC and TN hydraulic loading at each depth at all sampling locations, as given in Table 7-4, Table 7-5 and Table 7-6. This lead to the calculation of the hydraulic loading density profiles for both TOC and TN, which are given in Figure 7-10 and Figure 7-11, respectively.

Table 7-4: Estimated internal TOC and TN hydraulic loading **12cm** below the wetland surface

Date	21-Jul-16							
Depth	12cm below bed surface							
x (cm)	**ρ_{veg} (stems/m^2)**	**Q (L/hr)**	**TOC (mg/L)**	**m_{TOC} (g/d)**	**HLR_{TOC} (g/m^3.d)**	**TN (mg/L)**	**m_{TN} (g/d)**	**HLR_{TN} (g/m^3.d)**
0	0	5.8790	92.43	13.04	11.280	42.72	6.028	5.213
108	324	5.7306	20.82	2.863	2.477	15.35	2.111	1.826
225.5	309	5.6423	15.77	2.135	1.847	3.13	0.424	0.367
297	275	5.5127	33.18	4.390	3.797	4.54	0.601	0.520
373	219	5.3627	11.18	1.439	1.245	2.03	0.261	0.226
527	157	5.2354	9.95	1.25	1.081	1.61	0.202	0.175
600	0	5.1311	16.10	1.983	1.715	3.17	0.390	0.338

Table 7-5: Estimated internal TOC and TN hydraulic loading **24cm** below the wetland surface

Date	21-Jul-16							
Depth	24cm below bed surface							
x (cm)	**ρ_{veg} (stems/m^2)**	**Q (L/hr)**	**TOC (mg/L)**	**m_{TOC} (g/d)**	**HLR_{TOC} (g/m^3.d)**	**TN (mg/L)**	**m_{TN} (g/d)**	**HLR_{TN} (g/m^3.d)**
0	0	5.8790	92.43	13.04	11.280	42.72	6.028	5.213
108	324	5.7306	22.33	3.071	2.656	21.17	2.912	2.518
225.5	309	5.6423	12.06	1.633	1.412	6.820	0.9235	0.799
297	275	5.5127	12.97	1.716	1.484	11.33	1.499	1.297
373	219	5.3627	11.82	1.521	1.316	2.46	0.317	0.274
527	157	5.2354	10.27	1.290	1.116	2.18	0.274	0.237
600	0	5.1311	16.10	1.983	1.715	3.17	0.390	0.338

Table 7-6: Estimated internal TOC and TN hydraulic loading **36cm** below the wetland surface

Date	21-Jul-16							
Depth	36cm below bed surface							
x (cm)	**ρ_{veg} (stems/m^2)**	**Q (L/hr)**	**TOC (mg/L)**	**m_{TOC} (g/d)**	**HLR_{TOC} (g/m^3.d)**	**TN (mg/L)**	**m_{TN} (g/d)**	**HLR_{TN} (g/m^3.d)**
0	0	5.8790	92.43	13.04	11.280	42.72	6.028	5.213
108	324	5.7306	21.47	2.953	2.554	22.84	3.141	2.717
225.5	309	5.6423	11.24	1.522	1.316	11.98	1.622	1.403
297	275	5.5127	10.92	1.445	1.250	14.24	1.884	1.629
373	219	5.3627	12.30	1.583	1.369	4.42	0.569	0.492
527	157	5.2354	12.37	1.554	1.344	2.49	0.313	0.271
600	0	5.1311	16.10	1.983	1.715	3.17	0.390	0.338

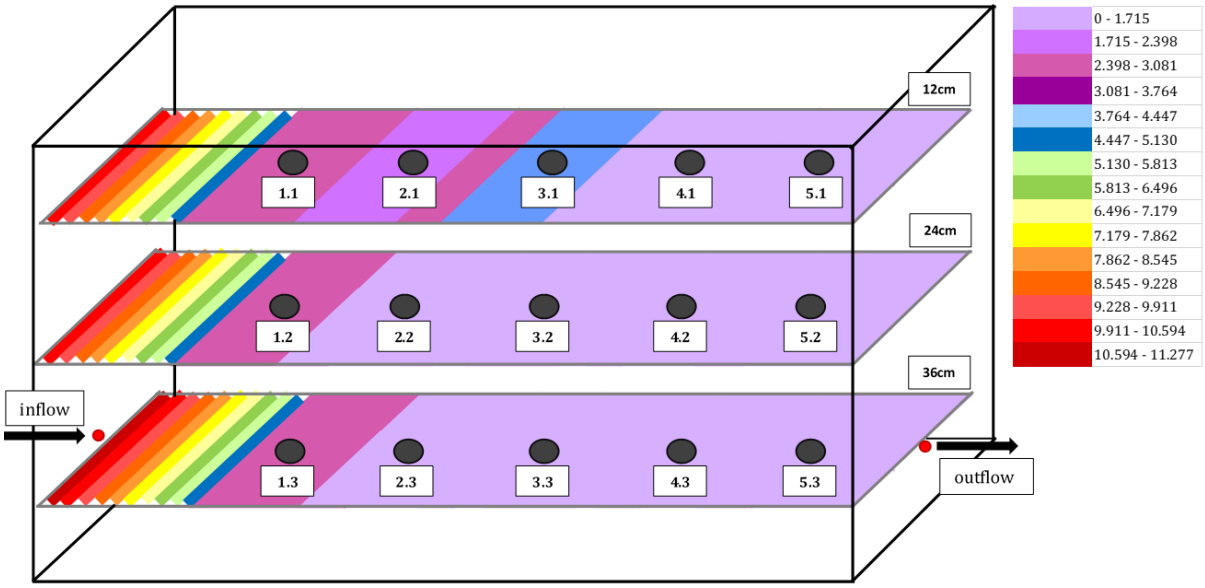


Figure 7-10: The TOC hydraulic loading density profile for the week 15th – 21st July 2016 (key in top right-hand side indicates range of hydraulic loading rates in g/m^3.d).

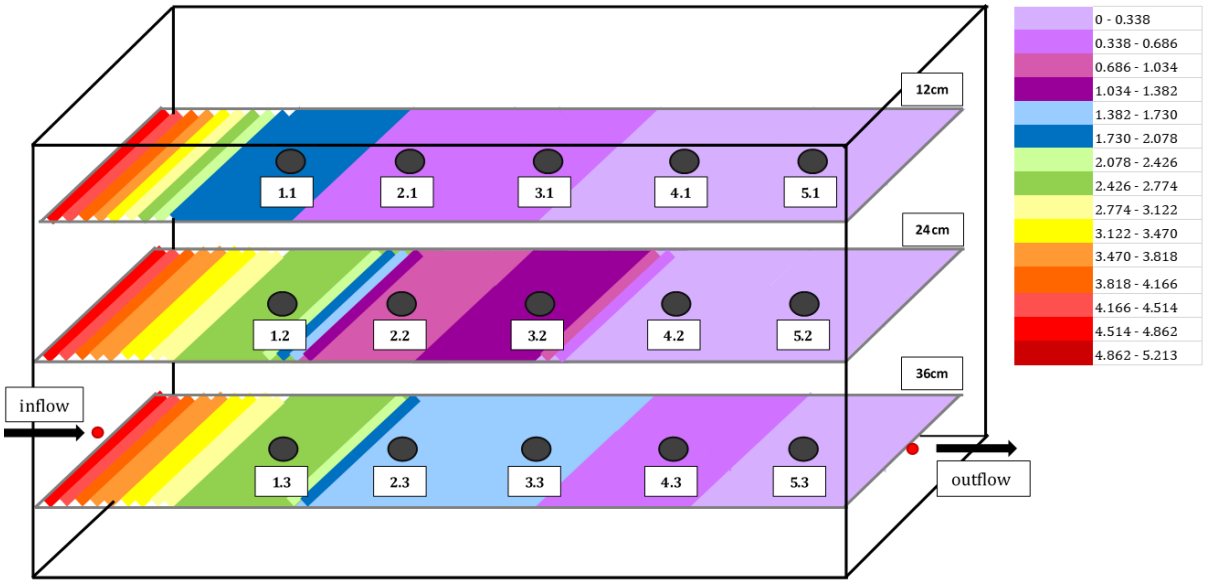


Figure 7-11: The TN hydraulic loading density profile for the week 15th – 21st July 2016 (key in top right-hand side indicates range of hydraulic loading rates in g/m^3.d).

The accuracy of the assumption that the highest concentrations reach depth 2 and depth 1 when the inlet is located at the bottom of the wetland (as indicted in Figure 7-10 and Figure 7-11) could be questioned. This assumption was made because the gravel bed should have, ideally, aided in uniform dispersion of the Uranine. However, in a black box system such as a CW, and with the data gathered in the time permitted for this research project, it is not possible to say what the reality really is. This could only be determined by inserting more sampling points within the first 108cm of the CW.

Figure 7-10 and Figure 7-11 show a depth distinction in the chemical hydraulic loads of both TOC and TN. In general, TN persists for longer in the bed than TOC. While organic carbon is degraded relatively quickly in CW systems, nitrogen is transformed from one species to another; hence the persistence of higher levels of TN in the bed.

Figure 7-10 shows that the TOC load had dropped to its lowest measured level within the first 150cm; although the TOC load at depth 1 was higher than at depths 2 and 3 until approximately half-way down the wetland. There was also an increase in TOC load between sample ports 2 (2.225 m) and 3 (2.97 m); such that a higher TOC concentration was measured at port 3 than at port 2. This could indicate hold-up in the vicinity of ports 2 and 3. A similar trend is seen at depth 2 for TN in Figure 7-11. There is a decrease in TN load from the inlet to port 2, followed by a slight increase between port 2 and port 3 and then a continual decrease to the lowest detectable level towards the wetland outlet. The central basket (Figure 3-5) was located at sampling location 3, which could have been a contributor to flow impediment, but then it would be expected to see the same patterns of higher TOC and TN load between port 2 and port 3 at all three depths but this is not the case. The vegetation density was also greater in the first half of the bed and at its highest in zones 1 and 2 up to 2.225 m (Figure E6, Appendix E). The thicker root mat in these areas of higher plant density could also cause hold-up within the bed.

In the hydraulic study (Chapter 6), tracer tests were performed at multiple locations and depths throughout the wetland. As such, RTDs were generated at each of the sampling points shown in Figure 7-10 and Figure 7-11 and at all three depths (Figure 6-4). In all cases, it was found that $\bar{t}_m$ was greater than τ, which indicated a deviation from plug flow and mixing effects.

The increase in TOC load was observed between ports 2 and 3 at depth 1. Considering the RTD for port 2 at 12cm below the bed surface (Figure 6-4b), the straight elongated tail and peak at $\theta = 0.5$ indicates a moderate amount of dead space. The multiple, small peaks on the tail also indicate hold-up within the system. The RTD for sampling location 3.1 in Figure 7-10 corresponds to that of port 4 (alongside the basket) in Figure 6-4b. This RTD has twin peaks, indicating hold-up within the system, and both the θ position of 0.5 – 0.6 and the straight elongated tail both allude to a moderate amount of dead space.

The increase in TN load was observed between ports 2 and 3 at depth 2. The corresponding RTDs are those of port 2 and port 4 in Figure 6-4c, respectively. The RTD for port 2 in Figure 6-4c shows a sharper peak and $E(\theta) \approx 1.9$ as compared to $E(\theta) \approx 1.5$ in Figure 6-4b. Similarly, the RTD for port 4 in Figure 6-4c shows $E(\theta) \approx 1.3 – 1.4$ as compared to $E(\theta) \approx 1.6$ in Figure 6-4b. Otherwise, the shapes of the RTDs at ports 2 and 4 at 12 cm and 24 cm below the bed surface indicate the same; namely dead space and hold-up within the wetland system.

In summary, it is thought that the measured increase in TOC and TN loads between ports 2 and 3 at depth 1 and 2, respectively, could be the result of dead-space or a stagnant zone. This results in water

becoming trapped, or spending a greater amount of time in this area, and consequently a build-up of concentration. This result is supported by the results of the hydraulic study, but would require further experimental validation.

Chapter 8 Discussion and concluding remarks

8.1. Discussion

This thesis is comprised of three research papers and one publication submitted for peer review, all of which already contain a detailed discussion and conclusion (Chapters 4 – 7). As such, this discussion and concluding remarks section summarizes the most important findings of the research papers in order to answer to the research objectives set out.

Tracer studies at the University of the Witwatersrand

The first research objective was to use impulse-response tracer tests to determine the hydraulic characteristics of the IMWaRU pilot-scale CWs. Specifically, the RTD, velocity profiles, reactor behaviour, location of dead zones and areas of short-circuiting/bypass would be determined. Thereafter, step-change tracer tests would be conducted, in the same systems, in order to compare and validate the findings. These results have been published in *Ecological Engineering* (Chapter 4).

Two gravel-filled HSSF CWs were used; one of which contained five different wetland plant species and the second left unplanted. Both systems were identical, with the exception of the vegetation, and were subjected to the same tests (impulse-response and step-change tracer tests). In each of the experiments, the tracer concentration was measured at multiple depths and locations throughout the wetlands, as well as at the outlet. The experimental data (tracer concentration versus time) was used both to plot the RTD and feed one of three mathematical models to compare reactor hydraulic behaviour. Ideally, the hydraulic output should have been the same irrespective of the model chosen.

The models chosen for the purpose of this investigation were:

i. The impulse-response model
ii. The step-change derivative model
iii. The step-change integral model

The following hydraulic parameters were considered:

- τ, the theoretical retention time (V/Q)
- $\bar{t}_m$, the nominal, or actual, residence time which is calculated from the RTD
- N, the number of CSTRs in series (a model output and indicator of reactor size and behaviour)
- Pe, the Peclet number (indicating the degree of dispersion in the system and the type of flow behaviour i.e. complete mixed flow, plug flow or somewhere in between)

In the unplanted system, $\bar{t}_m > \tau$ for all three methodologies (suggesting 100% utilization of the bed volume). Both of the step-change methods indicated identical hydraulic behaviour, but the impulse-response method yielded a higher $\bar{t}_m$ and showed a lower degree of dispersion. For the planted system,

all three methodologies indicated different hydraulic behaviours with regards to effective volume utilisation, degree of dispersion and percentage of dead-volume.

It is evident that various factors can impact upon the results of the hydraulic calculations:

- The introduction of plants into the wetland affects the fluid flow behaviour and the output of each of the three models.
- The impulse-response model is more sensitive to the experimental method or design. Specifically, insufficient concentration-time data in the vicinity of the peak changes the shape of the RTD and, thus, the hydraulic calculations. This is not a factor in a step-change experiment. Tracer dispersion, which is a largely unavoidable phenomenon in a packed bed, also has a larger impact on the impulse-response output than on the step-change output.
- The method of numerical integration is also of importance. Simpson's 1/3 rule was used in this study and it was determined that varying the size of the sub-intervals affects the hydraulic output. This is not a desirable feature of any reproducible wetland model, but the step-change derivative methodology is the least sensitive. However, the process of differentiation to calculate E(t) in this method intensifies background noise which could, equally, skew the hydraulic results.

All three modelling methodologies required the collection of data in the field to plot the RTD. However, each RTD model suggested a different hydraulic behaviour for the same wetland system. Prior to these experiments, it was expected that each method would yield the same hydraulic output for the system as each was fed by the same data. However, with this not being the case, it was not possible to validate the hydraulic results of the impulse-response tracer test using either of the step-change methods. The differences are thought to be the result of the mathematics behind each method and it cannot be said that one methodology is more correct than the other two.

It was determined that the unplanted reactor had no dead volume, in contrast to the planted system. It was difficult to determine the exact location of the dead-zones, but the hydraulic calculations in the planted system indicated between 2% and 4% dead space by the step-change derivative and impulse-response techniques, respectively. Interestingly, the step-change integral method showed no dead volume. The θ peak positions did not show significant short-circuiting, or bypass. This is supported by the high effective volume utilisation calculated by all methodologies. It was not possible to determine a velocity profile as there was no means of finding the local flow rate at each sampling point inside the wetland bed. This would be a suggestion for future research, as well as the development of an analytical method for the selection of the most suitable modelling methodology.

Tracer studies at the Helmholtz UFZ in Leipzig

The second research objective was to investigate the hydraulic and chemical kinetic performance of a pilot-scale CW during the start-up phase at the Helmholtz Centre for Environmental Research (Helmholtz UFZ) in Leipzig, Germany. The investigative method was to be chosen based on the conclusions drawn from Objective 1.

The experiments carried out at the University of the Witwatersrand in April through to June 2015 (Bonner et. al, 2017b) were an opportunity to conduct a literature review; learn, in a practical manner, about the different tracer test techniques available and collaborate on a research paper in order to guide the design of the experiments at the Helmholtz UFZ.

The impulse-response methodology was chosen for the experiments at the Helmholtz UFZ for a number of reasons:

i. This was the recommendation of Dr Uwe Kappelmeyer who designed and built the CWs at the Helmholtz UFZ in Leipzig.
ii. The experimental set-up at the UFZ is fully automated. The system is fed directly by municipal water whose flow rate is controlled via a system of gear pump, motor and frequency controller. A metering pump is available to administer a solution of tracer dye, but due to the mechanics of this feed configuration, it is difficult to ensure a constant concentration of tracer entering the wetland for the duration of a step-change tracer study.
iii. This is the most widely used tracer technique in the literature, it is a reliable method (even though the results could not be validated using the step-change technique) and the mathematics is slightly less complex (preferable for the large number of tracer experiments to be conducted and commensurate amount of data to be gathered).

Two HSSF CWs, filled with glacial gravel and planted with *Phragmites australis*, were available at the Helmholtz UFZ. The wetlands were allowed an 18 month period of establishment (October 2013 to August 2015). The experimental campaign comprised of two parts:

- Part 1 – July to December 2015: the very first tracer studies at mid-depth and multiple locations, determination of the baseline chemical composition and introduction of artificial waste water. This research was published in *Water SA* (Chapter 5).
- Part 2 – April to October 2016: follow up tracer studies at multiple depths and locations, determination of the new baseline chemical composition and the re-introduction of artificial wastewater with monitoring over a longer period. The hydraulic results were published in *Science of the Total Environmen*t (Chapter 6). The chemical data is given in Chapter 7 and will be submitted to *Science of the Total Environmen*t as a follow up paper.

Chemical kinetic performance 2015

A hydraulic tracer test is a prerequisite to any chemical kinetic investigation as this indicates how effectively the wetland volume will be used in the treatment of any contaminants introduced into the system and is the basis of the calculation of the reaction rate constants. The impulse-response tracer tests showed 100% tracer recovery, which is the first indicator of a successful tracer test. The RTD was multi-modal with an elongated tail; indicating by-pass flow, diffusive mixing and the presence of stagnant zones; all of which should be minimized for effective contaminant treatment. By-pass means that some contaminants will leave the wetland untreated and stagnation means that contaminants are held up in the bed; thereby creating zones of hyper-concentration. As CWs are designed to receive and effectively treat a certain contaminant load, zones of stagnation and hyper-concentration could ultimately push the system concentration above the design load and, consequently, the discharge may not meet local standards. Despite this, an average of 93% reduction in both TOC and TN were observed even in the late fall and early winter when ambient temperatures had dropped and plant activity was reduced.

The Tanks-In-Series model was chosen for the first kinetic calculations in this system. Seven weeks of data was gathered, but only the last five were used for the calculation of the reaction rate and rate constant. The first two weeks were discarded for the purposes of these calculations owing to large fluctuations in the volumetric flow rate. Contrary to the literature, a constant value for the TOC and TN rate constants was not obtained. There were a few factors that could have had an impact. Firstly, there were small fluctuations in the volumetric flow rate which could not have been prevented and, as such, the system was not strictly at steady-state. Secondly, the temperature in the bed dropped over the five week period as the season moved from fall into winter and a drop in the reaction rate constant (and reaction rate) were observed. In future, better control should be exerted over the volumetric flow rate and the kinetic calculations should be performed by season.

Hydraulic performance 2016

The focus of the 2015 hydraulic study was the RTD at the system outlet because the research aim was to study the kinetic performance of the system as a whole, as a starting point (Aylward et al., 2017). Impulse-response flow tests were, however, also performed at each of the six internal sampling locations. The follow up hydraulic study in 2016 involved repeating these flow tests at mid-depth (12 cm below the gravel bed surface), as well as conducting additional tracer experiments at 12 cm and 36 cm below the bed surface. This gave greater insight into the fluid flow behaviour inside the system.

From the results of the 2015 kinetic study (Aylward et al., 2017), it was evident that, despite the high level of automation, it was not possible to ensure a constant inflow and outflow rate for the full duration of the flow tests and the full chemical sampling campaign as these experiments were carried out over a period of 5 months. It was also noted that fluctuations in the outflow could have been related to climatic

conditions (for example, high temperatures and evapotranspiration in the summer or heavy rain events). These first experiments provided valuable learnings and it was decided to build these factors (variable flow rate and climatic conditions) into the design of the 2016 experiments rather than to try to engineer the system to avoid them. This would, after all, neither be representative of the reality in CW systems nor founded upon biomimetic design principles.

Considering that the volumetric flow rate would almost certainly be subject to some natural variation and that climatic conditions would play a part in this, the volumetric flow rate was closely monitored and climatic data gathered such that the impact of the method of hydraulic calculation, seasonality and weather events could be investigated. Two methods of calculation were considered:

1. The standard method of calculating the RTD and its related parameters, as reported by Levenspiel (1972, 1999a,b) and Fogler (1999, 2006).
2. The modified method developed by Werner and Kadlec (1996).

In general, the volumetric flowrate decreased from inlet to outlet owing to evapotranspiration and low to no outflow was recorded in the height of summer. The only exception to the decrease in flow rate was during a rain event, when a surge in outflow was the only way for the system to maintain the wetland level. The RTDs produced by both methods showed diffusive mixing and low to moderate volumes of dead space, but it was determined that the RTDs generated by the standard method (and subject to the assumption of steady-state flow) were significantly different whereas those calculated by the modified method were statistically similar. For this reason, the variable method and close monitoring of the volumetric flowrate would be the recommendation; even for steady-flow systems. Werner and Kadlec's (1996) variable flow method would yield the same result as the standard method for a steady-flow system, but its use regardless comes with an in-built safety factor of accounting for any unforeseen, unexpected or unknown variation in the volumetric flowrate.

The importance of regularly and accurately monitoring the volumetric flow rate was highlighted in this study, as well as the fact that climatic data should be collected to complete an accurate mass balance over the wetland system. Hydraulic studies could be further improved by:

- Determining the porosity of the gravel and investigating the interaction with both the chosen tracer and the contaminants under study before the commencement of any experiments. It is important to know whether sorption to the gravel may impact upon the mass balance and tracer recovery (tracer recovery in the 2016 experiments was low at 31% - 36%) and also whether the contaminants under study may interact with the bed matrix; specifically under which conditions of pH, temperature etc. they may sorb and desorb.
- Quantifying the extent of plant uptake before the commencement of a tracer test would indicate how much tracer could be lost in this way, if any. It will also ensure proper closure of the mass

balance. A large increase in vegetation density was observed between the end of fall 2015 and the end of summer 2016, during which time many flow tests were carried out. This impact is likely larger for systems in the early start-up phase.

- The value of calculating the RTD using the modified method for variable flow systems is highlighted in this study. According to the best knowledge of the authors, equations and/or correlations for the determination of various hydraulic parameters (with the exception of the hydraulic moments) have not been fully developed. Hence, developing the mathematical relationships for the determination of these parameters would enhance this field of research.

Contaminant degradation/transformation 2016

The results of the follow-up experiments investigating TOC degradation in and TN removal from the pilot-scale wetland at the Helmholtz UFZ are presented in Chapter 7. The baseline measurements of TOC and TN are useful points of reference with regards to the natural levels of each in the CW system. After the introduction of wastewater into the system, the outlet TOC and TN concentrations, or chemical hydraulic loads, would not fall below the background values. The baseline pH of the system (which was in the region of pH 6.0 – 7.0) is common of many natural wetland and water ecosystems and that which is required to support aquatic plants and micro-organisms. A large increase or decrease in the system pH would be harmful to aquatic life. With the introduction of artificial wastewater into the system, it was observed that the pH increased slightly but that the CW had a good buffering capacity. It was also observed that the wetland was naturally low in oxygen, with a low (either slightly positive or slightly negative) redox potential, and that the water entering the system was saturated with oxygen. This oxygen was consumed within the first 1.0 – 1.5 m of the bed.

The artificial wastewater feed was also high in oxygen, with a positive redox potential, when fed into the wetland. There was a large decrease in both DO and potential within the first 1.50m. The largest percentage removal of TOC and TN occurs within the first 1.50 m of the bed where oxygen is more readily available. It is, thus, thought that oxidative processes (which produce a drop in potential) and root exudate transformations occur largely in the first quarter of the bed and that the TOC degradation and TN transformation that occurs thereafter is largely anaerobic and occurs more gradually. As these mechanisms proceed, the redox potential increases steadily towards the system outlet.

To aid visualisation of what was happening inside the bed and to open up the ‘black box’, so to speak, a method was developed to combine all of the data describing the chemical hydraulic loading at five internal sampling locations and three depths below the bed surface into one three dimensional graphic. It is clear (see Figure 7-10 and Figure 7-11) that the highest contaminant loadings occur in the distance between the wetland inlet and the second sampling point (2.225 m) for TOC and the third sampling point (2.97 m) for TN. The full length of the CW is 6 m. It can also be seen that nitrogen persists for a longer period of time, as compared to organic carbon. Organic carbon is in abundance and is more

readily utilisable as source of nutrients for aquatic plants and micro-organisms. Nitrogen is also transformed from one form to another, rather than degraded, hence its extended presence in the system in the sum parameter measured as TN. The contaminant load had dropped to its lowest detected levels towards the back end of the wetland and the percentage removal from port 3 to 4 to 5 would be lower than from the inlet to port 1 to port 2. The vegetation was also noticeably less dense at the back end of the wetland than at the front. This could largely be due to the lack of nutrients received by the plants there, as compared to at the inlet. Although a somewhat crude starting point, the chemical hydraulic loading density map does give some useful insight. This is only an estimation and the methodology requires refining; particularly in terms of gathering more data (increasing the number of sampling points) in the first 1.50 m of the bed and inserting internal flow sensors rather than relying on the method of relating the local internal flow rate to the vegetation density.

The artificial wastewater fed into the pilot-scale wetland for the purposes of this investigation was modelled on the effluent from a wastewater treatment plant. Due to the limitations of the dosing pump regulating the inlet flow rate of the wastewater, the CW received a higher contaminant load that what would be found in water being released from a wastewater treatment facility of Class 2 in Germany. Hence, CWs are effective in removing relatively high quantities of TOC and TN, but pre-treatment will be required to remove suspended solids (which could clog the system) and to balance the design load with the wetland size and retention time requirement to ensure that the effluent water meets local municipal standards. In certain instances, when compared to a high throughput industrial wastewater treatment plant, this is not economically feasible.

Framework for improved constructed wetland design

The third research objective was to collate and analyse the data collected with the aim of developing a framework for improved CW design. This would be done from the perspective of optimizing fluid flow pathways and maximizing fluid residence time in the areas of the bed where the rates of contaminant removal are greatest. Combining biomimetic design principles with the outcomes of the published papers and additional data analysed, the following recommendations can be made:

- In general, a biomimetic approach would involve carefully observing and deepening one's understanding of a natural process before moving into the design phase. Applied to CW design, a multi-disciplinary approach to studying as many natural wetland systems as possible should be taken. In other words, the fields of engineering, microbiology, chemistry, climate studies and biomimicry should be combined.

- There are many guidelines for CW design published in the literature, but the process of CW design will always be one of trial and error and finding the best combination of parameters to suit the treatment objectives. Often, the designer may have to compromise on one aspect to achieve another

more important objective. Bonner et al. (2017b) have shown that different RTD modelling methodologies can yield different hydraulic results for the same wetland system and that each methodology has its own advantages and disadvantages. The choice of reactor model should, therefore, be largely dependent on the limitations of the experimental equipment (which technique will yield the best data and what tools are available for its accurate analysis) and on the preference of the CW designer or operator (with which technique the designer most confident to work in terms of mathematical complexity and interpreting the results). Once the model is selected, it must be used consistently throughout the design phase.

- Although subject to some strict design criteria, CWs are still natural, dynamic systems and in a continual state of flux. Once the construction phase is complete, the system should be allowed to establish for at least one year before the first baseline samples are taken. The wetlands at the Helmholtz UFZ were allowed an 18 month period of establishment (root development) before experiments commenced, but the systems at Wits University were allowed only one month. It is expected that the hydraulic results from these systems would change as the plant root systems developed further. Wetland establishment is proceeded by a hydraulic investigation (tracer tests; at least in duplicate) to understand fluid flow behaviour and how well the system has been designed. This will highlight any changes that need to be made before contaminants are introduced into the system. The kinetic study will begin with the introduction of wastewater into the system and continual sampling over an extended period. The greater the quantity of data available, the better the results will be, but this should be balanced with time and cost. It is recommended that the tracer flow tests and kinetic studies are repeated into long term operation to better understand the internal development of the system. The suggestion would be seasonal repetition, but the frequency is at the designer's discretion.

- The multiple-location and multiple-depth sampling approach is recommended, again to understand the internal development of the system.

- There is conflicting opinion in the literature with regards to the need to plant CWs with different types of vegetation. The pilot wetlands at Wits University were planted with five different species of aquatic plant; each of which has a different capacity for treatment of different chemical pollutants. No firm conclusion can be draw from this because the experiments on these systems were not extended to introduction of wastewater and the monitoring of contaminant removal. The wetlands at the Helmholtz UFZ, however, were planted with only *Phragmites australis* but performed well with regards to the removal of TOC and TN from an artificial wastewater which was formulated based on the effluent from a wastewater treatment plant of Class 2 in Germany. Careful selection of multiple-species of macrophyte can be a good solution for treating wastewaters with specific contaminants not ordinarily encountered in domestic wastewater (such as heavy metals,

petrochemical residues, acid mine drainage etc.); otherwise the commonly used *Phragmites australis* will offer sufficient and effective treatment.

- Fluid flow pathways are impacted by the physical design of a CW and, by the nature of the system, cannot always be predicted or controlled. However, there are various aspects of the design on which to focus in order to optimise flow through the bed. From this research in particular, the impact of the inlet and outlet positioning is highlighted. The pilot scale CWs at the University of the Witwatersrand contained identical inlet and outlet manifolds comprising 13 evenly distributed ports (Figure 3-1 and Figure 3-2). On the other hand, the CW systems at the Helmholtz UFZ had three evenly distributed inlet ports located 5 cm above the base of the wetland and a single outlet port, also 5 cm above the base of the wetland. According to the results of the hydraulic study on the systems at Wits University in Chapter 4 (Bonner et al., 2017b), the dead volume was in the region of 0% to 4%, which is low. The hydraulic study on the CWs at the Helmholtz UFZ showed a moderate amount of dead space. It is thought that the manifold designs on the Wits systems would have induced more streamlined flow and a more even distribution of water in the system. The design of the inlet and outlet ports on the CWs at the UFZ could have induced a more hull-shaped flow profile which, in turn, lead to the dead space. The wetlands at the UFZ were also more densely vegetated, which could create areas of hold-up. This is not, necessarily, undesirable as long as the contaminants are in good contact with the root zone. Nevertheless, it is important to prevent areas of stagnation in the bed in which contaminants become trapped and remain untreated and, thus, the manifold-type design on the inlet and outlet would be the design recommendation.

- The percentage removal of TOC and TN was greatest in the first 1.50 m of the bed; likely due to the better availability of oxygen. Hence, the designer would endeavor to ensure that contaminated water remains in this section of the wetland for sufficient time to allow for maximum removal of contaminants before flowing into the anaerobic regions further down the bed where the removal processes occur at a lower rate. For this, dead zones and by-pass flow should be avoided, especially within the first half of the bed. As discussed in the preceding paragraph, the inlet distribution network can be designed to ensure even flow distribution and prevent zones of stagnation. In addition to the inlet configuration, gravel particles of uniform size, relatively even vegetation density, a root system penetrating all the way to the base of the wetland and a carefully selected flow rate can prevent by-pass flow. Although low to moderate dead volume was indicated by the hydraulic calculations, there was no evidence of by-pass flow in any of the hydraulic studies on both sets of pilot wetland systems.

- The modified RTD theory for variable flow systems developed by Werner and Kadlec (1996) should be used preferentially. This is particularly important for variable flow systems to which the assumption of steady-state flow and the application of the standard RTD methods does not apply. In the special case of steady-state flow, the modified method will yield the same result as the standard

method. If in doubt about the nature of the flow, a preliminary investigation applying both methods to the same data and comparing the results statistically should be undertaken. It is also vitally important to carefully and regularly monitor the system inlet and outlet volumetric flow rates and account for climatic conditions in performing a system mass balance.

Selection of a suitable tracer

Tracers are most often chemical dyes. Seeing as the application of the biomimetic approach to wetland research heightens one's awareness of the environment, part of this research was to investigate alternative tracer materials which would eliminate the need to introduce foreign, artificial substances into a natural or biomimetic system.

The feasibility of using a salt tracer

The fourth objective was, thus, to compare the impulse-response performance of a fluoride probe with that of a fluorescent chemical tracer to investigate the suitability of a salt-based tracer. To do this, a concentrated solution of calcium fluoride would be injected into the bed (in the same way as a pulse of chemical tracer) and its concentration measured over time using the fluoride probe.

In order to determine whether the plants would be able to withstand an elevated concentration of fluoride, small experiments were conducted in the Phytotechnikum at the Helmholtz UFZ. *Phragmites australis* were harvested from the pilot wetland stock and placed in five brown bottles containing solutions of five different fluoride concentrations and the plant activity (specifically leaf stomal porosity) was measured over a period of seven days, or up until plant activity was not registered. The experimental results are summarized in Appendix F.

All levels of fluoride tested resulted in plant activity dramatically decreasing and the leaves and stems eventually turning brown and drying out. This experiment was then discontinued as the risk of injecting a fluoride solution of high concentration into the pilot-scale system was too large and time did not allow for further investigation into a more suitable salt tracer; if any exists. This presents an area for future research.

The feasibility of using a micro-biological tracer

The fifth, and final, objective was to determine whether micro-organisms could be used as reliable tracers. *Phragmites australis* were to be harvested from the wetland and the micro-organisms in the root zone isolated and identified. Based on these results, a genetically unrelated micro-organism would be chosen. Small-scale laboratory experiments would then be conducted, similar to those for the salt tracer test, in which *Phragmites* would be placed in brown glass bottles and exposed to different levels of the foreign micro-organism. Samples would be drawn regularly and both the foreign and indigenous strains identified to investigate the interactions. In other words, would the foreign strains out-compete the

natural strains, would they die off or would they survive a sufficient amount of time, at a detectable level, to qualify as a potential microbiological tracer?

This part of the experiment was to be carried out in conjunction with a microbiology student as the microbiological techniques were complex and quite a large amount of time would have been necessary to fully master them. However, the student's internship was cancelled before its commencement. As a result, this part of the research was not completed, but would also present an interesting area for future research.

8.2. Conclusion

CWs are man-made systems, modelled on natural wetlands, which are successfully used for the remediation of a wide variety of wastewaters. They contain a soil or gravel matrix and are planted with one or more types of aquatic macrophyte. The size of the CW is dependent upon whether the system will be used for primary, secondary or tertiary treatment; the type of CW selected (horizontal flow, vertical flow, hybrid etc.); the availability of land; the volume of wastewater to be received; the expected contaminant loading of the influent water and the allowable contaminant concentrations in the wetland discharge; amongst other factors. It is recommended to remove as large a quantity of suspended solids as possible from the wastewater before it enters the treatment wetland. Suspended solid particles become easily entrapped and can lead to clogging and a greatly reduced effective volume utilisation.

The majority of published research has treated CW systems as black boxes. Hence, this research was an extension of the work by Sheridan et al. (2014a, b) in which a multiple internal sampling location regime was developed. In addition to sampling at multiple locations, this research included sampling at multiple depths at each location. In this way, greater insight into and understanding of the internal operation of a pilot-scale CW was gained. It was also seen that CW research and design is a multi-disciplinary field in which elements of chemistry, chemical engineering, physics, microbiology, climate studies and biomimicry all combine. In particular, some important learnings were taken:

- CWs, although man-made and well-engineered and designed, are dynamic systems in a continual state of flux and the internal behaviour (flow regime, treatment efficiency etc.) changes over time.
- The presence of vegetation has a definite impact upon hydraulic behaviour.
- Numerous wetland modelling methodologies exist and each will produce different results for the same system. CW design is not an exact science, but rather done by trial and error and will require balancing a number of parameters to find the most suitable design. Hence, wetland design will be specific to location and objective and there is never one definitively 'correct' design.

- The importance of monitoring and knowing the volumetric flow rate cannot be understated, as it is the basis of all hydraulic and kinetic calculations. From a hydraulic and kinetic calculation, as well as design and modelling, point of view it cannot be assumed that a CW operates at steady-state when there is variation in the flow rate.
- A pilot-scale CW can achieve high levels of TOC and TN removal despite being in the established but early-start-up phase; exposed to higher contaminant loading than the norm for such a system and subject to great variations in temperature. Hence, these systems are robust and self-maintaining with good buffering capacity.

In summary, the following were identified as areas for future research:

- A method for the determination of the velocity profile within a CW system.
- The development of an analytical method for the selection of the most suitable hydraulic modelling methodology for CW systems.
- Finding the mathematical relationships for various hydraulic parameters and correlations, such as the Peclet and Dispersion numbers, which could be used with Werner and Kadlec's (1996) modified RTD theory for variable flow systems.
- Publication of the findings from long-term studies on the same wetland system (from start-up into steady operation over some years) which employs the multiple depth and location sampling approach and where hydraulic and kinetic studies are repeated seasonally.

Chapter 9 References

ADLER, P. R., TAKEDA, F., GLENN, D. M., WADE, E. M., SUMMERFELT, S. T. & HARPER, J. K. 1996. Nutrient removal: ecological process sows a cost-saving idea for enhancing water quality. *Water Environment & Technology,* 8**,** 23-24.

ALAOUI, A., CADUFF, U., GERKE, H. H. & WEINGARTNER, R. 2011. A preferential flow effect on infiltration and runoff in grassland and forest soils. *Vadose Zone Journal,* 10**,** 367-377.

ALBERTINI, A. V. P., REIS, A. L. S., TELES, F. R. R., SOUZA, J. C., FILHO, J. L. R., FREIRE, V. N., SANTOS, R. P., MARTINS, J. L., CAVADA, B. S., MARTINS, D. B. G., MARTÍNEZ, C. R. & FILHO, J. L. L. 2012. The new flow system approach in packed bed reactor applicable for immobilized enzyme. *Journal of Molecular Catalysis B: Enzymatic,* 79**,** 1-7.

ALBERTSON, M. L. 1998. Constructed Wetlands for Wastewater Treatment: A Proposed Research Program *Wetlands Engineering and River Restoration Conference 1998* Denver, Colorado: American Society of Civil Engineers.

ALBUQUERQUE, A., OLIVEIRA, J., SEMITELA, S. & AMARAL, L. 2009. Influence of bed media characteristics on ammonia and nitrate removal in shallow horizontal subsurface flow constructed wetlands. *Bioresource Technology,* 100**,** 6269-6277.

ALCOCER, D. J. R., VALLEJOS, G. G. & CHAMPAGNE, P. 2012. Assessment of the plug flow and dead volume ratios in a sub-surface horizontal-flow packed-bed reactor as a representative model of a sub-surface horizontal constructed wetland. *Ecological Engineering,* 40**,** 18-26.

ANDERSON, A. E., WEILER, M., ALILA, Y. & HUDSON, R. O. 2009. Dye staining and excavation of a lateral preferential flow network. *Hydrology and Earth System Sciences,* 13**,** 935-944.

ARMSTRONG, J. & ARMSTRONG, W. 1988. *Phragmites australis* - a preliminary study of soil-oxidising sites and internal gas transport pathways. *New Phytologist,* 108**,** 373-382.

ARMSTRONG, J. & ARMSTRONG, W. 1991. A convective through-flow of gases in Phragmites australis (Cav.) Trin. ex Steud. *Aquatic Botany,* 39**,** 75-88.

ARMSTRONG, W. 1979. Aeration in higher plants. *Advances in Botanical Research,* 7**,** 225-332.

ATKINS, P. & DE PAULA, J. 2006. *Atkins' Physical Chemistry,* Oxford, Oxford University Press.

AYLWARD, L., BONNER, R., SHERIDAN, C. & KAPPELMEYER, U. 2019. Hydraulic study of a non-steady horizontal sub-surface flow constructed wetland during start-up. *Science of the Total Environment,* 646**,** 880-892.

AYLWARD, L., KAPPELMEYER, U., BONNER, R., HECHT, P. & SHERIDAN, C. M. 2017. Investigation into the kinetics of wetland degradation processes as a precursor to biomimetic design. *Water SA,* 43**,** 655-665.

BAETZ, U. & MARTINOIA, E. 2014. Root exudates: the hidden part of plant defense. *Trends in Plant Science,* 19**,** 90-98.

BAVOR, H. J., ROSER, D. J., MCKERSIE, S. A. & BREEN, P. 1988. Joint study on sewage treatment using shallow lagoon aquatic plant systems. Sydney: Hawkesbury Agricultural College/CSIRO/Sydney Water Board.

BELLINGHAM, K. 2012. Physicochemical properties of natural waters. Portland, Oregon: Stevens Water Monitoring Systems Inc.

BENYUS, J. M. 2017. Biomimicry 3.8 Resource Handbook. Available: http://static.biomimicry.org/wp-content/uploads/2012/02/Biomimicry_Resource_Handbook_Excerpt.pdf [Accessed 14 October 2017].

BEQUETTE, B. W. 2003. *Process Control: Modeling, Design and Simulation.* , New Jersey, Prentice Hall.

BERNET, N., DANGCONG, P., DELEGENES, J. P. & MOLETTA, R. 2001. Nitrification at low oxygen concentration in biofilm reactor. *Journal of Enviornmental Energy,* 127**,** 266-271.

BIOMIMICRY.SA. 2015. *Biomimicry 101 Training Manual,* Cape Town, Biomimicry Institute of South Africa.

BIOMIMICRY.SA. 2018. *Our Biomimicry Projects: GENIUS OF SPACE PROJECT - LANGRUG* [Online]. Cape Town: Biomimicr S.A. Available: https://www.biomimicrysa.co.za/our-projects/ [Accessed 21 March 2018].

BONNER, R., AYLWARD, L., HARLEY, C., KAPPELMEYER, U. & SHERIDAN, C. M. 2017a. Heat as a hydraulic tracer for horizontal subsurface flow constructed wetlands. *Journal of Water Process Engineering,* 16**,** 183-192.

BONNER, R., AYLWARD, L., KAPPELMEYER, U. & SHERIDAN, C. 2018. Combining tracer studies and biomimetic design principles to investigate clogging in constructed wetlands. *Water SA,* 44**,** 764-770.

BONNER, R., AYLWARD, L., KAPPELMEYER, U. & SHERIDAN, C. M. 2017b. A comparison of three different residence time distribution modelling methodologies for horizontal subsurface flow constructed wetlands. *Ecological Engineering,* 99**,** 99-113.

BRADLEY, B. R., DAIGGER, G. T., RUBIN, R. & TCHOBANOGLOUS, G. 2002. Evaluation of onsite wastewater treatment technologies using sustainable development criteria. *Clean Technologies and Environmental Policy,* 4**,** 87-99.

BRISSON, J. & CHAZARENC, F. 2008. Maximising pollutant removal in constructed wetlands: should we pay more attention to macrophyte species selection? *Science of the Total Environment,* 407**,** 3923-3930.

BRIX, H. 1994a. Functions of macrophytes in constructed wetlands. *Water Science and Technology,* 29**,** 71-78.

BRIX, H. 1994b. Use of Constructed Wetlands in Water Pollution Control: Historical Development, Present Status and Future Perspectives. *Water Science and Technology,* 30**,** 209-223.

BRIX, H. 1997. Do macrophytes play a role in constructed treatment wetlands? *Water Science and Technology,* 35**,** 11-17.

BURESH, R. J., CASSELMAN, M. E. & PATRICK JR, W. H. 1980. Nitrogen fixation in flooded soil systems: a review. *Advances in Agronomy,* 33**,** 149-192.

BURGIN, A. J. & HAMILTON, S. K. 2007. Have we overemphasized the role of denitirification in aquatic ecosystems? A review of nitrate removal pathways. *Frontiers in Ecology and the Environment,* 5**,** 89-96.

CHA, L. C. & FAN, L. T. 1963. Age distribution for flow systems. *Canadian Journal of Chemical Engineering,* 41**,** 62-66.

CHAZARENC, F., MERLIN, G. & GONTHIER, Y. 2003. Hydrodynamics of horizontal subsurface flow constructed wetlands. *Ecological Engineering,* 21**,** 165-173.

COETZEE, C., JEFTHAS, E. & REINTEN, E. 1999. Indigenous Plant Genetic Resources of South Africa. *In:* JANICK, J. (ed.) *Perspectives on new crops and new uses.* Virginia: ASHS Press.

CUI, Y., WOOSTER, J. K., BAKER, P. F., DUSTERHOFF, S. R., SKLAR, L. S. & DIETRICH, W. E. 2008. Theory of Fine Sediment Infiltration into Immobile Gravel Bed. *Journal of Hydraulic Engineering,* 134**,** 1421-1429.

CWC. 2015. *Consolidated Water Conditioning (CWC): residential, commercial and industrial water purification systems* [Online]. Johannesburg: Consolidated Water Conditioning SA (Pty) Ltd. Available: http://www.cwc.co.za/index.html [Accessed 21 March 2018].

DAMA-FAKIR, P., JANISCH, C., O'CONNOR, C., OTTO, D. & WELZ, P. 2015. Biomimicry and Wetlands Literature Survey - Draft Final Report for WRC Project No. K5/2096/1. Pretoria: Water Research Commission.

DOE. 2018. *Coal resources* [Online]. Pretoria: South African Department of Energy (DOE). Available: http://www.energy.gov.za/files/coal_frame.html [Accessed 21 March 2018].

DORDIO, A. V. & CARVALHO, A. J. P. 2013. Organic xenobiotics removal in constructed wetlands, with emphasis on the importance of the support matrix. *Journal of Hazardous Materials,* 252**,** 272-292.

DOTRO, G., LARSEN, D. & PALAZOLO, P. 2011. Preliminary Evaluation of Biological and Physical–Chemical Chromium Removal Mechanisms in Gravel Media Used in Constructed Wetlands. *Water, Air, and Soil Pollution,* 215**,** 507-515.

DRIZO, A., FROST, C. A., GRACE, J. & SMITH, K. A. 1999. Physico-chemical screening of phosphate-removing substrates for use in constructed wetland systems. *Water Research,* 33**,** 3595-3602.

DUWIG, C., DELMAS, P., MÜLLER, K., PRADO, B., REN, K., MORIN, H. & WOODWARD, A. 2008. Quantifying fluorescent tracer distribution in allophanic soils to image solute transport. *European Journal of Soil Science,* 59**,** 94-102.

EL HAMOURI, B., NAZIH, J. & LAHJOUJ, J. 2007. Subsurface-horizontal flow constructed wetland for sewage treatment under Moroccan climate conditions. *Desalination,* 215**,** 153-158.

ERIKSSON, N., GUPTA, A. & DESTOUNI, G. 1997. Comparative analysis of laboratory and field tracer tests for investigating preferential flow and transport in mining waste rock. *Journal of Hydrology,* 194**,** 143-163.

FLEMING-SINGER, M. S. & HORNE, A. J. 2002. Enhanced Nitrate Removal Efficiency in Wetland Microcosms Using an Episediment Layer for Denitrification. *Environmental Science & Technology,* 36**,** 1231-1237.

FLORES, H. E., VIVANCO, J. M. & LOYOLA-VARGAS, V. M. 1999. "Radicle" biochemistry: the biology of root-specific metabolism. *Trends in Plant Science,* 4**,** 220-226.

FMJC. 2001. German Federal Law Gazette (Bundesgesetzblatt): Regulations around Requirements Regarding the Discharge of Wastewater. *2450 – 2451*. Germany: Bundesanzeiger Verlagsgesellschaft mbH.

FOCHT, D. D. & VERSTRAETE, W. 1977. Biochemical ecology of nitrification and denitrification. *Advances in Microbial Ecology,* 1**,** 135-214.

FOGLER, H. S. 1999. *Elements of Chemical Reaction Engineering,* Massachusetts, Prentice Hall.

FOGLER, H. S. 2006. *Elements of Chemical Reaction Engineering, 4th Edition,* Massachusetts, Prentice Hall.

FRASER, L. F. & KEDDY, P. 1997. The role of experimental microcosms in ecological research. *Trends in Ecology and Evolution,* 12.

FROMENT, G. F., BISCHOFF, K. B. & DE WILDE, J. 2011. *Chemical Reactor Analysis and Design, 3rd Ed.*, New York, John Wiley & Sons.

GALLETTI, A., VERLICCHI, P. & RANIERI, E. 2010. Removal and accumulation of Cu, Ni and Zn in horizontal subsurface flow constructed wetlands: Contribution of vegetation and filling medium. *Science of The Total Environment,* 408**,** 5097-5105.

GALVÃO, A. F., MATOS, J. S., FERREIRA, F. S. & CORREIA, F. N. 2010. Simulating flows in horizontal subsurface flow constructed wetlands operating in Portugal. *Ecological Engineering,* 36**,** 596-600.

GARCÍA, J., CHIVA, J., AGUIRRE, P., ÁLVAREZ, E., SIERRA, J. P. & MUJERIEGO, R. 2004. Hydraulic behaviour of horizontal subsurface flow constructed wetlands with different aspect ratio and granular medium size. *Ecological Engineering,* 23**,** 177-187.

GARCIA, J., ROUSSEAU, D. P. L., MORATÓ, J., LESAGE, E., MATAMOROS, V. & BAYONA, J. M. 2010. Contaminant Removal Processes in Subsurface-Flow Constructed Wetlands: A Review. *Critical Reviews in Environmental Science and Technology,* 40**,** 561-661.

GEANKOPLIS, C. J. 1993. *Transport Processes and Unit Operations, 3rd Ed.,* New Jersey, Prentice-Hall International, Inc.

GOVT.SA. 2017. *Water and Sanitation* [Online]. Pretoria: Government of South Africa. Available: http://www.gov.za/about-sa/water-affairs#nwrs [Accessed 17 February 2017].

GREENCAPE 2016. Water: Market Intelligence Report 2016. Cape Town.

GUTOWSKI, L., OLIVER, O., LANGE, J. & KÜMMERER, K. 2015. Photolytic transformation products and biological stability of the hyrdological tracer Uranine. *Science of the Total Environment,* 533**,** 446-453.

HABERL, R., GREGO, S., LANGERGRABER, G., KADLEC, R. H., CICALINI, A.-R., MARTINS-DIAS, S., NOVIAS, J. M., AUBERT, S., GERTH, A., THOMAS, H. & HEBNER, A. 2003. Constructed wetlands for the treatment of organic pollutants. *Journal of Soils & Sediments,* 3**,** 109-124.

HAUCK, R. D. 1984. Atmospheric Nitrogen. Chemistry, Nitrification, Denitrification, and their Interrelationships. In: The Natural Environment and the Biogeochemical Cycles

The Handbook of Environmental Chemistry. Heidelberg: Springer.

HEADLEY, T. R., DAVISON, L., HUETT, D. O. & MÜLLER, R. 2012. Evapotranspiration from subsurface horizontal flow wetlands planted with Phragmites australis in sub-tropical Australia. *Water Research,* 46**,** 345-354.

HEADLEY, T. R. & KADLEC, R. H. 2007. Conducting Hydraulic Tracer Studies of Constructed Wetlands: A Practical Guide. *Ecohydrology and Hydrobiology,* 7**,** 269-282.

HOLLAND, J. F., MARTIN, J. F., GRANATA, T., BOUCHARD, V., QUIGLEY, M. & BROWN, L. 2004. Effects of wetland depth and flow rate on residence time distribution characteristics. *Ecological Engineering,* 23**,** 189-203.

HUETT, D. O., MORRIS, S. G., SMITH, G. & HUNT, N. 2005. Nitrogen and phosphorus removal from plant nursery runoff in vegetated and unvegetated subsurface flow wetlands. *Water Research,* 39**,** 3259-72.

IWA 2000. Constructed Wetlands for Pollution Control: Process, Performance, Design and Operation. London: International Water Association.

JAKUBASZEK, A. & WOJCIECH, M. 2014. Statistical Analysis of Nitrogen in the Soil of Constructed Wetland with Horizontal Sub-Surface Flow. *Civil And Environmental Engineering Reports,* 12**,** 33-43.

JETTEN, M. S. M., LOGEMANN, S., MUYZER, G. M., ROBERTSON, L. A., DEVRIES, S., VAN LOOSDRECHT, M. C. M. & KEUNEN, J. G. 1997. Novel principles in the microbial conversion of nitrogen compounds. *Antonie van Leeuwenhoek Journal of Microbiology,* 71**,** 75-93.

JOHNSTON, C. 1993. Mechanisms of Wetland-water Quality Interaction. *Constructed Wetlands for Water Quality Improvement.* Michigan: Lewis Publishers.

JOHNSTON, C. A. 1991. Sediments and nutrient retention by freshwater wetlands: effects on surface water quality. *CRC Critical Reviews in Environmental Control,* 21**,** 491-565.

JTED 2014. John Todd Ecological Design Eco-Machine® Waste Treatment and Remediation Systems. Massachusetts.

KADLEC, R. H. 1994. Detention and mixing in free water wetlands. *Ecological Engineering,* 3**,** 345-380.

KADLEC, R. H. & KNIGHT, R. 1996. *Treatment Wetlands,* Boca Raton, CRC Press.

KADLEC, R. H. & WALLACE, S. D. 2009. *Treatment Wetlands,* New York, CRC Press.

KAPPELMEYER, U., WIEßNER, A., KUSCHK, P. & KÄSTNER, M. 2002. Operation of a universal test unit for planted soil filters – Planted Fixed Bed Reactor. *Engineering in Life Science,* 2**,** 311-315.

KARATHANASIS, A. D., POTTER, C. L. & COYNE, M. S. 2003. Vegetation effects on fecal bacteria, BOD, and suspended solid removal in constructed wetlands treating domestic wastewater. *Ecological Engineering,* 20**,** 157-169.

KASNAVIA, T., VU, D. & SABATINI, D. A. 1999. Fluorescent dye and media properties affecting sorption and tracer selection. *Ground Water,* 37**,** 376-381.

KÄSS, W. 1998. *Tracing technique in geohydrology,* Rotterdam, A.A. Balkema.

KÄSS, W. 2004. *Geohydrologische Markierungstechnik (Tracing Technique in Geohydrology),* Stuttgart, Borntraeger.

KASSIM, K. 2007. Modelling of Fecal Coliform Removal Using the Stella Software: A Case of Horizontal Sub-surface Flow Constructed Wetland in Tanzania. Harare: University of Zimbabwe.

KAUFFMAN, S. 1993. *The Origins of Order: Self Organization and Selection in Evolution,* London, Oxford University Press.

KENNY, J., DESHA, C., KUMAR, A. & HARGROVES, C. 2012. Using biomimicry to inform urban infrastructure design that addresses 21st century needs. 1st International Conference on Urban Sustainability and Development, 2012. London.

KEYES, W. J., O'MALLEY, R. C., KIM, D. & LYNN, D. G. 2000. Signaling organogenesis in parasitic angiosperms: xenognosin generation, perception, and response. *Journal of Plant Growth Regulation,* 19**,** 217-231.

KIM, S.-W., MIYAHARA, M., FUSHINOBU, S., WAKAGI, T. & SHOUN, H. 2010. Nitrous oxide emission from nitrifying activated sludge dependent on denitrification by ammonia-oxidizing bacteria. *Bioresource Technology,* 101**,** 3958-3963.

KIVAISI, A. K. 2001. The Potential for Constructed Wetlands for Wastewater Treatment and Reuse in Developing Countries - A Review. *Ecological Engineering,* 16**,** 545-560.

KNOWLES, P., DOTRO, G., NIVALA, J. & GARCÍA, J. 2011. Clogging in subsurface-flow treatment wetlands: Occurrence and contributing factors. *Ecological Engineering,* 37**,** 99-112.

KNOWLES, P. R. & DAVIES, P. A. 2010. A Finite Element Approach to Modelling the Hydrological Regime in Horizontal Subsurface Flow Constructed Wetlands for Wastewater Treatment. *In:* VYMAZAL, J. (ed.) *Water and Nutrient Management in Natural and Constructed Wetlands.* Dordrecht: Springer.

KOKO, M. 2018. *Coal is the lifeblood of the South African economy* [Online]. Johannesburg: Eskom. Available: http://www.eskom.co.za/Pages/CoaL.aspx [Accessed 2018-03-21].

KRANJC, A. 1997. *Tracer Hydrology 97,* Rotterdam, A.A. Balkema.

KRITZINGER, E. M., VAN VUUREN, R. J., WOODWARD, B., RONG, I. H., SPREETH, M. H. & M.M., S. 1997. Elimination of External and internal Contaminants in Rhizomes of Zantedeschia Aethiopica with Commercial Fungicides and Antibiotics. *In:* A.C., C. (ed.) *Pathogen and Microbial Contamination Management in Micropropagation: Developments in Plant Pathology.* Dordrecht: Springer.

LANGE, J., SCHUETZ, T., GREGOIRE, C., ELSÄSSER, D., SCHULZ, R., PASSEPORT, E. & TOURNEBIZE, J. 2011. Multi-tracer experiments to characterise contaminant mitigation capacities for different types of artificial wetlands. *International Journal of Environment Analytical Chemistry,* 91**,** 768-785.

LEE, B.-H. & SCHOLZ, M. 2007. What is the role of Phragmites australis in experimental constructed wetland filters treating urban runoff? *Ecological Engineering,* 29**,** 87-95.

LETO, C., TUTTOLOMONDO, T., LA BELLA, S., LEONE, R. & LICATA, M. 2013. Effects of plant species in a horizontal subsurface flow constructed wetland – phytoremediation of treated urban wastewater with Cyperus alternifolius L. and Typha latifolia L. in the West of Sicily (Italy). Part A. *Ecological Engineering,* 61**,** 282-291.

LEVENSPIEL, O. 1972. *Chemical Reaction Engineering, 2nd Ed.,* New York, John Wiley & Sons.

LEVENSPIEL, O. 1999a. Chemical Reaction Engineering. *Industrial and Engineering Chemistry Research,* 38**,** 4140-4143.

LEVENSPIEL, O. 1999b. *Chemical Reaction Engineering, 3rd Ed.,* New York, John Wiley & Sons.

LIGI, T., OOPKAUP, K., TRUU, M., PREEM, J.-K., NÕLVAK, H., MITSCH, W. J., MANDER, Ü. & TRUU, J. 2014. Characterization of bacterial communities in soil and sediment of a created riverine wetland complex using high-throughput 16S rRNA amplicon sequencing. *Ecological Engineering,* 72**,** 56-66.

LIMA, D. M. F. & ZAIAT, M. 2012. The influence of the degree of back-mixing on hydrogen production in an anaerobic fixed-bed reactor. *International Journal of Hydrogen Energy,* 37**,** 9630-9635.

LÜDERITZ, V. & GERLACH, F. 2002. Phosphorus Removal in Different Constructed Wetlands. *Engineering in Life Science,* 22**,** 91-99.

LÜNSMANN, V., KAPPELMEYER, U., BENNDORF, R., MARTÍNEZ-LAVANCHY, P. M., TAUBERT, A., ADRIAN, L., DUARTE, M., PIEPER, D. H., VON BERGEN, M., MÜLLER, J. A., HEIPIEPER, H. J. & JEHMLICH, N. 2016. In situ protein-SIP highlights Burkholderiaceae as key players degrading toluene by para ring hydroxylation in a constructed wetland model. *Environmental Microbiology,* 18**,** 1176-1186.

MARCHAND, L., MENCH, M., JACOB, D. L. & OTTE, M. L. 2010. Metal and metalloid removal in constructed wetlands, with emphasis on the importance of plants and standardized measurements: A review. *Environmental Pollution,* 158**,** 3447-3461.

MARSCHNER, H. 1995. *Mineral Nutrition of Higher Plants, 2nd Ed.,* London, Academic Press

MARSILI-LIBELLI, S. & CHECCHI, N. 2005. Identification of dynamic models for horizontal subsurface constructed wetlands. *Ecological Modelling,* 187**,** 201-218.

MATAGI, S. V., SWAI, D. & MUGABE, R. 1998. A review of heavy metal removal mechanisms in wetlands. *African Journal of Tropical Hydrobiology and Fisheries,* 8**,** 23-25.

MAYO, A. W. 2014. Modelling dynamics of organic carbon in water hyacinth Eichhornia Crassipes (Mart.) Solms artificial wetlands. *International Journal of Water Resources and Environmental Engineering,* 6**,** 121-130.

MCCORD, J. R. 1972. A stochastic analysis of the extremes of micromixing in a nonsteady-state continuous flow chemical reactor. *Chemical Engineering Science,* 27**,** 1613-1626.

MEGONIGAL, J. P., HINES, M. E. & VISSCHER, P. T. 2004. Anaerobic Metabolism: Linkage to Trace Gases and Aerobic Processes. *In:* SCHLESIGNER, W. H. (ed.) *Biogeochemistry.* Oxford: Elsevier-Pergamon.

MENDOZA, J. L., GRANADOS, M. R., DE GODOS, I., ACIÉN, F. G., MOLINA, E., BANKS, C. & HEAVEN, S. 2013. Fluid-dynamic characterization of real-scale raceway reactors for microalgae production. *Biomass and Bioenergy,* 54**,** 267-275.

MERCK 2011. Uranine Fluorescent Dye. Darmstadt, Germany: Millipore Corporation.

MIDDLETON, L. 2012. South Africa: Rural School Running on Methane Biogas. *Inter Press Service News Agency* [Online]. Available: http://www.ipsnews.net/2012/03/south-africa-rural-school-running-on-methane-bio-gas/ [Accessed 16 April 2015].

MIKULLA, C., EINSEIDL, F., SCHLUMPRECHT, C. & WOHNLICH, S. 1997. Sorption of uranine and eosine on an aquifer material containing high organic carbon. *In:* KRANJC, A. (ed.) *Tracer Hydrology 97.* Rotterdam: A.A. Balkema.

MILLER, P. A. & CLESCERI, N. L. 2002. *Waste Sites as Biological Reactors: Characterization and Modelling,* London, CRC Press.

MULDER, A., VAN DE GRAAF, A. A., ROBERTSON, L. A. & KUENEN, J. G. 1995. Anaerobic ammonium oxidation discovered in a denitrifying fluidized bed reactor. *FEMS Microbiology Ecology,* 16**,** 177-184.

NARDI, S., CONCHERI, G., PIZZEGHELLO, D., STURARO, A., RELLA, R. & PARVOLI, G. 2000. Soil organic matter mobilization by root exudates. *Chemosphere,* 5**,** 653-658.

NAUMANN, E. B. 1969. Residence time distributuon theory for unsteady stirred tank reactors. *Chemical Engineering Science,* 24.

NERALLA, S., WEAVER, R. W., LESIKAR, B. J. & PERSYN, R. A. 2000. Improvement of Domestic Water Quality by Subsurface Flow Constructed Wetlands. *Bioresource Technology,* 75**,** 19 - 25.

NIMBUS. 2017. *Nimbus Water Purification Solutions* [Online]. Johannesburg: Nimbus Water (Pty) Ltd. Available: http://www.nimbuswater.co.za/home.php#contact [Accessed 21 March 2018].

NOORVEE, A., PÕLDVERE, E. & MANDER, Ü. 2007. The effect of pre-aeration on the purification processes in the long-term performance of a horizontal subsurface flow constructed wetland. *Science of The Total Environment,* 380**,** 229-236.

ONG, S. A., UCHIYAMA, K., INADAMA, D., ISHIDA, Y. & YAMAGIWA, K. 2010. Performance evaluation of laboratory scale up-flow constructed wetlands with different designs and emergent plants. *Bioresour Technol,* 101**,** 7239-44.

PALMER-FELGATE, E. J., MORTIMER, R. J. G., KROM, M. D. & JARVIE, H. P. 2010. Impact of Point-Source Pollution on Phosphorus and Nitrogen Cycling in Stream-Bed Sediments. *Environmental Science & Technology,* 44**,** 908-914.

PAUL, E. A. & CLARK, F. E. 1996. *Soil microbiology and biochemistry 2nd Ed.,* San Diego, California, Academic Press.

PERSSON, J., SOMES, N. L. G. & WONG, T. H. F. 1999. Hydraulic Efficiency of Constructed Wetlands and Ponds. *Water Science and Technology,* 40**,** 291-300.

POZRIKIDIS, C. 1998. *Numerical Computation in Science and Engineering,* New York, Oxford University Press.

RANIERI, E., GORGOGLIONE, A. & SOLIMENO, A. 2013. A comparison between model and experimental hydraulic performances in a pilot-scale horizontal subsurface flow constructed wetland. *Ecological Engineering,* 60**,** 45-49.

REDDY, K. R. & D'ANGELO, E. M. 1997. Biogeochemical indicators to evaluate pollutant removal efficiency in constructed wetlands. *Water Science and Technology,* 35**,** 1-10.

REDDY, K. R., D'ANGELO, E. M. & DEBUSK, T. A. 1989. Oxygen transport through aquatic macrophytes: the role in wastewater treatment. *Journal of Environment Quality,* 19**,** 261-270.

REDDY, K. R. & PATRICK, W. H. 1984. Nitrogen transformations and loss in flooded soils and sediments. *CRC Critical Reviews in Environmental Control,* 13**,** 273-309.

REDDY, L. D., KUMAR, D. & ASOLEKAR, S. R. 2014. Typologies for Successful Operation and Maintenance of Horizontal Sub-Surface Flow Constructed Wetlands. *International Journal of Engineering Research,* 18-19**,** 2347-5013.

REED, S. C. 1993. Subsurface Flow Constructed Wetlands for Wastewater Treatment: A Technology Review. Washington DC: U.S. EPA Office of Water.

REED, S. C., CRITES, R. W. & MIDDLEBROOKS, E. J. 1995. *Natural Systems for Waste Management and Treatment, 2nd Ed.,* New York, McGraw Hill.

REINTEN, E. Y., COETZEE, J. H. & VAN WYK, B. E. 2011. The potential of South African indigenous plants for the international cut flower trade. *South African Journal of Botany,* 77**,** 934-946.

RENGERS, E. E., DA SILVA, J. B., PAULO, P. L. & JANZEN, J. G. 2016. Hydraulic performance of a modified constructed wetland system through a CFD based approach. *Journal of Hydro-environment Research,* 12**,** 91-104.

RÍOS, A. D., VÉLEZ, T. A. F., PEÑA, M. R. & PARRA, M. C. A. 2009. Changes of flow patterns in a horizontal subsurface flow constructed wetland treating domestic wastewater in tropical regions. *Ecological Engineering,* 35**,** 274-280.

ROSE, A. H. 1976. *Chemical Microbiology,* New York, Plenum Press.

ROUSSEAU, D. P. L. & SANTA, S. Quantification of oxygen transfer pathways inhorizontal subsurface-flow constructed wetlands. *In:* MANDER, Ü., KOIV, M. V. & VOHLA, C., eds. 2nd International Symposium on Wetland Pollutant Dynamics and Control 2007 Estonia.

ROUSSEAU, D. P. L., VANROLLEGHEM, P. A. & DE PAUW, N. 2004. Model-based design of horizontal subsurface flow constructed treatment wetlands: a review. *Water Research,* 38**,** 1484-1493.

RSA 1997. (Republic of South Africa) Water Services Act. Act No. 108 of 1997. Government Gazette No. 18522. Cape Town: Government Printer.

RSA 1998. (Republic of South Africa) National Water Act. Act No. 36 of 1998. Government Gazette No. 19182. Cape Town: Government Printer.

RUBIN, F., PALMER, A. R. & TYSON, C. 2001. Patterns of endemism within the Karoo National Park, South Africa. *Bothalia African Biodiversity and Conservation,* 31**,** 17.

RÜDISÜLI, M., SCHILDHAUER, T. J., BIOLLAZ, S. M. A. & VAN OMMEN, J. R. 2012. Scale-up of bubbling fluidized bed reactors — A review. *Powder Technology,* 217**,** 21-38.

SANBI. 2014. *Investing in Ecological Infrastructure: The Practice and the Payoff for Water Security* [Online]. Pretoria: South African National Biodiversity Institute (SANBI). Available: http://www.grasslands.org.za/news/entry/investing-in-ecological-infrastructure-the-practice-and-the-payoff-for-water-security [Accessed 26 July 2015].

SAVANT, N. K. & DEDATTA, S. K. 1982. Nitrogen transformations in wetland rice soils. *Advances in Agronomy,* 35**,** 241-302.

SCHIEGL, S., STOCKHAMMER, P., SCOTT, C. & WADLEY, L. 2004. A mineralogical and phytolith study of the Middle Stone Age hearths in Sibudu Cave, KwaZulu-Natal, South Africa : Sibudu Cave. *South African Journal of Science,* 100**,** 185-194.

SCHMIDT, I., SLIEKERS, O., SCHMID, M., BOCK, E., FUERST, J., KUENEN, J. G., JETTEN, M. S. & STROUS, M. 2003. New concepts of microbial treatment process for the nitrogen removal from wastewaters. *FEMS Microbiology Review,* 27**,** 481-492.

SCHMIDT, I., ZART, D. & BOCK, E. 2001. Effects of gaseous NO2 on cells of Nitrosomonas eutropha previously incapable of using ammonia as an energy source. *Antonie van Leeuwenhoek Journal of Microbiology,* 79.

SCHNEGG, P.-A. 2002. An inexpensive field fluorometer for hydrogeological tracer tests with three tracers and turbidity measurement. *Groundwater and Human Development.* London: CRC Press.

SCHOLZ, M. & HEDMARK, A. 2010. Constructed wetlands treating runoff contaminated with nutrients. *Water, Air, and Soil Pollution,* 205.

SEAL. 2018. *SEAL Water Tech: Water Purification & Equipment* [Online]. Port Elizabeth: SEAL Water Tech. Available: https://www.sealwatertech.co.za/ [Accessed 21 March 2018].

SHENKER, M., SEITELBACH, S., BRAND, S., HAIM, A. & LITAOR, M. I. 2005. Redox reactions and phosphorus release in re-flooded soils of an altered wetland. *European Journal of Soil Science,* 54**,** 515-525.

SHEORAN, A. S. & SHEORAN, V. 2006. Heavy metal removal mechanism of acid mine drainage in wetlands: A critical review. *Minerals Engineering,* 19**,** 105-116.

SHERIDAN, C., GLASSER, D. & HILDEBRANDT, D. A calculation of the hydraulic properties of a vegetated gravel bed filter using an impulse-response tracer experiment to quantify non-ideal behaviour. 12th International Conference on Environmental Science and Technology, Global Network on Environmental Science and Technology, 2011 Rhodes, Greece. 1711-1716.

SHERIDAN, C., HARDING, K., KOLLER, E. & DE PRETTO, A. 2013. A comparison of charcoal- and slag-based constructed wetlands for acid mine drainage remediation. *Water SA,* 39**,** 369-374.

SHERIDAN, C. M., GLASSER, D. & HILDEBRANDT, D. 2014a. Estimating Rate Constants of Contaminant Removal in Constructed Wetlands Treating Winery Effluent: A Comparison of Three Different Methods. *Process Safety and Environmental Protection,* 92**,** 903-916.

SHERIDAN, C. M., HILDEBRANDT, D. & GLASSER, D. 2014b. Turning wine (waste) into water: toward technological advances in the use of constructed wetlands for winery effluent treatment. *Journal of American Institute of Chemical Engineers,* 60**,** 420-431.

SMART, P. L. & LAIDLAW, I. M. S. 1977. An evaluation of some fluorescent dyes for water tracing. *Water Resources Research,* 13**,** 15-33.

SMITH, E., GORDON, R., MADANI, A. & STRATTON, G. 2005. Pathogen Removal by Agricultural Constructed Wetlands in Cold Climates. *Journal of Environmental Informatics,* 6**,** 46 - 50.

SMITH, K. 1997. Constructed Wetlands for Treating Acid Mine Drainage. *University of Minnesota Student On-Line Journal,* 2**,** 1-7.

STAMOU, A. I. & NOUTSOPOULOS, G. 1994. Evaluating the effect of inlet arrangement in settling tanks using the hydraulic efficiency diagram. *Water SA,* 20**,** 77-83.

STEWART, W. D. P. 1973. Nitrogen Fixation. *In:* CARR, N. G. & WHITTON, B. A. (eds.) *The biology of blue-green algae.* Berkeley, California: University of California Press.

STOTTMEISTER, U., WIEßNER, A., KUSCHK, P., KAPPELMEYER, U., KÄSTNER, M., BEDERSKI, O., MÜLLER, R. A. & MOORMANN, H. 2003. Effects of plants and microorganisms in constructed wetlands for wastewater treatment. *Biotechnology Advances,* 22**,** 93-117.

STROUS, M., VAN GERVEN, E., KUENEN, J. G. & JETTEN, M. S. 1997. Effects of aerobic and microaerobic conditions on anaerobic ammonium-oxidizing (anammox) sludge. *Applied and Environmental Microbiology,* 63**,** 2446-2448.

SUBRAMANIAN, R. S. 2004. Flow through packed beds and fluidized beds. Available: http://www.pdfdrive.com/flow-through-packed-beds-and-fluidized-beds-clarkson-university-e1826488.html [Accessed 2017-02-21].

SULIMAN, F., FRENCH, H. K., HAUGEN, L. E. & SØVIK, A. K. 2006a. Change in flow and transport patterns in horizontal subsurface flow constructed wetlands as a result of biological growth. *Ecological Engineering,* 27**,** 124-133.

SULIMAN, F., FUTSAETHER, C., OXAAL, U., HAUGEN, L. E. & JENSSEN, P. 2006b. Effect of the inlet–outlet positions on the hydraulic performance of horizontal subsurface-flow wetlands constructed with heterogeneous porous media. *Journal of Contaminant Hydrology,* 87**,** 22-36.

SWARTZ, C. D. 2009. A PLANNING FRAMEWORK TO POSITION RURAL WATER TREATMENT IN SOUTH AFRICA FOR THE FUTURE - WRC Report No. TT 419/09. Pretoria: Water Research Commission.

TANNER, C. C. 1996. Plants for constructed wetland treatment systems — A comparison of the growth and nutrient uptake of eight emergent species. *Ecological Engineering,* 7**,** 59-83.

TANNER, C. C. 2001. Plants as ecosystems engineers in subsurface flow treatment wetlands. *Water Science and Technology,* 44**,** 9-17.

TANNER, C. C., KADLEC, R. H., GIBBS, M. M., SUKIAS, J. P. S. & NGUYEN, M. L. 2002. Nitrogen processing gradients in subsurface-flow treatment wetlands—influence of wastewater characteristics. *Ecological Engineering,* 18**,** 499-520.

TANNER, C. C., SUKIAS, J. P. S., HEADLEY, T. R., YATES, C. R. & STOTT, R. 2012. Constructed wetlands and denitrifying bioreactors for on-site and decentralised wastewater treatment: Comparison of five alternative configurations. *Ecological Engineering,* 42**,** 112-123.

TEEFY, S. 1996. *Tracer studies in water treatment facilities: a protocol and case studies,* Denver, Colorado, American Water Works Association.

TEIXEIRA, E. C. & SIQUEIRA, R. 2008. Performance Assessment of Hydraulic Efficiency Indexes. *Journal of Environmental Engineering,* 134**,** 851-859.

THACKSTON, E. L., SHIELDS, F. D. & SCHROEDER, P. R. 1987. Residence Time Distributions of Shallow Basins. *Journal of Environment Engineering,* 113**,** 1319-1332.

TODD, J. & JOSEPHSON, B. 1996. The design of living technologies for waste treatment. *Ecological Engineering,* 6**,** 109-136.

U.S.EPA 2002. Wastewater Technology Fact Sheet: The Living Machine® - EPA 832-F-02-025. Washington: United States Environmental Protection Agency.

VAN DE GRAAF, A. A., MULDER, A., DE BRUIJN, P., JETTEN, M. S. M., ROBERTSON, L. A. & KUENEN, J. G. 1995. Anaerobic oxidation of ammonium is a biologically mediated process. *Applied and Environmental Microbiology,* 61**,** 1246-1251.

VAN DE MOORTEL, A. M. K., MEERS, E., DE PAUW, N. & TACK, F. M. G. 2010. Effects of Vegetation, Season and Temperature on the Removal of Pollutants in Experimental Floating Treatment Wetlands. *Water, Air, and Soil Pollution,* 212**,** 281-297.

VERBERK, W. C. E. P., BILTON, D. T., CALOSI, P. & SPICER, J. I. 2011. Oxygen supply in aquatic ectotherms: Partial pressure and solubility together explain biodiversity and size patterns. *Ecology,* 92**,** 1565-1572.

VOGEL, S. & MÜLLER-DOBLIES, U. 2001. Desert geophytes under dew and fog: The "curly-whirlies" of Namaqualand (South Africa). *Flora,* 206**,** 3-31.

VOHLA, C., KÕIV, M., BAVOR, H. J., CHAZARENC, F. & MANDER, Ü. 2011. Filter materials for phosphorus removal from wastewater in treatment wetlands—A review. *Ecological Engineering,* 37**,** 70-89.

VYMAZAL, J. 2005. Horizontal sub-surface flow and hybrid constructed wetlands systems for wastewater treatment. *Ecological Engineering,* 25**,** 478-490.

VYMAZAL, J. 2007. Removal of nutrients in various types of constructed wetlands. *Science of the Total Environment,* 380**,** 48-65.

VYMAZAL, J., BRIX, H., COOPER, P. F., GREEN, M. B. & HABERL, R. 1998. *Constructed wetlands for wastewater treatment in Europe, Leiden,* The Netherlands, Backhuys Publishers.

VYMAZAL, J. & KRŐPFELOVÁ, L. 2005. Growth of Phragmites australis and Phalaris arundinacea in constructed wetlands for wastewater treatment in the Czech Republic. *Ecological Engineering,* 25**,** 606-621.

VYMAZAL, J. & KRŐPFELOVÁ, L. 2009. Removal of organics in constructed wetlands with sub-surface flow: a review of field experience. *Science of the Total Environment,* 407**,** 3911-3922.

W.M.O. 2008. *Guide to Hydrological Practices, Volume I, Hydrology - From Measurement to Hydrological Information,* Switzerland, World Meteorological Organization.

WAHL, M. D., BROWN, L. C., SOBOYEJO, A. O., MARTIN, J. F. & DONG, B. 2010. Quantifying the hydraulic performance of treatment wetlands using the moment index. *Ecological Engineering,* 36**,** 1691-1699.

WALKER, T. S., PAL BAIS, H., GROTEWOLD, E. & VIVANCO, J. M. 2003. Root Exudation and Rhizosphere Biology. *Plant Physiology,* 132**,** 44-51.

WARNEKE, S., SCHIPPER, L. A., MATIASEK, M. G., SCOW, K. M., CAMERON, S., BRUESEWITZ, D. A. & MCDONALD, I. R. 2011. Nitrate removal, communities of denitrifiers and adverse effects in different carbon substrates for use in denitrification beds. *Water Research,* 45**,** 5463-75.

WEN, F., CURLANGO-RIVERA, G. & HAWES, M. C. 2007a. Article Addendum - Proteins Among the Polysaccharides: A New Perspective on Root Cap Slime. *Plant Signalling and Behavior,* 2**,** 410-412.

WEN, F., VANETTEN, H. D., TSAPRAILIS, G. & HAWES, M. C. 2007b. Extracellular Proteins in Pea Root Tip and Border Cell Exudates. *Plant Physiology,* 143**,** 773-783.

WEN, F., WHITE, G. J., VANETTEN, H. D., XIONG, Z. & HAWES, M. C. 2009. Extracellular DNA Is Required for Root Tip Resistance to Fungal Infection. *Plant Physiology,* 151**,** 820-829.

WEN, Y., CHEN, Y., ZHENG, N., YANG, D. & ZHOU, Q. 2010. Effects of plant biomass on nitrate removal and transformation of carbon sources in subsurface-flow constructed wetlands. *Bioresource Technology,* 101**,** 7286-92.

WERNER, T. M. & KADLEC, R. H. 1996. Application of residence time distributions to stormwater treatment systems. *Ecological Engineering,* 7**,** 213-234.

WERNER, T. M. & KADLEC, R. H. 2000. Wetland residence time distribution modelling. *Ecological Engineering,* 15**,** 77-90.

WWF-SA 2016. Water: Facts and Futures - Rethinking South Africa's Water Future. Cape Town.

YALCUK, A., PAKDIL, N. B. & TURAN, S. Y. 2010. Performance evaluation on the treatment of olive mill waste water in vertical subsurface flow constructed wetlands. *Desalination,* 262**,** 209-214.

YANG, H., LI, D. T. & ZHU, Z. Y. 2001. Autotrophic ammonium removal of sludge liquor. *Environmental Science,* 22**,** 105-107.

ZURITA, F., DE ANDA, J. & BELMONT, M. A. 2006. performance of laboratory-scale wetlands planted with tropical ornamental plants to treat domestic wastewater. *Water Quality Research Journal of Canada,* 41**,** 410-417.

Appendix A: Experimental Data, UFZ Leipzig

This appendix contains the raw experimental data collected from the outdoor, pilot CWs and the Helmholtz UFZ in Leipzig, Germany. It is divided into two sections; namely baseline data (before the introduction of the artificial wastewater) and artificial wastewater data (the period during which artificial wastewater was being fed continually into the system over a number of weeks). Samples were taken from the inlet, the outlet and at six internal locations within the system (±100cm, 225.5cm, 297cm (both inside and alongside the removable basket), 373cm and 527cm from the wetland inlet). Samples were also taken at three depths (12cm, 24cm and 36cm below the gravel bed surface) at each of the six sampling points.

Baseline Data for 2015

Table A1: Baseline data collected on 7th August 2015

7-Aug-15	Depth (cm)																	
	12						24						36					
Dist. from Inlet (cm)	DO (µg/L)	Temp (°C)	Redox (mV)	pH	Temp (°C)	TOC (mg/L)	DO (µg/L)	Temp (°C)	Redox (mV)	pH	Temp (°C)	TOC (mg/L)	DO (µg/L)	Temp (°C)	Redox (mV)	pH	Temp (°C)	TOC (mg/L)
0	3150		344.20	6.09	36.0	4.19	3150		344.20	6.09	36.0	4.19	3150		344.20	6.09	36.0	4.19
88.5	1010		174.28	6.75	21.2	4.72	759		223.10	6.66	21.5	4.06	588		83.70	6.72	21.7	4.09
225.5	1070		143.80	6.75	22.0	3.77	560		158.56	6.73	22.4	4.09	387		217.26	6.79	22.9	4.01
297	1580		304.64	5.34	44.2	3.43	1600		375.40	5.37	44.5	3.00	10600		298.64	5.33	44.2	3.07
373	585		174.14	6.87	23.1	3.58	452		241.90	7.00	23.5	2.79	407		267.84	6.88	23.6	3.61
521	725		188.20	6.83	26.0	3.59	494		214.80	6.87	26.5	3.42	439		239.48	6.94	26.9	3.35
600	160		211.64	7.00	26.7	7.96	160		211.64	7.00	26.7	7.96	160		211.64	7.00	26.7	7.96
297 (basket)	12030		390.56	4.69	44.3	4.21	1440		366.84	5.01	40.2	3.24	1160		366.68	4.63	45.4	4.05

Table A2: Baseline data collected on 7th September 2015

7-Sep-15	Depth (cm)																	
	12						24						36					
Dist. from Inlet (cm)	DO (µg/L)	Temp (°C)	Redox (mV)	pH	Temp (°C)	TOC (mg/L)	DO (µg/L)	Temp (°C)	Redox (mV)	pH	Temp (°C)	TOC (mg/L)	DO (µg/L)	Temp (°C)	Redox (mV)	pH	Temp (°C)	TOC (mg/L)
0																		
88.5	7800	20.6	415.64	7.83		4.69	9380	20.7	425.58	7.81		3.98	8500	20.8	447.52	7.69		2.95
225.5	4400	21.2	583.28	7.14		3.32	4740	21.0	558.40	7.27		3.17	6350	20.9	542.46	7.43		2.25
297																		
373	6450	20.3	484.82	7.48		3.55	6610	20.3	458.82	7.45		3.49	7460	20.2	459.88	7.54		3.80
521	10510	20.3	360.82	7.47		4.11	9850	20.2	418.88	7.30		3.47	9230	20.2	422.88	7.37		3.13
600																		
297 (basket)	10550	23.5	480.90	7.72		3.46	9280	20.2	481.88	7.65		3.88	6910	20.3	482.82	7.67		3.44

Table A3: Baseline data collected on 6th October 2015

6-Oct-15	Depth (cm)																	
	12						24						36					
Dist. from Inlet (cm)	DO (µg/L)	Temp (°C)	Redox (mV)	pH	Temp (°C)	TOC (mg/L)	DO (µg/L)	Temp (°C)	Redox (mV)	pH	Temp (°C)	TOC (mg/L)	DO (µg/L)	Temp (°C)	Redox (mV)	pH	Temp (°C)	TOC (mg/L)
0	9010	15.1	514.04	7.98	18.7	2.33	9010	15.1	514.04	7.98	18.7	2.33	9010	15.1	514.04	7.98	18.7	2.33
88.5	6620	13.7	473.52	7.29	15.6	3.07	9960	13.5	457.00	7.81	15.0	2.23	10920	13.5	462.06	8.06	14.9	2.11
225.5	6070	14.0	489.96	7.28	16.3	3.14	8180	13.9	484.36	7.56	15.8	2.42	8960	13.8	490.20	7.68	16.0	3.23
297	7680	14.4	502.88	7.42	16.4	1.96	7920	14.2	487.88	7.44	16.4	3.30	10300	14.1	482.88	7.74	16.4	2.34
373	3600	14.7	530.64	7.11	16.7	2.90	6310	14.6	527.48	7.33	16.9	2.38	6830	14.4	517.48	7.39	16.9	2.75
521	4540	15.0	526.08	7.24	17.4	2.62	5050	14.9	522.48	7.29	16.9	2.54	5320	14.8	517.40	7.29	17.0	3.27
600	5330	15.0	535.12	7.18	18.6	4.08	5330	15.0	535.12	7.18	18.6	4.08	5330	15.0	535.12	7.18	18.6	4.08
297 (basket)	2650	14.6	410.20	7.33	16.0	2.90	1360	14.6	356.04	7.45	16.2	3.25	1240	14.5	358.88	7.57	16.4	2.98

Baseline Data for 2016

Table A4: Baseline data collected on 13th April 2016

13-Apr-16	Depth (cm)																	
	12						24						36					
Dist. from Inlet (cm)	DO (µg/L)	Temp (°C)	Redox (mV)	pH	Temp (°C)	TOC (mg/L)	DO (µg/L)	Temp (°C)	Redox (mV)	pH	Temp (°C)	TOC (mg/L)	DO (µg/L)	Temp (°C)	Redox (mV)	pH	Temp (°C)	TOC (mg/L)
0						2.66						2.66						2.66
88.5	325	15.1	56.92	6.30	17.5	3.08	221	15.1	57.92	6.54	17.0	3.11	524	15.2	-14.16	6.56	17.2	2.76
225.5	330	15.0	-10.00	6.78	19.1	4.65	360	14.9	-21.94	6.78	19.2	4.94	485	14.9	-18.94	6.44	19.4	3.97
297	221	13.9	-29.34	6.59	20.1	4.20	233	13.9	-29.34	6.61	20.1	3.92	250	13.8	-38.28	6.58	20.1	4.11
373	211	15.5	-24.40	6.53	19.5	4.85	208	15.5	-21.40	6.51	19.5	4.24	345	15.5	-35.40	6.62	19.5	4.44
521	202	14.9	-14.94	5.98	19.5	5.52	185	14.8	-28.88	6.09	19.4	5.71	199	14.8	-28.88	6.34	19.4	6.12
600	155	17.8	-101.24	6.82	16.6	8.55	155	17.8	-101.24	6.82	16.6	8.55	155	17.8	-101.24	6.82	16.6	8.55
297 (basket)	302	14.1	20.54	6.62	20.2	4.94	260	14.1	21.54	6.51	20.8	4.80	335	14.0	39.60	6.61	20.7	5.36

Table A5: Baseline data collected on 29th April 2016

29-Apr-16	Depth (cm)																	
	12						24						36					
Dist. from Inlet (cm)	DO (µg/L)	Temp (°C)	Redox (mV)	pH	Temp (°C)	TOC (mg/L)	DO (µg/L)	Temp (°C)	Redox (mV)	pH	Temp (°C)	TOC (mg/L)	DO (µg/L)	Temp (°C)	Redox (mV)	pH	Temp (°C)	TOC (mg/L)
0	12448	7.8	437.44	7.61	12.6	3.34	12448	7.8	437.44	7.61	12.6	3.34	12448	7.8	437.44	7.61	12.6	3.34
88.5	470	7.8	26.88	7.45	16.4	3.43	562	7.7	145.60	7.52	15.5	3.78	3880	7.6	320.12	7.26	14.8	4.36
225.5	314	9.4	-6.88	6.59	14.8	4.83	279	9.3	-16.64	6.72	14.4	3.79	689	9.5	-35.60	7.05	17.0	3.62
297	295	8.5	-36.20	6.62	16.5	3.66	226	8.5	-43.92	6.81	13.2	3.84	261	8.5	-44.34	6.72	13.9	3.38
373	343	10.8	5.12	6.83	18.6	2.88	300	10.6	-21.08	7.22	17.6	3.19	262	10.6	-9.58	7.66	14.3	3.27
521	408	9.9	-5.88	6.31	21.4	7.42	423	9.8	-0.88	6.30	20.6	253.80	525	9.8	-0.84	6.40	19.8	265.50
600	70	11.6	-20.32	6.32	15.4	223.70	70	11.6	-20.32	6.32	15.4	223.70	70	11.6	-20.32	6.32	15.4	223.70
297 (basket)	348	10.0	38.48	6.79	16.9	3.84	470	9.7	4.72	7.12	19.1	2.92	689	9.5	25.44	7.41	18.2	3.33

Table A6: Baseline data collected on 11th May 2016

11-May-16	Depth (cm)																	
	12						24						36					
Dist. from Inlet (cm)	DO (µg/L)	Temp (°C)	Redox (mV)	pH	Temp (°C)	TOC (mg/L)	DO (µg/L)	Temp (°C)	Redox (mV)	pH	Temp (°C)	TOC (mg/L)	DO (µg/L)	Temp (°C)	Redox (mV)	pH	Temp (°C)	TOC (mg/L)
0	10572	15.9	374.28	8.08	15.9	8.21	10572	15.9	374.28	8.08	15.9	8.21	10572	15.9	374.28	8.08	15.9	8.21
88.5	267	14.7	-13.36	7.12	16.7	7.01	306	14.7	37.64	7.20	16.7	6.01	360	14.7	85.72	7.21	16.6	6.03
225.5	281	16.3	73.22	6.91	21.3	6.39	333	16.2	75.34	6.99	21.1	6.14	408	16.2	97.70	7.09	20.5	6.27
297	302	16.5	-6.56	7.06	22.6	5.95	363	16.5	-0.50	7.12	22.5	5.17	506	16.4	12.50	7.08	22.5	2.69
373	718	16.5	2.42	6.79	24.3	5.09	715	16.5	-8.52	6.84	24.2	5.10	947	16.5	-13.28	6.91	23.8	5.80
521	222	17.5	-21.64	6.54	24.4	3.25	313	17.5	-12.70	6.64	24.5	3.78	260	17.5	-12.58	6.55	24.3	5.09
600	0	22.7	11.64	6.80	20.6	6.20	0	22.7	11.64	6.80	20.6	6.20	0	22.7	11.64	6.80	20.6	6.20
297 (basket)	382	16.4	34.56	7.15	22.4	5.60	448	16.4	37.80	7.09	22.0	5.98	642	16.3	54.04	6.88	21.6	6.19

Table A7: Baseline data collected on 1st June 2016

1-Jun-16	Depth (cm)																	
	12						24						36					
Dist. from Inlet (cm)	DO (µg/L)	Temp (°C)	Redox (mV)	pH	Temp (°C)	TOC (mg/L)	DO (µg/L)	Temp (°C)	Redox (mV)	pH	Temp (°C)	TOC (mg/L)	DO (µg/L)	Temp (°C)	Redox (mV)	pH	Temp (°C)	TOC (mg/L)
0	9890	18.5	416.28	7.36	18.4	6.49	9890	18.5	416.28	7.36	18.4	6.49	9890	18.5	416.28	7.36	18.4	6.49
88.5	268	18.3	-6.28	6.69	19.1	7.81	378	18.3	73.72	6.79	19.1	5.42	1140	18.3	282.88	7.13	18.9	4.70
225.5	189	18.8	-10.44	6.55	19.3	7.04	213	18.7	-25.36	6.63	19.2	7.33	277	18.7	25.64	6.67	19.2	7.48
297	235	19.1	-34.68	6.58	19.6	5.96	268	19.0	-8.68	6.60	19.6	6.26	392	19.0	-0.68	6.62	19.6	6.67
373	180	19.1	-13.68	6.42	19.6	8.80	227	19.1	-17.68	6.48	19.6	7.50	315	19.1	-7.68	6.56	19.6	7.61
521	150	19.5	-16.60	6.41	19.5	6.36	160	19.5	-13.52	6.44	19.4	6.52	208	19.5	2.40	6.50	19.5	7.87
600	282	19.8	30.72	6.53	19.1	9.22	282	19.8	30.72	6.53	19.1	9.22	282	19.8	30.72	6.53	19.1	9.22
297 (basket)	271	19.0	-47.68	6.58	19.6	6.59	384	19.0	24.32	6.61	19.6	6.21	460	19.0	16.48	6.60	19.4	6.59

Table A8: Baseline data collected on 15th June 2016

15-Jun-16	Depth (cm)																	
	12						24						36					
Dist. from Inlet (cm)	DO (µg/L)	Temp (°C)	Redox (mV)	pH	Temp (°C)	TOC (mg/L)	DO (µg/L)	Temp (°C)	Redox (mV)	pH	Temp (°C)	TOC (mg/L)	DO (µg/L)	Temp (°C)	Redox (mV)	pH	Temp (°C)	TOC (mg/L)
0	9620	18.3	466.28	7.08	18.4	4.91	9620	18.3	466.28	7.08	18.4	4.91	9620	18.3	466.28	7.08	18.4	4.91
88.5	356	17.3	110.28	6.09	18.4	5.12	450	17.3	183.36	6.22	18.3	5.14	3450	17.3	385.36	6.35	18.3	5.11
225.5	239	17.6	71.88	5.95	18.9	6.54	264	17.5	39.96	5.97	18.8	5.16	303	17.5	78.04	5.97	18.7	4.76
297	190	18.1	33.82	5.94	20.3	7.04	211	18.1	65.70	5.90	20.5	6.34	213	18.1	57.00	5.93	20.0	6.64
373	180	18.3	5.22	5.93	21.3	6.44	186	18.3	15.52	5.96	20.8	5.68	205	18.2	29.52	5.94	20.8	6.14
521	126	22.1	13.92	6.09	21.8	8.03	164	20.2	18.62	5.87	22.3	5.75	235	19.4	19.20	5.79	23.0	5.90
600	313	23.5	34.96	6.24	23.4	10.39	313	23.5	34.96	6.24	23.4	10.39	313	23.5	34.96	6.24	23.4	10.39
297 (basket)	209	18.1	56.40	5.94	19.5	7.63	220	18.0	80.56	5.93	19.3	5.68	260	18.0	89.72	5.90	19.1	6.87

AWW Data for 2015

The tables in this section give the data collected at three depths at each internal sampling location up to 7 weeks after the introduction of artificial wastewater into the system. The data from the wetland inlet and outlet for these experiments is given in Chapter 3 (section 3.2.4).

Table A9: Artificial wastewater data collected on 28th October 2015 (week 1)

28-Oct-16	DO (mg/L)	Temp (°C)	Redox (mV)	pH	Temp (°C)	TOC (mg/L)	TN (mg/L)	NH_4^+ (mg/L)
Dist. from Inlet (cm)	**Depth: 12cm**							
88.5	0.220	6.8	86.56	7.19	12.4	44.21	19.42	7.40
225.5	0.311	7.5	262.84	7.26	13.6	42.55	15.99	2.70
297	0.784	8.5	304.92	7.12	15.1	7.11	1.58	0.00
373	0.390	9.7	294.76	7.03	15.3	30.46	9.83	0.90
521	0.279		287.00	7.20	15.0	18.95	5.90	0.40
600	0.720	10.6	339.24	7.17	14.6	19.18	5.93	0.20
297 (basket)	0.290	9.1	295.54	7.33	14.1	22.95	7.53	1.50
Dist. from Inlet (cm)	**Depth: 24cm**							
88.5	0.231	6.7	193.74	7.37	12.1	43.06	20.29	8.0
225.5	0.290	7.2	268.26	7.53	12.9	41.41	17.58	5.7
297	0.259	8.1	283.84	7.20	13.6	31.69	10.87	1.8
373	0.403	9.5	289.84	7.16	15.2	34.17	11.78	2.0
521	0.253	10.2	281.00	7.21	15.0	21.74	6.66	1.1
600	0.720	10.6	339.24	7.17	14.6	19.18	5.93	0.2
297 (basket)	0.328	9.1	297.84	7.41	13.6	8.89	2.43	0.0
Dist. from Inlet (cm)	**Depth: 36cm**							
88.5	0.272	6.7	171.38	7.41	12.7	48.99	21.52	8.4
225.5	0.371	7.1	258.26	7.34	12.9	39.94	17.76	6.3
297	0.368	7.8	260.60	7.41	14.0	54.59	22.80	7.1
373	0.490	9.4	291.24	7.23	14.6	34.88	12.81	2.8
521	0.390	10.0	302.18	7.19	14.7	25.10	7.78	0.7
600	0.720	10.6	339.24	7.17	14.6	19.18	5.93	0.2
297 (basket)	0.433	8.7	265.48	7.44	14.2	12.78	3.56	0.3

Table A10: Artificial wastewater data collected on 4th November 2015 (week 2)

4-Nov-15	DO (mg/L)	Temp (°C)	Redox (mV)	pH	Temp (°C)	TOC (mg/L)	TN (mg/L)	NH_4^+ (mg/L)
Dist. from Inlet (cm)	**Depth: 12cm**							
88.5	0.343	7.5	32.58	7.16	10.7	22.08	10.20	4.20
225.5	0.121	8.1	-2.56	7.21	12.6	17.66	8.65	3.90
297	0.259	8.7	133.78	7.15	13.7	10.00	3.17	0.20
373	0.294	8.5	62.84	7.12	13.6	13.45	5.56	2.30
521	0.211	8.9	171.32	7.15	12.8	11.71	5.56	1.50
600	0.357	9.5	148.96	7.10	16.3	16.49	5.98	1.70
297 (basket)	0.260	9.3	206.02	7.37	13.3	12.97	5.97	2.30
Dist. from Inlet (cm)	**Depth: 24cm**							
88.5	0.366	7.4	70.58	7.24	10.7	24.20	11.80	4.2
225.5	0.177	7.9	-45.98	7.23	13.3	17.03	8.88	4.3
297	0.301	8.5	70.96	7.11	13.4	14.86	5.87	1.8
373	0.315	8.5	110.90	7.20	13.5	10.58	6.06	5.5
521	0.216	8.8	175.26	7.15	12.9	15.32	5.94	2.0
600	0.357	9.5	148.96	7.10	16.3	16.49	5.98	1.7
297 (basket)	0.296	9.1	213.90	7.47	13.5	11.30	4.99	1.3
Dist. from Inlet (cm)	**Depth: 36cm**							
88.5	0.496	7.3	5.82	7.25	10.3	28.43	13.17	5.7
225.5	0.230	7.8	-4.42	7.34	10.7	18.86	9.48	3.6
297	0.448	8.3	-62.82	7.16	14.7	20.93	9.89	4.3
373	0.403	8.4	99.84	7.21	13.6	13.38	6.66	2.5
521	0.255	8.8	188.38	7.13	12.7	14.56	6.01	2.3
600	0.357	9.5	148.96	7.10	16.3	16.49	5.98	1.7
297 (basket)	0.396	9.0	192.20	7.55	13.0	11.50	3.96	0.0

Table A11: Artificial wastewater data collected on 11th November 2015 (week 3)

11-Nov-15	DO (mg/L)	Temp (°C)	Redox (mV)	pH	Temp (°C)	TOC (mg/L)	TN (mg/L)	NH_4^+ (mg/L)
Dist. from Inlet (cm)	**Depth: 12cm**							
88.5	0.222	12.7	-49.0	7.05	13.3	43.67	18.15	11.40
225.5	0.141	12.7	66.0	7.06	13.3	29.07	11.84	6.80
297	0.248	12.8	20.8	7.04	13.6	24.13	9.37	5.00
373	0.329	13.1	44.2	6.88	14.7	23.07	6.90	3.30
521	0.342	13.3	75.36	6.99	15.8	22.76	7.39	3.80
600	0.071	13.4	55.28	7.07	15.9	25.96	7.91	3.70
297 (basket)	0.267	12.8	134.6	7.23	14.0	19.94	6.82	3.80
Dist. from Inlet (cm)	**Depth: 24cm**							
88.5	0.270	12.7	-160.9	7.09	13.1	52.30	26.15	15.0
225.5	0.232	12.7	108.1	7.13	13.2	30.18	13.59	8.7
297	0.283	12.8	42.0	7.19	13.4	27.94	12.82	8.6
373	0.378	13.1	62.4	7.05	14.4	24.55	10.60	6.8
521	0.379	13.3	82.68	7.10	15.4	26.24	10.24	6.2
600	0.071	13.4	55.28	7.07	15.9	25.96	7.91	3.7
297 (basket)	0.336	12.8	119.6	7.29	14.0	17.29	5.95	2.2
Dist. from Inlet (cm)	**Depth: 36cm**							
88.5	0.416	12.6	-112.9	7.16	13.2	60.11	30.34	11.3
225.5	0.223	12.7	58.1	7.12	13.2	40.05	15.14	9.7
297	0.411	12.8	53.0	7.22	13.3	30.10	14.13	9.4
373	0.492	13.0	67.5	7.14	14.2	25.19	11.20	7.6
521	0.471	13.2	69.92	7.16	15.1	27.90	11.84	7.9
600	0.071	13.4	55.28	7.07	15.9	25.96	7.91	3.7
297 (basket)	0.430	12.8	87.7	7.31	13.9	20.14	7.74	4.4

Table A12: Artificial wastewater data collected on 17th November 2015 (week 4)

17-Nov-15	DO (mg/L)	Temp (°C)	Redox (mV)	pH	Temp (°C)	TOC (mg/L)	TN (mg/L)	NH_4^+ (mg/L)
Dist. from Inlet (cm)	**Depth: 12cm**							
88.5	0.278	10.7	0.2	7.34	11.4	14.75	8.60	6.30
225.5	0.182	10.2	5.9	7.25	11.8	14.03	7.74	4.90
297	0.253	10.5	50.6	7.24	12.4	7.00	6.55	3.50
373	0.307	10.7	15.7	7.29	12.2	7.48	8.60	7.30
521	0.293	10.8	67.4	7.26	12.6	11.91	6.29	3.50
600	0.563	10.9	126.1	7.22	13.2	13.65	8.92	6.50
297 (basket)	0.279	10.4	63.7	7.35	12.2	12.21	8.32	6.00
Dist. from Inlet (cm)	**Depth: 24cm**							
88.5	0.338	10.7	12.2	7.41	11.4	16.02	8.78	5.5
225.5	0.257	10.2	21.1	7.30	11.5	13.59	7.52	5.5
297	0.302	10.5	56.7	7.29	12.2	7.04	8.22	4.1
373	0.355	10.7	57.7	7.35	12.2	7.83	8.98	7.6
521	0.362	10.8	55.5	7.23	12.5	16.66	12.83	10.2
600	0.563	10.9	126.1	7.22	13.2	13.65	8.92	6.5
297 (basket)	0.279	10.4	88.9	7.40	11.8	15.11	7.92	4.8
Dist. from Inlet (cm)	**Depth: 36cm**							
88.5	0.400	10.7	31.3	7.43	11.2	17.24	10.60	7.4
225.5	0.374	10.1	34.2	7.34	11.4	11.86	7.41	4.9
297	0.398	10.4	64.8	7.21	12.0	14.96	10.66	8.1
373	0.534	10.7	53.5	7.34	12.5	21.70	18.80	15.3
521	0.437	10.7	62.6	7.30	12.3	23.55	25.10	21.5
600	0.563	10.9	126.1	7.22	13.2	13.65	8.92	6.5
297 (basket)	0.389	10.3	47.9	7.50	11.9	8.62	5.56	3.9

Table A13: Artificial wastewater data collected on 25th November 2015 (week 5)

25-Nov-15	DO (mg/L)	Temp (°C)	Redox (mV)	pH	Temp (°C)	TOC (mg/L)	TN (mg/L)	NH_4^+ (mg/L)
Dist. from Inlet (cm)	**Depth: 12cm**							
88.5	0.388	2.6	-12.6	7.32	5.8	25.55	19.69	14.70
225.5	0.274	2.9	4.4	7.30	5.7	26.92	19.79	16.60
297	0.309	3.2	49.1	7.21	6.1	18.76	7.53	5.20
373	0.753	3.6	82.6	7.23	6.7	21.13	9.24	5.70
521	0.520	3.9	99.6	7.19	5.5	12.56	7.30	5.70
600	0.648	3.9	104.7	7.22	5.4	63.31	19.62	12.20
297 (basket)	0.295	3.5	96.1	7.43	6.1	10.96	7.15	5.10
Dist. from Inlet (cm)	**Depth: 24cm**							
88.5	0.383	2.5	-0.8	7.38	6.0	42.20	21.70	12.8
225.5	0.334	2.8	23.5	7.38	5.6	30.74	22.73	17.5
297	0.316	3.1	41.2	7.29	5.9	29.77	15.07	11.6
373	1.057	3.5	90.9	7.28	6.4	30.99	13.94	9.8
521	0.543	4.0	101.4	7.27	5.8	28.63	11.47	7.5
600	0.648	3.9	104.7	7.22	5.4	63.31	19.62	12.2
297 (basket)	0.310	3.4	97.2	7.48	6.0	12.12	6.38	3.3
Dist. from Inlet (cm)	**Depth: 36cm**							
88.5	0.511	2.4	10.6	7.43	6.7	55.17	27.59	16.0
225.5	0.460	2.7	15.4	7.35	5.8	38.56	33.25	25.2
297	0.468	3.0	49.0	7.30	5.8	38.00	25.86	20.7
373	1.583	3.5	82.8	7.28	6.5	64.11	30.73	21.4
521	0.812	4.0	96.2	7.26	6.0	69.15	22.51	15.2
600	0.648	3.9	104.7	7.22	5.4	63.31	19.62	12.2
297 (basket)	0.380	3.4	99.0	7.56	6.3	27.37	10.07	5.7

Table A14: Artificial wastewater data collected on 2nd December 2015 (week 6)

2-Dec-15	DO (mg/L)	Temp (°C)	Redox (mV)	pH	Temp (°C)	TOC (mg/L)	TN (mg/L)	NH_4^+ (mg/L)
Dist. from Inlet (cm)	**Depth: 12cm**							
88.5	0.325	7.9	-20.2	7.05	10.3	36.83	24.50	21.0
225.5	0.209	7.3	5.2	7.18	9.7	16.37	17.87	14.0
297	0.164	7.4	18.1	7.16	9.9	19.98	13.27	10.0
373	0.169	7.6	13.9	7.11	10.1	19.47	14.99	13.0
521	0.165	7.3	25.1	7.10	9.9	12.44	7.77	6.0
600	0.495	7.5	67.1	7.15	9.9	48.91	20.86	14.0
297 (basket)	0.180	7.3	22.2	7.16	9.8	17.90	10.92	7.0
Dist. from Inlet (cm)	**Depth: 24cm**							
88.5	0.381	7.9	-14.1	7.11	10.2	80.43	45.24	33.0
225.5	0.285	7.3	9.1	7.19	9.9	25.27	20.49	15.0
297	0.171	7.3	10.2	7.24	9.7	36.39	26.28	27.0
373	0.176	7.6	23.0	7.22	10.0	24.10	18.79	15.0
521	0.175	7.2	22.2	7.16	9.8	26.33	14.53	12.0
600	0.495	7.5	67.1	7.15	9.9	48.91	20.86	14.0
297 (basket)	0.165	7.3	31.2	7.21	9.8	18.72	11.03	8.0
Dist. from Inlet (cm)	**Depth: 36cm**							
88.5	0.541	7.8	-24.2	7.03	10.3	217.70	93.32	55.0
225.5	0.536	7.3	-31.4	7.12	10.7	110.00	53.29	39.0
297	0.175	7.3	4.2	7.18	9.7	98.84	43.02	31.0
373	0.232	7.6	-12.1	7.18	10.1	145.00	62.44	41.0
521	0.205	7.2	17.2	7.19	9.8	62.69	31.11	25.0
600	0.495	7.5	67.1	7.15	9.9	48.91	20.86	14.0
297 (basket)	0.182	7.3	-7.8	7.15	9.8	126.60	42.60	24.0

Table A15: Artificial wastewater data collected on 8th December 2015 (week 7)

8-Dec-15	DO (mg/L)	Temp (°C)	Redox (mV)	pH	Temp (°C)	TOC (mg/L)	TN (mg/L)	NH_4^+ (mg/L)
Dist. from Inlet (cm)	**Depth: 12cm**							
88.5	0.281	6.6	-10.9	6.56	13.1	46.98	16.84	12.00
225.5	0.232	6.3	15.7	6.62	15.4	26.72	14.85	12.00
297	0.204	6.4	-0.8	6.55	14.7	40.81	10.80	8.00
373	0.173	7.2	-27.9	6.63	14.9	39.68	15.67	12.00
521	0.139	6.7	5.0	6.72	16.2	71.54	16.66	12.00
600	0.383	6.7	37.0	6.55	16.3	47.18	18.40	15.00
297 (basket)	0.200	6.8	6.5	7.03	12.5	37.96	15.64	15.00
Dist. from Inlet (cm)	**Depth: 24cm**							
88.5	0.368	6.5	10.3	6.77	11.1	60.77	19.01	12.0
225.5	0.269	6.2	12.4	6.65	14.4	40.51	15.68	12.0
297	0.238	6.3	-19.7	6.74	14.5	47.71	17.30	14.0
373	0.219	7.0	-33.2	6.59	15.3	43.14	16.81	13.0
521	0.254	6.5	-5.6	6.94	15.7	43.47	17.67	13.0
600	0.383	6.7	37.0	6.55	16.3	47.18	18.40	15.0
297 (basket)	0.231	6.8	8.0	7.02	13.3	48.77	13.68	12.0
Dist. from Inlet (cm)	**Depth: 36cm**							
88.5	0.541	6.3	-12.5	6.94	10.9	63.84	23.12	15.0
225.5	0.367	6.1	10.5	6.92	14.1	43.45	17.47	16.0
297	0.241	6.2	-45.3	6.77	13.9	54.21	19.64	16.0
373	0.365	6.9	-2.8	6.57	14.6	38.96	17.24	15.0
521	0.318	6.4	-9.4	7.07	15.5	46.03	18.06	15.0
600	0.383	6.7	37.0	6.55	16.3	47.18	18.40	15.0
297 (basket)	0.325	6.8	2.9	7.14	13.5	75.87	14.42	10.0

AWW Data for 2016

The tables in this section give the data collected at three depths at each internal sampling location up to 10 weeks after the introduction of artificial wastewater into the system. The data from the wetland inlet and outlet for these experiments is given in Chapter 3 (section 3.2.4).

Table A16: Artificial wastewater data collected on 1st July 2016 (week 1)

1-Jul-16	DO (mg/L)	Temp (°C)	Redox (mV)	pH	Temp (°C)	TOC (mg/L)	TN (mg/L)	NH_4^+ (mg/L)
Dist. from Inlet (cm)	**Depth: 12cm**							
108	1.010	19.5	-52.52	6.22	26.9	5.88	20.56	1.80
225.5	0.349	20.0	-27.96	6.05	28.7	4.36	17.34	0.00
297	0.352	20.6	-13.36	6.16	29.2	4.88	21.60	0.00
373	0.433	20.8	-45.20	6.41	32.0	4.24	13.48	0.50
527	0.451	23.9	17.76	6.32	30.4	1.97	11.16	0.00
600	0.463	24.7	25.28	6.65	31.2	3.31	14.05	0.00
297 (basket)	0.382	20.6	-0.92	6.46	27.4	3.77	13.47	0.00
Dist. from Inlet (cm)	**Depth: 24cm**							
108	1.500	19.4	-20.36	6.44	26.7	23.82	13.37	6.60
225.5	0.425	19.8	-49.92	6.38	27.4	28.88	4.95	0.00
297	0.422	20.6	-29.76	6.07	29.7	20.06	4.79	0.10
373	0.448	20.7	-43.90	6.26	31.5	13.57	4.30	0.40
527	0.683	23.9	14.92	6.30	31.8	13.20	3.48	0.20
600	0.463	24.7	25.28	6.65	31.2	14.05	3.31	0.00
297 (basket)	0.445	20.6	14.44	6.23	28.2	10.92	4.23	0.10
Dist. from Inlet (cm)	**Depth: 36cm**							
108	2.670	19.3	6.96	6.85	26.3	35.52	19.93	7.90
225.5	0.554	19.7	-50.84	6.55	27.3	25.40	7.34	1.90
297	0.522	20.5	-18.08	6.34	27.6	19.30	5.43	1.30
373	0.583	20.7	-36.90	6.43	31.5	14.28	4.34	0.20
527	0.937	23.8	16.98	6.29	31.7	12.67	3.62	0.00
600	0.463	24.7	25.28	6.65	31.2	14.05	3.31	0.00
297 (basket)	0.646	20.6	24.28	6.28	28.4	13.64	3.58	0.10

Table A17: Artificial wastewater data collected on 7th July 2016 (week 2)

7-Jul-16	DO (mg/L)	Temp (°C)	Redox (mV)	pH	Temp (°C)	TOC (mg/L)	TN (mg/L)	NH_4^+ (mg/L)
Dist. from Inlet (cm)	**Depth: 12cm**							
108	0.864	16.2	-27.24	6.57	20.4	24.98	9.98	6.20
225.5	0.470	16.7	-15.28	6.20	23.8	17.04	4.42	0.00
297	0.449	17.7	-24.56	5.76	28.2	22.33	5.68	0.50
373	0.646	17.8	-56.92	5.48	29.9	15.61	4.92	0.60
527	0.360	18.9	-8.60	5.44	29.5	10.99	3.19	4.70
600	0.540	18.9	41.44	5.50	25.7	14.56	3.59	2.00
297 (basket)	0.466	17.7	1.00	6.45	25.0	16.67	4.52	0.90
Dist. from Inlet (cm)	**Depth: 24cm**							
108	1.101	16.1	-25.54	6.60	20.9	34.37	21.35	13.20
225.5	0.343	16.7	-49.38	6.24	22.3	23.83	4.83	0.20
297	0.565	17.7	-28.84	6.08	27.3	19.83	10.73	3.50
373	0.425	17.8	-58.32	5.63	27.9	17.29	6.07	3.30
527	0.353	18.8	7.20	5.56	28.5	14.60	3.73	0.00
600	0.540	18.9	41.44	5.50	25.7	14.56	3.59	2.00
297 (basket)	0.551	17.6	14.92	6.43	25.1	17.69	4.94	1.20
Dist. from Inlet (cm)	**Depth: 36cm**							
108	1.940	16.1	-36.52	6.79	19.4	37.52	25.72	22.60
225.5	0.447	16.7	-38.92	6.44	23.2	24.97	9.95	5.80
297	0.735	17.7	-42.84	6.28	27.3	19.54	12.00	7.70
373	0.460	17.8	-47.80	5.77	28.5	16.82	5.50	1.80
527	0.324	18.8	3.40	5.57	27.0	14.22	3.79	1.30
600	0.540	18.9	41.44	5.50	25.7	14.56	3.59	2.00
297 (basket)	0.749	17.6	20.94	6.28	20.1	15.79	4.50	2.10

Table A18: Artificial wastewater data collected on 15th July 2016 (week 3)

15-Jul-16	DO (mg/L)	Temp (°C)	Redox (mV)	pH	Temp (°C)	TOC (mg/L)	TN (mg/L)	NH_4^+ (mg/L)
Dist. from Inlet (cm)	**Depth: 12cm**							
108	0.434	16.1	-98.72	6.94	15.9	5.71	13.01	15.30
225.5	0.310	16.4	-45.12	6.61	16.4	5.53	1.32	0.30
297	0.255	16.8	-60.20	6.56	16.5	11.51	2.58	1.60
373	0.351	16.7	-15.44	6.59	16.8	5.88	1.84	0.60
527	0.343	16.9	13.28	6.32	18.4	4.39	1.03	1.00
600	0.518	16.9	7.36	6.30	18.3	5.63	1.43	1.00
297 (basket)	0.459	16.3	-15.08	6.56	17.6	5.82	1.84	0.70
Dist. from Inlet (cm)	**Depth: 24cm**							
108	0.516	16.1	-100.56	6.91	15.7	11.50	15.72	17.5
225.5	0.338	16.3	-81.88	6.68	16.1	10.67	2.25	0.7
297	0.305	16.8	-85.44	6.55	16.8	10.45	6.49	6.9
373	0.429	16.7	-16.44	6.56	16.8	4.94	1.35	0.5
527	0.318	16.8	-9.68	6.52	17.1	5.29	1.50	0.9
600	0.518	16.9	7.36	6.30	18.3	5.63	1.43	1.0
297 (basket)	0.571	17.1	-2.04	6.64	18.8	6.79	1.92	1.0
Dist. from Inlet (cm)	**Depth: 36cm**							
108	0.777	16.1	-88.56	6.98	15.7	10.18	12.65	15.4
225.5	0.382	16.3	-102.96	6.76	16.2	9.13	9.15	8.1
297	0.336	16.8	-70.44	6.56	16.8	13.51	5.82	8.7
373	0.630	16.7	-17.60	6.57	17.0	5.46	1.62	1.5
527	0.346	16.8	-11.76	6.58	17.2	4.89	1.18	0.8
600	0.518	16.9	7.36	6.30	18.3	5.63	1.43	1.0
297 (basket)	0.645	17.1	-1.92	6.71	17.4	3.76	1.52	1.7

Table A19: Artificial wastewater data collected on 21st July 2016 (week 4)

21-Jul-16	DO (mg/L)	Temp (°C)	Redox (mV)	pH	Temp (°C)	TOC (mg/L)	TN (mg/L)	NH_4^+ (mg/L)
Dist. from Inlet (cm)	**Depth: 12cm**							
108	0.427	20.5	-125.96	6.82	21.6	20.82	15.35	8.30
225.5	0.322	20.8	-81.56	6.50	22.6	15.77	3.13	0.00
297	0.563	21.1	-95.28	6.47	23.8	33.18	4.54	0.00
373	0.317	21.2	-36.00	6.25	25.0	11.18	2.03	0.00
527	0.327	22.2	-19.08	6.27	27.6	9.95	1.61	0.00
600	1.073	23.6	4.68	6.24	27.9	16.10	3.17	0.00
297 (basket)	0.466	20.9	-28.74	6.47	22.9	10.87	2.81	0.00
Dist. from Inlet (cm)	**Depth: 24cm**							
108	0.500	20.5	-133.90	7.01	21.5	22.33	21.17	12.8
225.5	0.364	20.8	-111.44	6.67	22.4	12.06	6.82	0.5
297	0.774	21.1	-109.28	6.56	23.8	12.97	11.33	4.7
373	0.327	21.2	-51.82	6.26	24.7	11.82	2.46	0.0
527	0.333	22.1	-25.84	6.30	27.3	10.27	2.18	0.0
600	1.073	23.6	4.68	6.24	27.9	16.10	3.17	0.0
297 (basket)	0.567	20.9	-18.80	6.55	23.0	10.35	3.04	0.0
Dist. from Inlet (cm)	**Depth: 36cm**							
108	0.720	20.5	-124.78	7.04	21.3	21.47	22.84	12.4
225.5	0.396	20.8	-119.26	6.71	22.1	11.24	11.98	5.1
297	1.127	21.1	-100.98	6.56	23.3	10.92	14.24	4.7
373	0.371	21.2	-74.76	6.27	24.6	12.30	4.42	1.2
527	0.367	22.1	-38.20	6.31	26.5	12.37	2.49	0.0
600	1.073	23.6	4.68	6.24	27.9	16.10	3.17	0.0
297 (basket)	0.781	20.9	-30.80	6.59	23.0	11.16	3.95	0.0

Table A20: Artificial wastewater data collected on 29th July 2016 (week 5)

29-Jul-16	DO (mg/L)	Temp (°C)	Redox (mV)	pH	Temp (°C)	TOC (mg/L)	TN (mg/L)	NH_4^+ (mg/L)
Dist. from Inlet (cm)	**Depth: 12cm**							
108	0.532	26.1	-62.44	6.81	26.8	11.82	3.53	0.50
225.5	0.361	28.6	-75.48	7.11	28.1	18.62	3.02	0.00
297	0.321	27.3	-155.48	6.81	28.1	15.63	1.55	0.00
373	0.409	30.4	-87.18	6.31	30.3	25.69	1.74	0.00
527	0.309	29.1	-37.36	6.91	30.6	17.27	1.94	0.00
600	0.690	31.6	18.48	6.80	29.4	61.55	9.53	0.00
297 (basket)	0.422	31.1	-27.36	6.71	29.2	15.96	1.58	0.00
Dist. from Inlet (cm)	**Depth: 24cm**							
108	0.492	27.1	-53.76	7.12	27.2	9.68	4.36	1.9
225.5	0.482	29.2	-87.12	6.86	30.2	21.49	4.72	0.5
297	0.347	29.1	-142.68	6.28	29.6	13.53	1.54	0.0
373	0.426	28.1	-89.68	6.66	29.6	29.50	1.72	0.0
527	0.312	30.1	-42.12	6.79	30.2	10.44	1.56	0.0
600	0.690	31.6	18.48	6.80	29.4	61.55	9.53	0.0
297 (basket)	0.421	28.1	-47.18	6.57	30.3	18.61	2.97	0.0
Dist. from Inlet (cm)	**Depth: 36cm**							
108	0.473	27.2	-59.84	7.02	27.3	12.86	6.90	2.4
225.5	0.390	30.0	-89.06	6.83	30.1	24.92	4.83	1.4
297	0.329	30.6	-118.48	6.39	28.1	15.66	1.42	0.0
373	0.400	28.6	-77.12	6.68	28.9	39.34	3.02	3.1
527	0.322	30.2	-44.48	6.81	30.8	12.09	1.61	0.0
600	0.690	31.6	18.48	6.80	29.4	61.55	9.53	0.0
297 (basket)	0.433	27.2	-78.72	6.67	31.2	23.48	5.08	0.9

Table A21: Artificial wastewater data collected on 4th August 2016 (week 6)

4-Aug-16	DO (mg/L)	Temp (°C)	Redox (mV)	pH	Temp (°C)	TOC (mg/L)	TN (mg/L)	NH_4^+ (mg/L)
Dist. from Inlet (cm)	**Depth: 12cm**							
108	0.620	26.0	-48.80	6.26	26.0	29.42	3.47	
225.5	0.595	26.3	-91.08	6.32	27.6	17.55	1.35	
297	0.596	26.1	-37.52	6.36	26.9	4.89	1.03	
373	0.452	27.4	-16.00	6.44	30.0	5.65	1.35	
527	0.431	27.2	-10.84	6.34	27.3	11.15	1.24	
600	0.982	27.1	57.94	6.32	30.1	38.81	5.41	
297 (basket)	0.528	26.8	-63.44	6.36	26.8	9.63	1.60	
Dist. from Inlet (cm)	**Depth: 24cm**							
108	0.592	26.0	-63.96	6.24	26.2	29.08	3.38	
225.5	0.692	26.3	-77.84	6.27	27.3	20.21	1.96	
297	0.629	26.2	-76.04	6.32	26.3	6.18	1.16	
373	0.491	27.4	-18.48	6.45	30.8	6.82	1.38	
527	0.460	27.2	-15.06	6.38	30.1	8.62	1.36	
600	0.982	27.1	57.94	6.32	30.1	38.81	5.41	
297 (basket)	0.532	26.8	-75.52	6.31	26.9	13.27	2.19	
Dist. from Inlet (cm)	**Depth: 36cm**							
108	0.587	26.0	-67.76	6.28	27.2	37.48	4.98	
225.5	0.780	26.1	-61.16	6.38	27.7	23.06	3.31	
297	0.686	26.2	-70.48	6.27	25.6	8.58	1.35	
373	0.339	27.4	-7.60	6.61	27.0	11.76	2.05	
527	0.423	27.2	-7.12	6.31	30.2	8.15	1.42	
600	0.982	27.1	57.94	6.32	30.1	38.81	5.41	
297 (basket)	0.614	26.8	-83.52	6.38	26.9	20.81	2.63	

Table A22: Artificial wastewater data collected on 11th August 2016 (week 7)

11-Aug-16	DO (mg/L)	Temp (°C)	Redox (mV)	pH	Temp (°C)	TOC (mg/L)	TN (mg/L)	NH_4^+ (mg/L)
Dist. from Inlet (cm)	**Depth: 12cm**							
108	0.507	14.6	-98.20	6.40	19.0	19.30	26.93	22.50
225.5	0.416	15.2	-48.00	5.89	20.0	13.20	3.84	1.10
297	0.397	15.7	-8.52	5.56	19.4	12.24	1.62	0.00
373	0.377	16.7	-27.20	5.45	26.5	10.92	1.69	0.00
527	0.285	16.6	3.56	5.55	22.4	10.37	1.62	0.00
600	0.481	19.9	-14.18	6.08	20.3	23.52	3.02	0.00
297 (basket)	0.430	16.0	-33.96	5.76	18.7	11.26	4.17	1.90
Dist. from Inlet (cm)	**Depth: 24cm**							
108	0.592	14.6	-115.16	6.59	17.7	10.02	18.06	16.0
225.5	0.466	15.7	-84.06	5.98	20.1	20.72	17.11	14.7
297	0.479	15.6	-69.00	5.56	20.0	21.28	3.91	1.4
373	0.442	16.6	-39.44	5.48	26.8	8.76	1.56	0.0
527	0.670	16.5	-34.74	5.59	22.9	14.15	1.89	0.0
600	0.481	19.9	-14.18	6.08	20.3	23.52	3.02	0.0
297 (basket)	0.511	16.0	-23.04	5.76	18.8	11.69	3.69	0.5
Dist. from Inlet (cm)	**Depth: 36cm**							
108	0.813	14.5	-111.36	6.73	16.7	25.12	26.09	23.1
225.5	0.469	14.9	-93.76	6.04	19.7	18.55	17.09	16.8
297	0.766	16.0	-81.16	5.69	23.6	26.12	17.00	14.0
373	0.530	16.6	-63.80	5.52	26.0	10.03	7.24	8.3
527	1.046	16.5	-44.74	5.52	22.9	30.29	7.11	4.3
600	0.481	19.9	-14.18	6.08	20.3	23.52	3.02	0.0
297 (basket)	0.785	15.9	-7.76	5.83	19.7	10.69	3.78	1.5

Table A23: Artificial wastewater data collected on 18th August 2016 (week 8)

18-Aug-16	DO (mg/L)	Temp (°C)	Redox (mV)	pH	Temp (°C)	TOC (mg/L)	TN (mg/L)	NH_4^+ (mg/L)
Dist. from Inlet (cm)	**Depth: 12cm**							
108	0.449	15.4	-85.86	6.22	23.1	29.63	34.47	20.30
225.5	0.391	15.7	-71.30	5.86	30.5	10.52	2.25	0.00
297	0.485	16.7	-80.94	6.02	34.9	12.93	2.29	0.10
373	0.458	17.7	-35.46	5.81	34.1	7.15	1.37	0.00
527	0.425	18.5	-17.16	6.06	33.6	9.25	1.47	0.00
600	0.658	22.2	-2.82	6.98	34.7	17.28	2.49	0.00
297 (basket)	0.552	16.4	-81.16	5.99	33.6	9.59	2.32	0.00
Dist. from Inlet (cm)	**Depth: 24cm**							
108	0.473	15.3	-133.92	6.66	19.9	11.05	24.73	20.5
225.5	0.444	15.7	-101.56	5.91	28.2	23.32	10.63	5.0
297	0.596	16.6	-99.64	6.12	34.4	16.99	12.08	7.9
373	0.548	17.6	-53.76	5.83	34.6	7.66	1.39	0.0
527	0.473	18.4	-45.40	5.99	34.0	9.37	1.63	0.0
600	0.658	22.2	-2.82	6.98	34.7	17.28	2.49	0.0
297 (basket)	0.647	16.4	-42.14	6.02	31.9	11.44	3.12	0.0
Dist. from Inlet (cm)	**Depth: 36cm**							
108	0.879	15.4	-127.96	6.90	18.7	12.76	8.71	4.6
225.5	0.522	15.6	-86.92	6.03	27.4	29.61	17.82	11.2
297	0.919	16.4	-95.16	6.26	33.6	43.44	17.81	13.8
373	0.778	17.5	-87.94	5.89	34.9	37.14	4.83	1.1
527	0.799	18.2	-31.58	6.05	34.3	10.54	2.03	0.0
600	0.658	22.2	-2.82	6.98	34.7	17.28	2.49	0.0
297 (basket)	0.829	15.8	-8.02	6.06	31.7	9.38	2.69	0.0

Table A24: Artificial wastewater data collected on 25th August 2016 (week 9)

25-Aug-16	DO (mg/L)	Temp (°C)	Redox (mV)	pH	Temp (°C)	TOC (mg/L)	TN (mg/L)	NH_4^+ (mg/L)
Dist. from Inlet (cm)	**Depth: 12cm**							
108	0.449	18.9	-110.04	6.22	26.3	18.84	9.50	5.60
225.5	0.391	19.7	-41.28	5.42	33.8	3.94	1.05	0.00
297	0.485	21.4	-64.80	5.64	38.5	5.67	0.7356	0.00
373	0.458	21.2	-25.32	5.94	40.4	6.44	0.7424	0.00
527	0.425	22.2	-19.84	5.46	42.3	10.62	0.9675	0.00
600	0.658	22.3	-74.42	6.02	30.7	6.32	1.80	0.10
297 (basket)	0.552	21.2	0.44	5.75	35.7	7.79	1.81	0.00
Dist. from Inlet (cm)	**Depth: 24cm**							
108	0.893	18.9	-128.46	6.73	24.1	24.02	21.97	17.6
225.5	0.710	19.6	-63.20	5.82	32.0	5.98	1.17	0.0
297	0.761	21.4	-73.40	5.43	38.0	3.62	1.14	0.0
373	0.686	21.2	-55.68	5.66	39.6	6.23	0.8010	0.0
527	0.598	22.2	-44.36	5.51	41.7	8.29	0.9111	0.0
600	0.056	22.3	-74.42	6.02	30.7	6.32	1.80	0.1
297 (basket)	0.310	21.2	-108.44	6.00	32.4	4.72	1.33	0.0
Dist. from Inlet (cm)	**Depth: 36cm**							
108	1.531	18.9	-122.32	6.95	22.2	24.18	28.62	22.6
225.5	0.848	19.6	-96.30	6.01	30.5	13.75	3.75	1.7
297	0.957	21.3	-98.00	5.86	37.5	6.59	6.55	4.9
373	1.027	21.1	-52.16	5.36	40.2	5.38	1.17	0.0
527	0.735	22.1	-27.48	6.05	40.6	7.25	0.8736	0.0
600	0.056	22.3	-74.42	6.02	30.7	6.32	1.80	0.1
297 (basket)	3.026	21.1	-8.16	5.52	35.2	7.28	1.37	0.0

Table A25: Artificial wastewater data collected on 1st September 2016 (week 10)

1-Sep-16	DO (mg/L)	Temp (°C)	Redox (mV)	pH	Temp (°C)	TOC (mg/L)	TN (mg/L)	NH_4^+ (mg/L)
Dist. from Inlet (cm)	**Depth: 12cm**							
108	0.501	18.2	-101.16	6.46	23.6	17.55	6.54	5.90
225.5	0.654	17.5	-85.68	6.57	22.8	17.27	5.82	0.00
297	0.624	18.8	-65.58	5.99	24.3	20.37	1.89	0.00
373	0.468	18.6	-48.64	5.84	28.3	14.95	1.65	0.00
527	0.438	19.6	-30.08	5.77	31.8	12.72	1.32	0.00
600	0.082	19.6	-71.24	6.34	27.8	10.99	1.23	0.00
297 (basket)	1.171	17.6	-65.64	6.12	25.8	14.63	6.20	4.30
Dist. from Inlet (cm)	**Depth: 24cm**							
108	0.618	18.2	-111.28	6.07	23.8	16.39	7.61	4.9
225.5	0.503	17.4	-118.80	6.50	23.0	10.94	9.80	8.6
297	0.640	18.7	-109.16	5.93	25.2	24.21	8.46	6.6
373	0.638	18.6	-78.60	5.99	27.0	15.90	1.76	0.0
527	0.519	19.5	-75.08	5.84	31.8	14.81	1.46	0.0
600	0.082	19.6	-71.24	6.34	27.8	10.99	1.23	0.0
297 (basket)	0.780	17.5	-120.04	6.73	26.3	11.61	5.88	5.1
Dist. from Inlet (cm)	**Depth: 36cm**							
108	1.030	17.8	-108.52	6.12	24.2	14.17	10.00	8.6
225.5	0.820	17.4	-107.28	6.56	23.8	9.94	11.57	10.7
297	1.150	18.7	-97.16	6.78	25.2	24.13	8.66	6.0
373	1.040	18.6	-97.00	6.13	25.0	10.26	6.07	0.0
527	0.533	19.4	-62.12	5.88	30.2	9.61	1.49	0.0
600	0.082	19.6	-71.24	6.34	27.8	10.99	1.23	0.0
297 (basket)	0.928	17.5	-90.04	6.69	23.4	12.88	6.47	3.6

Calculation of the contaminant loading for the 2016 AWW experiments

The data used to support the calculation of the inlet and outlet contaminant loading is shown below. The AWW was first introduced into the system on 23rd June 2016.

Table A26: Average weekly ambient temperatures, bed temperatures, inlet and outlet dissolved oxygen concentrations and inlet and outlet redox potentials during the 2016 artificial wastewater experiments

	Date (2016)	Avg. temp (°C)	Bed temp (°C)	Sat. O_2 (mg/L)	DO inlet (mg/L)	DO outlet (mg/L)	Redox inlet (mV)	Redox outlet (mV)
week 1	1-Jul	29.4	21.7	8.83	8.560	0.463	155.3	25.28
week 2	7-Jul	26.1	18.0	9.50	8.938	0.540	95.9	41.44
week 3	15-Jul	17.1	16.8	9.74	9.220	0.518	187.7	7.36
week 4	21-Jul	24.5	21.4	8.88	8.290	1.073	81.5	4.68
week 5	29-Jul	28.9	26.2	8.13	9.001	0.690	94.1	18.48
mean					*8.802*			
std dev.					*0.372*			
week 6	4-Aug	27.8	26.0	8.16	8.530	0.982	113.3	57.94
week 7	11-Aug	20.9	16.8	9.74	8.770	0.481	40.7	-14.18
week 8	18-Aug	32.1	17.9	9.52	9.100	0.658	78.0	-2.82
week 9	25-Aug	35.4	21.1	8.92	10.450	0.056	157.7	-74.42
week 10	1-Sep	26.3	20.9	8.96	7.730	0.082	87.9	-71.24
mean					*8.916*			
std dev.					*0.995*			

Tables A28 and A29 show the calculations of the hydraulic loading rates. Table A27 shows the chemical species labelling and the average baseline data for comparison.

Table A27: Average baseline TOC (A) and TN (B) loading during the 2016 period of observation

Chemical Species	Symbol	Avg. baseline concentration (mg/L)		
		Apr '16	May '16	June '16
TOC	A	4.24	5.42	6.46
TN	B	3.58	2.16	1.14

Table A28: Average weekly inlet and outlet wetland flow rates with the measured inlet and outlet concentrations of TOC and the corresponding hydraulic loads for the 2016 experimental period

	Date (2016)	[a]Q_{in} (L/h)	Q_{in} (L/d)	τ (d)	[b]Q_{out} (L/h)	Q_{out} (L/d)	C_{A0} (mg/L)	m_{A0} (g/d)	HLR_{A0} ($g/m^2.d$)	HLR_{A0} ($g/m^3.d$)	C_A (mg/L)	m_A (g/d)	HLR_A ($g/m^2.d$)	HLR_A ($g/m^3.d$)
week 1	1-Jul	6.35	152.5	7.58	5.90	141.7	82.99	12.65	1.84	10.95	14.05	1.99	0.290	1.722
week 2	7-Jul	5.99	143.7	8.05	5.17	124.2	82.62	11.87	1.73	10.27	14.56	1.81	0.263	1.564
week 3	15-Jul	6.07	145.6	7.94	5.17	124.2	66.21	9.64	1.40	8.34	5.63	0.70	0.102	0.605
week 4	21-Jul	6.63	159.2	7.26	5.72	137.2	92.43	14.72	2.14	12.73	16.10	2.21	0.322	1.910
week 5	29-Jul	5.75	138.0	8.38	4.74	113.8	68.60	9.46	1.38	8.19	16.16	1.84	0.268	1.590
mean		*6.2*	*147.8*		*5.3*	*128.2*	*78.57*	*11.79*	*1.72*	*10.1*				
std dev.		*0.3*	*7.4*		*0.4*	*10.0*	*10.96*	*8.39*	*1.22*	*1.7*				
week 6	4-Aug	3.70	88.7	13.0	2.60	62.5	352.0	31.22	4.54	27.00	38.81	2.42	0.353	2.096
week 7	11-Aug	4.63	111.1	10.4	4.60	110.3	97.01	10.78	1.57	9.32	23.52	2.59	0.378	2.244
week 8	18-Aug	3.38	81.1	14.3	4.13	99.1	69.45	5.63	0.82	4.87	17.28	1.71	0.249	1.481
week 9	25-Aug	11.69	280.6	4.12	13.0	312.8	4.31	1.21	0.18	1.05	6.32	1.98	0.288	1.710
week 10	1-Sep	6.56	157.5	7.34	3.72	89.4	93.32	14.70	2.14	12.72	10.99	0.98	0.143	0.849

[a]average weekly inlet flowrate

[b]average weekly outlet flowrate

Table A29: Average weekly inlet and outlet wetland flow rates with the measured inlet and outlet concentrations of TN and the corresponding hydraulic loads for the 2016 experimental period

	Date (2016)	[a]Q_{in} (L/h)	Q_{in} (L/d)	τ (d)	[b]Qo_{ut} (L/h)	Q_{out} (L/d)	C_{B0} (mg/L)	m_{B0} (g/d)	HLR_{B0} ($g/m^2.d$)	HLR_{B0} ($g/m^3.d$)	C_B (mg/L)	m_B (g/d)	HLR_B ($g/m^2.d$)	HLR_B ($g/m^3.d$)
week 1	1-Jul	6.35	152.5	7.58	5.90	141.7	36.04	5.50	0.80	4.75	3.31	0.469	0.0683	0.406
week 2	7-Jul	5.99	143.7	8.05	5.17	124.2	35.65	5.12	0.75	4.43	3.59	0.446	0.0649	0.386
week 3	15-Jul	6.07	145.6	7.94	5.17	124.2	31.18	4.54	0.66	3.93	1.43	0.178	0.0258	0.154
week 4	21-Jul	6.63	159.2	7.26	5.72	137.2	42.72	6.80	0.99	5.88	3.17	0.435	0.0633	0.376
week 5	29-Jul	5.75	138.0	8.38	4.74	113.8	30.12	4.16	0.60	3.59	9.53	1.084	0.1578	0.938
mean		*6.2*	*147.8*		*5.3*	*128.2*	*35.1*	*5.31*	*0.77*	*4.5*				
std dev.		*0.3*	*7.4*		*0.4*	*10.0*	*5.0*	*3.73*	*0.54*	*0.8*				
week 6	4-Aug	3.70	88.7	13.0	2.60	62.5	156.10	13.85	2.02	11.97	5.41	0.338	0.0492	0.292
week 7	11-Aug	4.63	111.1	10.4	4.60	110.3	44.63	4.96	0.72	4.29	3.02	0.333	0.0485	0.288
week 8	18-Aug	3.38	81.1	14.3	4.13	99.1	28.29	2.29	0.33	1.98	2.49	0.247	0.0359	0.213
week 9	25-Aug	11.69	280.6	4.12	13.0	312.8	1.54	0.43	0.06	0.37	1.80	0.563	0.0820	0.487
week 10	1-Sep	6.56	157.5	7.34	3.72	89.4	38.45	6.06	0.88	5.24	1.23	0.110	0.0160	0.095

[a]average weekly inlet flowrate

[b]average weekly outlet flowrate

Internal contaminant degradation and transformation

The TOC, TN, DO and redox profiles at depths 1 (12 cm) and 3 (36 cm) for the 2016 experimental period are presented in Figures A1 and A2 below. The plots for depth 2 are presented in Chapter 7 (Figure 7-8 and Figure 7-9).

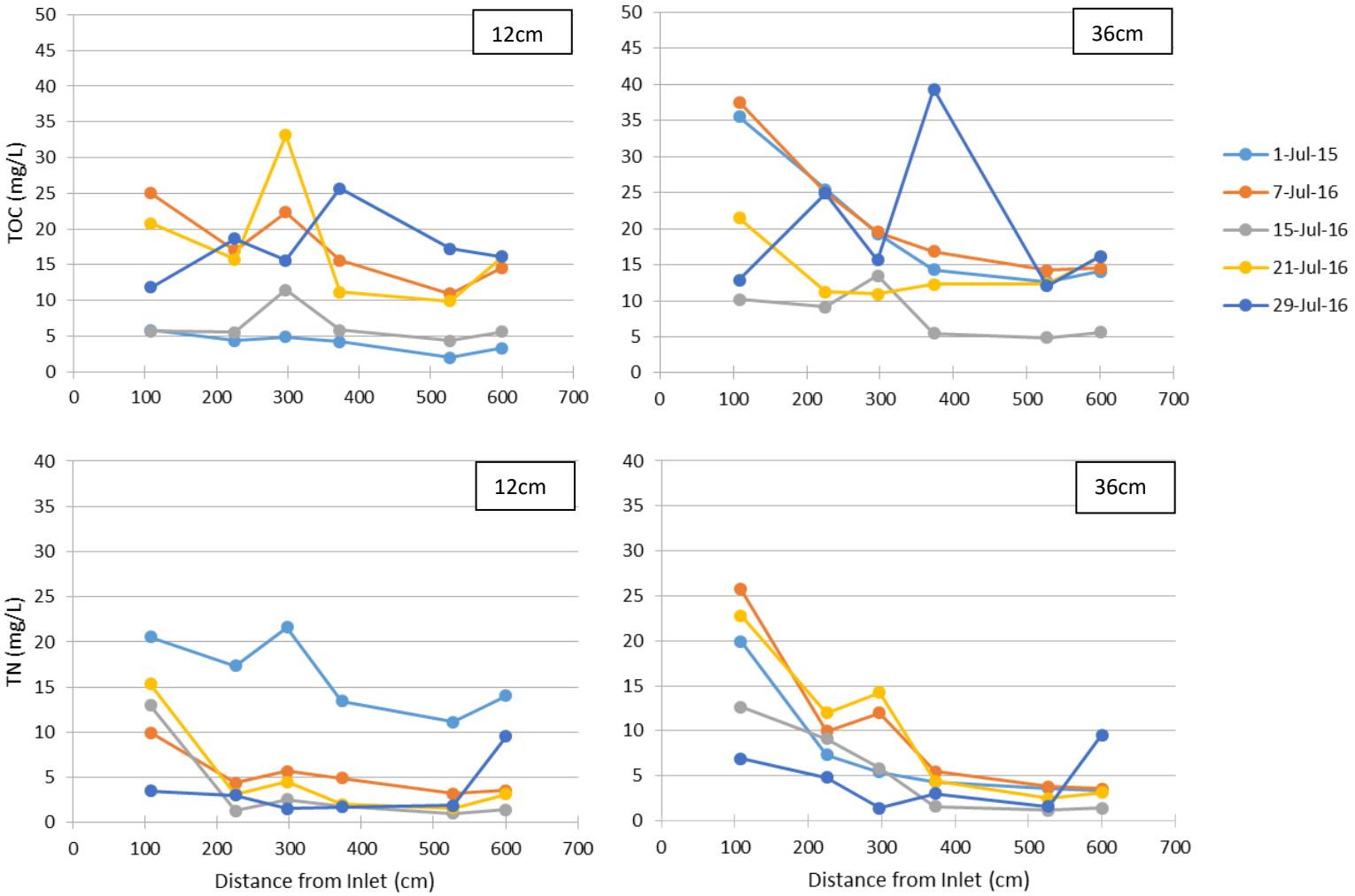


Figure A1: TOC and TN profiles at 12 cm and 36 cm below the surface during the 2016 experimental period

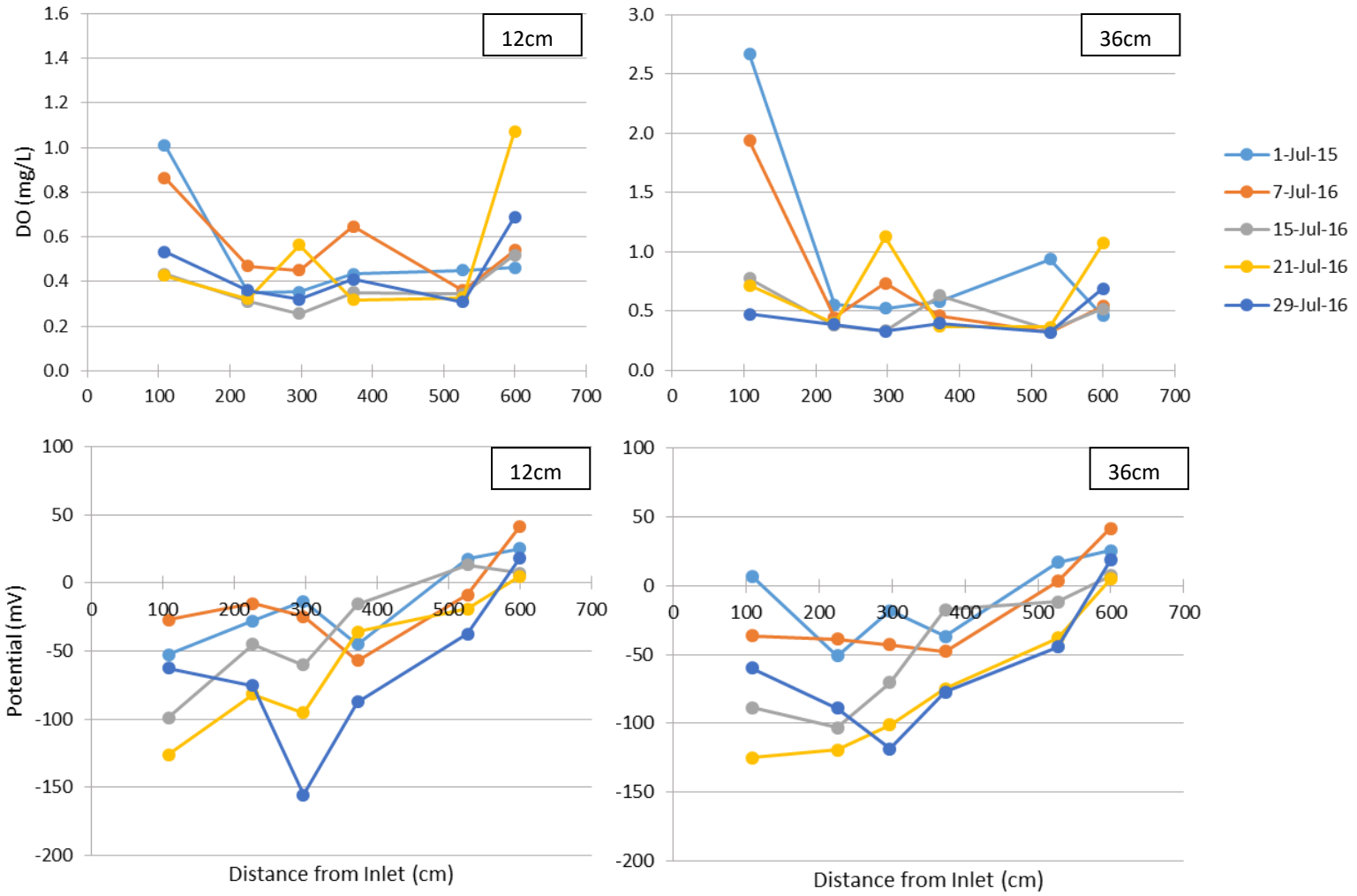


Figure A2: DO and redox potential profiles at 12 cm and 36 cm below the surface during the 2016 experimental period

Internal contaminant loading profile

This section gives the data and calculations supporting the development of the concentration density profile in Chapter 7. The linear correlation between the volumetric flow rate and distance from the wetland inlet is illustrated in Figure A3. The measured vegetation density for the period April to November 2016 is summarized in Table A30 and is the basis of Figure E6 (Appendix E). Finally, vegetation density is plotted against the distance from the wetland inlet in Figure A4 and the best fit trend line determined by trial and error.

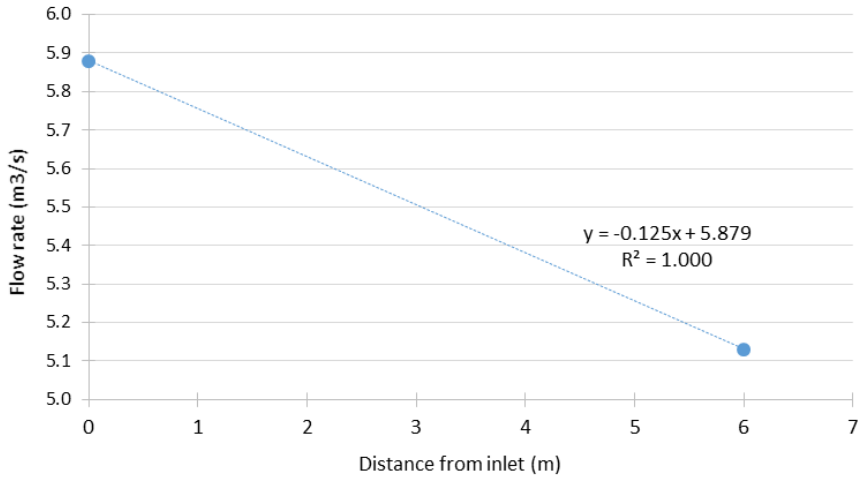


Figure A3: The linear correlation (by assumption) between the volumetric flow rate and the distance from the wetland inlet

Table A30: Measured vegetation density from April to November 2016

Zone	Zone Designation (cm)	Vegetation density, ρ_{veg} (stems/m^2)							
		April	May	June	July	August	September	October	November
1	0 to 108	84	118	314	325	361	408	438	460
2	108 to 225.5	79	133	313	322	354	398	425	445
3	225.5 to 297	41	97	284	296	330	375	404	425
4	297 to 373	75	83	245	255	285	324	349	368
5	373 to 527	66	79	176	183	202	225	240	251
6	527 to 600	50	65	124	130	143	156	166	173

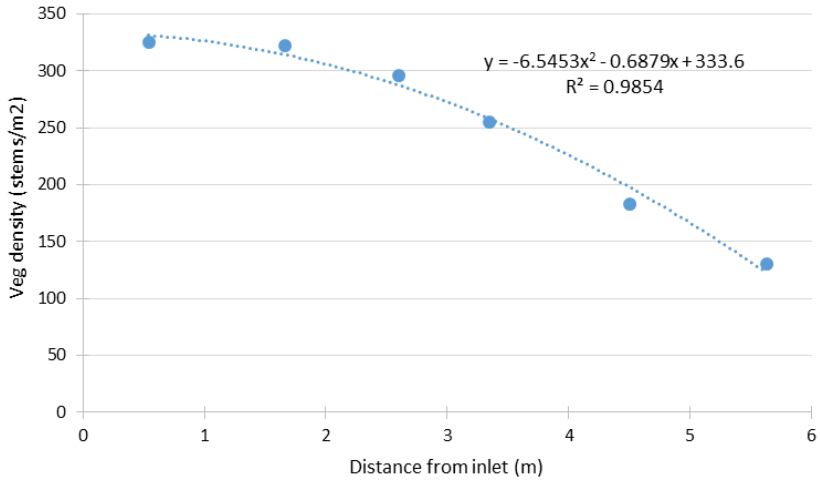


Figure A4: Vegetation density versus distance from the wetland inlet with the best fit trend line (polynomial, degree 2)

Appendix B: Matlab Code for Flow Test Data Analysis

This section presents the Matlab code written for the analysis of the tracer flow test data. The code was written with the help of Dr Marie Kurz, formerly a scientist in the Department of Hydrogeology at the Helmholtz UFZ in Leipzig, Germany. The code was written as a series of master execution files; each calling on various function .m files. The running of the code is first, briefly, described and then provided below in fully annotated format.

The field data was generated by the field fluorometers, which detected the Uranine and recorded a milli-volt (mV) signal which was related to the concentration of Uranine in solution. At the completion of each flow test, the .mV file was downloaded from the instrument using a specialised software (GGUN Fluorometer) and then run through the Matlab code, which is described in Table B1. The .mV files are provided on the CD due to data volume. The inputs and outputs of the MasterCals_SS.m and MasterCalcs_NSS.m execution codes are presented in the flow test data in Appendix C.

Table B1: Description of the Matlab master execution files and the related function .m files

Matlab execution file name	**Function .m file name (required by execution file)**	**Description**
MasterDataProc.m		Processes the raw experimental data.
	read.m	The input is the .mV data file from the fluorometer (provided on the CD).
	cal.m	Data calibration script (converts mV data from fluorometer to corresponding concentration of Uranine).
	extract.m	Extracts the data from the start of the tracer flow test to the end of the tracer flow test.
	myfilter.m	To smooth experimental data (remove excessive noise).
MasterTailFit.m		Performs a best approximation exponential curve fit to the tail of the data (only in the isolated cases where the flow test was terminated early). The input is the converted, calibrated and extracted data from MasterDataProc.m.
	append.m	Mathematically computes the RTD tail using the raw experimental data and an exponential trendline.
	myfilter.m	To smooth experimental data (remove excessive noise).
MasterCalcs_SS		Performs the hydraulic calculations **assuming** a steady-state volumetric flow rate (i.e. using the average of the volumetric flow rates recorded by the inlet and outlet

		pump data loggers). The input is the smoothed concentration/time data from MasterDataProc.m or MasterTailFit.m.
	volume.m	Calculates the volume of the wetland, taking into account the gravel porosity.
	Inflow.m	Data collected from the inlet pump.
	Outflow.m	Data collected from the outflow pump.
MasterCals_NSS		Performs the hydraulic calculations **using the modified method for non-steady flow** (i.e. using the complete volumetric flow rate vectors recorded by the inlet and outlet pump data loggers). The input is the smoothed concentration/time data from MasterDataProc.m or MasterTailFit.m.
	Inflow.m	Data collected from the inlet pump.
	Outflow.m	Data collected from the outflow pump.

```
% MasterDataProc.m
% Pre-processing of experimental data
close all
clear all

% => USER TO SPECIFY THE FOLLOWING:
     path(path,'C:/users/aylward/Desktop/MATLAB/Final2017')        % working directory
     flu_file = '7iii_f025.mv';                                    % experimental data file
     f = 625;                                                      % number of fluorometer
     c_cal_Uranine = 70.0;                                         % Uranine calibration conc. (ppb)
     P1I = datenum([2016 08 22 12 35 00]);                         % Time of injection (YYYY MM DD hh mm ss)
     P1F = datenum([2016 09 15 12 32 00]);                         % End Time of flow test (YYYY MM DD hh mm ss)

     %-------------------------------------------------------------------------------------------------------------
     % User instructions for this sub-section:
     % 1. Set P1S_ind = 0 (see next OPTIONAL section below)
     % 2. Run script to _____BREAK 1_____
     % 3. In Figure (1), determine calibration windows:
% =>
            ind_ura = 104:105;                                     % Uranine calibration window (by data index)
            ind_blank = 27220:32820;                               % Baseline calibration window (by data index)
     % 4. Comment out section (2.1)
     % 5. Re-run script to _____BREAK 2_____ - check figure (2)
     %-------------------------------------------------------------------------------------------------------------

     %=============================================================================================================
     % THIS SECTION IS OPTIONAL
     %  Determine 'data start time' (P1S) by visual inspection
     %    To eliminate false +ve conc. before the peak
     %    (set all conc. prior to first attainment of 0ppb to zero)

     % User instructions for this section:
     %  1. Run script to _____BREAK 2_____
     %  2. In Figure (2), find the first zero conc. after calibration but before the peak
     %  3. Export cursor data to workspace and record 'DataIndex':
% =>          DataIndex =
            P1S_ind = 27111;
     %  4. Comment out section (2.2)
```

```
%  5. Re-run script to _____BREAK 3_____ - check figure (3)

%=========================================================================================================

% NOW PROCEED TO RUNNING REMAINING SECTIONS AFTER _____BREAK 3_____
% It is recommended that each new section be run individually and in numerical order
% Follow instructions as they appear

%% (1) Import data into MATLAB
       [DateNum, Uranine_mv, Temperature] = read(flu_file);

%% (2) Calibrate data & convert mV to conc. (ppb)

% %      (2.1) Plot Uranine mV data to determine calibration windows
%              figure(21)
%              plot(Uranine_mv, 'g');
%              xlabel('Data index')
%              ylabel('Uranine mV')
%              title('Raw data for determination of calibration window')

%_____________________________________BREAK 1_____________________________________________________

       [C1] = cal(Uranine_mv, Temperature, c_cal_Uranine, ind_ura, ind_blank);

% %      (2.2) Plot calibrated Uranine conc. data
%              figure(22)
%              plot(DateNum, C1(:,1), 'g');
%              datetick('x', 'dd/mm-HH', 'keepticks', 'keeplimits');
%              xlabel('Date & time (dd/mm-hr)');
%              ylabel('[Uranine] (ppb)');
%              title('Calibrated Uranine conc.');

%_____________________________________BREAK 2_____________________________________________________

%% (3) Extract BTC from full time series (starting @ time of injection)
       [E1] = extract(DateNum, C1, P1I, P1S_ind, P1F);
% =>
       save('7iii_BTC_E1', 'E1')
```

```
%     (3.1) Plot Uranine BTC (i.e Uranine conc. (ppb) vs time (hrs since inj))
              figure(31)
              plot(E1(:,3), E1(:,2)); hold on
              xlabel('Time since injection (hr)');
              ylabel('[Uranine] (ppb)');
              title('Uranine BTC')

%_____________________________________BREAK 3_____________________________________________

%% ============================================================================================
%% Exponential Tail Fit
%  If a tail fit is required:
%     -> Run MasterTailFit.m using E1 matrix now
%     -> MasterDataProc.m can be closed because the SG Filter will run in MasterTailFit.m
%  If a tail fit is not required:
%     -> continue to section (4) below
%% ============================================================================================

%% (4) Applies the Savitsky-Golay (SG) filter to smooth the extracted data
       % User instructions for this section:
       % 1. Comment out section (3.1)
       % 2. Update figure title and figure name
       % 3. Run script to end of section (4)

       [F1] = myfilter(E1);
% =>
       save('7ii_BTC_F1', 'F1')

%      (4.1) Plot Uranine BTC (Uranine conc. (ppb) vs time (hrs since inj)
              figure(41)
              plot(E1(:,3), E1(:,2), 'g.'); hold on
              plot(F1(:,3), F1(:,2), 'm-', 'LineWidth', 1.25); hold off
              legend('Raw data', 'Filtered data (SG deg5)', 'Location', 'northeast');
              xlabel('Time since injection (hr)');
              ylabel('[Uranine] (ppb)')
% =>           Specify domain and range:
              xlim([0 450])
```

```
            ylim([0 6])
% =>
            % title('BTC for Port 2 (12cm below gravel surface)');
            % title('BTC for Port 2 (24cm below gravel surface)');
            % title('BTC for Port 2 (36cm below gravel surface)');
            title('BTC for Port 7ii');
% =>
            % savefig('2_1_FilterPlot.fig');
            % savefig('2_2_FilterPlot.fig');
            % savefig('2_3_FilterPlot.fig');
            savefig('7ii_FilterPlot.fig');



function [DateNum, Uranine_mv, Temperature] = read(flu_file)
% Reads and re-formats fluorometer (experimental) data
fid = fopen(flu_file);
T = textscan(fid, '%*s %s %*s %f %f %f %f %f %f %f %*s', 'headerlines', 3);
fclose(fid);

Date = T{1};
DateNum = datenum(Date, 'dd/mm/yy-HH:MM:SS');     % Generate numerical date
Uranine_mv = T{2};
Temperature = T{8};



function [C1] = cal(Uranine_mv, Temperature, c_cal_Uranine, ind_ura, ind_blank)
% Calibrates experimental data (Uranine mV signals)
% Converts Uranine mV signal to corresponding Uranine conc. (ppb)
% Plots calibrated conc.
calib_conc = c_cal_Uranine;
blank = mean(Uranine_mv(ind_blank));
L1_ura = mean(Uranine_mv(ind_ura));

C1 = zeros(length(Temperature),1);
    for i = 1:length(Temperature)
        Raw_signals_minusblank = (Uranine_mv - blank)';
        coeff1 = (L1_ura-blank(1))/calib_conc;
```

```
        C1(i,:) = (coeff1\Raw_signals_minusblank(:,i))';
    end
C1(C1 < 0) = 0;                             % Sets -ve conc. to zero



function [E1] = extract(DateNum, C1, P1I, P1S_ind, P1F)
% Extracts BTC from full time series (starting @ time of injection)

C1(C1 < 0) = 0;                             % Sets -ve conc. to zero

for n = 1:P1S_ind
    C1(n,1) = 0;
end

[~,P1I_ind] = min(abs(DateNum-P1I));
[~,P1F_ind] = min(abs(DateNum-P1F));

E1(:,1) = DateNum(P1I_ind:P1F_ind);         % time (DateNum)
E1(:,2) = C1(P1I_ind:P1F_ind,:);            % [Uranine] (ppb)
E1(:,3) = (E1(:,1) - P1I).*24;              % time (hrs since inj)
end



function [F1] = myfilter(E1)
% Applies the Savitsky-Golay (SG) filter to smooth the extracted data
%  SG is a generalized, moving-average filter
%     It performs an unweighted, linear, least-squares fit using a polynomial (whose degree can be specified)
%        Higher degree polynomials capture the heights and widths of narrow peaks more accurately, but perform
poorly when smoothing broad peaks
%  SG is often used for spectroscopic data
%     It is effective at preserving higher moments, but less successful at rejecting noise

% Savitzky-Golay Filter:
%   yy = smooth(x, y, span, 'sgolay', degree)
%   **span must be odd (default 5)
%   **degree must be less than span (default 2)
```

```
%   x = E1(:,3) => time (hrs since injection)
%   y = E1(:,2) => [Uranine] (ppb)

SGfilt_d5 = smooth(E1(:,2), 1500, 'sgolay', 5);     % span = 1500; degree = 5
SGfilt_d5(SGfilt_d5 < 0) = 0;

F1(:,1) = E1(:,1);       % time (DateNum)
F1(:,2) = SGfilt_d5;     % [Uranine] (ppb)
F1(:,3) = E1(:,3);       % time (hrs since inj)
```

%% MasterTailFit.m

```
% Fits an exponential tail to the experimental data
%    Run this script if flow test was terminated too early or if tail was completed manually
%    Determines 'theoretical' end of flow test

% Fits an exponential tail (one-term exponential decay function) to flow test data
%    y = a.e^(-b.x)
%    Then extrapolates to [Uranine] = 0ppb to determine t_end

% User instructions for this section:
% 1. Load correct data file
% 2. Section (1.1): Enter % of tail data points to be used for the tail fit
%                   into 'inf_find' OR determine by visual inspection from
%                   figure (3) in MasterDataProc.m
% 3. Section (1.2): Enter x co-ordinate (INDEX) of 'inf_find' into 'ind'
% 4. Run script until _____Break 1______
% 5. Enter the values of the fit parameters 'a' and 'b' in section (1.3)
%    (they will be displayed to the Workspace)
% 6. Repeat run until section (1) until satisfied with tail fit
% 7. Run section (2) to check plot of tail fit
% 8. Run section (3) to save F1 matrix

%% (1) Exponential Tail Fit
close all
clear all
% =>
```

```
load C:/users/aylward/Desktop/MATLAB/Final2017/7iii_BTC_E1

% (1.1) Exponential Curve Fit
   E1(1,3) = 0;
   X = E1(:,3);      % time (hrs since inj)
   Y = E1(:,2);      % [Uranine] (ppb)

% => Determine from figure (3) in MasterDataProc.m (use +/- the final 50% of
%       data points after the peak)
%    Position = (270.3; 6.0541)
%    DataIndex = 97217

% =>   Enter x co-ordinate (INDEX) of ind_find:
       ind = 97217;
       t = X(ind:end);
       C = Y(ind:end);
       params = fit(t,C, 'exp1');
       disp('exp1 parameters')
       disp(params)

% (1.2) Plot tail data with exponential curve
        figure(12)
        plot(params,t,C);
        xlabel('Time since injection (hrs)')
        ylabel('[Uranine] (ppb)')
        title('Exponential Decay of RTD tail (one-term)')

%_____________________________________BREAK 1_____________________________________________

% (1.3) Determine flowtest end time
%        C = a*exp(b*t)
%        -> t = [ln(a) - ln(c)]/b
%        At what time will C = 0.01?
% =>
              a = 195.1;
% =>
              b = -0.01276;
```

```
                t_end_hrs = (log(a) - log(0.01))/abs(b);
                t_term = X(end,1);
                [x,y] = size(E1);
                t_term_ind = x;
                total_points = round(t_end_hrs)*360;         % no. of 10s intervals
                points = total_points - x;

%% (2) Append experimental flow test data at 10s intervals
%       Add data points for RTD tail using exponential function determined in section (1)
        [A1] = append(E1, points, a, b);
% =>
         save('7iii_BTC_A1', 'A1')
%        A1(:,1) = time (hrs since injection)
%        A1(:,2) = [Uranine] (ppb)

% (2.1) Plot RTD with extended tail
         figure(21)
         plot(A1(:,1), A1(:,2), 'm-'); hold on
         xlabel('Time since injection (hrs)');
         ylabel('[Uranine] (ppb)')
% =>     Specify domain and range:
         xlim([0 800])
         ylim([0 14])
% =>
         title('BTC with exponential tail - Port 7iii');
% =>
         savefig('7iii_TailFitPlot.fig')

%% (3)  Applies the Savitsky-Golay (SG) filter to smooth the extracted data
%       Applies the Savitsky-Golay (SG) filter to smooth the extracted data
%       SG is a generalized, moving-average filter
%          It performs an unweighted, linear, least-squares fit using a polynomial (whose degree can be specified)
%          Higher degree polynomials capture the heights and widths of narrow peaks more accurately,
%          but perform poorly when smoothing broad peaks
%       SG is often used for spectroscopic data
%          It is effective at preserving higher moments, but less successful at rejecting noise

% (3.1) Apply Savitzky-Golay Filter:
%       yy = smooth(x, y, span, 'sgolay', degree)
```

```
%       ** span must be odd (default 5)
%       ** degree must be less than span (default 2)
%       x = A1(:,1) => time (hrs since injection)
%       y = A1(:,2) => [Uranine] (ppb)

        SGfilt_d5 = smooth(A1(:,2), 1500, 'sgolay', 5);     % span = 1500; degree = 5
        SGfilt_d5(SGfilt_d5 < 0) = 0;
        F1(:,1) = A1(:,1);                                  % time (hrs since inj)
        F1(:,2) = SGfilt_d5;                                % [Uranine] (ppb)
% =>
        save('7iii_BTC_F1', 'F1')

% (3.2) Plot Filtered Data
        figure(3)
        plot(A1(:,1), A1(:,2), 'g.'); hold on
        plot(F1(:,1), F1(:,2), 'm-', 'LineWidth', 1.25); hold off
        legend('Raw data', 'Filtered data (SG deg5)', 'Location', 'northeast');
        xlabel('Time since injection (hr)');
        ylabel('[Uranine] (ppb)')
% =>    Specify domain and range:
%       xlim([0 220])
%       ylim([0 30])
% =>
        title('BTC for Port 7iii');
% =>
        savefig('7iii_FilterPlot.fig');


function [A1] = append(E1, points, a, b)
% Append experimental flowtest data at hourly intervals

[x,y] = size(E1);
tail_data = (x + points);

A1 = zeros(tail_data,2);
% A1(:,1) = hrs after injection
% A1(:,2) = conc.
```

```
for n = 1:119790;
    A1(n,1) = E1(n,3);
    A1(n,2) = E1(n,2);
end
for q = 119790:x;
    A1(q,1) = A1(q-1,1) + 0.0028;
    A1(q,2) = a*exp(b*A1(q,1));
for m = x : tail_data;
    A1(m,1) = A1(m-1,1) + 0.0028;
    A1(m,2) = a*exp(b*A1(m,1));
end
end
```

%% MasterCalcs_SS.m

```
% Calculates various hydraulic parameters assuming steady flow
% (i.e constant average volumetric flowrate)

% NOTE: Run Inflow.m and Outflow.m before continuing with MasterCalcs_SS.m

close all
clear all

%% USER DEFINED INPUTS
%  ALL UNITS SHOULD BE IN sec, L, ppb or ug/L

% INPUT 1: load correct data files
% =>
     load 'C:/users/Lara/Desktop/MATLAB/Final2017/7i_BTC_F1';
     % ** NOTE: Section (2) must agree with 'E' or 'F' in file name!
     % F1(:,1) = time (DateNum)
     % F1(:,2) = [Uranine] (ppb)
     % F1(:,3) = time (hrs since injection)
% =>
     load 'C:/users/Lara/Desktop/MATLAB/Final2017/7i_inflow';
     % Q_in = inlet volumetric flow rate (L/h)
% =>
```

```
    load 'C:/users/Lara/Desktop/MATLAB/Final2017/7i_outflow';
    % Q_out = outlet volumetric flow rate (L/h)

% INPUT 2: Experimental data variable assignment
%          ** Assign correct index to t_hr = F1() and C_t = F1() if data needs
%          to be truncated

%       2.1  If NO tail-fit has been performed:
%            Check index (must agree with F1 used in Inflow.m and Outflow.m)
% =>
%     t_hr = F1(:,3);            % (hr since inj)
%     t_sec = t_hr.*3600;        % (s since inj). hr -> s using 3600 s/hr
%     t_hr(1,1) = 0;

%       2.2  If a tail-fit HAS been performed:
%            Check index (must agree with F1 used in Inflow.m and Outflow.m)
% =>
    t_hr = F1(1:77604, 1);     % (hr since inj)
    t_sec = t_hr.*3600;        % (s since inj). hr -> s using 3600 s/hr
    t_hr(1,1) = 0;
%_____________________________________________________________________________
% =>
    C_t = F1(1:77604, 2);      % (ug/L) or (ppb)
    C_t(C_t < 0) = 0;          % set negative concentrations to zero

q_in = Q_in./3600;             % (L/s)
q_out = Q_out./3600;           % (L/s)

% INPUT 3: Mass of Uranine injected (g)
% =>
    M = 0.003*1000000;         % (ug). g converted to ug using 1,000,000 ug/g

% INPUT 4: System physical parameters

% Variable parameters:
% =>
    L = 6.000;                 % distance to sample port (m)
    h_H2O = 0.44;              % water level/height (m)
```

```
% Fixed parameters:
voidage = 0.3597;               % factional voidage of gravel
h = 0.70;                       % height of steel container (m)
h_gravel = 0.50;                % gravel/bed height (m)
B_top = 1.20;                   % breadth of steel container (surface) (m)
B_base = 1.0;                   % breadth of steel container (base) (m)

Dp = 0.006;                     % equivalent spherical diameter (4mm-8mm gravel) (m)
density_H2O = 998.2;            % (kg/m3) - Engineering Toolbox
viscosity_H2O = 1.002e-3;       % (Ns/m2) - Engineering Toolbox

%%  (1) GENERAL CALCULATIONS

% (1.1) Average system volumetric flow rates
Q_in_avg = mean(Q_in)                   % (L/hr)
Q_out_avg = mean(Q_out)                 % (L/hr)
Q_avg = (Q_in_avg + Q_out_avg)/2        % (L/hr)
q_in_avg = Q_in_avg/3600;               % (L/s)
q_out_avg = Q_out_avg/3600;             % (L/s)
q_avg = Q_avg/3600;                     % (L/s)

% (1.2) System fluid volume (up to the point of sample removal)
[V_bed_m3,  B_bed_base, base, h_perp] = volume(L, h_H2O, voidage, h, B_top, B_base);
V_bed_L = V_bed_m3 * 1000               % (L). m3 -> L using 1000 L/m3.

% (1.3) Reynold's Number (Re < 10 for laminar flow)

% Superficial velocity (m/s) = volumetric flowrate / cross sectional area
Us = (q_avg*0.001)/((B_bed_base*h_H2O) + (0.5*base * h_perp));

% Reynolds number for a packed bed
Re = (Dp*Us*density_H2O) / ((1-voidage)*viscosity_H2O)

%% (2) STEADY STATE CALCULATIONS

% (2.1) Percentage recovery of tracer
```

```
dt = (t_sec(3,1) - t_sec(2,1));      % (s)
m = q_avg * (sum(C_t)*dt)            % (ug)
recovery = m/M * 100

% (2.2) Nominal retention time, tau
tau_sec = V_bed_L/q_avg;             % (s)
tau_hr = tau_sec/3600                % (hr)

% (2.3) The RTD function
E_t = C_t ./ (sum(C_t)*dt);          % (1/s)

% (2.4) Mean residence time, t_m
%       ! CHECK: Does t_m = tau?

t_m_sec = sum(t_sec.*E_t)*dt;        % (s)
t_m_hr = t_m_sec/3600                % (hr)

% (2.5) Normalized (dimensionless) time, theta
theta = t_hr ./ t_m_hr;
theta(1,1) = 0;

% (2.6) The dimensionless RTD, C_theta
C_theta = C_t .* (V_bed_L/m);

% (2.7) The normalized RTD function, E_theta
E_theta = E_t .* t_m_sec;

% (2.8) Plot C(theta) vs theta and E(theta) vs theta
%       ! CHECK: Does C_theta vs theta  =  E_theta vs theta?

figure(28)
subplot(2,1,1)
plot(theta, C_theta, 'g'); hold on
xlabel('theta')
ylabel('C-theta')
% =>
     xlim([0 2.0])
     %ylim([0 1.0])
```

```
% =>
     % title('Dimensionless RTD for Port 1 (12cm below gravel surface) - steady flow')
     title('Dimensionless RTD for Port 7 (12th April 2016) - steady flow assumption')

subplot(2,1,2)
plot(theta, E_theta, 'b')
xlabel('theta')
ylabel('E-theta')
% =>
     xlim([0 2.0])
     %ylim([0 2.5])
% =>
     % title('Normalized RTD function for Port 1 (12cm below gravel surface) - steady flow')
     title('Normalized RTD function for Port 7 (12th April 2016) - steady flow assumption')
hold off

% (2.9) Mode (peak time)
%       ! CHECK: Do Cpeak_ppb & tpeak_hr agree with FilterPlot.fig?
%       ! CHECK: Do Cpeak_norm & tpeak_norm agree with normalized RTD plots in figure(28)?

Cpeak_ppb = max(C_t);             % Peak conc. (ppb)
Cpeak_norm = max(C_theta);        % Normalized peak conc.
[~,max_ind] = max(C_t);
tpeak_hr = t_hr(max_ind)          % Peak time (hr)
tpeak_norm = theta(max_ind)       % Normalized peak time

% (2.10) Moment Analysis

% 0th Moments
% ! CHECK: Does M0(E) = 1?
% ! CHECK: Does M0(C') = 1?
% ! CHECK: Does M0(E') = 1?

M0_Et = sum(E_t) * dt
d_theta = dt/t_m_sec;
M0_Ctheta = sum(C_theta) * d_theta
M0_Etheta = sum(E_theta) * d_theta
```

```
% 1st Moments
% ! CHECK: Does M1_Et = tau?
% ! CHECK: Does M1(C') = 1?
% ! CHECK: Does M1(E') = 1?

M1_Et_hr = t_m_hr
M1_Ctheta = sum(theta.*C_theta) * d_theta
M1_Etheta = sum(theta.*E_theta) * d_theta

% 2nd Moment
M2_Et = ( sum((t_sec).^2 .* E_t) * dt ) - t_m_sec^2;                % (s^2)
M2_Ctheta = sum( (theta - M1_Ctheta).^2 .* C_theta ) * d_theta
StdDev = sqrt(M2_Ctheta)

%% (3) Hydraulic Performance Calculations
%      Performed for Port 7 (outlet) only to investigate overall system performance

% (3.1) Tanks in Series Model
%          No. of tanks in series, N
sigma_sqd = M2_Et;
N = t_m_sec^2 / sigma_sqd

% (3.2) Dispersed Plug Flow Model
%          Pectlet no., Pe, & dispersion no., D
%          Calculations performed using Microsoft Excel Solver


% (3.3) Effective volume utilization, e
e = t_m_sec/tau_sec

% (3.4) Hydraulic efficiency, lambda
lambda = e * (1 - (1/N))

% (3.5) Efficiency Indexes
m0_all = sum(C_t).*dt;
[r,c] = size(C_t);
m0_inc = zeros(r,1);
for n = 1 : r
```

```
    m0_inc(n,1) = sum(C_t(1:n)).*dt;
end

t10_ind = find(m0_inc > (m0_all*0.10),1);
t10_hr = t_hr(t10_ind)
theta10 = t10_hr / t_m_hr

t90_ind = find(m0_inc > (m0_all*0.90),1);
t90_hr = t_hr(t90_ind)
MDI = t90_hr / t10_hr

% Find the index at which theta = 1.000
% Enter into THETA_ind
% =>
     THETA_ind = 27980;

MI_theta = theta(1:THETA_ind);
MI_C_theta = C_theta(1:THETA_ind);
MI = 1 - ( sum( (1-MI_theta) .* MI_C_theta ) * d_theta )

%% (4) Save data
% =>
     Data7i(:,1) = theta;
     Data7i(:,2) = C_theta;
     Data7i(:,3) = E_theta;

% =>
     save('7i_BTC_Data', 'Data7i')
```

%% MasterCalcs_NSS.m

```
% Calculates various hydraulic parameters for a variable flow system
%   Based on the method developed by Werner & Kadlec for the application of
%   residence time distribution theory to stormwater treatment systems
%   -> Ecol. Eng. 7 (1996) 213-214
```

```
% NOTE: Run Inflow.m and Outflow.m before continuing with MasterCalcs_SS.m
%       Run MasterCalcs_SS.m before continuing with MasterCalcs_NSS.m
close all
clear all

%% USER DEFINED INPUTS
%  ALL UNITS SHOULD BE IN sec, L, ppb or ug/L

% INPUT 1: load correct data files
% =>
     load 'C:/users/Lara/Desktop/MATLAB/Final2017/2_3_BTC_F1';
     % ** NOTE: Section (2) must agree with 'E' or 'F' in file name!
     % F1(:,1) = time (DateNum)
     % F1(:,2) = [Uranine] (ppb)
     % F1(:,3) = time (hrs since injection)
% =>
     load 'C:/users/Lara/Desktop/MATLAB/Final2017/2_3_inflow';
     % Q_in = inlet volumetric flow rate (L/h)
% =>
     load 'C:/users/Lara/Desktop/MATLAB/Final2017/2_3_outflow';
     % Q_out = outlet volumetric flow rate (L/h)
% =>
     load 'C:/users/Lara/Desktop/MATLAB/Final2017/2_3_BTC_data';
     % Steady state data from MasterCalcs_SS.m
     % Data#(:,1) = theta;
     % Data#(:,2) = C_theta;
     % Data#(:,3) = E_theta;

% INPUT 2: Experimental data variable assignment
%          ** Assign correct index to t_hr = F1() and C_t = F1() if data needs
%          to be truncated

%       2.1  If NO tail-fit has been performed:
%            Check index (must agree with F1 used in Inflow.m and Outflow.m)
% =>
     t_hr = F1(:,3);             % (hr since inj)
     t_sec = t_hr.*3600;         % (s since inj). hr -> s using 3600 s/hr
     t_hr(1,1) = 0;
```

```
%       2.2  If a tail-fit HAS been performed:
%            Check index (must agree with F1 used in Inflow.m and Outflow.m)
% =>
%      t_hr = F1(1:120532, 1);    % (hr since inj)
%      t_sec = t_hr.*3600;        % (s since inj). hr -> s using 3600 s/hr
%      t_hr(1,1) = 0;
%_____________________________________________________________________________
% =>
     C_t = F1(:,2);              % (ug/L) or (ppb)
     C_t(C_t < 0) = 0;           % set negative concentrations to zero

q_in = Q_in./3600;               % (L/s)
q_out = Q_out./3600;             % (L/s)

% INPUT 3: Mass of Uranine injected (g)
% =>
     M = 0.015*1000000;          % (ug). g converted to ug using 1,000,000 ug/g

% INPUT 4: System physical parameters

% Variable parameters:
% =>
     L = 2.225;                  % distance to sample port (m)
     h_H2O = 0.44;               % water level/height (m)

% Fixed parameters:
voidage = 0.3597;                % factional voidage of gravel
h = 0.70;                        % height of steel container (m)
h_gravel = 0.50;                 % gravel/bed height (m)
B_top = 1.20;                    % breadth of steel container (surface) (m)
B_base = 1.0;                    % breadth of steel container (base) (m)

Dp = 0.006;                      % equivalent spherical diameter (4mm-8mm gravel) (m)
density_H2O = 998.2;             % (kg/m3) - Engineering Toolbox
viscosity_H2O = 1.002e-3;        % (Ns/m2) - Engineering Toolbox

%%  (1) GENERAL CALCULATIONS
```

```
% (1.1) Average system volumetric flow rates
Q_in_avg = mean(Q_in);                  % (L/hr)
Q_out_avg = mean(Q_out);                % (L/hr)
Q_avg = (Q_in_avg + Q_out_avg)/2;       % (L/hr)
q_in_avg = Q_in_avg/3600;               % (L/s)
q_out_avg = Q_out_avg/3600;             % (L/s)
q_avg = Q_avg/3600;                     % (L/s)

% (1.2) System fluid volume (up to the point of sample removal)
[V_bed_m3,  B_bed_base, base, h_perp] = volume(L, h_H2O, voidage, h, B_top, B_base);
V_bed_L = V_bed_m3 * 1000;      % (L). m3 -> L using 1000 L/m3.

% (1.3) Reynold's Number (Re < 10 for laminar flow)

% Superficial velocity (m/s) = volumetric flowrate / cross sectional area
Us = (q_avg*0.001)/((B_bed_base*h_H2O) + (0.5*base * h_perp));

% Reynolds number for a packed bed
Re = (Dp*Us*density_H2O) / ((1-voidage)*viscosity_H2O);

%% (2) NON-STEADY STATE CALCULATIONS

% (2.1) Percentage recovery of tracer
dt = (t_sec(3,1) - t_sec(2,1));      % (s)
m2 = sum(C_t .* q_out)*dt            % (ug)
recovery2 = m2/M * 100

% (2.2) Nominal retention time, tau
%       NOT APPLICABLE

% (2.3) The RTD function
E_t2 = (C_t .* q_out)./m2;           % (1/s)

% (2.4) Mean residence time, t_m
t_m_sec = sum(t_sec.*E_t2)*dt;       % (s)
t_m_hr = t_m_sec/3600                % (hr)
```

```
% (2.5) Flow Weighted Time, phi
%          phi = V_out / V_system for each time point
%          V_out (L) = volume of water that has exited in t_inj -> t_hr
%          Assume that V_system is approximately constant because of the
%             syphon controlling the water level

[a,b] = size(t_hr);
V_out = zeros(a,1);
V_out(1,1) = 0;
for n = 2 : a
    V_out(n,1) = Q_out(n-1,1)*( t_hr(n,1) - t_hr(n-1,1) ) + V_out(n-1,1);
end
phi = V_out ./ V_bed_L;

% (2.6) The dimensionless RTD, C_phi
C_phi = C_t .* (V_bed_L/m2);
C_phi(C_phi < 0) = 0;

% (2.7) The normalized RTD function, E_theta
%       NOT APPLICABLE

% (2.8) Plot C(phi) vs phi and C(theta) vs theta
%       ! CHECK: Compare plots

figure(28)
subplot(2,1,1)
plot(phi, C_phi, 'b'); hold on
xlabel('phi')
ylabel('C-phi')
% =>
     xlim([0 5.5])
     %ylim([0 0.8])
% =>
     title('Non-steady flow RTD for Port 2 (36cm below gravel surface)')
     %title('Non-steady flow RTD for Port 7 (2nd May 2016)')

subplot(2,1,2)
plot(Data23(:,1), Data23(:,2), 'g');
```

```
xlabel('theta')
ylabel('C-theta')
% =>
     xlim([0 5.5])
     %ylim([0 0.8])
% =>
     title('Steady-flow RTD for Port 2 (36cm below gravel surface)')
     %title('Steady flow RTD for Port 7 (2nd May 2016)')

% =>
     %savefig('2_3_NormRTDs')

% (2.9) Mode (peak time)
%       ! CHECK: Do Cpeak_norm & tpeak_norm agree with normalized RTD plot in figure(28)?
Cpeak_norm = max(C_phi);       % Normalized peak conc.
[~,max_ind] = max(C_phi);
tpeak_norm = phi(max_ind)      % Normalized peak time

% (2.10) Moment Analysis

% 0th Moments
% ! CHECK: Does M0(E) = 1?
% ! CHECK: Does M0(C') = 1?

M0_E_t = sum(E_t2) * dt

[r,c] = size(C_phi);
d_phi = zeros(r,1);
d_phi(1,1) = 0.00056;
for N = 2 : r
    d_phi(N,1) = (V_out(N,1) - V_out(N-1,1)) ./ V_bed_L;
end
M0_Cphi = sum(C_phi .* d_phi)

% 1st Moments
% ! CHECK: Does M1(C') = 1?
M1_Et2_sec = (sum(t_sec.*E_t2)*dt);
M1_Et2_hr = M1_Et2_sec/3600
```

```
M1_Cphi = sum(phi .* C_phi .* d_phi)

% 2nd Moment
M2_Et2 = ( sum((t_sec).^2 .* E_t2) * dt ) - M1_Et2_sec^2;                % (s^2)
M2_Cphi = sum((phi - M1_Cphi).^2 .* C_phi .* d_phi)
StdDev2 = sqrt(M2_Cphi)

%% (3) Hydraulic Performance Calculations
%      Performed for Port 7 (outlet) only to investigate overall system performance

% (3.1) Tanks in Series Model
%          No. of tanks in series, N
sigma_sqd = M2_Et2;
N = M1_Et2_sec^2 / sigma_sqd

%% (4) Save Data
%      **** Update data matrix name [Data##(:,n)] and file name ****
Data23(:,4) = phi;
Data23(:,5) = C_phi;

% =>
     save('2_3_BTC_Data', 'Data23')



function [V_bed_m3, B_bed_base, base, h_perp] = volume(L, h_H2O, voidage, h, B_top, B_base)
% Calculates the volume of water in the constructed wetland system
%    The volume returned (Vsys) is the system fluid volume up to the point
%     of sample removal (or up to the specified sample port)
%    Volume = volume of rectangular section + volume of triangular section

% Volume of rectangular section
B_bed_base = B_base;                                % breadth of gravel/bed (base of wetland) (m)
L_bed = L;
V_rect = L_bed * B_bed_base * h_H2O * voidage;      % (m3)


% Volume of triangular section (see diagram in lab book for varibale definitions)
```

```
ao = B_top - B_base;                                % (m)
bo = h;                                             % (m)
ho = sqrt((ao*ao) + (bo*bo));                       % (m) - Pythagoras' theorem
bi = h_H2O;                                         % (m)
hi = (bi/bo) * ho;                                  % (m) - Ratio of sides of right angled triangle
ai = sqrt((hi*hi) - (bi*bi));                       % (m) - Pythagoras' theorem
base = ai;                                          % (m)
h_perp = bi;                                        % (m)
V_tri = L_bed * 0.5*base * h_perp * voidage;        % (m3)

% Volume of bed
V_bed_m3 = V_rect + V_tri;      % (m3)
```

%% Inflow.m

```
%  To create a vector of inlet volumetric flowrates for every flowtest sampling time
%  (i.e. 10s intervals from time of injection to time of termination)
%  NOTE: ' => ' indicates where user inputs are required

%  Requires:
%           1. full flowtest sampling time vector - hrs since injection format (time)
%              -> already calibrated and extracted
%           2. inflow cycle DateTime [ t_in ] and corresponding volumetric flowrate [ q_in ]

%  Creates a zero matrix of size(time) to represent Q_in
%  Compares every (time) to (t_in)
%    Then assigns a volumetric flowrate to replace each zero for every sample time
%    **** (time) and (Q_in) must have the same dimensions ****

%% User Instructions:
%  1. Follow instructions as they are given below

close all
clear all


%% (1) Load experimental data: time & [Uranine]
```

```
% =>
     load C:/users/Lara/Desktop/MATLAB/Final2017/1_2_BTC_F1.mat
     % F1(:,1): time (DateNum)
     % F1(:,2): [Uranine] (ppb)
     % F1(:,3): time (hrs since inj)

% *** Injection time = 12 April 2016, 12:21:20 ***
% =>
     t_inj = datenum([2016 04 12 12 21 20]);

% *** End of Flowtest = 18 April 2016, 09:43:30 ***
% =>
     t_end = datenum([2016 04 18 09 43 30]);

%% (2) Fluoro flowtest data

% (2.1) If NO tail-fit has been performed:
time = F1(:,3);
time_end = time(end,1);
time(1,1) = 0;

% (2.2) If a tail-fit HAS been performed:
%       ! CHECK: index corresponding to t_end
% =>
%      time = F1(1:120532, 1);
%
% time_end = time(end,1);
% time(1,1) = 0;
%_____________________________________________________________________________
%
% conc: for each time (from injectin to termination)
% ! CHECK: index corresponding to t_end
% =>
     conc = F1(:,2);

conc(conc < 0) = 0;

%% (3) Inflow LOG data
```

```
%      Save Excel file (LOG#.xlsx) containing flow rate data into MATLAB current folder
%      (see LOG_Template.xlsx for required spreadsheet layout)
%      ! CHECK: start & end time of LOG data = start & end time of flow test

%  (3.1) ENTER spreadsheet name & cell references for 'Log_in' & 'q_in'
% =>
     Log_in = xlsread('LOG1.xlsx', 'LogData', 'A2:A479');         % Inflow cycle start DateTime (Excel numeric
format)

t_in = datetime(Log_in,'ConvertFrom','excel');
T_in = datenum(t_in);
T_in_hr = (T_in - t_inj).*24;                                     % time since injection (hrs)

% =>
     q_in = xlsread('LOG1.xlsx', 'LogData', 'C2:C479');           % Inlet volumetric flowrate (L/h)

%  (3.2) ! CHECK: agreement between 'in' start & end times
%        1. Run script now, up until the end of section (3.2)
%        2. If start & end times are in agreement, continue with (3.3)
start_in = T_in_hr(1,1);
stop_in = T_in_hr(end,1);
check_start_in = abs(time(1,1) - start_in);     % should be zero if both entries represent the same DateTime
check_stop_in = abs(time_end - stop_in);        % should be zero if both entries represent the same DateTime

%  (3.3) ! CHECK: time vectors
%        1. Adjust LOG spreadsheet indexes and assign Q_in(1,1) now before
%           continuing to section (4) (explanation follows directly below and
%           an example is contained in Example_Adjustment_Inflow_section3_3.m)

%   time(2,1) may not be 0.0028hr (10s) after t_inj = 0
%   -> open time and T_in_hr in the variable window
%   -> if time(2,1) does not = t_inj + 0.0028hr (10s) &
%         time(2,1) > T_in_hr(2,1)
%      then t_in from LOGx.xlsx must be set = to time(2,1) by adjusting the
%      cells referenced from the Excel log data spreadsheet in 'Log_in'
%   -> * it will also then be neccessary to manually assign the correct q_in
%      @ t_inj to Q_in(1,1) directly after the 'for' loop in section (4)
%% (4) Assign volumetric flowrates to all flowtest times
```

```
[r,c] = size(time);
[a,b] = size(T_in_hr);
Q_in = zeros(r,1);
count = 1;
for m = 1 : r
    if time(m,1) < T_in_hr(count+1,1)
        Q_in(m,1) = q_in(count,1);
    elseif time(m,1) == T_in_hr(count+1,1)
        Q_in(m,1) = q_in(count+1,1);
    elseif time(m,1) > T_in_hr(count+1,1) && count < a
        count = count + 1;
        Q_in(m,1) = q_in(count,1);
    elseif count >= a
        disp('count IN exceeds time steps')
        r = r + 1;
    end
end

% =>
     % Q_in(1,1) = 6.8000;     % see Sectiion (3.3) for explanation

% =>
     save('1_2_inflow', 'Q_in')

%% (5) Export data to Excel (UPDATE WORKSHEET NAME)
%       ! CHECK: that the correct volumetric flowrates are assigned to each experimental sampling time
       warning('off','MATLAB:xlswrite:AddSheet');
% =>
     xlswrite('LOG1.xlsx', time, 'CheckData1_2', 'A2');     % Flow test sample time (hrs since inj)
     xlswrite('LOG1.xlsx', conc, 'CheckData1_2', 'B2');     % Uranine conc. (ppb)
     xlswrite('LOG1.xlsx', Q_in, 'CheckData1_2', 'C2');     % Inlet volumetric flowrate corresponding to each
                                                              flowtest sample time
```

```
%% Outflow.m
%  To create a vector of outlet volumetric flowrates for every flowtest sampling time
%  (i.e. 10s intervals from time of injection to time of termination)
%  NOTE: ' => ' indicates where user inputs are required

%  Requires:
%           1. full flowtest sampling time vector - hrs since injection format (time)
%              => already calibrated and extracted
%           2. outflow cycle DateTime [ t_out ] and corresponding volumetric flowrate [ q_out ]

%  Creates a zero matrix of size(time) to represent Q_out
%  Compares every (time) to (t_out)
%    Then assigns a volumetric flowrate to replace each zero for every sample time
%    **** (time) and (Q_out) must have the same dimensions ****

%% User Instructions:
%  1. Follow instructions as they are given below

close all
clear all

%% (1) Load experimental data: time & [Uranine]
% =>
     load C:/users/Lara/Desktop/MATLAB/Final2017/1_2_BTC_F1.mat
     % F1(:,1): time (DateNum)
     % F1(:,2): [Uranine] (ppb)
     % F1(:,3): time (hrs since inj)

% *** Injection time = 12 April 2016, 12:21:20 ***
% =>
     t_inj = datenum([2016 04 12 12 21 20]);

% *** End of Flowtest = 18 April 2016, 09:43:30 ***
% =>
     t_end = datenum([2016 04 18 09 43 30]);
```

```
%% (2) Fluoro flowtest data

% (2.1) If NO tail-fit has been performed:
time = F1(:,3);
time_end = time(end,1);
time(1,1) = 0;

% (2.2) If a tail-fit HAS been performed:
%       ! CHECK: index corresponding to t_end
% =>
%      time = F1(1:120532, 1);
%
% time_end = time(end,1);
% time(1,1) = 0;
%_____________________________________________________________________________
%
% conc: for each time (from injectin to termination)
% ! CHECK: index corresponding to t_end
% =>
     conc = F1(:,2);

conc(conc < 0) = 0;

%% (3) Inflow LOG data
%      Save Excel file (LOG#.xlsx) containing flow rate data into MATLAB current folder
%      (see LOG_Template.xlsx for required spreadsheet layout)
%      ! CHECK: start & end time of LOG data = start & end time of flow test

%  (3.1) ENTER spreadsheet name & cell references for 'Log_out' & 'q_out'
% =>
     Log_out = xlsread('LOG1.xlsx', 'LogData', 'E2:E988');         % Outflow Cycle Time - Excel numeric format

t_out = datetime(Log_out,'ConvertFrom','excel');
T_out = datenum(t_out);
T_out_hr = (T_out - t_inj).*24;                                    % time since injection (hrs)

% =>
     q_out = xlsread('LOG1.xlsx', 'LogData', 'G2:G988');           % Outlet volumetric flowrate (L/h)
```

```
%  (3.2) ! CHECK: agreement between 'out' start & end times
%        1. Run script now, up until the end of section (3.2)
%        2. If start & end times are in agreement, continue with (3.3)
start_out = T_out_hr(1,1);
stop_out = T_out_hr(end,1);
check_start_out = abs(time(1,1) - start_out);     % should be zero if both entries represent the same DateTime
check_stop_out = abs(time(end,1) - stop_out);     % should be zero if both entries represent the same DateTime

%  (3.3) ! CHECK: time vectors
%        1. Adjust LOG spreadsheet indexes and assign Q_out(1,1) now before
%           continuing to section (4) (explanation follows directly below and
%           an example is contained in Example_Adjustment_Inflow_section3_3.m

%   time(2,1) may not be 0.0028hr (10s) after t_inj = 0
%   -> open time and T_out_hr in the variable window
%   -> if time(2,1) does not = t_inj + 0.0028hr (10s) &
%         time(2,1) > T_out_hr(2,1)
%      then t_out from LOGx.xlsx must be set = to time(2,1) by adjusting the
%      cells referenced from the Excel log data spreadsheet in 'Log_out'
%   -> * it will also then be neccessary to manually assign the correct q_in
%      @ t_inj to Q_out(1,1) directly after the 'for' loop in section (4)

%% (4) Assign volumetric flowrates to all flowtest times
[r,c] = size(time);
[a,b] = size(T_out_hr);
Q_out = zeros(r,1);
count = 1;
for m = 1 : r
    if time(m,1) < T_out_hr(count+1,1)
        Q_out(m,1) = q_out(count,1);
    elseif time(m,1) == T_out_hr(count+1,1)
        Q_out(m,1) = q_out(count+1,1);
    elseif time(m,1) > T_out_hr(count+1,1) && count < a
        count = count + 1;
        Q_out(m,1) = q_out(count,1);
    elseif count >= a
        disp('count IN exceeds time steps')
        r = r + 1;
```

```
    end
end

% =>
     % Q_out(1,1) = 6.4731;      % see Sectiion (3.3) for explanation

% =>
     save('1_2_outflow', 'Q_out')

%% (5) Export data to Excel (UPDATE WORKSHEET NAME)
%      ! CHECK: that the correct volumetric flowrates are assigned to each experimental sampling time
warning('off','MATLAB:xlswrite:AddSheet');
% =>
     xlswrite('LOG1.xlsx', Q_out, 'CheckData1_2', 'D2');      % Outlet volumetric flowrate corresponding to each flow
                                                                test sample time
```

Appendix C: Tracer Flow Test Data, UFZ Leipzig

The Matlab code to extract and analyse this data has been given in Appendix B. Due to the volume of data generated, the size of the text files and concern for the number of printed pages, this section presents the raw experimental data in the form of concentration breakthrough curves (plots of tracer concentration versus time as measured by the field fluorometers). The examples sets chosen are for the wetland outlet. The fluorometer data can be found in electronic form on the CD submitted with this thesis.

Flow Tests in 2015

The series of flow tests that were performed in 2015 are summarized in this section. The sample port numbers correspond to those given in Figure 3-4 a) of Chapter 3. The experimental concentration/time data for the flow test conducted at the wetland outlet (before any normalization or calculations were performed) is presented in Figure C1. The matlab data inputs and outputs for the flow tests are summarized in Tables C1 and C2 below.

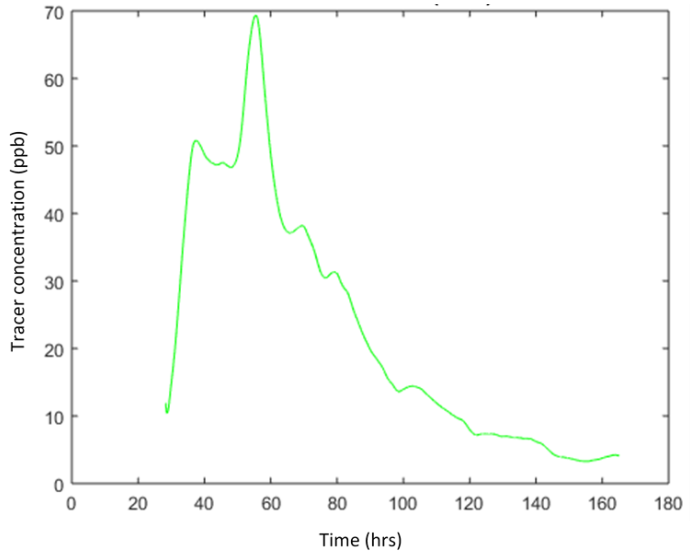


Figure C1: The concentration breakthrough curve at the wetland outlet for the 2015 flow test (29th September 2015)

Table C1: Summary of the Matlab code inputs for the flow tests performed in the pilot-scale CWs at the Helmholtz UFZ in 2015

Variable Description	Variable name	(unit)	Port 1 29th Sept Depth 2 (24cm)	Port 2 22nd Oct Depth 2 (24cm)	Port 3 13th Oct Depth 2 (24cm)	Port 4 13th Oct Depth 2 (24cm)	Port 5 13th Oct Depth 2 (24cm)	Port 6 29th Sept Depth 2 (24cm)	Port 7 29th Sept Depth 2 (24cm)
Data pre-processing - MasterDataProc.m									
raw data mV file	**flu_file**		Port1_f051_2015	Port2_f050_2015	Port3_f050_2015	Port4_f025_2015	Port5_f023_2015	Port6_f050_2015	Port7_f025_2015
fluorometer no.	**f**		651	650	650	625	623	650	625
calibration conc. Uranine	**c_cal_Uranine**	*(ppb)*	70	70	70	70	70	70	70
calibration window Uranine	**ind_ura**		165 : 168	158 : 160	59416 : 59418	59474 : 59476	59488 : 59490	154 : 146	149 : 150
calibration window baseline	**ind_blank**		286 : 471	5675 : 7110	1202 : 1489	1229 : 1761	5381 : 5385	179 : 207	188 : 212
date/time of injection	**P1I**		2015 09 29 13 00 30	2015 10 22 12 10 10	2015 10 13 13 24 00	2015 10 13 13 24 00	2015 10 13 13 24 00	2015 09 29 13 00 30	2015 09 29 13 00 30
date/time of end of flow test	**P1F**		2015 09 30 08 54 20	2015 10 26 13 30 10	2015 10 20 09 35 30	2015 10 20 09 40 00	2015 10 20 09 38 50	2015 10 05 11 05 30	2015 10 06 10 03 40
Hydraulic calculations - MasterCalcs_SS.m									
data file			1_BTC_F1	2_BTC_F1	3_BTC_F1	4_BTC_F1	5_BTC_F1	6_BTC_F1	7_BTC_F1
average volumetric flow rate	**q_avg**	*(L/h)*	22.73	21.94	20.02	20.02	20.02	22.73	22.73
mass of Uranine injected	**M**	*(mg)*	42	30	30	30	30	42	42
distance to sample port	**L**	*(m)*	66	225.5	297	297	373	500	600
water level	**h_h20**	*(m)*	0.50	0.50	0.50	0.50	0.50	0.50	0.50

Table C2: Summary of the Matlab code outputs for the flow tests performed in the pilot-scale CWs at the Helmholtz UFZ in 2015

MasterCalcs_SS.m Variable Description	Variable name	(unit)		Port 1 29th Sept Depth 2 (24cm)	Port 2 22nd Oct Depth 2 (24cm)	Port 3 13th Oct Depth 2 (24cm)	Port 4 13th Oct Depth 2 (24cm)	Port 5 13th Oct Depth 2 (24cm)	Port 6 29th Sept Depth 2 (24cm)	Port 7 29th Sept Depth 2 (24cm)
System fluid volume (up to sample port)	**V_bed_L**	*(L)*		127.1796	434.5304	572.3084	572.3084	718.7577	963.4821	1156.2
Reynold's Number	**Re**			0.0957	0.0735	0.0806	0.0806	0.0806	0.1072	0.1078
Mass of tracer recovered	**m**	*(ug)*		34101	1846.2	22993	19467	28865	60945	69288
Percentage recovery	**recovery**	*(%)*		81.1921	6.1542	76.6426	64.8904	96.2179	145.1063	164.9711
Nominal retention time	**tau_hr**	*(hr)*		6.4330	28.6252	34.3522	34.3522	43.1427	43.5177	51.8931
Mean residence time	**t_m_hr**	*(hr)*		4.2807	47.084	48.8675	44.5112	48.8536	50.7857	69.4055

				Port 1 29th Sept Depth 2 (24cm)	Port 2 22nd Oct Depth 2 (24cm)	Port 3 13th Oct Depth 2 (24cm)	Port 4 13th Oct Depth 2 (24cm)	Port 5 13th Oct Depth 2 (24cm)	Port 6 29th Sept Depth 2 (24cm)	Port 7 29th Sept Depth 2 (24cm)
Does $t_m = \tau$?				N	N	N	N	N	N	N
Does $C'(\theta) = E'(\theta)$?				N	N	N	N	N	N	N
Peak time	**tpeak_hr**	*(hr)*		2.5639	42.8861	33.3111	20.1556	32.7750	32.5167	55.4139
Normalized peak time	**tpeak_norm**			0.5989	0.9108	0.6817	0.4528	0.6709	0.6403	0.7984
0th moments:	**M0_E**		1	1.0000	1.0000	1.0000	1.0000	1.0000	1.0000	1.0000
	M0_C'		1	1.5028	0.6080	0.7030	0.7718	0.8831	0.8569	0.7477
	M0_E'		1	1.0000	1.0000	1.0000	1.0000	1.0000	1.0000	1.0000
1st moments:	**M1_E**	*(hr)*	t_m	4.2807	47.0840	48.8675	44.5112	48.8536	50.7857	69.4055
	M1_C'		1	1.5028	0.6080	0.7030	0.7718	0.8831	0.8569	0.7477
	M1_E'		1	1.0000	1.0000	1.0000	1.0000	1.0000	1.0000	1.0000
2nd moment	**M2_C'**			0.9260	0.1211	0.2874	0.3497	0.2659	0.1903	0.1813
Standard deviation	**StdDev**			0.9623	0.3481	0.5361	0.5914	0.5156	0.4363	0.4258
Number of tanks in series	**n**			2.7519	21.9472	3.1185	2.4934	3.4794	4.9594	5.5927
	t_m			1.5411E+04	1.6950E+05	1.7592E+05	1.6024E+05	1.7587E+05	1.8283E+05	1.8682E+05
	σ^2			8.6300E+07	1.3091E+09	9.9242E+09	1.0298E+10	8.8899E+09	6.7400E+09	1.1163E+10
Peclet Number	**Pe**			4.2166	42.7744	4.9953	3.6577	5.7505	8.7856	10.0689
Dispersion Number	**D**			0.23716	0.02338	0.20019	0.27340	0.17390	0.11382	0.09932
Effective volume utilization	**e**			0.6654	1.6448	1.4225	1.2957	1.1324	1.167	1.3375
Hydraulic efficieincy	**λ**			0.4236	1.5699	0.9664	0.7761	0.8069	0.9317	1.0983
Efficiency Indexes	**t_{10}**			1.8139	35.3944	25.8917	19.2667	27.6667	29.1139	37.9528
	θ_{10}			0.4237	0.7517	0.5298	0.4328	0.5663	0.5733	0.5468
	t_{90}			7.4167	61.3833	84.0694	77.2833	80.7417	81.9944	112.8806
	MDI			4.0888	1.7343	3.247	4.0112	2.9184	2.8163	2.9742
	MI			0.6761	0.9467	0.8598	0.8223	0.8361	0.8551	0.8751

Flow Tests in 2016

The series of flow tests that were performed in 2016 are summarized in this section. The quantity of flow test experiments in 2016 was increased to include RTDs from multiple depths at each sample port; rather that just at mid-depth as in 2015. The sample port numbers correspond to those given in Figure 3-4 a) of Chapter 3. The experimental concentration/time data for the three flow tests conducted at the wetland outlet (before any data normalization or calculations were performed) is presented in Figures C2, C3 and C4. This section also includes the daily average flow rate data for the April to September 2016 experimental period (Tables C3 and C4). The flowrate was monitored more closely in 2016 due to the observation of the extent of flow rate fluctuation during the 2015 experiments. The inflow rate was monitored daily and the outflow rate only during the flow tests; until the introduction of the AWW on 23rd June 2016. Hyphens indicate where data was not logged by the control system. The matlab data inputs for the 2016 flow tests are summarized in Tables C5 to C11 and the outputs in Tables C12 to C15. The Peclet and Dispersion numbers (Tables C16 – C19) were calculated using the dispersed plug flow model and *Microsoft Excel Solver*.

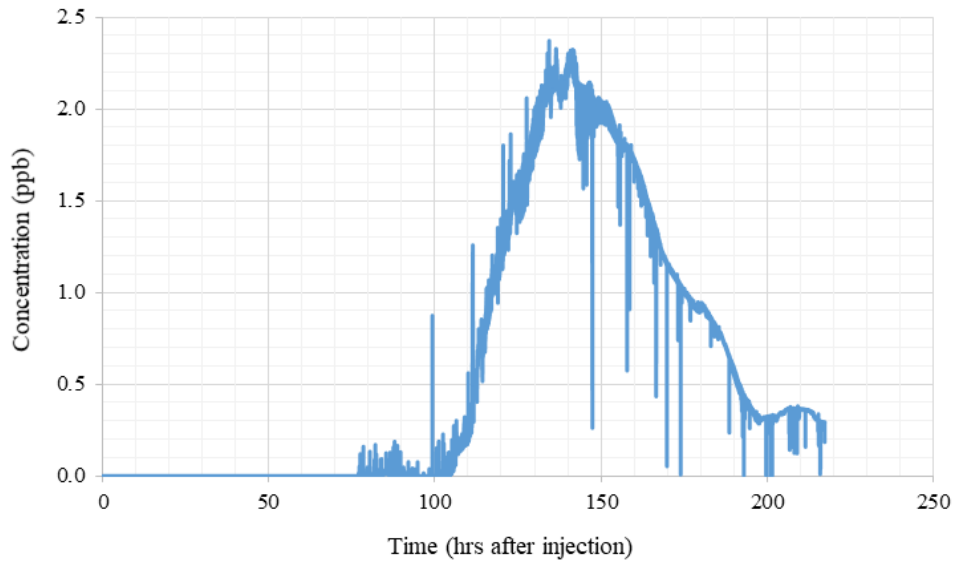


Figure C2: Concentration breakthrough curve at the wetland outlet for the 1st flow test (12th April 2016)

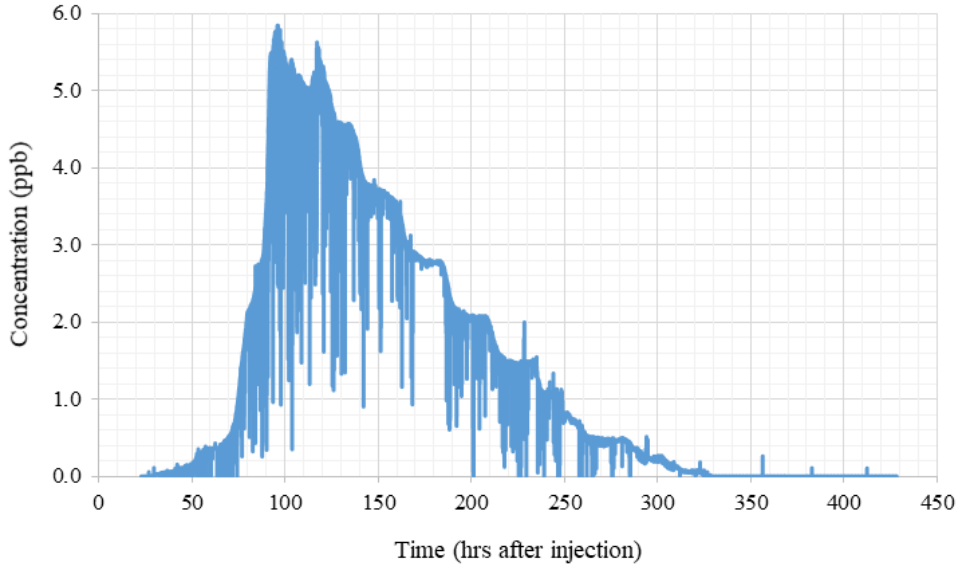


Figure C3: Concentration breakthrough curve at the wetland outlet for the 2nd flow test (2nd May 2016)

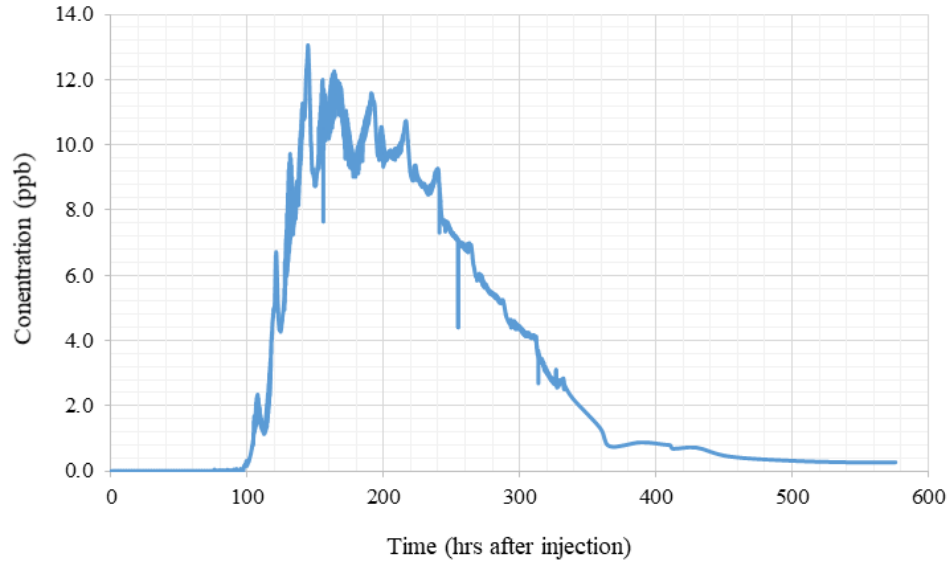


Figure C4: Concentration breakthrough curve at the wetland outlet for the 3rd flow test (22nd August 2016)

Table C3: Inlet, outlet and average daily flow rate for April, May and June 2016

Month	April 2016			May 2016			June 2016		
Date	Inflow	Outflow	(in + out)/2	Inflow	Outflow	(in + out)/2	Inflow	Outflow	(in + out)/2
1				8.1275			8.5955		
2				7.9896	8.7202	8.3549	8.6076		
3				8.1275	9.7003	8.9139	8.6319		
4				8.1383	6.5742	7.3563	8.6197		
5				8.1275	8.2098	8.1687	8.6319		
6				8.1600	8.0413	8.1007	8.6441	8.1304	8.3873
7				8.1709	7.8462	8.0086	8.6563	7.9574	8.3069
8				8.1818	7.8645	8.0232	8.6686	8.5431	8.6059
9				8.2038	7.9387	8.0713	8.6441	8.6977	8.6709
10				8.2148	7.9387	8.0768	8.6563	8.0913	8.3738
11				8.2148	7.9200	8.0674	8.6319	8.5215	8.5767
12	7.2857	6.4731	6.8794	8.2369	8.0334	8.1352	8.6441	11.5670	10.1056
13	3.7685	6.7186	5.2436	8.2258	8.3731	8.2995	8.2369	12.5597	10.3983
14	5.1689	5.0846	5.1268	8.2038	8.3731	8.2885	8.3607	8.0334	8.1971
15	5.2487	6.4114	5.8301	8.1818	10.4534	9.3176	8.3836	4.5060	6.4448
16	7.8764	8.7885	8.3325	8.1600	9.4286	8.7943	8.1928	8.5867	8.3898
17	7.8764	9.8134	8.8449	8.1818			7.8161	16.5813	12.1987
18	7.2255	5.8539	6.5397	8.2038			8.5714		
19	7.8663			8.2038			8.6686		
20	6.7032			8.2480			8.6809		
21	3.4615			8.2258			8.0845		
22	6.3750			8.2148			6.8841		
23	4.2530			20.1316			6.8076	5.5545	6.1811
24	2.4838			15.9791			6.7849	7.1314	6.9582
25	3.8131			16.2766			-	-	-
26	8.1818			15.7732			-	-	-
27	8.1709			16.7213			6.1078	5.5728	5.8403
28	8.1818			15.1485			6.6522	6.0000	6.3261
29	8.1709			8.1275			6.0118	5.4821	5.7470
30	8.2148			-			5.7573	5.6762	5.7168
31				8.2038					

Key:

sampling day introduction of AWW **Flow test running**

Table C4: Inlet, outlet and average daily flow rate for July, August and September 2016

Month	July 2016			August 2016			September		
Date	Inflow	Outflow	(in + out)/2	Inflow	Outflow	(in + out)/2	Inflow	Outflow	(in + out)/2
1	6.6522	5.4466	6.0494	5.7143	1.8545	3.7844	6.7699	4.6880	5.7290
2	5.8960	5.8949	5.8955	4.6050	5.2186	4.9118	6.8151	4.9427	5.8789
3	6.0000	4.9793	5.4897	4.0610	3.0297	3.5454	6.6958	4.3043	5.5001
4	5.6406	4.6685	5.1546	0.9171	1.3097	1.1134	6.5385	6.6260	6.5823
5	6.2449	5.3770	5.8110	5.2397	8.6530	6.9464	6.4557	7.5640	7.0099
6	5.4790	4.6750	5.0770	6.1017	5.1864	5.6441	6.3750	5.7051	6.0401
7	6.5736	5.5728	6.0732	5.1777	3.3294	4.2536	6.4353	4.8996	5.6675
8	6.6958	7.3015	6.9987	5.2487	2.8647	4.0567	6.3684	4.2128	5.2906
9	6.8456	4.9500	5.8978	4.7925	3.3493	4.0709	6.4353	4.6815	5.5584
10	4.8456	3.1080	3.9768	4.9315	7.4800	6.2058	6.6306	4.8642	5.7474
11	4.7962	2.7058	3.7510	3.9974	2.7036	3.3505	6.3950	4.5000	5.4475
12	5.3637	3.8077	4.5857	3.5233	4.3043	3.9138	6.9467	3.3065	5.1266
13	6.0000	5.6762	5.8381	2.4324	3.0768	2.7546	7.0915	3.1370	5.1143
14	7.4002	8.2703	7.8353	0.5849	-	0.5849	7.0426	3.0684	5.0555
15	6.1078	6.2103	6.1591	2.1779	-	2.1779	6.7624	3.3294	5.0459
16	6.0059	4.7813	5.3936	4.4967	5.1944	4.8456	6.1881	6.1311	6.1596
17	5.7955	6.6000	6.1978	6.4353	5.3684	5.9019	6.6958	6.1989	6.4474
18	8.0952	6.3629	7.2291	5.5235	4.9793	5.2514	6.7032	6.2449	6.4741
19	7.6025	6.1536	6.8781	15.8961	14.8938	15.3950	6.6739	4.5984	5.6362
20	6.1964	4.1918	5.1941	20.1980	21.5769	20.8875	6.6594	5.7935	6.2265
21	5.8790	5.1311	5.5051	19.1250	19.0169	19.0710	6.5948	6.2218	6.4083
22	6.8304	5.1077	5.9690	8.3379	15.5115	11.9247	6.4831	5.6954	6.0893
23	5.7196	3.7358	4.7277	6.2195	11.2575	8.7385	6.6594	5.4554	6.0574
24	5.2895	3.3327	4.3111	6.5315	3.9929	5.2622	7.0023	6.3271	6.6647
25	5.3637	3.9140	4.6389	6.5665	3.5544	5.0605	6.9625	5.8438	6.4032
26	6.0296	6.7590	6.3943	6.5665	3.1109	4.8387	6.9943	6.5614	6.7779
27	5.3826	5.6762	5.5294	6.4557	3.6389	5.0473	7.2598	6.9402	7.1000
28	5.4937	4.2716	4.8827	6.3950	3.0297	4.7124	7.1831	6.1536	6.6684
29	5.3663	1.9169	3.6416	6.6739	4.0215	5.3477	7.1163	5.0617	6.0890
30	1.2341	0.9915	1.1128	6.6594	4.5121	5.5858	6.9545	7.1314	7.0430
31	1.1930	-	-	6.6306	4.1970	5.4138			

Key:

sampling day introduction of AWW **Flow test running**

Table C5: Summary of the Matlab code inputs for the flow tests performed at three depths at port 1 in the pilot-scale CWs at the Helmholtz UFZ in 2016

Variable Description	Variable name	*(unit)*	Port 1, Depth 1 (12cm) 12th April	Port 1, Depth 2 (24cm) 12th April	Port 1, Depth 3 (36cm) 12th April
MasterDataProc.m					
raw data mV file	**flu_file**		1_1_f023.mv	1_2_f024.mv	1_3_f025.mv
fluorometer no.	**f**		623	624	625
calibration conc. Uranine	**c_cal_Uranine**	*(ppb)*	70	70	70
calibration window Uranine	**ind_ura**		143 : 145	150 : 151	139 : 140
calibration window baseline	**ind_blank**		1309 : 1546	1393 : 1590	791 : 912
date/time of injection	**P1I**	*[YYYY MM DD hh mm ss]*	2016 04 12 12 21 20	2016 04 12 12 21 20	2016 04 12 12 21 20
date/time of end of flow test					
chosen data end	**P1F**	*[YYYY MM DD hh mm ss]*	2016 04 18 09 43 30	2016 04 18 09 43 30	2016 04 16 16 35 50
fluoro data end		*[YYYY MM DD hh mm ss]*	2016 04 18 09 43 30	2016 04 18 09 43 30	2016 04 15 16 45 10
index - start of experimental data	**P1S_ind**		1389	608	879
Tail fit required? (Y/N)			N	N	Y
2_#_FilterPlot.fig					
x values for filter plot	**domain (x)**	*(hrs since injection)*	[0 150]	[0 150]	[0 100]
y values for filter plot	**range (y)**	*(ppb)*	[0 12]	[0 12]	[0 10]
Figure (3)					
Co-ordinate - start of tail fit			-	-	(69.7, 2.768)
Index of coordinate	**ind**		-	-	25072
MasterTailFit.m Params returned by MATLAB 'fit' fcn with 'exp1' specified					y = a*exp(b*x)
C = a*exp(b*t)	**a**		-	-	9.892E+05
C = a*exp(b*t)	**b**		-	-	-0.1836
Time of fluoro data termination	**t_term**	*(hr)*	-	-	76.3972
Conc. @ t_term (read from **F1** matrix)		*(ppb)*	-	-	0.8075
Index @ t_term (size of **E1**)			-	-	27484
Time of fluoro data termination	**t_end**	*(hr)*	-	-	100.242
Conc. @ t_end (read from **F1** matrix)		*(ppb)*	-	-	0.0101
Index @ t_end (read from **F1** matrix)			-	-	36000

Variable Description	Variable name	*(unit)*	Port 1, Depth 1 (12cm) 12th April	Port 1, Depth 2 (24cm) 12th April	Port 1, Depth 3 (36cm) 12th April
Inflow.m					
data file			1_1_BTC_F1	1_2_BTC_F1	1_3_BTC_F1
date/time of injection	**t_inj**	*[YYYY MM DD hh mm ss]*	2016 04 12 12 21 20	2016 04 12 12 21 20	2016 04 12 12 21 20
date/time of end of flow test	**t_end**	*[YYYY MM DD hh mm ss]*	2016 04 18 09 43 30	2016 04 18 09 43 30	2016 04 18 09 43 30
Excel data log file			LOG1.xlsx	LOG1.xlsx	LOG1.xlsx
Date/time data from *LOGn.xlsx*	**Log_in**	*(Excel date/time)*	A2:A478	A2:A479	A2:A287
Flow rate data from *LOGn.xlsx*	**q_in**	*(L/hr)*	C2:C478	C2:C479	C2:C287
Outflow.m					
data file			1_1_BTC_F1	1_2_BTC_F1	1_3_BTC_F1
date/time of injection	**t_inj**	*[YYYY MM DD hh mm ss]*	2016 04 12 12 21 20	2016 04 12 12 21 20	2016 04 12 12 21 20
date/time of end of flow test	**t_end**	*[YYYY MM DD hh mm ss]*	2016 04 18 09 43 30	2016 04 18 09 43 30	2016 04 18 09 43 30
Excel data log file			LOG1.xlsx	LOG1.xlsx	LOG1.xlsx
Date/time data from *LOGn.xlsx*	**Log_out**	*(Excel date/time)*	E2:E987	E2:E988	E2:E584
Flow rate data from *LOGn.xlsx*	**q_out**	*(L/hr)*	G2:G987	G2:G988	G2:G584
MasterCalcs_			**(1) _SS.m** / **(2) _NSS.m**	**(1) _SS.m** / **(2) _NSS.m**	**(1) _SS.m** / **(2) _NSS.m**
data file			1_1_BTC_F1	1_2_BTC_F1	1_3_BTC_F1
inlet flow rate file from *Inflow.m*			1_1_inflow	1_2_inflow	1_3_inflow
outlet flow rate file from *Outflow.m*			1_1_outflow	1_2_outflow	1_3_outflow
			- / 1_1_BTC_Data	- / 1_2_BTC_Data	- / 1_3_BTC_Data
mass of Uranine injected	**M**	*(mg)*	3	3	3
distance to sample port	**L**	*(m)*	1.08	1.08	1.08
water level	**h_h20**	*(m)*	0.5	0.5	0.5

Table C6: Summary of the Matlab code inputs for the flow tests performed at three depths at port 2 in the pilot-scale CWs at the Helmholtz UFZ in 2016

Variable Description	Variable name	*(unit)*	Port 2, Depth 1 (12cm) 2nd May	Port 2, Depth 2 (24cm) 2nd May	Port 2, Depth 3 (36cm) 2nd May
MasterDataProc.m					
raw data mV file	**flu_file**		2_1_f023.mv	2_2_f024.mv	2_3_f025.mv
fluorometer no.	**f**		623	624	625
calibration conc. Uranine	**c_cal_Uranine**	*(ppb)*	70	70	70
calibration window Uranine	**ind_ura**		157 : 158	158 : 159	136 : 137
calibration window baseline	**ind_blank**		1446 : 1896	1264 : 1559	1515 : 1906
date/time of injection	**P1I**	*[YYYY MM DD hh mm ss]*	2016 05 02 16 52 00	2016 05 02 16 52 00	2016 05 02 16 52 00
date/time of end of flow test					
chosen data end	**P1F**	*[YYYY MM DD hh mm ss]*	2015 05 11 07 41 10	2016 05 11 07 41 10	2016 05 11 07 41 10
fluoro data end		*[YYYY MM DD hh mm ss]*	2016 05 11 07 41 10	2016 05 11 07 41 10	2016 05 11 07 41 10
index - start of experimental data	**P1S_ind**		1174	746	1154
Tail fit required? (Y/N)			**N**	**N**	**N**
2_#_FilterPlot.fig					
x values for filter plot	**domain (x)**	*(hrs since injection)*	[0 220]	[0 220]	[0 220]
y values for filter plot	**range (y)**	*(ppb)*	[0 30]	[0 40]	[0 55]
Inflow.m					
data file			2_1_BTC_F1	2_2_BTC_F1	2_3_BTC_F1
date/time of injection	**t_inj**	*[YYYY MM DD hh mm ss]*	2016 05 02 16 52 00	2016 05 02 16 52 00	2016 05 02 16 52 00
date/time of end of flow test	**t_end**	*[YYYY MM DD hh mm ss]*	2016 05 11 07 41 10	2016 05 11 07 41 10	2016 05 11 07 41 10
Excel data log file			LOG2.xlsx	LOG2.xlsx	LOG2.xlsx
Date/time data from *LOGn.xlsx*	**Log_in**	*(Excel date/time)*	A2 : A994	A2 : A994	A2 : A994
Flow rate data from *LOGn.xlsx*	**q_in**	*(L/hr)*	C2 : C994	C2 : C994	C2 : C994
Outflow.m					
data file			2_1_BTC_F1	2_2_BTC_F1	2_3_BTC_F1
date/time of injection	**t_inj**	*[YYYY MM DD hh mm ss]*	2016 05 02 16 52 00	2016 05 02 16 52 00	2016 05 02 16 52 00
date/time of end of flow test	**t_end**	*[YYYY MM DD hh mm ss]*	2016 05 11 07 41 10	2016 05 11 07 41 10	2016 05 11 07 41 10
Excel data log file			LOG2.xlsx	LOG2.xlsx	LOG2.xlsx
Date/time data from *LOGn.xlsx*	**Log_out**	*(Excel date/time)*	E4 : E1161	E4 : E1161	E4 : E1161
Flow rate data from *LOGn.xlsx*	**q_out**	*(L/hr)*	G4 : G1161	G4 : G1161	G4 : G1161

Variable Description	Variable name	*(unit)*	Port 2, Depth 1 (12cm) 2nd May		Port 2, Depth 2 (24cm) 2nd May		Port 2, Depth 3 (36cm) 2nd May	
MasterCalcs.m			**(1) _SS.m**	**(2) _NSS.m**	**(1) _SS.m**	**(2) _NSS.m**	**(1) _SS.m**	**(2) _NSS.m**
data file			2_1_BTC_F1		2_2_BTC_F1		2_3_BTC_F1	
inlet flow rate file from *Inflow.m*			2_1_inflow.mat		2_2_inflow.mat		2_3_inflow.mat	
outlet flow rate file from *Outflow.m*			2_1_outflow.mat		2_2_outflow.mat		2_3_outflow.mat	
other data required			-	2_1_BTC_data	-	2_2_BTC_data	-	2_3_BTC_data
mass of Uranine injected	**M**	*(mg)*	15		15		15	
distance to sample port	**L**	*(m)*	2.255		2.255		2.255	
water level	**h_h20**	*(m)*	0.44		0.44		0.44	

Table C7: Summary of the Matlab code inputs for the flow tests performed at three depths at port 3 in the pilot-scale CWs at the Helmholtz UFZ in 2016

Variable Description	Variable name	*(unit)*	Port 3, Depth 1 (12cm) 7th November	Port 3, Depth 2 (24cm) 22nd August	Port 3, Depth 3 (36cm) 6th June
MasterDataProc.m					
raw data mV file	**flu_file**		3_1_f025.mv	3_2_f023.mv	3_3_f051.mv
fluorometer no.	**f**		625	623	651
calibration conc. Uranine	**c_cal_Uranine**	*(ppb)*	70	70	70
calibration window Uranine	**ind_ura**		196:197	108:109	104 : 105
calibration window baseline	**ind_blank**		2000:2090	4166:4886	3750:3850
date/time of injection	**P1I**	*[YYYY MM DD hh mm ss]*	2016 11 07 15 15 00	2016 08 22 12 35 00	2016 06 06 13 02 00
date/time of end of flow test					
chosen data end	**P1F**	*[YYYY MM DD hh mm ss]*	2016 11 14 13 04 20	2016 09 16 10 11 50	2016 06 22 06 43 20
fluoro data end		*[YYYY MM DD hh mm ss]*	2016 11 14 13 04 20	(2016 09 05 09 34 50)	(2016 06 15 16 23 00)
index - start of experimental data	**P1S_ind**		2239	766	3319
Tail fit required? (Y/N)			N	Y	Y
2_#_FilterPlot.fig					
x values for filter plot	**domain (x)**	*(hrs since injection)*	[0 180]	[0 600]	[0 400]
y values for filter plot	**range (y)**	*(ppb)*	[0 7]	[0 30]	[0 60]
Figure (3)					
Co-ordinate - start of tail fit			-	-	-
Index of coordinate	**ind**		-	82322	49326
MasterTailFit.m					
Params returned by MATLAB 'fit' fcn with 'exp1' specified				y = a*exp(b*x)	y = a*exp(b*x)
C = a*exp(b*t)	**a**		-	66.93	97.54
C = a*exp(b*t)	**b**		-	-0.01474	-0.02432
Time of fluoro data termination	**t_term**	*(hr)*	-	576.0333	219.3472
Conc. @ t_term (read from **F1** matrix)		*(ppb)*	-	0.0137	0.306
Index @ t_term (size of **E1**)			-	119796	78667
Time of fluoro data termination	**t_end**	*(hr)*	-	597.64	377.69
Conc. @ t_end (read from **F1** matrix)		*(ppb)*	-	0.01	0.01
Index @ t_end (read from **F1** matrix)			-	214287	135218

Variable Description	Variable name	*(unit)*	Port 3, Depth 1 (12cm) 7th November		Port 3, Depth 2 (24cm) 22nd August		Port 3, Depth 3 (36cm) 6th June	
Inflow.m								
data file			3_1_BTC_F1		3_2_BTC_F1		3_3_BTC_F1	
date/time of injection	**t_inj**	*[YYYY MM DD hh mm ss]*	2016 11 07 15 15 00		2016 08 22 12 35 00		2016 06 06 13 02 00	
date/time of end of flow test	**t_end**	*[YYYY MM DD hh mm ss]*	2016 11 14 13 04 20		2016 09 16 10 11 50		2016 06 22 06 43 20	
Excel data log file			LOG8-2.xlsx		LOG7iii.xlsx		LOG4.xlsx	
Date/time data from *LOGn.xlsx*	**Log_in**	*(Excel date/time)*	A3:A750		A3:A2213		A3:A1870	
Flow rate data from *LOGn.xlsx*	**q_in**	*(L/hr)*	C3:C750		C3:C2213		C3:C1870	
Outflow.m								
data file			3_1_BTC_F1		3_2_BTC_F1		3_3_BTC_F1	
date/time of injection	**t_inj**	*[YYYY MM DD hh mm ss]*	2016 11 07 15 15 00		2016 08 22 12 35 00		2016 06 06 13 02 00	
date/time of end of flow test	**t_end**	*[YYYY MM DD hh mm ss]*	2016 11 14 13 04 20		2016 09 16 10 11 50		2016 06 22 06 43 20	
Excel data log file			LOG8-2.xlsx		LOG7iii.xlsx		LOG4.xlsx	
Date/time data from *LOGn.xlsx*	**Log_out**	*(Excel date/time)*	E3:E1579		E3:E2677		E3:E3722	
Flow rate data from *LOGn.xlsx*	**q_out**	*(L/hr)*	G3:G1579		G3:G2677		G3:G3722	
MasterCalcs.m			**(1) _SS.m**	**(2) _NSS.m**	**(1) _SS.m**	**(2) _NSS.m**	**(1) _SS.m**	**(2) _NSS.m**
data file			3_1_BTC_F1		3_2_BTC_F1		3_3_BTC_F1	
inlet flow rate file from *Inflow.m*			3_1_inflow.mat		3_2_inflow.mat		3_3_inflow.mat	
outlet flow rate file from *Outflow.m*			3_1_outflow.mat		3_2_outflow.mat		3_3_outflow.mat	
			-	3_1_BTC_data	-	3_2_BTC_data	-	3_3_BTC_data
mass of Uranine injected	**M**	*(mg)*	30.4		30		30.2	
distance to sample port	**L**	*(m)*	2.970		2.970		2.970	
water level	**h_h20**	*(m)*	0.44		0.44		0.44	
figure (28) domain	**xlim**		[0 3.0]	[0 3.5]	[0 4.5]	[0 5.5]	[0 5.0]	[0 7.0]
index at which θ = 1	**THETA_ind**		20734	-	49039	-	27590	-

Table C8: Summary of the Matlab code inputs for the flow tests performed at three depths at port 4 in the pilot-scale CWs at the Helmholtz UFZ in 2016

Variable Description	Variable name	*(unit)*	Port 4, Depth 1 (12cm) 6th June	Port 4, Depth 2 (24cm) 6th June	Port 4, Depth 3 (36cm) 6th June
MasterDataProc.m					
raw data mV file	**flu_file**		4_1_f023.mv	4_2_f024.mv	4_3_f025.mv
fluorometer no.	**f**		623	624	625
calibration conc. Uranine	**c_cal_Uranine**	*(ppb)*	70	70	70
calibration window Uranine	**ind_ura**		106 : 107	105 : 106	107 : 108
calibration window baseline	**ind_blank**		3637 : 4346	3396 : 4037	4931 : 5200
date/time of injection	**P1I**	*[YYYY MM DD hh mm ss]*	2016 06 06 13 02 00	2016 06 06 13 02 00	2016 06 06 13 02 00
date/time of end of flow test					
chosen data end	**P1F**	*[YYYY MM DD hh mm ss]*	2016 06 21 05 50 40	2016 06 21 00 30 30	2016 06 20 13 36 40
fluoro data end		*[YYYY MM DD hh mm ss]*	(2016 06 15 16 23 00)	(2016 06 15 16 22 50)	(2016 06 15 16 23 00)
index - start of experimental data	**P1S_ind**		1284	0	0
Tail fit required? (Y/N)			Y	Y	Y
2_#_FilterPlot.fig					
x values for filter plot	**domain (x)**	*(hrs since injection)*	[0 400]	[0 350]	[0 350]
y values for filter plot	**range (y)**	*(ppb)*	[0 55]	[0 55]	[0 70]
Figure (3)					
Co-ordinate - start of tail fit				(74.36, 20.45)	(70.64, 25.04)
Index of coordinate	**ind**		23944	26752	25412
MasterTailFit.m Params returned by MATLAB 'fit' fcn with 'exp1' specified			y = a*exp(b*x)	y = a*exp(b*x)	y = a*exp(b*x)
C = a*exp(b*t)	**a**		165.3	158.4	189.9
C = a*exp(b*t)	**b**		-0.02753	-0.02783	-0.02927
Time of fluoro data termination	**t_term**	*(hr)*	219.3472	219.3472	219.3472
Conc. @ t_term (read from **F1** matrix)		*(ppb)*	0.5707	0.5437	0.4831
Index @ t_term (size of **E1**)			75398	78909	78664
Time of fluoro data termination	**t_end**	*(hr)*	352.812	347.4752	336.5776
Conc. @ t_end (read from **F1** matrix)		*(ppb)*	0.0100	0.0100	0.0100
Index @ t_end (read from **F1** matrix)			123064	124669	120532

Variable Description	Variable name	*(unit)*	Port 4, Depth 1 (12cm) 6th June		Port 4, Depth 2 (24cm) 6th June		Port 4, Depth 3 (36cm) 6th June	
Inflow.m								
data file			4_1_BTC_F1		4_2_BTC_F1		4_3_BTC_F1	
date/time of injection	**t_inj**	*[YYYY MM DD hh mm ss]*	2016 06 06 13 02 00		2016 06 06 13 02 00		2016 06 06 13 02 00	
date/time of end of flow test	**t_end**	*[YYYY MM DD hh mm ss]*	2016 06 21 05 50 40		2016 06 21 00 30 30		2016 06 20 13 36 40	
Excel data log file			LOG4.xlsx		LOG4.xlsx		LOG4.xlsx	
Date/time data from *LOGn.xlsx*	**Log_in**	*(Excel date/time)*	A3:A1759		A3:A1731		A3:A1675	
Flow rate data from *LOGn.xlsx*	**q_in**	*(L/hr)*	C3:C1759		C3:C1731		C3:C1675	
Outflow.m								
data file			4_1_BTC_F1		4_2_BTC_F1		4_3_BTC_F1	
date/time of injection	**t_inj**	*[YYYY MM DD hh mm ss]*	2016 06 06 13 02 00		2016 06 06 13 02 00		2016 06 06 13 02 00	
date/time of end of flow test	**t_end**	*[YYYY MM DD hh mm ss]*	2016 06 21 05 50 40		2016 06 21 00 30 30		2016 06 20 13 36 40	
Excel data log file			LOG4.xlsx		LOG4.xlsx		LOG4.xlsx	
Date/time data from *LOGn.xlsx*	**Log_out**	*(Excel date/time)*	E3:E3524		E3:E3468		E3:E3374	
Flow rate data from *LOGn.xlsx*	**q_out**	*(L/hr)*	G3:G3524		G3:G3468		G3:G3374	
MasterCalcs.m			**(1) _SS.m**	**(2) _NSS.m**	**(1) _SS.m**	**(2) _NSS.m**	**(1) _SS.m**	**(2) _NSS.m**
data file			4_1_BTC_F1		4_2_BTC_F1		4_3_BTC_F1	
inlet flow rate file from *Inflow.m*			4_1_inflow		4_2_inflow		4_3_inflow	
outlet flow rate file from *Outflow.m*			4_1_outflow		4_2_outflow		4_3_outflow	
			-	4_1_BTC_Data	-	4_2_BTC_Data	-	4_3_BTC_Data
mass of Uranine injected	**M**	*(mg)*	30.2		30.2		30.2	
distance to sample port	**L**	*(m)*	2.970		2.970		2.970	
water level	**h_h20**	*(m)*	0.44		0.44		0.44	
figure (28) domain	**xlim**		[0 5.0]	[0 7.0]	[0 6.0]	[0 7.0]	[0 6.0]	[0 7.0]
index at which θ = 1	**THETA_ind**		23315	-	23962	-	22705	-

Table C9: Summary of the Matlab code inputs for the flow tests performed at three depths at port 5 in the pilot-scale CWs at the Helmholtz UFZ in 2016

Variable Description	Variable name	*(unit)*	Port 5, Depth 1 (12cm) 20th September	Port 5, Depth 2 (24cm) 20th September	Port 5, Depth 3 (36cm) 20th September
MasterDataProc.m					
raw data mV file	**flu_file**		5_1_f023.mv	5_2_f024.mv	5_3_f025.mv
fluorometer no.	**f**		623	624	625
calibration conc. Uranine	**c_cal_Uranine**	*(ppb)*	70	70	70
calibration window Uranine	**ind_ura**		207 : 209	157 : 158	190 : 191
calibration window baseline	**ind_blank**		2100:2200	2489:2845	4323:4562
date/time of injection	**P1I**	*[YYYY MM DD hh mm ss]*	2016 09 20 12 07 00	2016 09 20 12 07 00	2016 09 20 12 07 00
date/time of end of flow test					
chosen data end	**P1F**	*[YYYY MM DD hh mm ss]*	2016 09 30 18 52 00	2016 09 30 09 07 10	2016 09 30 18 52 00
fluoro data end		*[YYYY MM DD hh mm ss]*	2016 09 30 18 52 00	**2016 09 30 09 07 10**	2016 09 30 18 52 00
index - start of experimental data	**P1S_ind**		8591	8389	4715
Tail fit required? (Y/N)			N	N	N
2_#_FilterPlot.fig					
x values for filter plot	**domain (x)**	*(hrs since injection)*	[0 250]	[0 250]	[0 250]
y values for filter plot	**range (y)**	*(ppb)*	[0 8]	[0 8]	[0 12]
Inflow.m					
data file			5_1_BTC_F1	5_2_BTC_F1	5_3_BTC_F1
date/time of injection	**t_inj**	*[YYYY MM DD hh mm ss]*	2016 09 20 12 07 00	2016 09 20 12 07 00	2016 09 20 12 07 00
date/time of end of flow test	**t_end**	*[YYYY MM DD hh mm ss]*	2016 09 30 18 52 00	2016 09 30 09 07 10	2016 09 30 18 52 00
Excel data log file			LOG5.xlsx	LOG5.xlsx	LOG5.xlsx
Date/time data from *LOGn.xlsx*	**Log_in**	*(Excel date/time)*	A3:A998	A3:A957	A3:A998
Flow rate data from *LOGn.xlsx*	**q_in**	*(L/hr)*	C3:C998	AC3:C957	C3:C998
Outflow.m					
data file			5_1_BTC_F1	5_2_BTC_F1	5_3_BTC_F1
date/time of injection	**t_inj**	*[YYYY MM DD hh mm ss]*	2016 09 20 12 07 00	2016 09 20 12 07 00	2016 09 20 12 07 00
date/time of end of flow test	**t_end**	*[YYYY MM DD hh mm ss]*	2016 09 30 18 52 00	2016 09 30 09 07 10	2016 09 30 18 52 00
Excel data log file			LOG5.xlsx	LOG5.xlsx	LOG5.xlsx
Date/time data from *LOGn.xlsx*	**Log_out**	*(Excel date/time)*	E3:E1605	E3:E1532	E3:E1605

Variable Description	Variable name	*(unit)*	Port 5, Depth 1 (12cm) 20th September		Port 5, Depth 2 (24cm) 20th September		Port 5, Depth 3 (36cm) 20th September	
MasterCalcs.m			**(1) _SS.m**	**(2) _NSS.m**	**(1) _SS.m**	**(2) _NSS.m**	**(1) _SS.m**	**(2) _NSS.m**
data file			5_1_BTC_F1		5_2_BTC_F1		5_3_BTC_F1	
inlet flow rate file from *Inflow.m*			5_1_inflow		5_2_inflow		5_3_inflow	
outlet flow rate file from *Outflow.m*			5_1_outflow		5_2_outflow		5_3_outflow	
			-	5_1_BTC_Data	-	5_2_BTC_Data	-	5_3_BTC_Data
mass of Uranine injected	**M**	*(mg)*	30		30		30	
distance to sample port	**L**	*(m)*	3.730		3.730		3.730	
water level	**h_h20**	*(m)*	0.44		0.44		0.44	
figure (28) domain	**xlim**		[0 2.5]	[0 2.5]	[0 2.5]	[0 2.5]	[0 3.0]	[0 3.0]
index at which θ = 1	**THETA_ind**		36790	-	36874	-	33492	-

Table C10: Summary of the Matlab code inputs for the flow tests performed at three depths at port 6 in the pilot-scale CWs at the Helmholtz UFZ in 2016

Variable Description	Variable name	*(unit)*	Port 6, Depth 1 (12cm) 17th October 2016	Port 6, Depth 2 (24cm) 17th October 2016	Port 6, Depth 3 (36cm) 17th October 2016
MasterDataProc.m					
raw data mV file	**flu_file**		6_1_f023.mv	6_2_f024.mv	6_3_f025.mv
fluorometer no.	**f**		623	624	625
calibration conc. Uranine	**c_cal_Uranine**	*(ppb)*	70	70	70
calibration window Uranine	**ind_ura**		183 : 184	194 : 195	196 : 197
calibration window baseline	**ind_blank**		683:993	2043:2409	2081:2429
date/time of injection	**P1I**	*[YYYY MM DD hh mm ss]*	2016 10 17 17 38 00	2016 10 17 17 38 00	2016 10 17 17 38 00
date/time of end of flow test					
chosen data end	**P1F**	*[YYYY MM DD hh mm ss]*	2016 10 28 17 05 30	2016 10 28 17 05 30	2016 10 28 17 05 30
fluoro data end		*[YYYY MM DD hh mm ss]*	(2016 10 28 17 06 40)	(2016 10 28 17 06 00)	2016 10 28 17 05 30
index - start of experimental data	**P1S_ind**		992	0	2356
Tail fit required? (Y/N)			N	N	N
2_#_FilterPlot.fig					
x values for filter plot	**domain (x)**	*(hrs since injection)*	[0 300]	[0 300]	[0 300]
y values for filter plot	**range (y)**	*(ppb)*	[0 2.5]	[0 5]	[0 6]
Inflow.m					
data file			6_1_BTC_F1	6_2_BTC_F2	6_3_BTC_F3
date/time of injection	**t_inj**	*[YYYY MM DD hh mm ss]*	2016 10 17 17 38 00	2016 10 17 17 38 00	2016 10 17 17 38 00
date/time of end of flow test	**t_end**	*[YYYY MM DD hh mm ss]*	2016 10 28 17 05 30	2016 10 28 17 05 30	2016 10 28 17 05 30
Excel data log file			LOG6.xlsx	LOG6.xlsx	LOG6.xlsx
Date/time data from *LOGn.xlsx*	**Log_in**	*(Excel date/time)*	A3:A883	A3:A883	A3:A883
Flow rate data from *LOGn.xlsx*	**q_in**	*(L/hr)*	C3:C883	C3:C883	C3:C883
Outflow.m					
data file			6_1_BTC_F1	6_2_BTC_F2	6_3_BTC_F3
date/time of injection	**t_inj**	*[YYYY MM DD hh mm ss]*	2016 10 17 17 38 00	2016 10 17 17 38 00	2016 10 17 17 38 00
date/time of end of flow test	**t_end**	*[YYYY MM DD hh mm ss]*	2016 10 28 17 05 30	2016 10 28 17 05 30	2016 10 28 17 05 30
Excel data log file			LOG6.xlsx	LOG6.xlsx	LOG6.xlsx
Date/time data from *LOGn.xlsx*	**Log_out**	*(Excel date/time)*	E3:E2139	E3:E2139	E3:E2139
Flow rate data from *LOGn.xlsx*	**q_out**	*(L/hr)*	G3:G2139	G3:G2139	G3:G2139

Variable Description	Variable name	*(unit)*	Port 6, Depth 1 (12cm) 17th October 2016		Port 6, Depth 2 (24cm) 17th October 2016		Port 6, Depth 3 (36cm) 17th October 2016	
MasterCalcs.m			**(1) _SS.m**	**(2) _NSS.m**	**(1) _SS.m**	**(2) _NSS.m**	**(1) _SS.m**	**(2) _NSS.m**
data file			6_1_BTC_F1		6_2_BTC_F2		6_3_BTC_F3	
inlet flow rate file from *Inflow.m*			6_1_inflow		6_2_inflow		6_3_inflow	
outlet flow rate file from *Outflow.m*			6_1_outflow		6_2_outflow		6_3_outflow	
			-	6_1_BTC_Data	-	6_2_BTC_Data	-	6_3_BTC_Data
mass of Uranine injected	**M**	*(mg)*	31.8		31.8		31.8	
distance to sample port	**L**	*(m)*	5.270		5.270		5.270	
water level	**h_h20**	*(m)*	0.44		0.44		0.44	
figure (28) domain	**xlim**		[0 2.5]	[0 2.5]	[0 2.5]	[0 2.5]	[0 2.5]	[0 2.5]
index at which θ = 1	**THETA_ind**		46228	-	49169	-	46083	-

Table C11: Summary of the Matlab code inputs for the flow tests performed at three depths at port 7 in the pilot-scale CWs at the Helmholtz UFZ in 2016

Variable Description	Variable name	*(unit)*	7i, Depth 1 (12cm) 12th April 2016	7ii, Depth 2 (24cm) 2nd May 2016	7iii, Depth 3 (36cm) 22nd August 2016
MasterDataProc.m					
raw data mV file	**flu_file**		7i_f025	7ii_f051	7iii_f025
fluorometer no.	**f**		625	651	625
calibration conc. Uranine	**c_cal_Uranine**	*(ppb)*	70	70	70
calibration window Uranine	**ind_ura**		139 : 140	138 : 139	104 : 105
calibration window baseline	**ind_blank**		791 : 912	2193 : 2366	27220 : 32820
date/time of injection	**P1I**	*[YYYY MM DD hh mm ss]*	2016 04 12 12 21 20	2016 05 02 16 52 00	2016 08 22 12 35 00
date/time of end of flow test					
chosen data end	**P1F**	*[YYYY MM DD hh mm ss]*	2016 04 24 17 52 00	2016 05 20 13 11 10	2016 09 23 18 46 30
fluoro data end		*[YYYY MM DD hh mm ss]*	(2016 04 21 13 47 10)	(2016 05 20 13 11 10)	(2016 09 05 09 36 10)
index - start of experimental data	**P1S_ind**		0	408	27111
Tail fit required? (Y/N)			Y	N	Y
2_#_FilterPlot.fig					
x values for filter plot	**domain (x)**	*(hrs since injection)*	[0 300]	[0 450]	[0 800]
y values for filter plot	**range (y)**	*(ppb)*	[0 2.5]	[0 6]	[0 14]
Figure (3)					
Co-ordinate - start of tail fit			(181.2, 0.9148)	-	(270.3, 6.0541)
Index of coordinate	**ind**		37394	-	97217
MasterTailFit.m Params returned by MATLAB 'fit' fcn with 'exp1' specified					
C = a*exp(b*t)	**a**		1072	-	195.1
C = a*exp(b*t)	**b**		-0.03946	-	-0.01276
Time of fluoro data termination	**t_term**	*(hr)*	217.4306	-	575.9500
Conc. @ t_term (read from **F1** matrix)		*(ppb)*	0.2444	-	0.1255
Index @ t_term (size of **E1**)			50428	-	119802
Time of fluoro data termination	**t_end**	*(hr)*	293.5239	-	774.1914
Conc. @ t_end (read from **F1** matrix)		*(ppb)*	0.0100	-	0.0100
Index @ t_end (read from **F1** matrix)			77604	-	277351

Variable Description	Variable name	*(unit)*	7i, Depth 1 (12cm) 12th April 2016		7ii, Depth 2 (24cm) 2nd May 2016		7iii, Depth 3 (36cm) 22nd August 2016	
Inflow.m								
data file			7i_BTC_F1		7ii_BTC_F1		7iii_BTC_F1	
date/time of injection	**t_inj**	*[YYYY MM DD hh mm ss]*	2016 04 12 12 21 20		2016 05 02 16 52 00		2016 08 22 12 35 00	
date/time of end of flow test	**t_end**	*[YYYY MM DD hh mm ss]*	2016 04 24 17 52 40		2016 05 11 13 11 10		2016 09 23 18 46 30	
Excel data log file			LOG1.xlsx		LOG2.xlsx		LOG7iii.xlsx	
Date/time data from *LOGn.xlsx*	**Log_in**	*(Excel date/time)*	A2 : A948		A2 : A2064		A3 : A2725	
Flow rate data from *LOGn.xlsx*	**q_in**	*(L/hr)*	C2 : C948		C2 : C2064		C3 : C2725	
Adjusted LOG data start time		*[YYYY MM DD hh mm ss]*	2016 04 15 17 13 50		2016 05 03 15 46 10		-	
Adjusted Date/time data from LOGn.xlsx	**Log_in**	*(Excel date/time)*	A178 : A949		A111 : A2065		-	
Adjusted flow rate data from LOGn.xlsx	**q_in**	*(L/hr)*	C178 : C949		C111 : C2065		-	
Flow rate @ t_inj	**Q_in(1,1)**	*(L/hr)*	6.8000		8.3836		-	
Outflow.m								
data file			7i_BTC_F1		7ii_BTC_F1		7iii_BTC_F1	
date/time of injection	**t_inj**	*[YYYY MM DD hh mm ss]*	2016 04 12 12 21 20		2016 05 02 16 52 00		2016 08 22 12 35 00	
date/time of end of flow test	**t_end**	*[YYYY MM DD hh mm ss]*	2016 04 24 17 52 40		2016 05 11 13 11 10		2016 09 23 18 46 30	
Excel data log file			LOG1.xlsx		LOG2.xlsx		LOG7iii.xlsx	
Date/time data from *LOGn.xlsx*	**Log_out**	*(Excel date/time)*	E2 : E1716		E4 : E3668		E3 : E3635	
Flow rate data from *LOGn.xlsx*	**q_out**	*(L/hr)*	G2 : G1716		G4 : G3668		G3 : G3635	
Adjusted LOG data start time		*[YYYY MM DD hh mm ss]*	2016 04 15 17 13 50		2016 05 03 15 46 10		-	
Adjusted Date/time data from LOGn.xlsx	**Log_in**	*(Excel date/time)*	E2 : E1716		E106 : E3668		-	
Adjusted flow rate data from LOGn.xlsx	**q_in**	*(L/hr)*	G2 : G1716		G106 : G3668		-	
Flow rate @ t_inj	**Q_out(1,1)**	*(L/hr)*	6.4731		0.0000		-	
MasterCalcs.m			**(1) _SS.m**	**(2) _NSS.m**	**(1) _SS.m**	**(2) _NSS.m**	**(1) _SS.m**	**(2) _NSS.m**
data file			7i_BTC_F1		7ii_BTC_F1		7iii_BTC_F1	
inlet flow rate file from *Inflow.m*			7i_inflow		7ii_inflow		7iii_inflow	
outlet flow rate file from *Outflow.m*			7i_outflow		7ii_outflow		7iii_outflow	
			-	7i_BTC_Data	-	7ii_BTC_Data	-	7iii_BTC_Data
mass of Uranine injected	**M**	*(mg)*	3		15		30	
distance to sample port	**L**	*(m)*	6		6		6	
water level	**h_h20**	*(m)*	0.44		0.44		0.44	
figure (28) domain	**xlim**		[0 2.0]	[0 2.0]	[0 3.0]	[0 3.5]	[0 3.5]	[0 4.0]
index at which θ = 1	**THETA_ind**		27980	-	45509	-	83176	-

Table C12: Summary of the Matlab code outputs for the flow tests performed at three depths at ports 1 and 2 in the pilot-scale CWs at the Helmholtz UFZ in 2016

	Port 1, 12cm		Port 1, 24cm		Port 1, 36cm		Port 2, 12cm		Port 2, 24cm		Port 2, 36cm	
	Steady flow	**Variable Flow**	**Steady flow**	**Variable Flow**	**Steady flow**	**Variable Flow**	**Steady flow**	**Variable Flow**	**Steady flow**	**Variable Flow**	**Steady flow**	**Variable Flow**
Q_{avg} (L/s)	6.96	-	6.96	-	6.31	-	7.72	-	7.72	-	7.72	-
τ (h)	29.9	-	29.9	-	33.0	-	48.5	-	48.5	-	48.5	-
θ_{peak} / Φ_{peak}	0.4894	0.7329	0.5658	0.7065	0.5735	0.6319	0.5041	0.2704	0.4143	0.2277	0.4624	0.1580
M_0 (E)	1.0000	1.0000	1.0000	1.0000	1.0000	1.0000	1.0000	1.0000	1.0000	1.0000	1.0000	1.0000
M_0 (C')	0.6493	1.0009	0.7923	1.1127	0.9899	1.0000	1.0307	1.0006	1.0172	1.0009	1.2189	1.0011
M_1 (E) = t_m	46.1	48.1	37.8	40.5	33.3	31.0	47.0	47.7	47.7	47.6	39.8	36.0
M_1 (C')	0.6943	1.4671	0.7923	1.5552	0.9899	0.9514	1.0307	0.7048	1.0172	0.7127	1.2189	0.4781
Recovery (%)	104.35	91.99	87.21	85.00	68.01	64.81	43.53	42.35	48.54	47.44	46.78	52.90
N	3.9342	3.5208	2.8200	2.6974	3.0085	2.7586	2.0524	1.9507	1.6597	1.5290	1.7595	1.4381
d	0.25	0.28	0.35	0.37	0.33	0.36	0.00	0.51	0.60	0.65	0.57	0.70
t_{10}	19.4833	-	14.0444	-	11.3528	-	18.4611	-	19.4583	-	18.3972	-
t_{90}	78.7611	-	74.8722	-	63.9917	-	93.5917	-	97.5833	-	79.2306	-
θ_{10}	0.4229	-	0.3720	-	0.3409	-	0.3924	-	0.4082	-	0.4625	-
MDI	4.0425	-	5.3311	-	5.6367	-	5.0697	-	5.0150	-	4.3067	-
MI	0.8688	-	0.8192	-	0.7596	-	0.7234	-	0.7080	-	0.6836	-

Table C13: Summary of the Matlab code outputs for the flow tests performed at three depths at ports 3 and 4 in the pilot-scale CWs at the Helmholtz UFZ in 2016

	Port 3, 12cm		Port 3, 24cm		Port 3, 36cm		Port 4, 12cm		Port 4, 24cm		Port 4, 36cm	
	Steady flow	Variable Flow	Steady flow	Variable Flow	Steady flow	Variable Flow	Steady flow	Variable Flow	Steady flow	Variable Flow	Steady flow	Variable Flow
Q_{avg} (L/s)	8.44	-	5.42	-	8.81	-	8.89	-	8.89	-	8.89	-
τ (h)	59.2	-	92.2	-	56.7	-	56.1809	-	56.2222	-	56.0959	-
θ_{peak} / Φ_{peak}	0.7644	0.8102	0.7612	0.6054	0.7087	0.8735	0.6980	0.8220	0.6538	0.7048	0.5802	0.5757
M_0 (E)	1.0000	1.0000	1.0000	1.0000	1.0000	1.0000	1.0000	1.0000	1.0000	1.0000	1.0000	1.0000
M_0 (C')	1.0279	1.0006	0.6759	1.0009	0.7395	1.0027	0.7533	1.1790	0.8440	1.0009	0.8886	1.0020
M_1 (E) = t_m	57.6	58.2	136.4	139.9	76.7	78.0	74.5794	76.2241	66.6129	68.1579	63.1254	64.8460
M_1 (C')	1.0279	1.0787	0.6759	0.9369	0.7395	1.3026	0.7533	1.3750	0.8440	1.1288	0.8886	1.0722
Recovery (%)	6.32	6.96	38.04	30.17	62.27	61.66	67.96	64.98	77.81	75.13	89.31	85.68
N	8.4136	8.7554	5.2424	4.8098	4.5141	4.3136	3.4887	3.6024	3.1252	3.1033	3.1562	3.0997
d	1.19E+05	0.11	0.19	0.21	0.22	0.23	0.29	0.28	0.32	0.32	0.32	0.32
t_{10}	37.5538	-	82.2861	-	45.4056	-	39.3833	-	33.0861	-	31.6750	-
t_{90}	85.6472	-	209.3306	-	121.6722	-	127.8111	-	115.7056	-	109.6056	-
θ_{10}	0.6518	-	0.6033	-	0.5920	-	0.5281	-	0.4967	-	0.5018	-
MDI	2.2804	-	2.5439	-	2.6797	-	3.2453	-	3.4971	-	3.4603	-
MI	0.8637	-	0.8948	-	0.8767	-	0.8544	-	0.8281	-	0.8202	-

Table C14: Summary of the Matlab code outputs for the flow tests performed at three depths at ports 5 and 6 in the pilot-scale CWs at the Helmholtz UFZ in 2016

	Port 5, 12cm		Port 5, 24cm		Port 5, 36cm		Port 6, 12cm		Port 6, 24cm		Port 6, 36cm	
	Steady flow	**Variable Flow**	**Steady flow**	**Variable Flow**	**Steady flow**	**Variable Flow**	**Steady flow**	**Variable Flow**	**Steady flow**	**Variable Flow**	**Steady flow**	**Variable Flow**
Q_{avg} (L/s)	6.50	-	6.49	-	6.50	-	6.70	-	6.70	-	6.70	-
τ (h)	96.5	-	96.7	-	96.5	-	132.4	-	132.4	-	132.4	-
θ_{peak} / Φ_{peak}	0.7139	0.6749	0.7098	0.6740	0.7064	0.6146	0.9143	1.0315	0.8219	0.9808	0.8228	0.9093
M_0 (E)	1.0000	1.0000	1.0000	1.0000	1.0000	1.0000	1.0000	1.0000	1.0000	1.0000	1.0000	1.0000
M_0 (C')	0.9437	1.0006	0.9440	1.0005	1.0386	1.0006	1.0294	1.0006	0.9679	1.0006	1.0328	1.0006
M_1 (E) = t_m	102.2	103.7	102.5	104.1	92.9	94.1	128.6	129.5	136.7	137.0	128.2	128.9
M_1 (C')	0.9437	0.9739	0.9440	0.9783	1.0386	0.8814	1.0294	1.1205	0.9679	1.1909	1.0328	1.1184
Recovery (%)	10.32	9.68	10.25	9.60	12.92	11.98	2.63	3.01	6.84	7.82	7.60	8.66
N	12.9628	13.1084	11.4012	11.5713	9.5289	9.5293	35.3293	31.9956	14.6623	15.2827	15.5762	15.9144
d	0.08	0.08	0.09	0.09	0.10	0.10	0.03	0.03	0.07	0.07	0.06	0.06
t_{10}	70.3111	-	68.6444	-	61.0556	-	101.9194	-	98.0000	-	92.9444	-
t_{90}	142.6806	-	145.5833	-	136.5667	-	159.3111	-	189.9028	-	171.1222	-
θ_{10}	0.6877	-	0.6699	-	0.6572	-	0.7927	-	0.7167	-	0.7252	-
MDI	2.0293	-	2.1208	-	2.2368	-	1.5631	-	1.9378	-	1.8411	-
MI	0.8943	-	0.8878	-	0.8663	-	0.9286	-	0.8993	-	0.8981	-

Table C15: Summary of the Matlab code outputs for the flow tests performed at three depths at port 7 in the pilot-scale CWs at the Helmholtz UFZ in 2016

	7ii (May 2016)		7iii (August 2016)	
	Steady flow	**Variable Flow**	**Steady flow**	**Variable Flow**
Q_{avg} (L/s)	8.20	-	5.76	-
τ (h)	123.1	-	175.2	-
θ_{peak} / Φ_{peak}	0.6352	0.5250	0.6247	0.4753
M_0 (E)	1.0000	1.0000	1.0000	1.0000
M_0 (C')	0.8240	1.0009	0.7577	1.0016
M_1 (E) = t_m	149.4	150.0	231.3	241.1
M_1 (C')	0.8240	0.9591	0.7577	0.9309
Recovery (%)	30.86	29.97	36.01	29.57
N	8.4973	8.3245	7.1699	7.4997
d	0.12	0.12	0.14	0.13
t_{10}	92.7639	-	141.3222	-
t_{90}	224.3306	-	343.9395	-
θ_{10}	0.6208	-	0.6111	-
MDI	2.4183	-	2.4337	-
MI	0.8851	-	0.8926	-

Appendix D: Climatic Data (2016)

This appendix summarizes the climatic data (temperature, rainfall, global radiation, relative humidity) that was gathered by the small weather station erected alongside the outdoor pilot-scale CWs at the Helmholtz UFZ, Leipzig. This data was used, in conjunction with the flow rate data recorded by the wetland control system, to perform a water mass balance over the wetland, which yielded the water loss due to evapotranspiration. In addition, investigating the climatic, or weather, conditions during the experiments gave an explanation of some of the fluctuations in flow rate which were observed. Only the climatic data collected during each tracer flow test or that supporting what is presented in Aylward et al. (2019) is given here.

Additional information needed to interpret the data given in Tables D1 to D6

Day cycle:	6am – 10pm
Night cycle:	10pm – 6am (+1)
Inflow cylinder volume:	1.7 L
Outflow cylinder volume:	0.935 L
Density of water:	1 kg/L
Gravel bed surface area:	6 870 000 mm^2

Note:

- The climatic data is analysed in two parts; namely a day cycle and a night cycle.
- The control system records the time taken to fill and then drain a cylinder of know volume at the inlet (*inflow cylinder*) and at the outlet (*outflow cylinder*). This makes it possible to calculate the inlet and outlet volumetric flowrates. The number of filling and draining cycles recorded during the designated day and night periods also give the total mass of water entering and leaving the system within these times.

$$\text{inflow mass (kg)} = \text{no. of cycles} \times \text{volume of inlet cylinder (L)} \times \text{density of water } (\frac{\text{kg}}{\text{L}})$$

$$\text{outflow mass (kg)} = \text{no. of cycles} \times \text{volume of outlet cylinder (L)} \times \text{density of water } (\frac{\text{kg}}{\text{L}})$$

- Temperature, global radiation and relative humidity are recorded by the weather station on an hourly basis. The following are reported in Tables D1 to D6 below:
  - The day time maximum temperature
  - The night time minimum temperature
  - The day time and night time global radiation maxima
  - The day time and night time average relative humidity

- Rainfall (mm) is measured from a rain gauge at the site.

$$\text{Rainfall (kg)} = \text{rainfall (mm)} \times \text{gravel bed surface area (mm}^2) \times \left(1 \times 10^{-6} \frac{\text{L}}{\text{mm}^3}\right) \times \frac{1\text{kg}}{\text{L}}$$

- The system water balance:

$$\text{inflow mass (kg)} + \text{rainfall (kg)} = \text{outflow mass (kg)} + \text{evapotranspiration (kg)}$$

- The volume of water lost due to evapotranspiration is

$$\text{evapotranspiration (mm)} = \frac{\text{evapotranspiration (kg)}}{\text{density of water } \left(\frac{\text{kg}}{\text{L}}\right) \times \text{gravel bed surface area (mm}^2) \times \frac{(1\times10^{-6})\text{L}}{\text{mm}^3}}$$

Table D1: Sub-set of data used to perform the water mass balance (masses of water entering and leaving the system) during the flow test in April 2016

Date (2016)	Inflow Cycles		Outflow Cycles		Inflow mass (kg)		Outflow mass (kg)		Rainfall (mm)		Rainfall (kg)		Evapotranspiration (kg)		Evapotranspiration (mm)	
	Day	Night	Day	Night	Day	Night	Day	Night	Day	Night	Day	Night	Day	Night	Day	Night
12-Apr	71	33	110	53	120.7	56.1	102.9	49.6	0.0	0.0	0.0	0.0	17.9	6.5	2.6	1.0
13-Apr	42	13	87	66	71.4	22.1	81.3	61.7	1.0	7.2	6.9	49.5	-3.1	9.9	-0.4	1.4
14-Apr	56	3	99	7	95.2	5.1	92.6	6.5	0.6	0.0	4.1	0.0	6.8	-1.4	1.0	-0.2
15-Apr	59	37	132	72	100.3	62.9	123.4	67.3	3.0	0.0	20.6	0.0	-2.5	-4.4	-0.4	-0.6
16-Apr	74	37	154	92	125.8	62.9	144.0	86.0	1.3	2.5	8.9	17.2	-9.3	-5.9	-1.3	-0.9
17-Apr	75	37	160	72	127.5	62.9	149.6	67.3	2.2	0.0	15.1	0.0	-7.0	-4.4	-1.0	-0.6
18-Apr	65	37	81	62	110.5	62.9	75.7	58.0	0.0	0.0	0.0	0.0	34.8	4.9	5.1	0.7

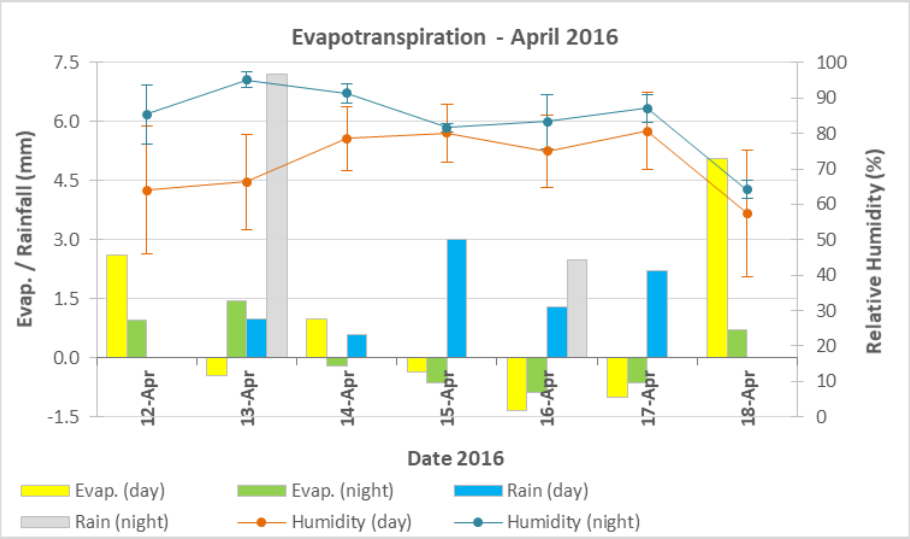


Figure D1: Amount of rainfall and evapotranspiration with the relative during the April 2016 flow test

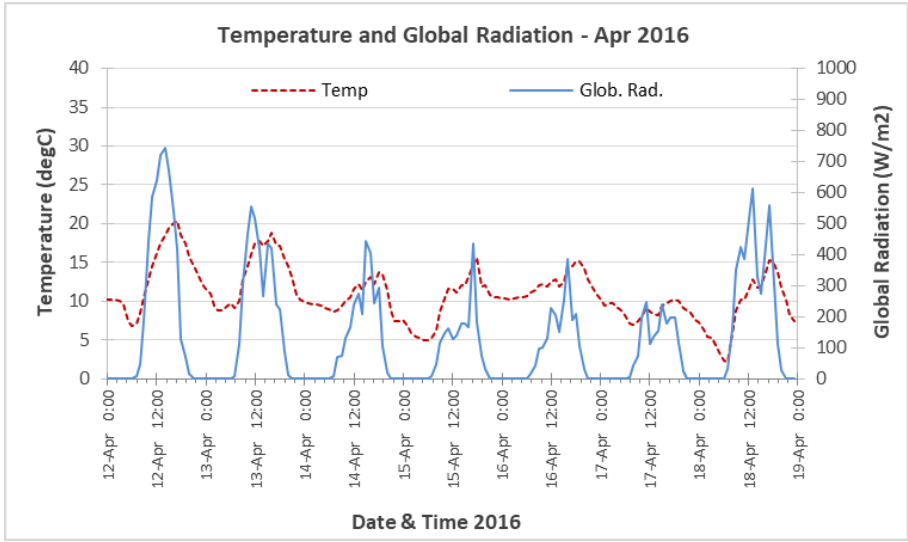


Figure D2: Daytime and night time temperature and global radiation during humidity the April 2016 flow test

Table D2: Sub-set of data used to perform the water mass balance (masses of water entering and leaving the system) during the flow test in May 2016

Date (2016)	Inflow Cycles		Outflow Cycles		Inflow mass kg)		Outflow mass kg)		Rainfall (mm)		Rainfall (kg)		Evapotranspiration (kg)		Evapotranspiration (mm)	
	Day	Night	Day	Night	Day	Night	Day	Night	Day	Night	Day	Night	Day	Night	Day	Night
2-May	74	38	79	0	125.8	64.6	73.9	0	0.0	0.0	0.0	0.0	51.9	64.6	2.9	-1.0
3-May	77	38	127	52	130.9	64.6	118.7	48.62	0.0	3.5	0.0	24.0	12.2	40.0	3.3	-0.7
4-May	76	39	121	75	129.2	66.3	113.1	70.1	0.0	0.0	0.0	0.0	16.1	-3.8	2.0	-0.5
5-May	77	38	135	76	130.9	64.6	126.2	71.1	0.0	0.0	0.0	0.0	4.7	-6.5	0.4	-0.7
6-May	77	39	131	74	130.9	66.3	122.5	69.2	0.0	0.0	0.0	0.0	8.4	-2.9	2.9	-1.0
7-May	77	38	128	74	130.9	64.6	119.7	69.2	0.0	0.0	0.0	0.0	11.2	-4.6	1.4	-1.0
8-May	77	39	127	75	130.9	66.3	118.7	70.1	0.0	0.0	0.0	0.0	12.2	-3.8	2.9	-1.6
9-May	77	38	129	75	130.9	64.6	120.6	70.1	0.0	0.0	0.0	0.0	10.3	-5.5	-4.7	2.1
10-May	78	38	129	76	132.6	64.6	120.6	71.1	0.0	0.0	0.0	0.0	12.0	-6.5	5.0	5.0
11-May	78	38	127	76	132.6	64.6	118.7	71.1	0.0	0.0	0.0	0.0	13.9	-6.5	9.2	0.5
12-May	78	39	129	77	132.6	66.3	120.6	72.0	0.0	0.0	0.0	0.0	12.0	-5.7	0.2	-4.6
13-May	77	39	139	75	130.9	66.3	130.0	70.1	0.6	0.0	4.1	0.0	5.1	-3.8	-0.7	-1.5
14-May	77	38	140	74	130.9	64.6	130.9	69.2	0.0	0.0	0.0	0.0	0.0	-4.6	1.8	-1.2
15-May	78	38	194	75	132.6	64.6	181.4	70.1	5.3	0.0	36.4	0.0	-12.4	-5.5	0.7	-1.2
16-May	77	38	166	75	130.9	64.6	155.2	70.1	2.3	0.0	15.8	0.0	-8.5	-5.5	1.4	-1.0
17-May	77	39	150	78	130.9	66.3	140.3	72.9	0.1	0.0	0.7	0.0	-8.7	-6.6	3.8	-0.4
18-May	77	38	143	77	130.9	64.6	133.7	72.0	0.0	0.0	0.0	0.0	-2.8	-7.4	2.8	-0.7
19-May	78	38	135	77	132.6	64.6	126.2	72.0	0.0	0.0	0.0	0.0	6.4	-7.4	2.9	-1.0
20-May	78	39	134	77	132.6	66.3	125.3	72.0	0.0	0.0	0.0	0.0	7.3	-5.7	3.3	-0.7

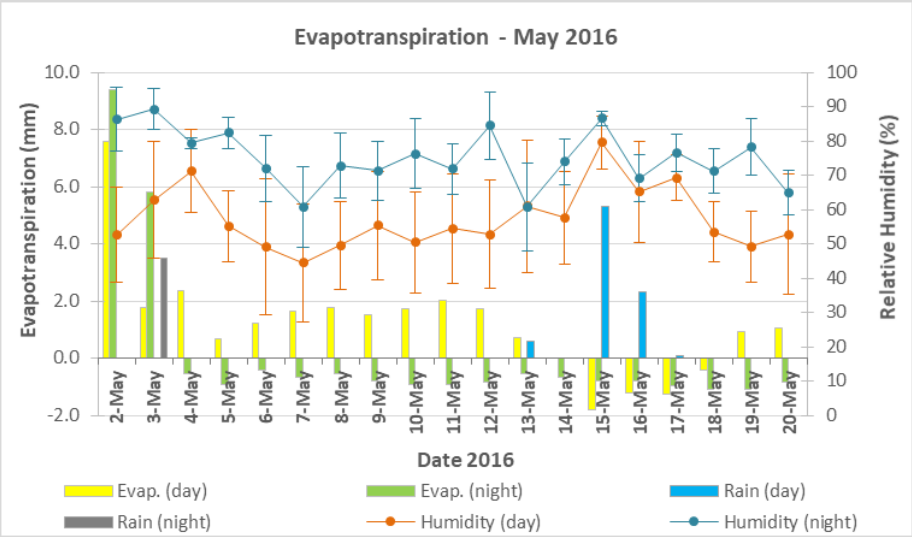


Figure D3: Amount of rainfall and evapotranspiration with the relative during the May 2016 flow test

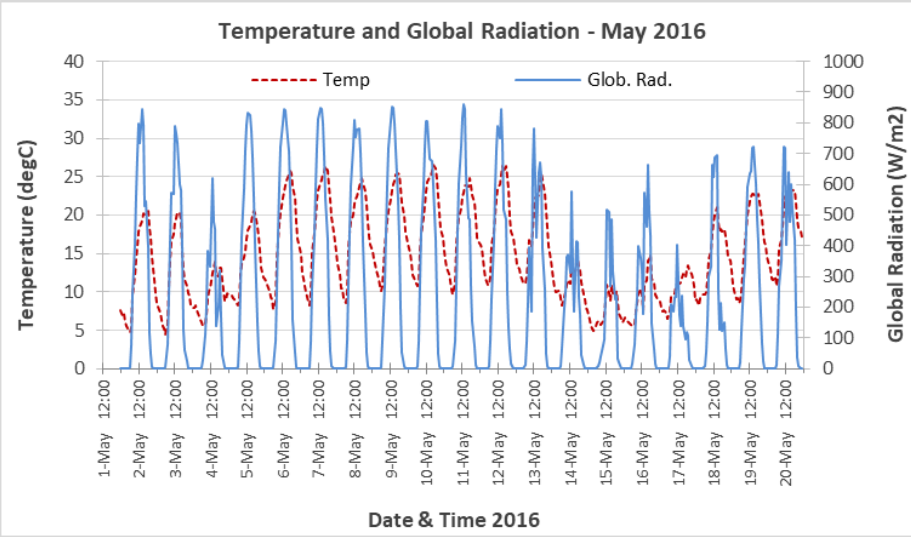


Figure D4: Daytime and night time temperature and global radiation during humidity the May 2016 flow test

Table D3: Sub-set of data used to perform the water mass balance (masses of water entering and leaving the system) during the flow test in June 2016

Date (2016)	Inflow Cycles		Outflow Cycles		Inflow mass (kg)		Outflow mass (kg)		Rainfall (mm)		Rainfall (kg)		Evapotranspiration (kg)		Evapotranspiration (mm)	
	Day	Night	Day	Night	Day	Night	Day	Night	Day	Night	Day	Night	Day	Night	Day	Night
6-Jun	82	40	128	80	139.4	68.0	119.7	74.8	0.0	0.0	0.0	0.0	19.7	-6.8	2.9	-1.0
7-Jun	82	41	125	80	139.4	69.7	116.9	74.8	0.0	0.0	0.0	0.0	22.5	-5.1	3.3	-0.7
8-Jun	81	41	139	79	137.7	69.7	130.0	73.9	0.9	0.1	6.2	0.7	13.9	-3.5	2.0	-0.5
9-Jun	81	41	144	80	137.7	69.7	134.6	74.8	0.0	0.0	0.0	0.0	3.1	-5.1	0.4	-0.7
10-Jun	82	40	128	80	139.4	68.0	119.7	74.8	0.0	0.0	0.0	0.0	19.7	-6.8	2.9	-1.0
11-Jun	82	40	139	80	139.4	68.0	130.0	74.8	0.0	0.0	0.0	0.0	9.4	-6.8	1.4	-1.0
12-Jun	81	41	209	100	137.7	69.7	195.4	93.5	11.3	1.9	77.6	13.1	19.9	-10.7	2.9	-1.6
13-Jun	76	38	231	64	129.2	64.6	216.0	59.8	7.9	1.4	54.3	9.6	-32.5	14.4	-4.7	2.1
14-Jun	80	39	149	37	136.0	66.3	139.3	34.6	5.5	0.4	37.8	2.7	34.5	34.5	5.0	5.0
15-Jun	79	39	80	67	134.3	66.3	74.8	62.6	0.5	0.0	3.4	0.0	62.9	3.7	9.2	0.5
16-Jun	80	35	144	144	136.0	59.5	134.6	134.6	0.0	6.3	0.0	43.3	1.4	-31.9	0.2	-4.6
17-Jun	73	37	278	79	124.1	62.9	259.9	73.9	19.1	0.1	131.2	0.7	-4.6	-10.3	-0.7	-1.5
18-Jun	82	41	141	83	139	70	132	78	0.7	0.0	4.8	0.0	12	-8	1.8	-1.2
19-Jun	82	41	144	83	139.4	69.7	134.6	77.6	0.0	0.0	0.0	0.0	4.8	-7.9	0.7	-1.2
20-Jun	81	41	137	82	137.7	69.7	128.1	76.7	0.0	0.0	0.0	0.0	9.6	-7.0	1.4	-1.0
21-Jun	75	34	127	65	127.5	57.8	118.7	60.8	2.6	0.0	17.6	0.0	26.3	-3.0	3.8	-0.4
22-Jun	64	32	96	63	108.8	54.4	89.8	58.9	0.0	0.0	0.0	0.0	19.0	-4.5	2.8	-0.7

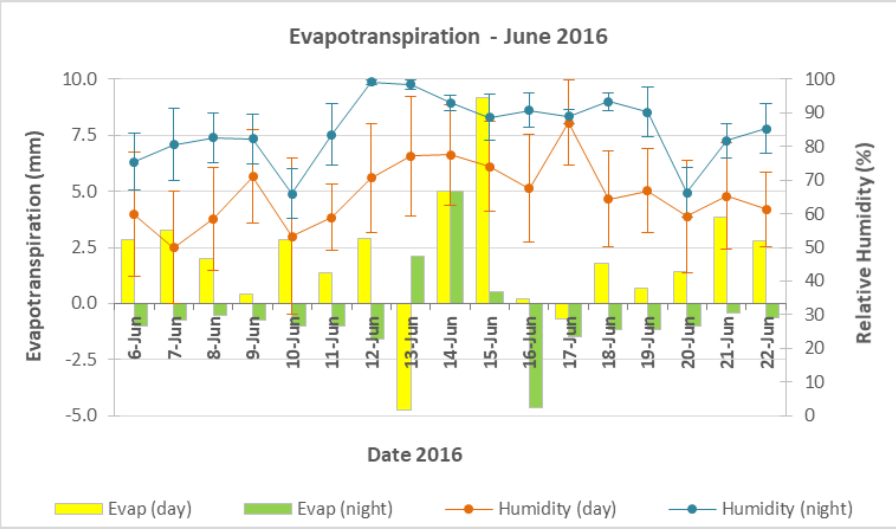


Figure D5: Amount of rainfall and evapotranspiration with the relative during the June 2016 flow test

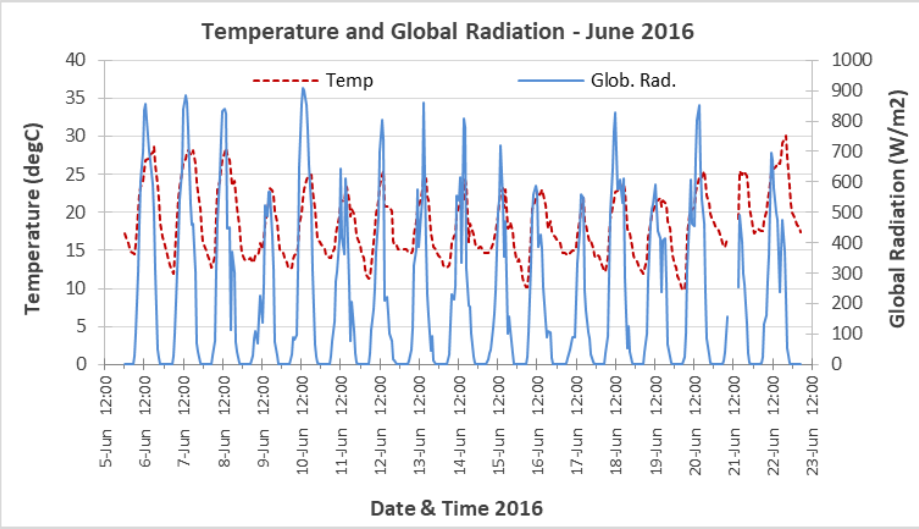


Figure D6: Daytime and night time temperature and global radiation during humidity the June 2016 flow test

Table D4: Sub-set of data used to perform the water mass balance (masses of water entering and leaving the system) during the flow test in July 2016

Date (2016)	Inflow Cycles		Outflow Cycles		Inflow mass (kg)		Outflow mass (kg)		Rainfall (mm)		Rainfall (kg)		Evapotranspiration (kg)		Evapotranspiration (mm)	
	Day	Night	Day	Night	Day	Night	Day	Night	Day	Night	Day	Night	Day	Night	Day	Night
18-Jul	77	39	106	74	130.9	66.3	99.1	69.2	0	0	0	0	31.8	-2.9	4.6	-0.4
19-Jul	71	30	89	57	120.7	51	83.2	53.3	0	0	0	0	37.5	-2.3	5.5	-0.3
20-Jul	58	27	53	49	98.6	45.9	49.6	45.8	0	0	0	0	49.0	0.1	7.1	0.0
21-Jul	56	26	82	49	95.2	44.2	76.7	45.8	0	0	0	0	18.5	-1.6	2.7	-0.2
22-Jul	69	30	81	54	117.3	51	75.7	50.5	0	0	0	0	41.6	0.5	6.1	0.1

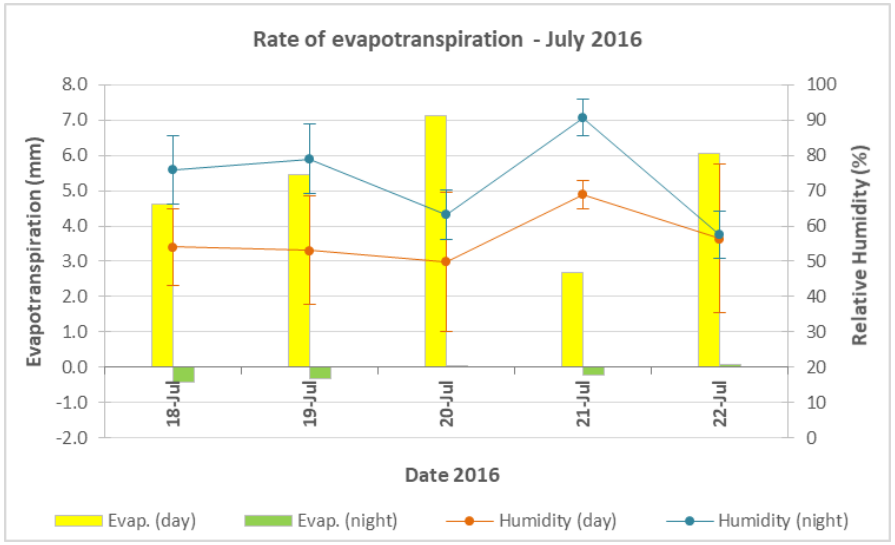


Figure D7: Amount of rainfall and evapotranspiration with the relative during the July 2016 flow test

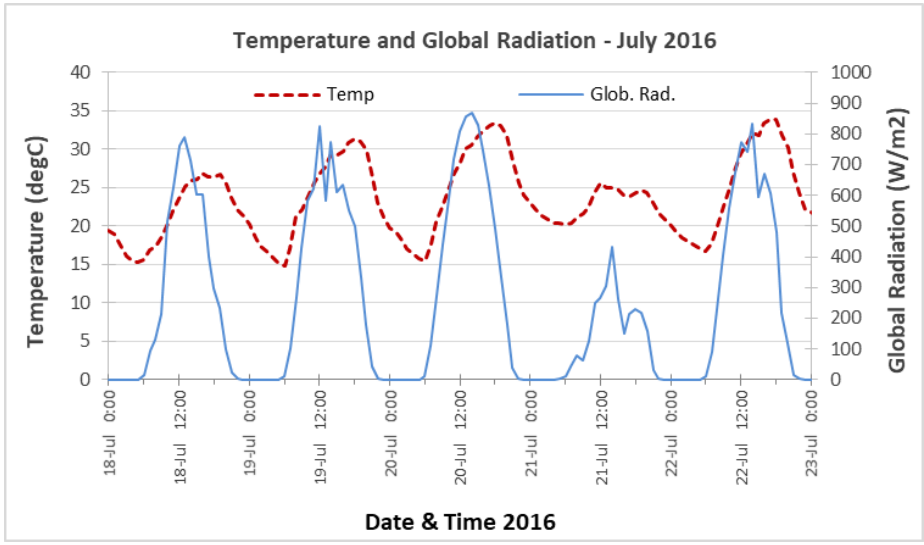


Figure D8: Daytime and night time temperature and global radiation during humidity the July 2016 flow test

Table D5: Sub-set of data used to perform the water mass balance (masses of water entering and leaving the system) during the flow test in August 2016

Date (2016)	Inflow Cycles		Outflow Cycles		Inflow mass (kg)		Outflow mass (kg)		Rainfall (mm)		Rainfall (kg)		Evapotranspiration (kg)		Evapotranspiration (mm)	
	Day	Night	Day	Night	Day	Night	Day	Night	Day	Night	Day	Night	Day	Night	Day	Night
22-Aug	53	3	86	0	90.1	5.1	80.4	0.0	0	0	0	0	9.7	5.1	1.4	0.7
23-Aug	36	29	0	44	61.2	49.3	0.0	41.1	0	0	0	0	61.2	8.2	8.9	1.2
24-Aug	62	30	48	56	105.4	51	44.9	52.4	0	0	0	0	60.5	-1.4	8.8	-0.2
25-Aug	62	31	36	54	105.4	52.7	33.7	50.5	0	0	0	0	71.7	2.2	10.4	0.3
26-Aug	62	30	27	53	105.4	51	25.2	49.6	0	0	0	0	80.2	1.4	11.7	0.2
27-Aug	61	30	40	53	103.7	51	37.4	49.6	0	0	0	0	66.3	1.4	9.7	0.2
28-Aug	61	29	27	51	103.7	49.3	25.2	47.7	0	0.2	0	1.4	78.5	3.0	11.4	0.4
29-Aug	62	31	50	57	105.4	52.7	46.8	53.3	0	0	0	0	58.7	-0.6	8.5	-0.1
30-Aug	63	31	59	58	107.1	52.7	55.2	54.2	0	0	0	0	51.9	-1.5	7.6	-0.2
31-Aug	63	30	50	56	107.1	51	46.8	52.4	0	0	0	0	60.4	-1.4	8.8	-0.2

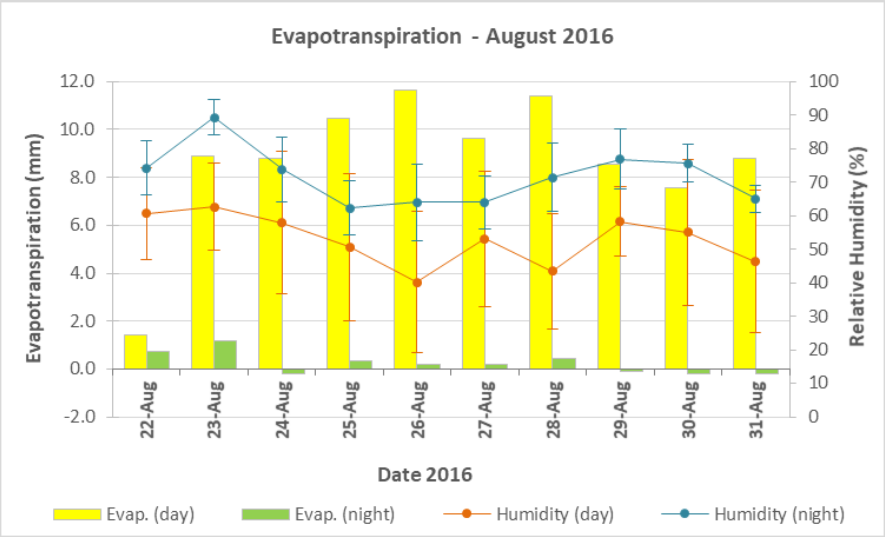


Figure D9: Amount of rainfall and evapotranspiration with the relative humidity during the August 2016 flow test

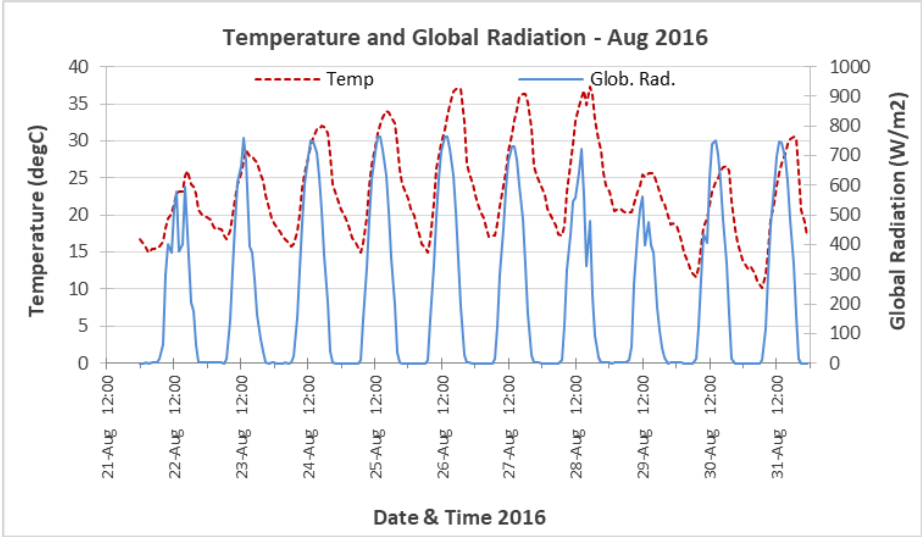


Figure D10: Daytime and night time temperature and global radiation during the August 2016 flow test

Table D6: Data used to perform the water mass balance (masses of water entering and leaving the system) during September 2016

Date (2016)	Inflow Cycles		Outflow Cycles		Inflow mass (kg)		Outflow mass (kg)		Rainfall (mm)		Rainfall (kg)		Evapotranspiration (kg)		Evapotranspiration (mm)	
	Day	Night	Day	Night	Day	Night	Day	Night	Day	Night	Day	Night	Day	Night	Day	Night
1-Sep	65	30	64	61	110.5	51.0	59.8	57.0	0	0	0	0	50.7	-6.0	7.37	-0.88
2-Sep	64	30	66	58	108.8	51.0	61.7	54.2	0	0	0	0	47.1	-3.2	6.85	-0.47
3-Sep	63	31	54	56	107.1	52.7	50.5	52.4	0	0	0	0	56.6	0.3	8.24	0.05
4-Sep	61	30	114	62	103.7	51.0	106.6	58.0	3.4	1.1	23.4	7.6	20.5	0.6	2.98	0.09
5-Sep	61	30	131	61	103.7	51.0	122.5	57.0	3	0	20.6	0	1.8	-6.0	0.27	-0.88
6-Sep	60	30	86	59	102	51.0	80.4	55.2	0	0	0	0	21.6	-4.2	3.14	-0.61
7-Sep	61	30	68	58	103.7	51.0	63.6	54.2	0	0	0	0	40.1	-3.2	5.84	-0.47
8-Sep	60	30	51	56	102	51.0	47.7	52.4	0	0	0	0	54.3	-1.4	7.91	-0.20
9-Sep	61	31	63	61	103.7	52.7	58.9	57.0	0	0	0	0	44.8	-4.3	6.52	-0.63
10-Sep	63	30	65	59	107.1	51.0	60.8	55.2	0	0	0	0	46.3	-4.2	6.74	-0.61
11-Sep	60	30	57	52	102	51.0	53.3	48.6	0	0	0	0	48.7	2.4	7.09	0.35
12-Sep	66	33	36	47	112.2	56.1	33.7	43.9	0	0	0	0	78.5	12.2	11.43	1.77
13-Sep	67	34	35	46	113.9	57.8	32.7	43.0	0	0	0	0	81.2	14.8	11.82	2.15
14-Sep	66	33	33	43	112.2	56.1	30.9	40.2	0	0	0	0	81.3	15.9	11.84	2.31
15-Sep	63	29	41	46	107.1	49.3	38.3	43.0	0	0	0	0	68.8	6.3	10.01	0.92
16-Sep	59	27	106	96	100.3	45.9	99.1	89.8	1.3	7.9	8.9	54.3	10.1	10.4	1.47	1.52
17-Sep	63	31	84	63	107.1	52.7	78.5	58.9	6	0	41.2	0	69.8	-6.2	10.16	-0.90
18-Sep	64	30	99	21	108.8	51.0	92.6	19.6	0	0	0	0	16.2	31.4	2.36	4.57
19-Sep	62	31	97	61	105.4	52.7	90.7	57.0	1.7	0	11.7	0	26.4	-4.3	3.84	-0.63
20-Sep	61	30	88	61	103.7	51.0	82.3	57.0	0	0	0	0	21.4	-6.0	3.12	-0.88
21-Sep	62	31	99	61	105.4	52.7	92.6	57.0	0	0	0	0	12.8	-4.3	1.87	-0.63
22-Sep	61	30	86	58	103.7	51.0	80.4	54.2	0	0	0	0	23.3	-3.2	3.39	-0.47
23-Sep	63	34	81	63	107.1	57.8	75.7	58.9	0	0	0	0	31.4	-1.1	4.57	-0.16
24-Sep	65	33	98	74	110.5	56.1	91.6	69.2	0	0	0	0	18.9	-13.1	2.75	-1.91
25-Sep	66	32	87	62	112.2	54.4	81.3	58.0	0	0	0	0	30.9	-3.6	4.49	-0.52
26-Sep	67	33	104	69	113.9	56.1	97.2	64.5	0	0	0	0	16.7	-8.4	2.43	-1.22

27-Sep	69	34	110	67	117.3	57.8	102.9	62.6	0	0	0	0	14.5	-4.8	2.10	-0.71
28-Sep	67	34	93	59	113.9	57.8	87.0	55.2	0	0	0	0	26.9	2.6	3.92	0.38
29-Sep	67	33	71	71	113.9	56.1	66.4	66.4	0	0	0	0	47.5	-10.3	6.92	-1.50
30-Sep	65	33	122	65	110.5	56.1	114.1	60.8	0.6	0	4.1	0	0.6	-4.7	0.08	-0.68

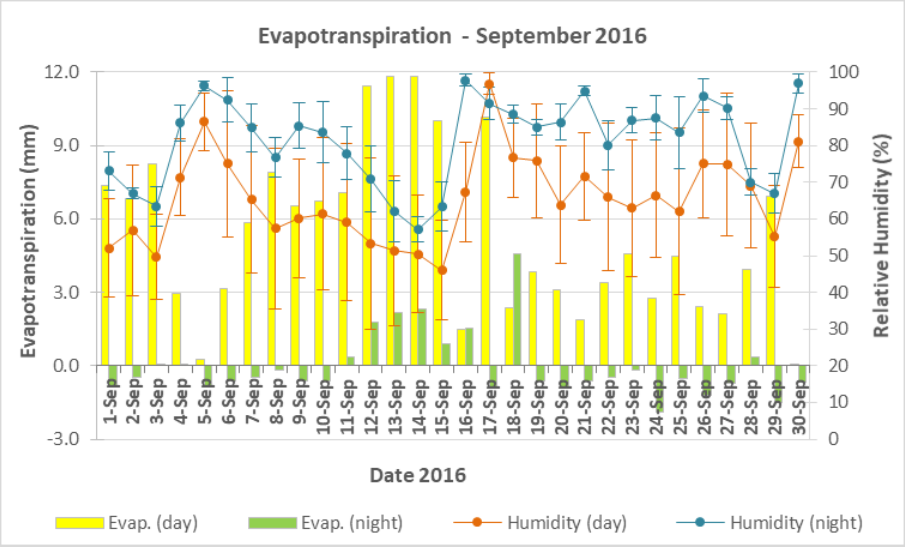


Figure D11: Amount of rainfall and evapotranspiration with the relative humidity during September 2016

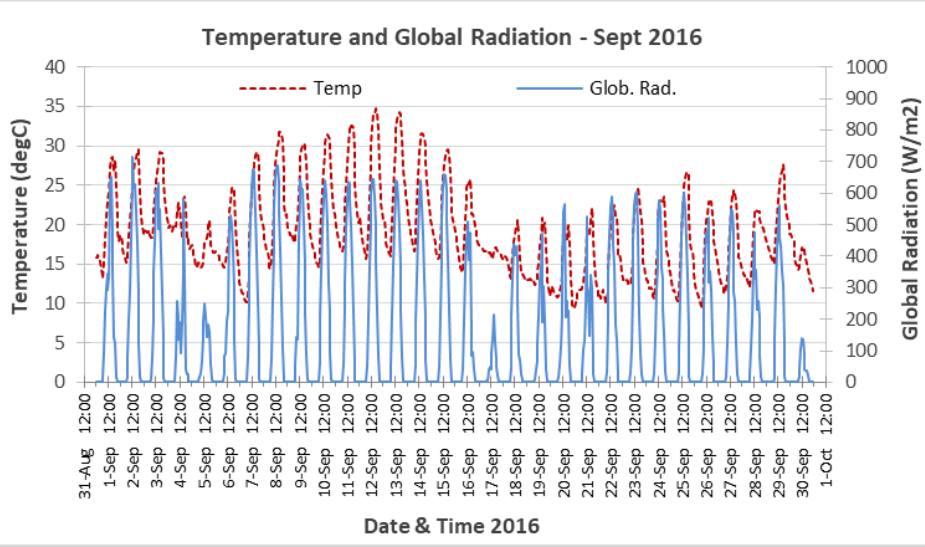


Figure D12: Daytime and night time temperature and global radiation during September 2016

Table D7: Sub-set of data used to perform the water mass balance (masses of water entering and leaving the system) during the flow test in October 2016

Date (2016)	Inflow Cycles		Outflow Cycles		Inflow mass (kg)		Outflow mass (kg)		Rainfall (mm)		Rainfall (kg)		Evapotranspiration (kg)		Evapotranspiration (mm)	
	Day	Night	Day	Night	Day	Night	Day	Night	Day	Night	Day	Night	Day	Night	Day	Night
17-Oct	51	25	90	53	86.7	42.5	84.2	49.6	0	0	0	0	2.6	-7.1	0.37	-1.03
18-Oct	53	26	156	74	90.1	44.2	145.9	69.2	7.6	0.6	52.2	4.1	-3.5	-20.9	-0.52	-3.04
19-Oct	54	27	108	53	91.8	45.9	101.0	49.6	4	0.5	27.5	3.4	18.3	-0.2	2.66	-0.03
20-Oct	56	29	165	63	95.2	49.3	154.3	58.9	7.8	0.6	53.6	4.1	-5.5	-5.5	-0.80	-0.80
21-Oct	57	28	119	63	96.9	47.6	111.3	58.9	1.3	0.7	8.9	4.8	-5.4	-6.5	-0.79	-0.95
22-Oct	56	28	144	59	95.2	47.6	134.6	55.2	3.5	0	24.0	0	-15.4	-7.6	-2.24	-1.10
23-Oct	56	28	113	58	95.2	47.6	105.7	54.2	0	0	0	0	-10.5	-6.6	-1.52	-0.97
24-Oct	55	26	194	88	93.5	44.2	181.4	82.3	10.2	3.1	70.1	21.3	-17.8	-16.8	-2.59	-2.44
25-Oct	51	25	121	54	86.7	42.5	113.1	50.5	2.2	0	15.1	0	-11.3	-8.0	-1.65	-1.16
26-Oct	54	27	106	56	91.8	45.9	99.1	52.4	0	0	0	0	-7.3	-6.5	-1.06	-0.94
27-Oct	56	28	116	59	95.2	47.6	108.5	55.2	1.1	0	7.6	0	-5.7	-7.6	-0.83	-1.10
28-Oct	57	29	125	62	96.9	49.3	116.9	58.0	2.2	0.7	15.1	4.8	-4.9	-3.9	-0.71	-0.56

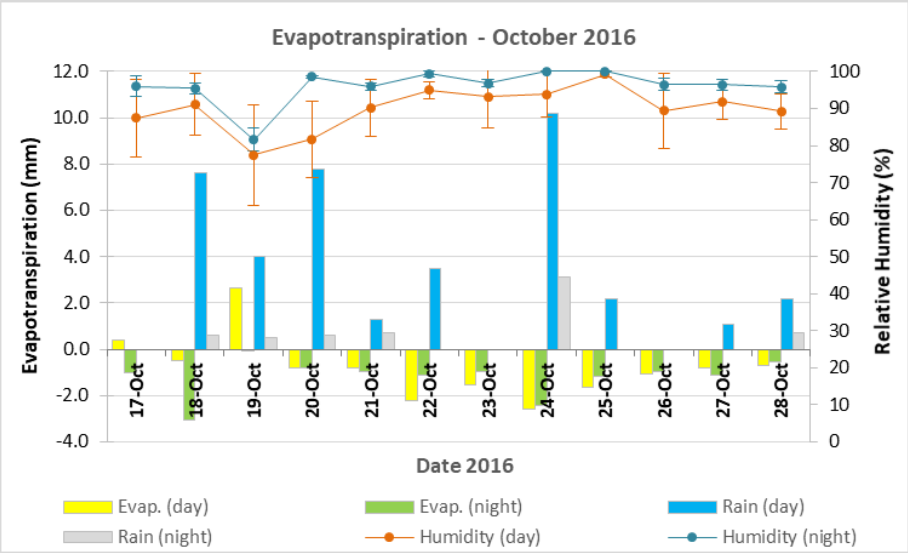


Figure D13: Amount of rainfall and evapotranspiration with the relative during the October 2016 flow test

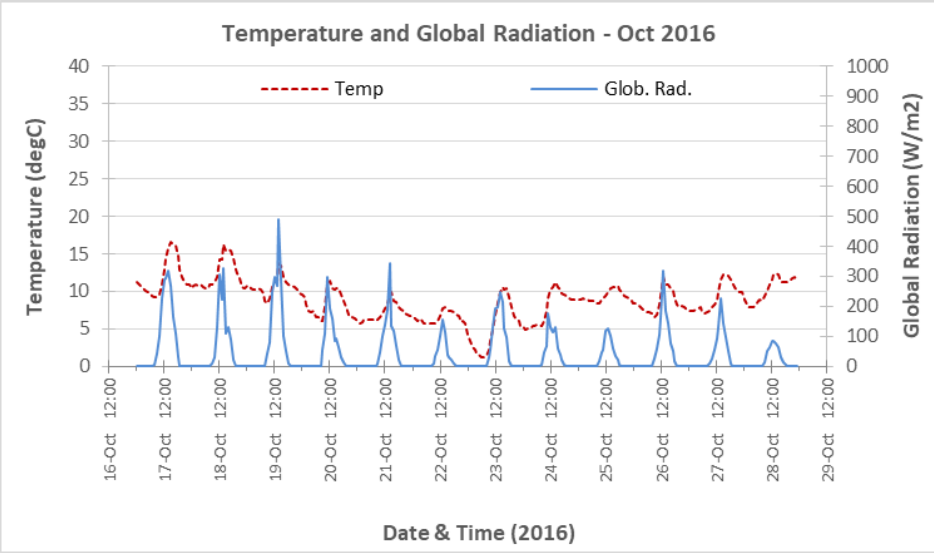


Figure D14: Daytime and night time temperature and global radiation during humidity the October 2016 flow test

Appendix E: Supplementary information for *Sci. Tot. Environ. (2019) Vol. 646 pp. 880-892*

The following section contains supplementary information for the paper by Aylward et al. (2019) entitled "Hydraulic study of a non-steady horizontal sub-surface flow constructed wetland during start-up".

Pilot-scale constructed wetlands at the Helmholtz UFZ in Leipzig, Germany

Photographs of the wetland systems are presented in this section.

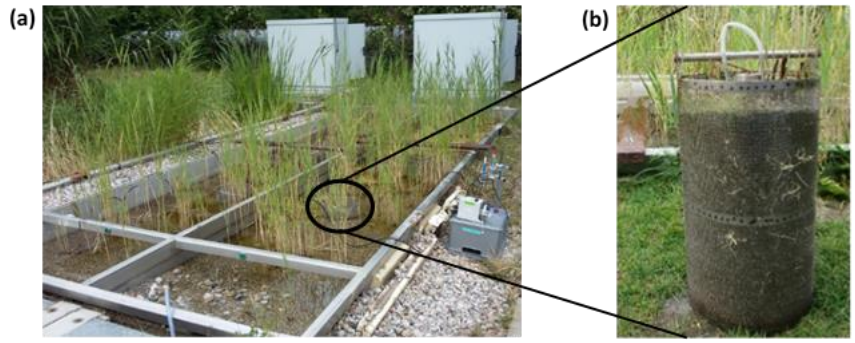


Figure E1: Photograph of the pilot, gravel horizontal subsurface flow constructed wetland at the Helmholtz UFZ, Leipzig (July 2015) **(a)** and the middle basket when removed from the wetland showing a well-developed root system (Sept 2015) **(b)**

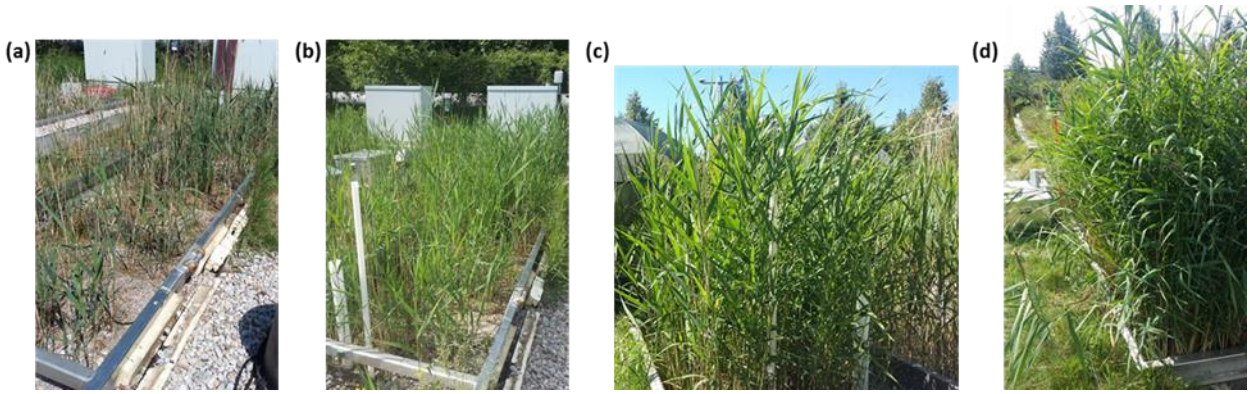


Figure E2: Photographs of the Helmholtz UFZ constructed wetland planted with *Phragmites Australis* in April **(a)**, May **(b)**, June **(c)** and August/September **(d)** of 2016

Experimental set-up for the impulse-response flow tests using the Fluorometers

The fluorometers were set-up to record the uranine concentration at regular intervals (10 seconds) as per the diagram below (Figure E3). Flow tests were run at 6 internal samples ports at three depths below the gravel surface, as well as at the system outlet.

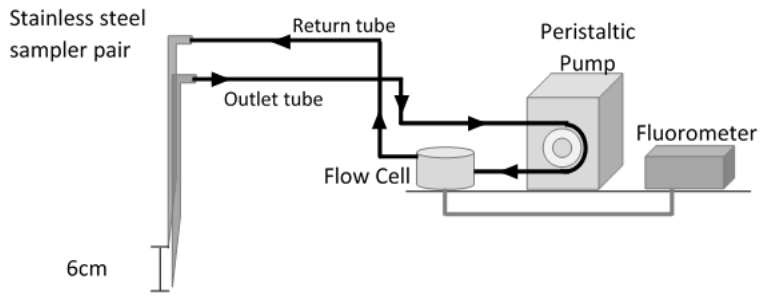


Figure E3: Stainless steel sampling devices (samplers), peristaltic pump, flow cell and fluorometer configuration for the impulse-response flow tests

Rainfall in Leipzig – April to October 2016

Rainfall, and other climatic data, was recorded at the weather station installed on site at the Helmholtz UFZ in Leipzig. The total monthly rainfall for this period is shown in Figure E4.

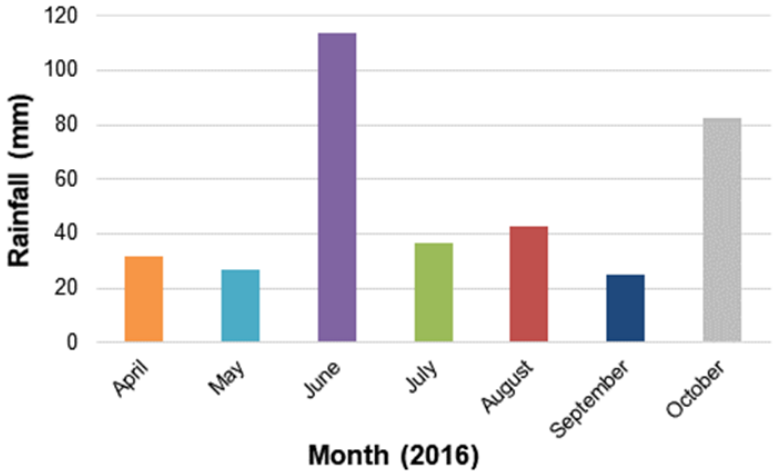


Figure E4: Total monthly rainfall in Leipzig from April to October 2016

Variation in Outlet Volumetric Flow Rate – April to October 2016

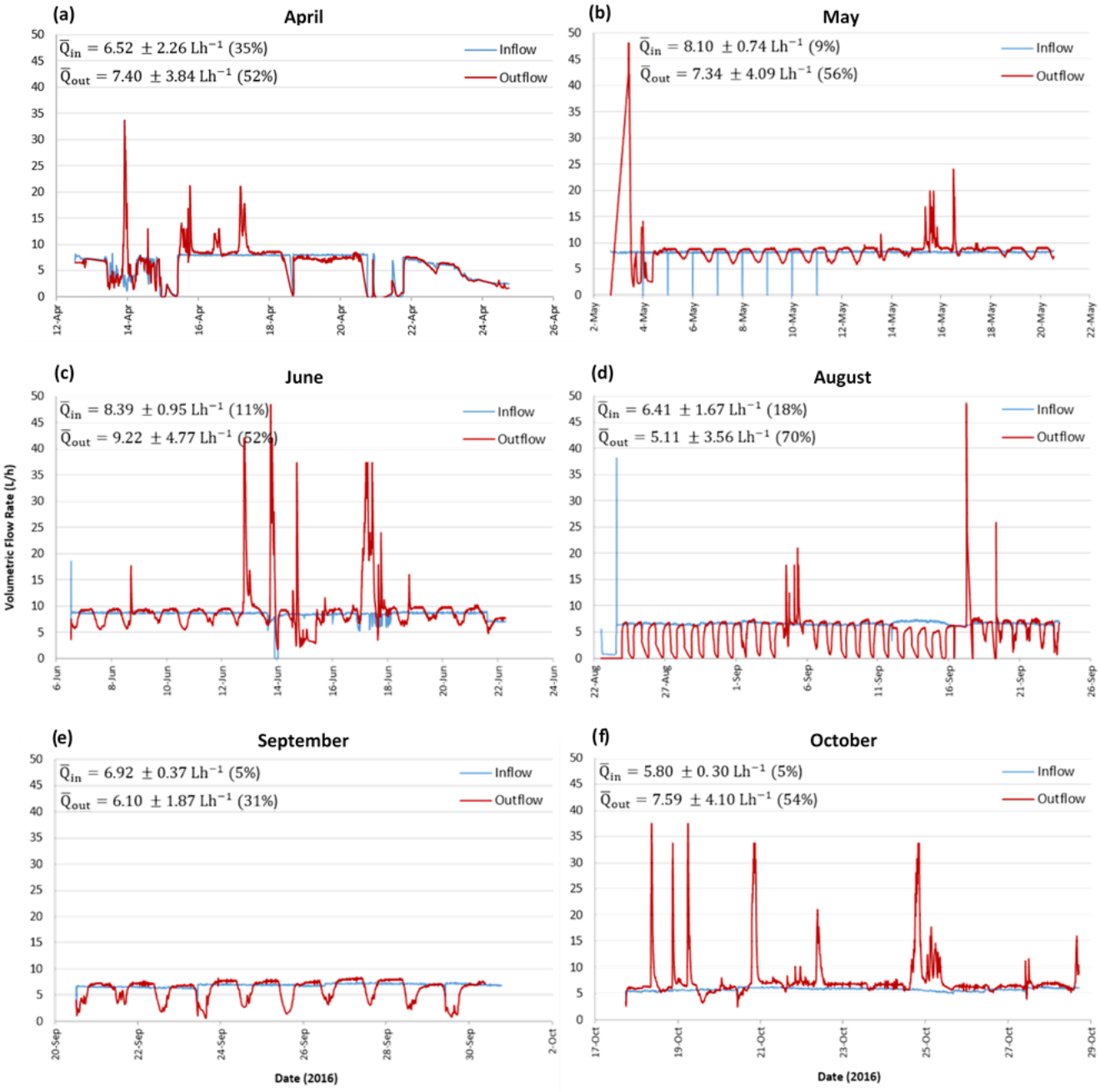


Figure E5: Variation in inlet and outlet volumetric flow rate for the duration of the flow tests (2016)

Measurements of Vegetation Density – April to October 2016

The vegetation density in constructed wetland was measured by the quadrat method. Figure E6 shows monthly measurements of *Phragmites autralis* stem density during 2016. Photographs of the vegetation development are included in Figure E2 of the supplementary material.

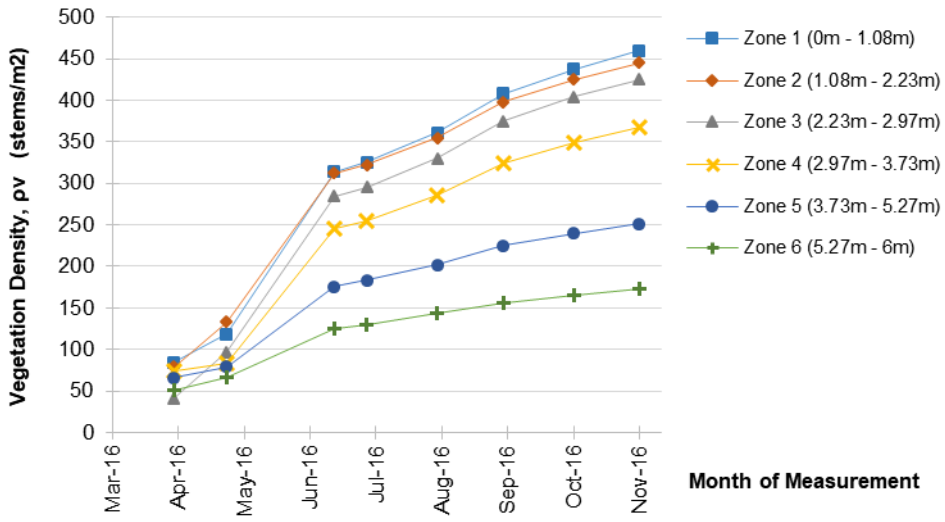


Figure E6: Monthly measurements of vegetation density (*Phragmites autralis*) in the Helmholtz UFZ constructed wetland during 2016

Estimation of the Local Internal Flow Rate

The expressions relating stem density to volumetric flow rate are:

$$\text{Port 2: } \rho_v = 135.05e^{-0.126\left(\frac{Q-8.10}{-0.1267}\right)} \quad [E1]$$

$$\text{Port 3 (24cm): } \rho_v = -7.5975\left(\frac{6.36-Q}{0.315}\right)^2 + 1.2229\left(\frac{6.36-Q}{0.315}\right) + 368.05 \quad [E2]$$

$$\text{Port 5: } \rho_v = -9.0973\left(\frac{6.91-Q}{0.1383}\right)^2 + 3.6579\left(\frac{6.91-Q}{0.1383}\right) + 413.85 \quad [E3]$$

The estimated local internal flow rates at three locations within the CW are given in Table E1. These were determined using the expressions in Eq. E1, E2 and E3 above in conjunction with the stem density estimates and the Microsoft Excel Solver tool. The months for the calculations (Table E1 below) were chosen because a decrease in flow rate was observed from inlet to outlet. The locations at which the internal flow rates have been calculated were chosen based on the sample port at which the flow test was conducted during the month in question.

The estimated internal flow rates for May (Port 2) and September (Port 5) were used to re-calculate the RTD. The calculation was not repeated for August (Port 3) because the internal volumetric flow rate

estimated is equal to the average system flow rate. For comparison, the RTD's calculated using the average system volumetric flow rate (see Equation 6-12) and the average outlet volumetric flow rate are plotted on the same set of axes. The RTD obtained using the variable flow methodology is also plotted for completeness. All plots are given in Figure E7.

Table E1: Estimate of the local volumetric flow rate at each sampling distance along the wetland during the May (Port 2), August (Port 3, mid-depth) and September (Port 5) flow tests (2016)

Distance (m)	**May**		**August**		**September**	
	ρ_v (stems/m^2)	**Q (L/hr)**	**ρ_v (stems/m^2)**	**Q (L/hr)**	**ρ_v (stems/m^2)**	**Q (L/hr)**
0	-	8.10	-	6.36	-	6.91
1.08	125	8.03	358	5.96	403	6.73
2.255	115	7.94	342	5.75	386	6.64
2.97	90	7.69	308	5.45	350	6.51
3.73	81	7.58	244	5.06	274	6.34
5.27	72	7.47	172	4.74	190	6.20
6.00	-	7.34	-	4.47	-	6.08
Avg.	**-**	**7.72**	**-**	**5.42**	**-**	**6.50**

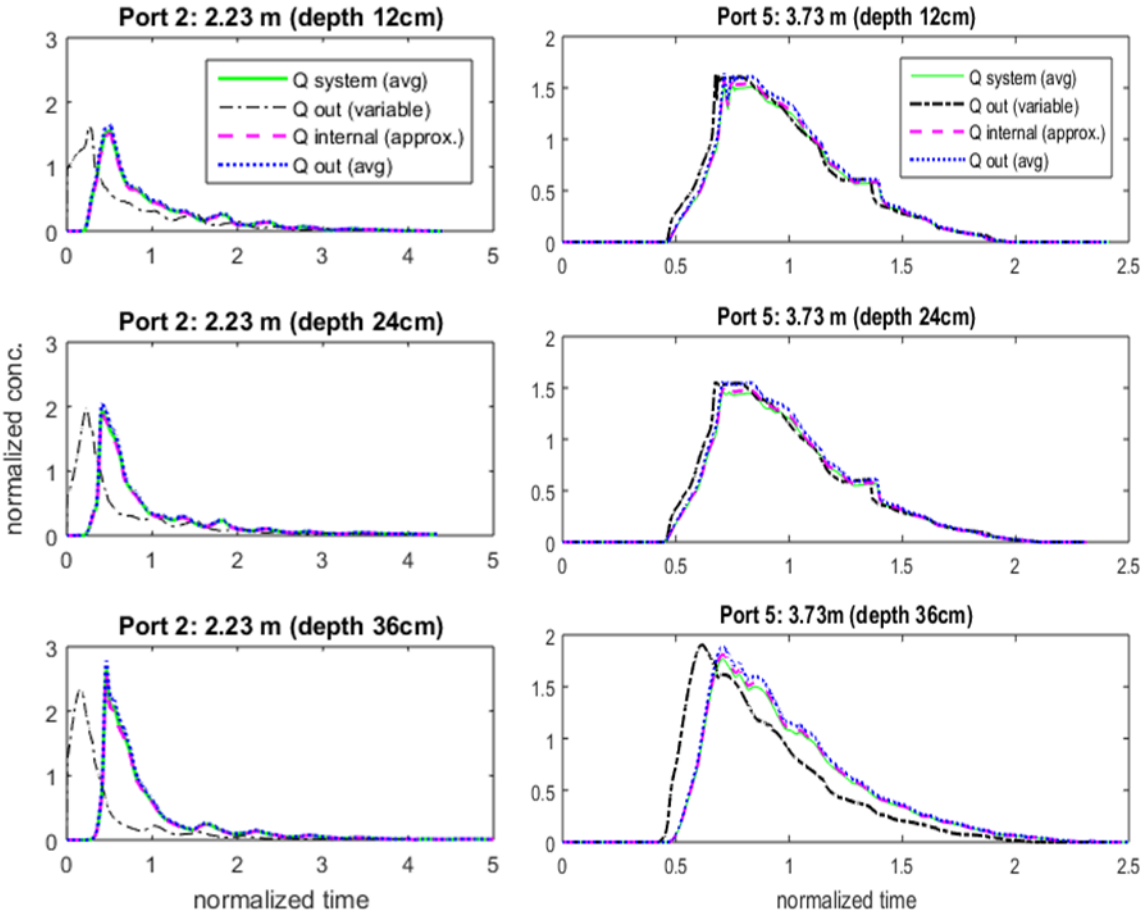


Figure E7: 2016 normalized RTDs at **Port 2** (2.97 m) and **Port 5** (5.27 m) comparing four methods of flow rate valuation with standard RTD theory. These are plotted with the RTD obtained using the variable flow methodology (black dash-dotted line)

Appendix F: *Phragmites australis* fluoride tolerance experiments

Before fluoride was injected into the pilot CWs at the Helmholtz UFZ in Leipzig, Germany, experiments were conducted to investigate the tolerance of *Phragmites australis* to fluoride ions in solution. This was done by harvesting *Phragmites* from the pilot wetlands and exposing them to solutions of varying concentrations of fluoride. This was done over a period of 14 days (24th August 2015 to 7th September 2015) and in three ways:

1. Visual observation of the Phragmites.
2. Measuring the stomatal resistance. The apertures of the stomata play a large role in controlling the diffusion of gasses (notably water vapor and carbon dioxide) into and out of the leaf. The lower the resistance of the stomata to the flow of gasses (and the wider the apertures), the healthier the plant. An AP4 Leaf Porometer (Delta-T Devices) was used to measure the diffusion resistance.
3. Measuring the amount of evapotranspiration.

Visual Observation

After two weeks, the plants in the bottles containing fluoride had all turned brown and needle-like. The leaves in the control bottle (containing only water) were dry but still green.

Stomatal Resistance

The results obtained from the Porometer for each experiment (different concentration of fluoride) are shown in Figures F1 to F5. The resistance to the diffusion increases with increasing fluoride concentration; indicating that plant health is negatively impacted by the presence of higher concentrations of fluoride ions. Readings outside the range of 0.2 – 40.0 $s.cm^{-1}$ should be treated with caution.

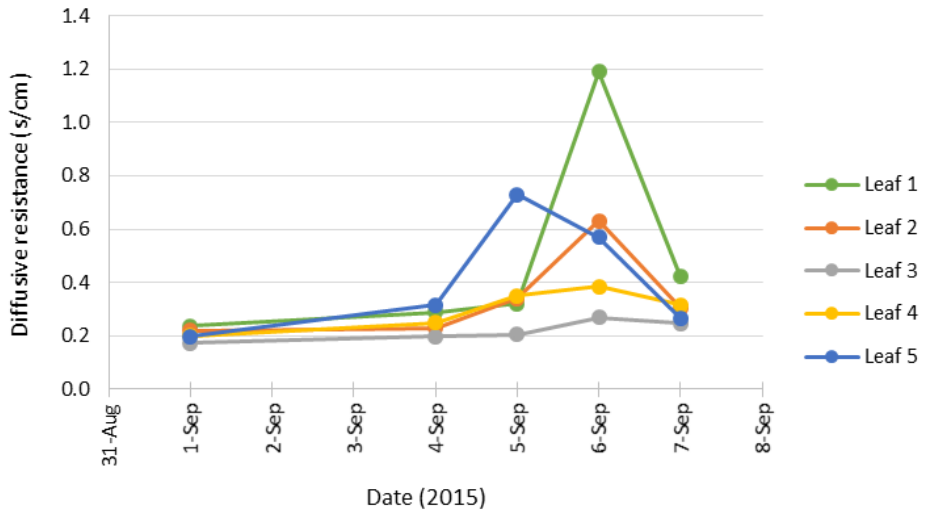


Figure F1: Diffusive resistance of *Phragmites australis* when stored in a brown bottle filled with water for two weeks. The data is taken from the second week.

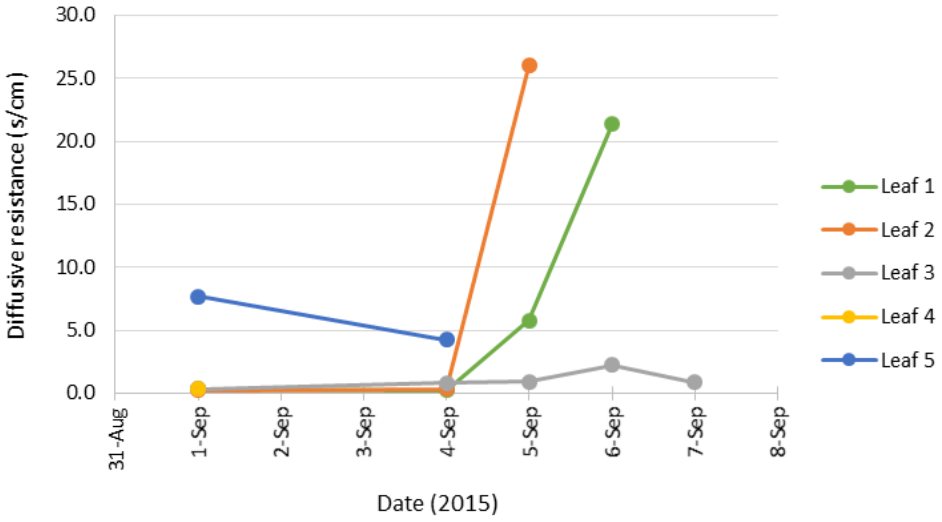


Figure F2: Diffusive resistance of *Phragmites australis* when stored in a brown bottle filled with a fluoride solution (concentration 0.5 g/L) for two weeks. The data is taken from the second week.

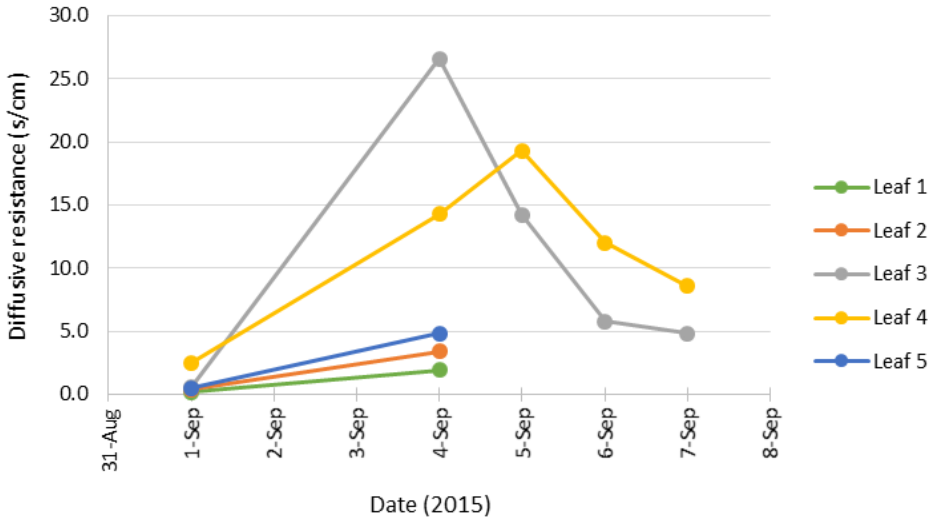


Figure F3: Diffusive resistance of *Phragmites australis* when stored in a brown bottle filled with a fluoride solution (concentration 1.0 g/L) for two weeks. The data is taken from the second week.

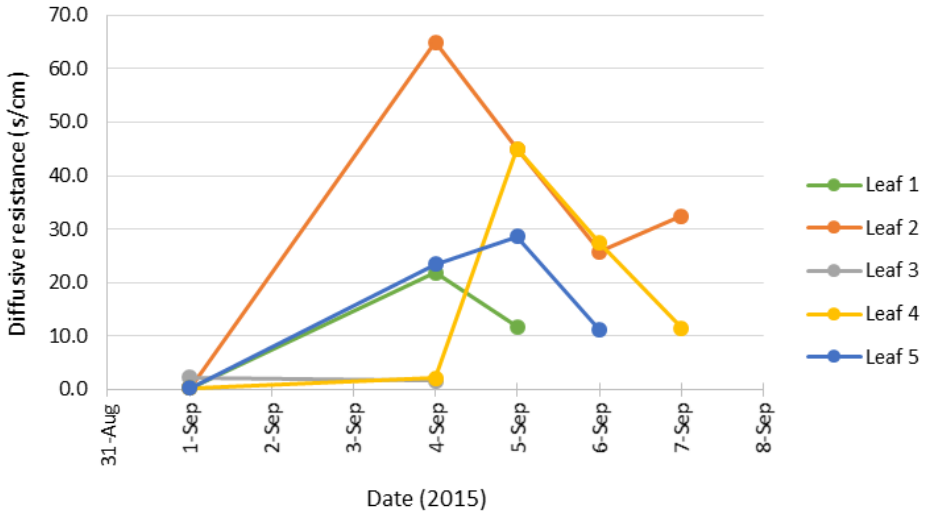


Figure F4: Diffusive resistance of *Phragmites australis* when stored in a brown bottle filled with a fluoride solution (concentration 2.0 g/L) for two weeks. The data is taken from the second week.

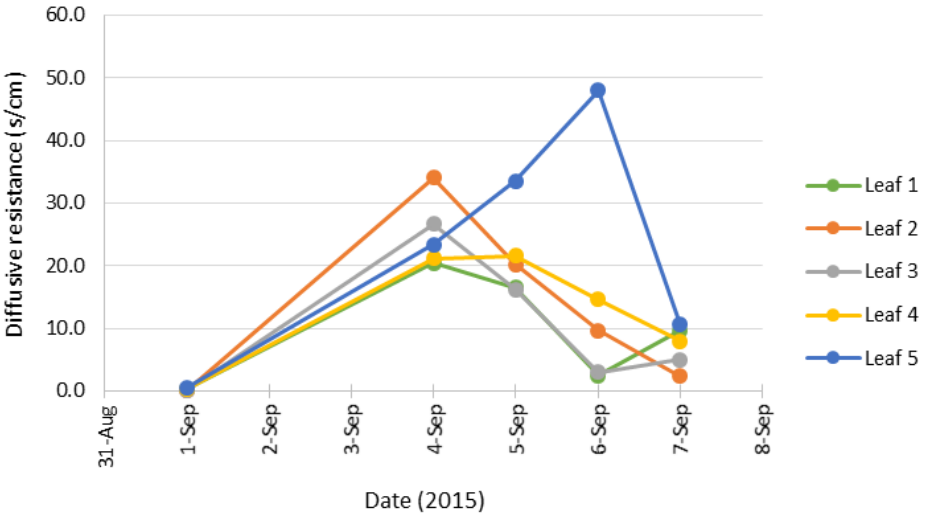


Figure F5: Diffusive resistance of *Phragmites australis* when stored in a brown bottle filled with a fluoride solution (concentration 5.0 g/L) for two weeks. The data is taken from the second week.

Water lost by evapotranspiration

Under controlled environmental conditions (such as in a laboratory), the amount of water lost due to evapotranspiration should not decrease dramatically in healthy plants. The calculation of the amount of evapotranspiration is shown in Tables F1 and F2. There is no immediately apparent correlation between fluoride concentration and the amount of evapotranspiration.

Table F1: Measurements of the initial and final mass of the experiments to perform a water balance

		A	B	C	D	E
[F^-] (g/L)		0	0.5	1	2	5
Date	**Time**	**Mass of bottle + solution + *Phragmites* (kg)**				
24-Aug-15	15h35	4.05	4.05	4.25	4.35	4.35
25-Aug-15	-	-	-	-	-	-
26-Aug-15	14h20	3.90	3.90	4.10	4.15	4.20
27-Aug-15	14h10	3.80	3.80	4.00	4.10	4.10
28-Aug-15	12h30	3.75	3.75	3.90	4.05	4.05
		4.50	**4.65**	**4.35**	**4.60**	**4.60**
29-Aug-15	11h50	4.25	4.30	4.20	4.35	4.35
30-Aug-15	15h20	4.00	4.10	3.95	4.15	4.10
		4.20	**4.15**	**4.25**	**4.35**	**4.40**
1-Sep-15	10h45	4.15	4.10	4.20	4.25	4.35
2-Sep-15	11h10	4.10	4.05	4.10	4.15	4.30
		4.35	**4.15**	**4.40**	**4.45**	**4.45**
3-Sep-15	08h40	4.25	4.05	4.30	4.40	4.35
		4.30	**4.40**	**4.40**	**4.40**	**4.30**
4-Sep-15	14h15	4.20	4.30	4.35	4.35	4.25
5-Sep-15	10h20	4.15	4.25	4.30	4.30	4.20
6-Sep-15	10h15	4.10	4.20	4.25	4.25	4.15
7-Sep-15	08h35	4.05	4.15	4.20	4.20	4.10

bold values indicate total mass after being topped up with water/fluoride solution

Table F2: Mass of water lost due to evapotranspiration (initial – final mass)

	A	B	C	D	E
[F-] (g/L)	0	0.5	1	2	5
	Evapotranspiration (kg)				
Day 1	0.00	0.00	0.00	0.00	0.00
Day 3	0.15	0.15	0.15	0.20	0.15
Day 4	0.10	0.10	0.10	0.05	0.10
Day 5	0.05	0.05	0.10	0.05	0.05
Day 6	0.25	0.35	0.15	0.25	0.25
Day 7	0.25	0.20	0.25	0.20	0.25
Day 8	0.05	0.05	0.05	0.10	0.05
Day 9	0.05	0.05	0.10	0.10	0.05
Day 10	0.10	0.10	0.10	0.05	0.10
Day 11	0.10	0.10	0.05	0.05	0.05
Day 12	0.05	0.05	0.05	0.05	0.05
Day 13	0.05	0.05	0.05	0.05	0.05
Day 14	0.05	0.05	0.05	0.05	0.05